

NATIONAL TEST PILOT SCHOOL



Professional Course

Volume 2

Aerodynamics for Flight Testers

Rev. 1 October 2021

1030 Flight Line
Mojave, California 93501-0658
United States of America
Phone: +1 661 824 2977
Fax: +1 661 824 2943
ntps@ntps.edu

Table of Contents

	Chapter	Update
Aerodynamics for Flight Testers		
Standard Atmosphere.....	1	10/01/2021
Dimensional Analysis.....	2	10/01/2021
Subsonic Aerodynamics.....	3	10/01/2021
Drag Polar.....	4	10/01/2021
Transonic Aerodynamics.....	5	10/01/2021
Supersonic Aerodynamics.....	6	10/01/2021
Pitot-Statics.....	7	10/01/2021
Glossary.....	A	10/01/2021
Standard Atmosphere Table.....	B	10/01/2021
NACA TR-1135.....	Annex	10/01/2021

Volume 2 – Aerodynamics for Flight Testers

Chapter 1

Standard Atmosphere

Table of Contents

1.1 Introduction.....	2
1.2 Altitude Definitions	2
1.2.1 Geometric Altitude	2
1.2.2 Absolute Altitude.....	2
1.2.3 Geopotential Altitude	3
1.3 Division of the Atmosphere	4
1.4 Standard Atmosphere Assumptions	6
1.5 Standard Atmosphere Equations.....	7
1.5.1 Pressure Altitude.....	10
1.5.2 Temperature Altitude.....	11
1.5.3 Density Altitude.....	11

1.1 Introduction

The performance of any flying machine will be greatly influenced by the atmosphere in which it is flying. This is true even for space shuttles, space probes etc. . . since at some point in their journey they will have to cross the atmosphere of the planet from which they are blasting off or re-entering.

The earth's atmosphere is a constantly changing system. The pressure and temperature variations are a function of altitude, geographical location around the earth, season, time of day etc. . . Since these atmospheric conditions cannot be duplicated at will to provide the exact environment in which a flight takes place, then a "standard atmosphere" must be devised to provide a common basis to relate all flight test, wind tunnel results, aircraft design and general performance.

The standard atmosphere will give mean values of pressure, temperature and density as a function of altitude. These values come from mathematical models supported by experimental data obtained from weather balloons and rocket probes.

There are several models of "standard atmosphere" published by various agencies. Minor differences based on mathematical constants used to calculate changes above 100,000 ft. may account for the variation between the models published, however, the differences are negligible in the region of the atmosphere in which modern aircraft fly.

1.2 Altitude Definitions

Although everyone considers altitude as the distance above the earth, more precise definitions must be used in setting up the mathematical models which will define the standard atmosphere.

1.2.1 Geometric Altitude

The geometric altitude is defined as the actual height of an object or aircraft above sea level. Consider a helicopter that takes off from sea level, climbs to a certain height and hovers at that constant height. A tape measure is dropped from the helicopter to sea level. The height of the helicopter indicated by the tape defines its geometric or "tapeline" altitude.

1.2.2 Absolute Altitude

To measure the absolute altitude of a helicopter, its height must be taken with respect to the center of the earth (Figure 1.1).

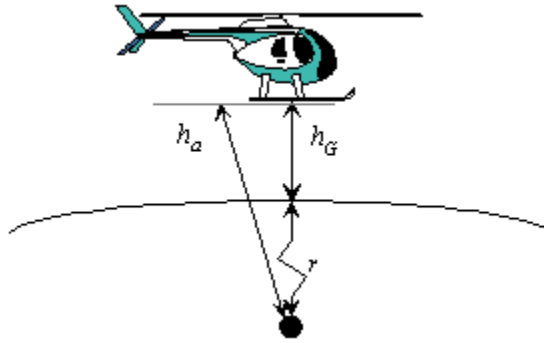


Figure 1.1 Geometric and Absolute Altitude

Absolute altitude is therefore the geometric (or tapeline) altitude plus the radius of the earth. Since the radius varies around the earth, so will the absolute altitude of an aircraft.

$$h_a = h_G + r$$

Absolute altitude is important in space flights because the local acceleration due to gravity varies as a function of the absolute altitude, h_a . Newton's law of gravitation says that 'g' varies inversely as the square of the distance from the earth's center. The term g_o denotes standard sea level acceleration ($g_o = 32.17 \text{ ft/sec}^2$) while g denotes gravitational acceleration at altitude. Although the earth's radius is not constant, it is approximately $20.9 \times 10^6 \text{ ft}$ at 35° latitude, sea level.

$$g = g_o \left(\frac{r}{h_a} \right)^2$$

or

$$g = g_o \left(\frac{r}{r + h_G} \right)^2 \quad (1.1)$$

This variation in 'g' with altitude must be taken into account when building mathematical models of the standard atmosphere. Note that $g = .99g_o$ at 100,000ft, $.999g_o$ at 10,000ft, and $.9999g_o$ at 1000 feet above sea level.

1.2.3 Geopotential Altitude

Because the gravitational acceleration changes as a function of height, there exists a requirement to define yet another altitude, the geopotential altitude. Potential energy is the product of true weight and tapeline altitude ($W \cdot h_G$). If an object's sea level weight is used instead ($W_{SL} = mg_o$), it will not need to go as high to obtain the same potential energy. This lower height is the geopotential height, Figure 1.2. In actual practice, however, the difference between geopotential and geometric height is insignificant unless dealing with space mechanics.

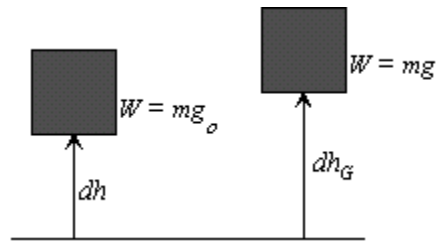


Figure 1.2

Therefore,

$$dhg_o = dh_Gg$$

where:

h : geopotential height

h_G : geometric height

g_o : gravitational constant: 32.17 ft/sec²

g : acceleration due to gravity

$$dh = dh_G \frac{g}{g_o}$$

1.3 Division of the Atmosphere

Figure 1.3 shows the layers of the atmosphere. There are five major divisions of the atmosphere: the troposphere, the stratosphere, the mesosphere, the thermosphere and the exosphere.

The troposphere is the closest region of the atmosphere surrounding the earth. It extends from the surface to approximately 28,000 feet at the poles and to 56,000 feet at the equator. This is the region which will be of most interest to us since it is the region in which most of the weather phenomenon occur and where most aircraft fly. The upper region of the troposphere is the tropopause. The height of this "pause" varies with seasons and also with latitudes.

The second division of the atmosphere is the stratosphere. It extends from the tropopause to approximately 14 miles outward. Depending on the latitude of flight, many aircraft do venture into the lower regions of the stratosphere. With the advent of new technology, many aircraft will someday fly on a routine basis well within the stratosphere.

One of the major characteristics of the lower stratosphere is that the temperature remains a constant. Although strong winds may be present at these high altitudes, they are generally constant in speed. The ever changing weather patterns we witness close to the earth do not occur in the stratosphere.

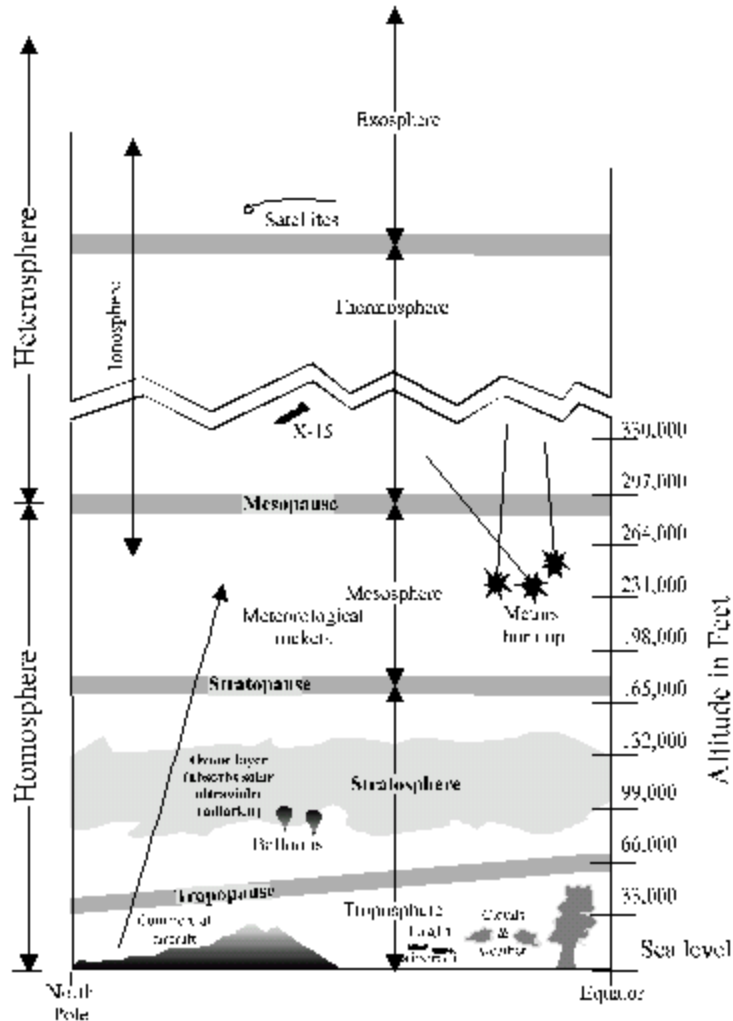


Figure 1.3

The composition of the earth's atmosphere per volume is approximately 78% nitrogen, 21% oxygen, 0.4% water vapor and a trace of other rare gases such as argon, carbon dioxide etc. . .

1.4 Standard Atmosphere Assumptions

1. The air is dry:

With only 0.4% of water vapor per volume in standard air, this is a very reasonable assumption.

2. The air is a perfect gas.

A perfect gas is one in which intermolecular forces are negligible. This is true up to an altitude of about 290,000 ft. This will also be true of the flow of air surrounding an aircraft at subsonic speed as well as supersonic speed. The air will therefore obey the equation of state for a perfect gas:

$$P = \rho RT$$

R is a gas constant which varies with the type of gas. For air, $R = 1716 \frac{lbft}{(slug)(^{\circ}R)}$. Note

that in some books, the equation of state may read:

$$P = \rho gRT$$

In this case, $R = 53.3 \frac{lb.sec^2}{(slug)(^{\circ}R)}$ and multiplying:

$$32.2 \frac{ft}{sec^2} \times 53.3 \frac{lb.sec^2}{(slug)(^{\circ}R)} 1716 \frac{lbft}{(slug)(^{\circ}R)}$$

3. Gravitational Field Decreases with Altitude $g = g_o \left(\frac{r}{r + h_G} \right)^2$

Newton's gravitational law leading to the definition of geopotential altitude has already been discussed.

4. Hydrostatic Equilibrium Exists

One basic law of physics states that the air will always flow from a region of high pressure to a region of low pressure. Why then, does the air surrounding the earth not flow outward into space and leave the earth in a void? Gravity.

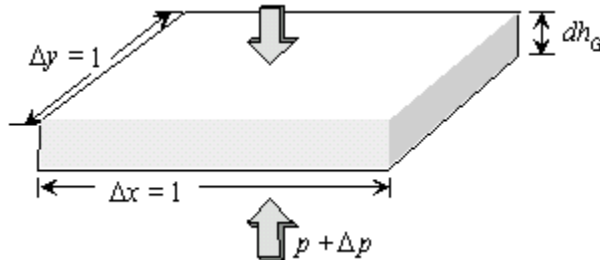


Figure 1.4 Hydrostatic Equilibrium

Considering a small cube of air of Δx and $\Delta y = 1$. If the cube of air is in equilibrium, i.e., not moving up, down, nor sideways, then the force holding the cube down must be equal to the weight of that element of air:

$$\Delta p(\Delta x \cdot \Delta y) = -W$$

The weight of the element of air is equal to its mass times the local acceleration, i.e., $(m \cdot g)$, and since the mass is the density, ρ , per unit volume, then:

$$\Delta p(\Delta x \cdot \Delta y) = -\rho g \Delta h_G (\Delta x \cdot \Delta y)$$

which simplifies to:

$$\Delta p = -\rho g \Delta h_G$$

This hydrostatic equation applies to any fluid of density ρ , i.e., air as well as water etc.. In order to make the equation useful in our aerodynamics calculations, some basic assumptions must be made: in layers of the atmosphere where aircraft generally fly, the variation of g with altitude is negligible. Therefore, by convention, g was considered to be a constant through the atmosphere and equal to g_o . To keep the equations consistent, since

$$dh_{g_o} = dh_{G} \tag{1.2}$$

the **hydrostatic equation** can now be written in its useful form:

$$\boxed{\Delta p = -\rho g_o \Delta h} \tag{1.4}$$

where h is the geopotential altitude. Geopotential altitude is a fictitious altitude which takes into consideration the change in local acceleration with altitude. Since $g \approx g_o$ then the geopotential altitude is the same as geometric altitude in the lower layers of the atmosphere.

1.5 Standard Atmosphere Equations

The three cornerstones of the standard atmosphere are accepted standard values for sea level pressure (P_o), temperature (T_o) and the variation of temperature with altitude (lapse rate). They are all based on experimental data:

$$P_o = 2116.22 \text{ lb/ft}^2 = 14.696 \text{ lb/in}^2 = 29.921 \text{ in Hg} = 1013 \text{ hPa} (mb) = 760 \text{ mm Hg}$$

$$T_o = 288.15 \text{ }^\circ\text{K} = 518.67 \text{ }^\circ\text{R} = 58.67 \text{ }^\circ\text{F} = 15^\circ\text{C}$$

The standard lapse rate is defined as 1.9812°C (3.57°F) per 1,000 geopotential feet up to an altitude of 36,088 feet (11,000 m). The standard temperature is a constant 216.65K between 36,088 ft and 65,616 ft (20,000 m) above this altitude, the temperature begins to actually increase at about $+3^\circ\text{C}$ per

1,000 ft, but these altitudes are outside the scope of this text. Using these cornerstones, the hydrostatic equation, and the perfect gas equation, a relationship can be derived to calculate pressure and density at any altitude.

Ratios

Most standard atmosphere tables will present the data in terms of ratios instead of carrying absolute values.

$$\delta \text{ (delta)} \equiv \text{pressure ratio} \equiv \frac{\text{pressure at altitude}}{\text{pressure sea level std day}} \equiv \frac{P_a}{P_o}$$

$$\theta \text{ (theta)} \equiv \text{temperature ratio} \equiv \frac{\text{temperature at altitude}}{\text{temperature sea level std day}} \equiv \frac{T_a}{T_o}$$

$$\sigma \text{ (sigma)} \equiv \text{density ratio} \equiv \frac{\text{density at altitude}}{\text{density sea level std day}} \equiv \frac{\rho_a}{\rho_o}$$

Recall the perfect gas equation:

$$P = \rho RT$$

From this relation, standard day sea level density is calculated as:

$$\rho_o = 0.002377 \text{ slgs/ft}^3 = 0.07647 \text{ lbm/in}^3 = 1.2284 \text{ kg/m}^3$$

The perfect gas equation applies at any condition. By dividing this relationship at some altitude by the same relation at sea level, we get:

$$\frac{P}{P_o} = \frac{\rho RT}{\rho_o RT_o} \text{ or } \delta = \sigma \theta \text{ or } \sigma = \frac{\delta}{\theta}$$

Dividing the hydrostatic equation by the perfect gas equation and integrating between various limits of pressure, temperature, and altitudes yields the standard atmosphere pressure, temperature, and density equations.

For geopotential altitudes below 36,089 feet, the equations, in terms of the ratios defined, are as follows:

$$\delta = \frac{P_a}{P_o} = (1 - k_1 H)^{k_2} \quad (1.5)$$

$$\theta = \frac{T_a}{T_o} = (1 - k_1 H) \quad (1.6)$$

$$\sigma = \frac{\rho_a}{\rho_o} = (1 - k_1 H)^{k_2 - 1} \quad (1.7)$$

where:

$$k_1 = \frac{L}{T_o} = 6.87559 \times 10^{-6} \text{ ft}^{-1}$$

and:

$$k_2 = \frac{g_0}{RL} = 5.2559$$

where R is the gas constant
 L is the temperature lapse rate
 T is the temperature in degrees Rankine

The k_1 and k_2 constants come from the integration process mentioned above.

For geopotential altitudes above 36,089 feet the temperature is constant to 65,616 feet. The Equations are as follows:

$$T_a = -56.5^\circ C = 216.65K = 389.99R \quad (1.8)$$

$$\delta = \frac{P_a}{P_o} = 0.22335e^{-k_3(H-36089)} \quad (1.9)$$

$$\sigma = \frac{\rho_a}{\rho_o} = 0.29707e^{-k_3(H-36089)} \quad (1.10)$$

where:

$$k_3 = \frac{G}{RT_a} = 4.80614 \times 10^{-5} \text{ geopotential foot}$$

This model is depicted graphically below and is tabulated in appendix B.

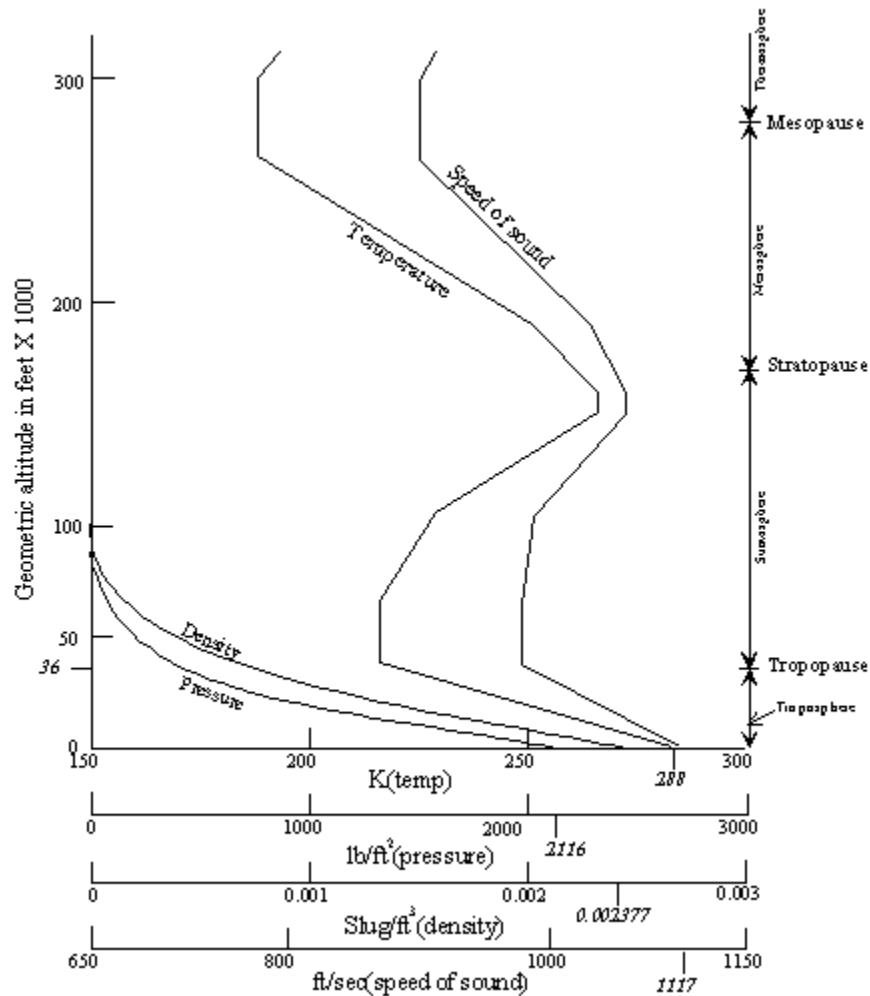


Figure 1.5 Geometric Altitude vs Temperature, Pressure, Density, Speed of Sound

1.5.1 Pressure Altitude

To make use of the standard atmosphere tables in flight testing aircraft, the absolute static pressure of the air is of primary importance. The static pressure of the air at any altitude results from the mass of air supported above that level. At standard sea level, the static pressure is 29.92 in Hg. A simple way of measuring the pressure at any altitude is by the use of the altimeter with the setting in the Kohlsman window set to standard sea level pressure. Since the altimeter is calibrated according to the standard atmosphere pressure variation equation with altitude, with the setting to 29.92 in. Hg., the indicated altitude read directly off the altimeter is pressure altitude. This may not reflect the *true geometric* altitude of the aircraft above mean sea level (MSL), but true altitude is not important in most flight test, pressure altitude is. Pressure altitude can always be duplicated by flying the same indicated altitude as long as the barometric setting is 29.92 in. Hg.

1.5.2 Temperature Altitude

Temperature altitude is defined as the altitude, on a standard day, at which the test day temperature would be found. Temperature altitude can be readily found by using a corrected outside air temperature gauge and the standard atmosphere table.

1.5.3 Density Altitude

Density altitude is the altitude, on a standard day, at which the test day density would be found. Because aircraft are not equipped with "density gauges", the test day density must be calculated. This is done knowing test day pressure (P_a), temperature (T_a) and the perfect gas law ($P_a = \rho_a P T_a$). Although all flight testing is performed with the altimeter set to the standard day sea level pressure, i.e., flying a pressure altitude, density altitude is very important to the performance of an aircraft, especially in the take-off and climb phases.

density altitude:

$$\rho = \frac{P}{RT_{test}}$$

or using the ratio equation:

$$\sigma = \frac{\delta}{\theta} = \frac{\delta T_o}{T_{test}}$$

where:

δ is the pressure ratio at the indicated pressure altitude, obtained directly from the atmospheric tables

T_o is the standard sea level temperature in °Kelvin or °Rankine

T is the test day temperature at the test altitude in °Kelvin or °Rankine

Volume 2 – Aerodynamics for Flight Testers

Chapter 2

Dimensional Analysis

Table of Contents

2.1 Introduction.....	2
2.1.1 Aerodynamic Factors.....	2
2.1.2 Dimensional Analysis Principles.....	3
2.1.3 Procedure.....	6
2.1.3.1 Step 1.....	6
2.1.3.2 Step 2.....	6
2.1.3.3 Step 3.....	7
2.1.3.4 Step 4.....	7
2.1.3.5 Step 5.....	8
2.1.4 Applications.....	12
2.1.5 Limitations.....	13
2.1.6 Engine Performance	13
2.1.6.1 Step 1.....	14
2.1.6.2 Step 2.....	14
2.1.6.3 Step 3.....	14
2.1.6.4 Step 4.....	15
2.1.6.5 Step 5.....	16
2.1.7 References	17

2.1 Introduction

Dimensional analysis is a tool which has been used by engineers for many years to reduce the number of variables when investigating or testing a particular physical problem or phenomena. The technique is to identify individual variables that are involved in the particular problem and then form groups of these variables into non-dimensional parameters. Care must be taken to ensure that the most significant variables are included in each parameter, otherwise the non-dimensional parameters are not significant. Using the Buckingham π Theorem, the number of parameters will be three less than the number of variables, thereby reducing the number of variables in testing program and allowing comparison of wind tunnel model and full scale flight data. The use of non-dimensional parameters can:

- Reduce wind tunnel and flight testing requirements;
- Provide a simpler method to standardize performance data;
- Provide a means to correlate wind tunnel and full scale test data;
- Facilitate comparison of different airframe and engine combinations.

The use of non-dimensional parameters to describe the performance and stability and control capabilities of different aircraft is normal in aeronautical engineering since it allows comparison of aircraft and engines irrespective of aircraft speed, size, or specific flight conditions.

A number of the non-dimensional parameters that are pertinent to aircraft and engine performance are developed to show that the basis of the parameters are mathematically sound and systematically derived.

2.1.1 Aerodynamic Factors

Consider an airfoil of a given shape immersed in airflow at a fixed angle of attack α as shown in

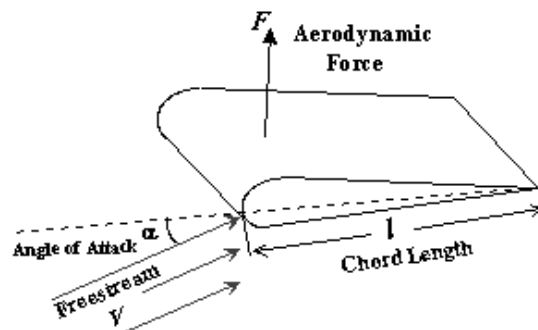


Figure 2.1.

Figure 2.1 Airfoil in airflow

Intuitively, the total force on the airfoil would be a function of the airflow characteristics, body characteristics and gravity.

$$F = f(\text{airflow characteristics, body characteristics, gravity})$$

Airflow characteristics which are important to this problem are velocity (V) density (ρ) viscosity (μ) and temperature (T). Important body characteristics are size, shape, orientation and roughness. For simplification, we will *restrict the body to an airfoil shape with a smooth surface at a fixed angle of attack*. The only variable is then the size which is represented by a reference length, the chord length (l).

Therefore:

$$F = f(V, \rho, \mu, T, l, g) \quad (2.1)$$

or equivalently

$$f(F, V, \rho, \mu, T, l, g) = 0$$

Six independent variables have been identified which are involved in the force produced on an airfoil in an airstream. By reducing the scope of the study to low supersonic flow conditions, then variation in the ratio of specific heats (γ), the universal gas constant (R) etc. . . can be ignored. It is important to ensure that all significant variables that could affect the results, are included in the analysis.

Equation 2.1 is a general functional relation which does not provide a means to directly calculate the force on the airfoil. The force could be determined experimentally in a wind tunnel or through flight test by measuring the variation in F due to variations in V , ρ , g , l , T and μ taken one at a time. This process of changing one parameter at a time and observing its effect is called a parametric analysis. The data obtained could be analyzed and an exact functional expression might be determined. However, a large amount of time and resources would be expended for parametric testing and analysis especially trying to separate the variables μ , g and T . The problem could be simplified and the testing reduced if the number of independent variables were reduced. This can be done by applying the dimensional analysis process to the problem.

2.1.2 Dimensional Analysis Principles

A set of fundamental dimensions must be established prior to starting the analysis process. For most mechanical engineering applications, the fundamental dimensions used are mass, $[M]$, length, $[L]$, and time, $[T]$. The use of brackets denotes a dimensional expression. Several systems of units are used to express the quantity or size associated with each fundamental dimension. For example, in the international system (SI) of units, mass is measured in kilograms, length in meters, and time in seconds. In the British engineering system, mass is in slugs, length in feet, and time in seconds. For the dimensional analysis process, we will use only the fundamental dimensions mass, length, and time.

For the variables in our aerodynamic problem, the dimensional expressions along with SI and British units are shown in table 2.1. The dimensions of force come from Newton's law of motion:

$$\text{Force} = \text{Mass} \times \text{Acceleration}$$

$$\text{Force} = M \frac{L}{T^2}$$

The dimensions of viscosity come from its definition:

$$\text{Viscosity} = \frac{\text{shear stress}(\tau)}{\text{velocity gradient} \left(\frac{dV}{dy} \right)}$$

where shear stress is a force applied over a given area. Hence:

$$\text{Viscosity} = \frac{\frac{ML}{T^2} / L^2}{\frac{L}{T} / L} = \frac{M}{LT}$$

The temperature (T) can be expressed in the units of mass length and time using the equation that defines the speed of sound (a) as a function of temperature (T). The use of the Equation

$$a = \sqrt{\gamma RT}$$

is reasonable since there are no restrictions to the transonic or supersonic flow in the analysis. The ratio of specific heat (γ) and the universal gas constant (R) are assumed constant therefore

$$a = k\sqrt{T}$$

and $T = f(a^2)$. Since (a) is a velocity, then

$$[T] = [a^2] = \frac{L^2}{T^2}$$

Variable	Symbol	Dimension	SI units	British units
Force	F	$\frac{ML}{T^2}$	N	lb
Velocity	V	$\frac{L}{T}$	$\frac{m}{sec}$	$\frac{ft}{sec}$
Density	ρ	$\frac{M}{L^3}$	$\frac{kg}{m^3}$	$\frac{slug}{ft^3}$
Viscosity	μ	$\frac{M}{LT}$	$\frac{kg}{m-sec}$	$\frac{lb\ sec}{ft^2}$
Chord Length	l	L	m	ft
Gravity	g	$\frac{L}{T^2}$	$\frac{m}{sec^2}$	$\frac{ft}{sec^2}$
Temperature	T	$\frac{L^2}{T^2}$	$^{\circ}K$	$^{\circ}R$

Table 2.1 Dimensional Equivalents

Dimensional analysis is based on the simple fact that in an equation dealing with a physical phenomenon, each side of the equation must have the same dimensions. For example, in the equation $\mathbf{A}=\mathbf{B}$, the dimensions of \mathbf{A} must equal the dimensions of \mathbf{B} . If \mathbf{A} is dimensionless, or non-dimensional, then \mathbf{B} must also be the same. The process used in dimensional analysis is expressed in the Buckingham π Theorem. This theorem essentially says:

If a physical phenomenon involves N dimensional variable which are expressed by K fundamental dimensions, then the phenomenon can be described by $N-K$ non-dimensional parameters called π

In the example expressed by Equation 2.1, there are seven dimensional variables, namely F , V , ρ , μ , g , T , and l . Therefore $N = 7$. Also $K = 3$ since three fundamental dimensions (M, L, T) are being used. Therefore according to the Buckingham π Theorem, there will be three ($7 - 3 = 4$) non-dimensional parameters. Symbolically, Buckingham's theorem is used to express a set of dimensional variables by an equivalent set of non-dimensional valuables:

$$\begin{aligned} \text{Dimensional:} & \quad f_1(x_1, x_2, x_3, \dots, x_N) = 0 \\ \text{Non-dimensional:} & \quad f_2(\pi_1, \pi_2, \dots, \pi_{N-K}) = 0 \end{aligned}$$

where each π parameter is a grouping of some of the x dimensional variables such that each parameter is non-dimensional.

2.1.3 Procedure

The procedure for determining each of the π parameters consists of:

1. Selecting the variables (factors) to place in each group;
2. Assigning arbitrary exponents to each of the variables;
3. Expressing each variable by its dimensional equivalent;
4. Solving for the unknown exponents so that each group of variables is non-dimensional.
5. Rearranging the non-dimensional parameters into a practical form.

2.1.3.1 Step 1

Of the ($N = 7$) dimensional variables identified, ($K = 3$) of them must be highlighted as the most important. These are called the "repeating" variables and are included in each of the π parameters. The remaining ($N - K = 4$) variables are split up, one each, among the ($N - K = 4$) π parameters. The selection of repeating variables is important and requires considerable engineering judgment and experience with the dimensional analysis process. Poor selection could result in meaningless non-dimensional parameters. For the aerodynamic example, velocity, V , density, ρ , and chord length, l are selected as repeating variables for each parameter. The remaining variables; force, F , viscosity, μ , temperature, T , and acceleration due to gravity, g , are distributed one in each parameter. Therefore,

$$\pi_1 = f(V, \rho, l, F)$$

$$\pi_2 = f(V, \rho, l, \mu)$$

$$\pi_3 = f(V, \rho, l, T)$$

$$\pi_4 = f(V, \rho, l, g)$$

2.1.3.2 Step 2

$$\pi_1 = f(V, \rho, l, F) = V^a \rho^b l^c F \quad (2.2)$$

$$\pi_2 = f(V, \rho, l, \mu) = V^d \rho^e l^f \mu \quad (2.3)$$

$$\pi_3 = f(V, \rho, l, T) = V^g \rho^h l^i T \quad (2.4)$$

$$\pi_4 = f(V, \rho, l, g) = V^j \rho^k l^m g \quad (2.5)$$

The grouping of the variables in each parameter is in the form of a product of powers of the variables as shown in equations (2.2), (2.3), (2.4), and (2.5). The arbitrary exponents a , b , and c are assigned to the variables V , ρ , and l . The fourth variable in each group is assigned as the dependent variable with the exponent of one.

2.1.3.3 Step 3

Each variable of Equations (2.2), (2.3), (2.4) and (2.5) is replaced by its dimensional equivalent from Table 2.1.

$$\pi_1 = \left[\frac{L}{T} \right]^a \left[\frac{M}{L^3} \right]^b [L]^c \left[\frac{ML}{T^2} \right] = [LT^{-1}]^a [ML^{-3}]^b [L]^c [MLT^{-2}] \quad (2.6)$$

$$\pi_2 = \left[\frac{L}{T} \right]^a \left[\frac{M}{L^3} \right]^b [L]^c \left[\frac{M}{LT} \right] = [LT^{-1}]^d [ML^{-3}]^e [L]^f [ML^{-1}T^{-1}] \quad (2.7)$$

$$\pi_3 = \left[\frac{L}{T} \right]^a \left[\frac{M}{L^3} \right]^b [L]^c \left[\frac{L^2}{T^2} \right] = [LT^{-1}]^g [ML^{-3}]^h [L]^i [L^2T^{-2}] \quad (2.8)$$

$$\pi_4 = \left[\frac{L}{T} \right]^a \left[\frac{M}{L^3} \right]^b [L]^c \left[\frac{L}{T^2} \right] = [LT^{-1}]^j [ML^{-3}]^k [L]^m [LT^{-2}] \quad (2.9)$$

2.1.3.4 Step 4

To solve for the unknown exponents, first simplify Equations (2.6), (2.7), (2.8), and (2.9). The following are the algebraic rules for operating with exponents:

$$A^x A^y = A^{x+y}$$

$$(A^x)^y = A^{xy}$$

$$A^0 = 1$$

Applying these rules to equations (2.6), (2.7), (2.8), and (2.9) yields:

$$\pi_1 = [L^a T^{-a}] [M^b L^{-3b}] [L^c] [MLT^{-2}] = [M^{b+1} L^{a-3b+c+1} T^{-a-2}] \quad (2.10)$$

$$\pi_2 = [L^a T^{-a}] [M^b L^{-3b}] [L^c] [ML^{-1}T^{-1}] = [M^{e+1} L^{d-3e+f-1} T^{-d-1}] \quad (2.11)$$

$$\pi_3 = [L^a T^{-a}] [M^b L^{-3b}] [L^c] [L^2 T^{-2}] = [M^h L^{g-3h+i+2} T^{-g-2}] \quad (2.12)$$

$$\pi_4 = [L^a T^{-a}] [M^b L^{-3b}] [L^c] [LT^{-2}] = [M^k L^{j-3k+m+1} T^{-j-2}] \quad (2.13)$$

By definition, each π parameter is non-dimensional or:

$$[\pi] = [M^0 L^0 T^0]$$

Therefore:

$$\pi_1: [M^0 L^0 T^0] = [M^{b+1} L^{a-3b+c+1} T^{-a-2}] \quad (2.14)$$

$$\pi_2: [M^0 L^0 T^0] = [M^{e+1} L^{d-3e+f-1} T^{-d-1}] \quad (2.15)$$

$$\pi_3: [M^0 L^0 T^0] = [M^h L^{g-3h+i+2} T^{-g-2}] \quad (2.16)$$

$$\pi_4: [M^0 L^0 T^0] = [M^k L^{j-3k+m+1} T^{-j-2}] \quad (2.17)$$

Now for Equations (2.14), (2.15), (2.16), and (2.17), simply equate the exponents of M , L , and T on each side, and solve for the unknown values of a , b , and c .

For π_1 :

$$M: 0 = b + 1$$

$$L: 0 = a - 3b + c + 1$$

$$T: 0 = -a - 2$$

Solving these Equations simultaneously yields:

$$a = -2$$

$$b = -1$$

$$c = -2$$

Therefore, from Equation (2.2):

$$\pi_1 = V^{-2} \rho^{-1} l^{-2} F = \frac{F}{\rho V^2 l^2} \quad (2.18)$$

Doing a similar analysis on π_2 , π_3 and π_4 , we get:

$$\pi_2 = \frac{\mu}{\rho V l} \rightarrow \frac{\rho V l}{\mu} \quad (2.19)$$

$$\pi_3 = \frac{T}{V^2} \rightarrow \frac{V^2}{T} \rightarrow \frac{V}{\sqrt{T}} \rightarrow \frac{V}{a} \quad (2.20)$$

$$\pi_4 = \frac{l g}{V^2} \rightarrow \frac{V^2}{l g} \rightarrow \frac{V}{\sqrt{l g}} \quad (2.21)$$

A non-dimensional parameter is still non-dimensional if inverted, and if the square root is taken - as shown in Equation (2.19), (2.20) and (2.21). π_3 which was reduced to $\frac{V}{\sqrt{T}}$ can be converted to $\frac{V}{a}$ since $a = \sqrt{TR\gamma}$ and R & γ are constant.

2.1.3.5 Step 5

The non-dimensional parameters resulting from dimensional analysis can be made more practical by slight modifications and substituting variables with similar dimensions. Equation (2.18) is known as the force coefficient C_F . In aerodynamics applications, the force coefficient expression is modified slightly as follows:

$$C_F = \frac{F}{\frac{1}{2} \rho V^2 S} \quad (2.22)$$

where $\frac{1}{2}$ is a numerical constant, and S is the wing area and is equal to the product of the wing chord and wing span. These modifications do not invalidate the dimensional analysis process since they do not affect the non-dimensional nature of the resulting parameter. The dimension of S is $[L^2]$ which is the same as the dimension of l^2 , and, of course, the fraction $\frac{1}{2}$ has no dimensions. The expression $\frac{1}{2} \rho V^2$ is defined as dynamic pressure, q .

A feel for q :

The kinetic energy of a moving object is calculated as $\frac{1}{2}mV^2_T$. The same is true of a block of moving air, $KE = \frac{1}{2}\rho(\text{volume})V^2_T$. Dividing through by volume yields $\frac{1}{2}\rho V^2_T$, an expression for the kinetic energy per volume of moving air. The dimensions are units of pressure (lb/ft² in the British system) and is called "Dynamic Pressure" or " q ". Think of q as the potential for converting each cubic foot of the airflow's kinetic energy into frontal stagnation pressure. This idea of q can be felt in everyday life by extending your hand out the window of a moving car. This discussion explains why engineers chose to divide the above force coefficient by 1/2 - doing so equates the flow's density & velocity to kinetic energy.

Equation (2.22) can be rewritten as:

$$C_F = \frac{F}{qS} \quad (2.23)$$

π_2 defines the Reynolds Number, Re , π_3 defines the Mach Number, M , and π_4 defines the Froude Number

$$Re = \frac{\rho V l}{\mu} \quad (2.24)$$

$$M = \frac{V}{a} \quad (2.25)$$

$$Fr = \frac{V}{\sqrt{l g}} \quad (2.26)$$

The Reynolds number $\frac{\rho V l}{\mu}$ is named after Dr. Reynolds who proved by pipe flow experiments that Reynolds number is significant in the prediction of transition from laminar to turbulent flow.

The ratio of true airspeed to the local speed of sound is called the Mach number after Dr. Mach who proved that this non-dimensional velocity is significant in aircraft drag at high subsonic Mach numbers. Mach effects are evident on aerodynamic forces and moments above $M = 0.3$.

The Froude number is essentially the ratio of aerodynamic to inertial forces. Froude number modeling is important in relating store trajectories from aircraft models in a wind tunnel to full scale flight. Summarizing Equations (2.23), (2.24), (2.25), and (2.26) we have:

$$f(C_F, Re, M, Fr) = 0$$

or

$$C_F = f(Re, M, Fr) \quad (2.27)$$

Equation (2.27) is an important result when compared with Equation (2.1). In Equation (2.1), F was a function of six independent variables. However, through dimensional analysis, we have shown that F can

be expressed as a non-dimensional force coefficient, C_F , which is a function of only Reynolds number, Mach number and Froude number.

Except for wind tunnel modeling of weapon trajectories, Froude number is not significant in most aerodynamic phenomena, therefore frequently Froude Number is neglected such that

$$C_F = f(Re, M) \quad (2.28)$$

By reducing the number of independent variables from six to two, the amount of wind tunnel or flight testing can be greatly reduced.

It is important to remember that in the above analysis we restricted the body to an airfoil shape with a given surface texture and a fixed angle of attack. However, removing the angle of attack restriction and letting it vary, Equation 2.27 is further generalized to:

$$C_F = f(Re, M, \alpha) \quad (2.29)$$

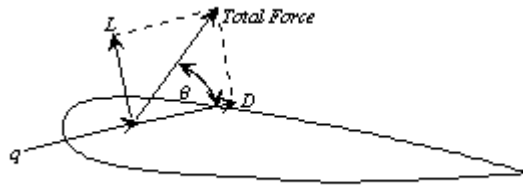
The above analysis only applies to aerodynamically similar shapes and bodies such as wings and fuselages etc. . . This means that using the non-dimensional parameters the force and moment coefficient data obtained from wind tunnel tests on an aerodynamically similar scale model will apply to the full scale aircraft - if the tests are performed at the same Mach and Reynolds numbers.

A feel for coefficients:

The term force coefficient C_F might seem a bit cryptic at first but is actually quite a simple concept. Rearranging equation 2.23 gives $C_F = \frac{F/S}{q}$ which is the ratio between the total

force pressure and the flow's dynamic pressure. This concept becomes more clear when the total force is broken into its lift and drag components. By definition, the lift force is the component of the total force, which is perpendicular to the freestream flow, while the drag is the component along the flow. Intuitively, increasing the flow's dynamic pressure generates a larger total force, and also increases lift and drag. Instead of discussing the total force coefficient and its orientation to the flow, engineers break it into lift and drag coefficients define as:

$$C_L \equiv \frac{L/S}{q} \quad \text{and} \quad C_D \equiv \frac{D/S}{q}$$



Think of lift coefficient as the "lift pressure per dynamic pressure" or how effective the object is at converting the flow's kinetic energy into lift pressure. Similarly, drag coefficient is a measure of the object's effectiveness at converting dynamic pressure into drag pressure. Dimensional analysis states that if experiments or comparisons are conducted for similar shapes at similar Re , M , and α , then the resulting coefficients will also be constant. Clearly then, doubling q will double the lift pressure (and the drag pressure). This principle makes it easy to "scale up" wind tunnel measurements.

There are actually many of these non-dimensional coefficients used in describing aircraft properties. They describe properties such as pitching moment, $C_m \equiv \frac{M}{qS_c}$ and elevator power, $C_{M_{\delta_e}} = \frac{dM}{qS_c d\delta_e}$.

They are widely used because they have two useful properties:

- ① The ability to simply scale up wind tunnel model data to the real aircraft at similar Flight conditions (M , Re , α).
- ② They allow a comparison of any aircraft property between different flight conditions. An example of this might be comparing directional stability, at high mach number vs low mach number.

To determine the effects of Reynolds number on an airfoil in a wind tunnel, the Mach number (M) is held constant and the lift is measured at various values of angle of attack. The results are plotted as lift coefficient (C_L) versus angle of attack (α) at one value of Re and M . Repeating the test at larger Reynolds numbers gives the data shown in Figure 2.2.

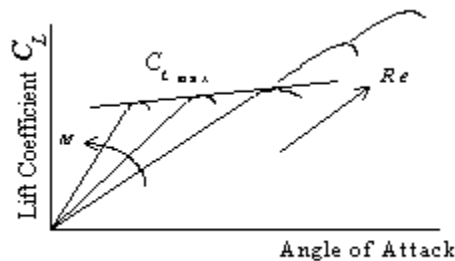


Figure 2.2 Variation of C_L versus α

Repeating the test at a constant Reynolds number (Re), but at various values of Mach number will show the effect of Mach number (M) on the $C_L \sim \alpha$ curve of an airfoil section (figure 2.2). An increase in

Reynolds number (Re) has no effect on the lift curve slope but will increase the maximum lift coefficient (C_{Lmax}). The increases in C_{Lmax} will have an effect on the stall speeds: i.e., an increase in altitude will reduce the C_{Lmax} which will result in an increase in stall speed.

An increase in Mach number will have little effect on the maximum lift coefficient (C_{Lmax}) but will increase the lift curve slope $C_{L\alpha}$, (Figure 2.2). This is valid below a Mach Number of one.

To simplify data analysis, in flight testing it is normal to restrict the tests to a test altitude with an appropriate data band to keep the Reynolds number constant. By performing the test at a test Mach number with small variations in Mach and altitude the $C_L \sim \alpha$ curves in Figure (2.2) can be reduced to a single $C_L \sim \alpha$ curve for one Reynolds and one Mach number.

2.1.4 Applications

The correlation of aerodynamic data from scale model wind tunnel test to full scale flight requires matching Reynolds number and Mach number. This matching often requires wind tunnels that must be pressurized to many atmospheres of pressure and which must be cooled or heated as necessary.

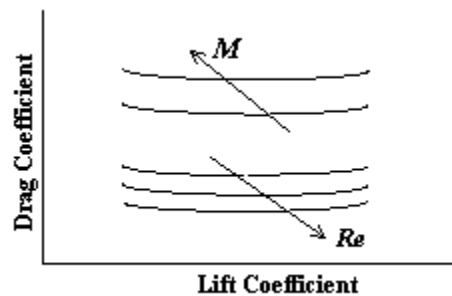


Figure 2.3 Variation of C_D versus C_L

It is appropriate to emphasize the usefulness of coefficients when working with aerodynamic forces. Even at the same Mach and Reynolds numbers, a real Boeing 727 will obviously create a lot more lift *force* than a scale model in a wind tunnel. Both the aircraft size and the air's energy ($1/2 \rho \alpha V^2_T$ or q) directly affect the amount of force generated. Dividing out these two factors gives the *coefficient of lift* [$(L/qS) = C_L$] as seen in Equation (2.23). The beauty of using such coefficients is that by dividing out the size and dynamic pressure for both the aircraft and the model, the lift coefficient (C_L) for the model and the aircraft are the same, Figure 2.4.

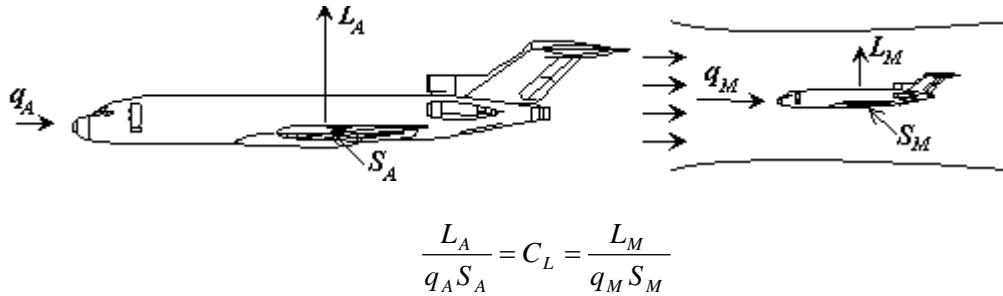


Figure 2.4 Equating Lift Coefficients for Aircraft and Models

Non-dimensional techniques are also used to reduce test day data to standard conditions of weight and altitude.

2.1.5 Limitations

The limitations of dimensional analysis must be observed when using the process. These are:

- The results of dimensional analysis show only how the variables can be grouped together, not how the groups are related;
- The resulting parameters are only as good as the original assumptions;
- All important variables must be included;
- Constants must remain constant;
- All modifications of the resulting parameters must be dimensionally consistent;
- Any discarded parameters or expressions must not be important.

2.1.6 Engine Performance

Dimensional analysis can also be used to analyze turbojet engine performance. The magnitude of the engine thrust, F , is dependent upon atmospheric characteristics and engine design characteristics. Important atmospheric characteristics are pressure (P), temperature (T), and velocity (V). Important engine design characteristics are the cross-sectional area represented by the engine diameter (D), and the engine speed (N). Functionally, this can be represented as:

$$F = f(P, T, V, D, N)$$

or $f(P, T, V, D, N, F) = 0$ (2.30)

Applying the Buckingham π theorem for six variables ($N = 6$) and three fundamental dimensions ($K = 3$), engine performance can be described by three ($N - K = 3$) non-dimensional parameters. Equation (2.30) can then be expressed as:

$$f(\pi_1, \pi_2, \pi_3) = 0$$

2.1.6.1 Step 1

Taking thrust, diameter, and engine speed as the significant variables, the π parameters can be expressed as:

2.1.6.2 Step 2

$$\pi_1 = f(F, D, N, V) = F^a D^b N^c V \quad (2.31)$$

$$\pi_2 = f(F, D, N, T) = F^d D^e N^f T \quad (2.32)$$

$$\pi_3 = f(F, D, N, P) = F^g D^h N^i P \quad (2.33)$$

The dimensional expressions and customary units for the variables in the engine problem are shown in Table 2.2.

Variable	Symbol	Dimension	SI units	British units
Force	F	$\frac{ML}{T^2}$	N	lb
Temperature	T	$\frac{L^2}{T^2}$	$^{\circ}K$	$^{\circ}R$
Pressure	P	$\frac{M}{LT^2}$	$\frac{N}{m^2}$	$\frac{lb}{ft^2}$
Velocity	V	$\frac{L}{T}$	$\frac{m}{sec}$	$\frac{ft}{sec}$
Diameter	D	L	m	ft
Engine Speed	N	$\frac{1}{T}$	$\frac{rad}{sec}$	$\frac{rad}{sec}$

Table 2.2 Dimensional Equivalents for Engine Variables

2.1.6.3 Step 3

Substituting the dimensions from Table 2.2 into Equations (2.31), (2.32), and (2.33) gives:

$$\pi_1 = \left[\frac{ML}{T^2} \right]^a [L]^b \left[\frac{1}{T} \right]^c \left[\frac{L}{T} \right] = [MLT^{-2}]^a [L]^b [T^{-1}]^c [LT^{-1}] \quad (2.34)$$

$$\pi_2 = \left[\frac{ML}{T^2} \right]^a [L]^b \left[\frac{1}{T} \right]^c \left[\frac{L^2}{T^2} \right] = [MLT^{-2}]^a [L]^b [T^{-1}]^c [L^2 T^{-2}] \quad (2.35)$$

$$\pi_3 = \left[\frac{ML}{T^2} \right]^a [L]^b \left[\frac{1}{T} \right]^c \left[\frac{M}{LT} \right] = [MLT^{-2}]^a [L]^b [T^{-1}]^c [ML^{-1} T^{-2}] \quad (2.36)$$

2.1.6.4 Step 4

Now using the algebraic rules for working with exponents Equations (2.34), (2.35), and (2.36) become:

$$\pi_1 = [M^a L^a T^{-2a}] [L^b] [T^{-c}] [L T^{-1}] = [M^a L^{a+b+1} T^{-2a-c-1}] \quad (2.37)$$

$$\pi_2 = [M^a L^a T^{-2a}] [L^b] [T^{-c}] [L^2 T^{-2}] = [M^a L^{d+e+2} T^{-2d-f-2}] \quad (2.38)$$

$$\pi_3 = [M^a L^a T^{-2a}] [L^b] [T^{-c}] [M L^{-1} T^{-2}] = [M^{g+1} L^{g+h-1} T^{-2g-i-2}] \quad (2.39)$$

Since each π parameter is non-dimensional then the Equations (2.37), (2.38), and (2.39) can be expressed as:

$$\pi_1: [M^0 L^0 T^0] = [M^a L^{a+b+1} T^{-2a-c-1}] \quad (2.40)$$

$$\pi_2: [M^0 L^0 T^0] = [M^d L^{d+e+2} T^{-2d-f-2}] \quad (2.41)$$

$$\pi_3: [M^0 L^0 T^0] = [M^{g+1} L^{g+h-1} T^{-2g-i-2}] \quad (2.42)$$

In Equations (2.40), (2.41), and (2.42) the exponents of M , L , and T on each side can be equated and solved for the unknown values of a , b , and c :

For π_1 :

$$\begin{aligned} M: 0 &= a \\ L: 0 &= a + b + 1 \\ T: 0 &= -2a - c - 1 \end{aligned}$$

Solving these equations simultaneously gives:

$$\begin{aligned} a &= 0 \\ b &= -1 \\ c &= -1 \end{aligned}$$

Therefore, from Equation (2.31):

$$\pi_1 = F^0 D^{-1} N^{-1} V = \frac{V}{ND} \quad (2.43)$$

Performing a similar analysis on π_2 and π_3 gives:

$$\pi_2 = \frac{T}{N^2 D^2} \text{ or } \frac{\sqrt{T}}{ND} \quad (2.44)$$

$$\pi_3 = \frac{D^2 P}{F} \quad (2.45)$$

The non-dimensional functional relationship for engine performance can be expressed as:

$$f\left(\frac{V}{ND}, \frac{\sqrt{T}}{ND}, \frac{D^2 P}{F}\right) = 0$$

or, by selecting the parameter which includes F as the dependent variable, gives:

$$\frac{D^2 P}{F} = f\left(\frac{V}{ND}, \frac{\sqrt{T}}{ND}\right) \quad (2.46)$$

2.1.6.5 Step 5

Equation (2.46) is simply a functional relationship of non-dimensional parameters. These parameters can be modified in certain ways as long as the non-dimensional nature of the parameter is not violated. Such modification is sometimes done to make the parameter more meaningful, or simply for convenience during analysis.

Aerodynamicists use ratios instead of dimensional numbers to discuss the properties of air. As an example, instead of saying the atmospheric pressure P_a at some altitude is 5 PSI, the ratio of local ambient pressure to standard day sea level pressure ($5/14.7$) or 0.34 is used. This pressure ratio, P_a/P_o is referred to as δ . Similarly, $\theta = T_a/T_o$ and $\sigma = \rho_a/\rho_o$. The subscript o denotes sea-level standard day conditions and are arbitrary constants.

The thrust parameter $\frac{D^2 P}{F}$, is first inverted, then P is replaced with $P_o \delta$ from the standard atmosphere relationships. Assuming that D is fixed for a given engine, the term $D^2 P_o$ in the denominator is constant and can be disregarded in the functional relationship. The thrust parameter is therefore reduced to;

$$\frac{D^2 P}{F} \rightarrow \frac{F}{D^2 P} \rightarrow \frac{F}{D^2 P_o \delta} \rightarrow \frac{F}{(\text{constant}) \delta} \rightarrow \frac{F}{\delta}$$

The resulting thrust parameter $\frac{F}{\delta}$, which is equivalent dimensionally to $\frac{D^2 P}{F}$, is called "corrected thrust".

The parameter $\frac{\sqrt{T}}{ND}$, is also inverted and T is replaced with $T_o \theta$ from the standard atmosphere relationships. Again assuming that D is fixed for a given engine, the term $\frac{D}{\sqrt{T_o}}$ is a constant and is disregarded in the functional relationship. The resulting parameter is:

$$\frac{\sqrt{T}}{ND} \rightarrow \frac{ND}{\sqrt{T}} \rightarrow \frac{ND}{\sqrt{T_o \theta}} \rightarrow (\text{constant}) \frac{N}{\sqrt{\theta}} \rightarrow \frac{N}{\sqrt{\theta}}$$

The resulting parameter is known as "corrected engine speed" or "corrected RPM".

Modifying the velocity parameter $\frac{V}{ND}$, ND is related to speed of sound a which has the same dimensions (recall from thermodynamics $a = \sqrt{\gamma RT} = 49\sqrt{T} \frac{ft}{s}$). Since $\frac{V}{a}$ is Mach Number by definition, then:

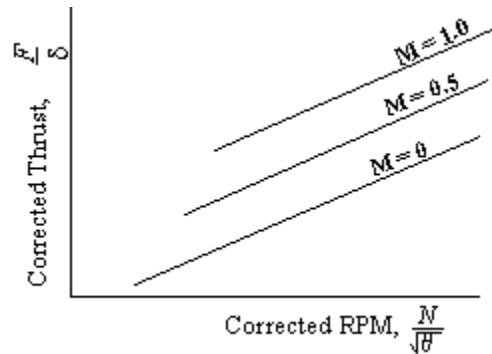
$$\frac{V}{ND} \rightarrow \frac{V}{a} \rightarrow M$$

Combining the modified parameters, the corrected thrust can be expressed as a function of Mach number and corrected RPM, and Equation (2.46) becomes:

$$\frac{F}{\delta} = f\left(M, \frac{N}{\sqrt{\theta}}\right) \quad (2.47)$$

In summary, Equation (2.47) shows that the corrected thrust parameter is a function of only Mach number and the corrected RPM parameter. The advantage of using the relationship in Equation (2.47) is shown in Figure 2.5 where the complete thrust characteristics of a simple turbojet engine can be presented on a single chart.

Figure 2.5 Variation of Corrected Thrust with Corrected RPM



2.1.7 References

- 2.1 Anderson, John D. Jr., *Fundamentals of Aerodynamics*, McGraw-Hill, Inc., 1991.
- 2.2 Hesse, W. J. and Mumford, N. V. S. Jr., *Jet propulsion for Aerospace Applications, 2d Ed.*, Pitman Publishing Corporation, 1964.
- 2.3 White, Frank M., *Fluid Mechanics*, McGraw-Hill Book Co., 1979.
- 2.4 U.S. Air Force Test Pilot School Text, *Aircraft Performance, Vol. 1*, Edwards AFB, June, 1987.

Aerodynamics for Flight Testers, Volume II

Chapter 3

Subsonic Aerodynamics

Table of Contents

3.1 Introduction.....	3
3.1.1 The Atmosphere	3
3.1.1.1 Atmospheric Structure.....	3
3.1.1.2 ICAO Standard Atmosphere.....	5
3.1.1.3 Weather	6
3.1.1.4 Drift	7
3.1.2 Aircraft Terminology.....	9
3.1.2.1 Introduction	9
3.1.2.2 Basic Terminology	9
3.1.2.3 Fuselage.....	10
3.1.2.4 Wings	11
3.1.2.5 Tail Assembly	12
3.1.2.6 Primary Flying Controls.....	13
3.1.2.7 Secondary Controls	14
3.1.2.8 Landing Gear.....	15
3.1.2.9 Powerplants	16
3.1.3 Aerodynamic Theory.....	17
3.1.3.1 Introduction	17
3.1.3.2 Simplifying Assumptions.....	17
3.1.3.3 Flow Visualization	17
3.1.3.4 Unsteady Flow.....	18
3.1.3.5 Rotational and Irrotational Flow	19
3.1.3.6 One-Dimensional Flow	21
3.1.3.7 Physical Laws.....	23
3.1.4 Basic Lift Theory.....	24
3.1.4.1 Model of Vorticity around an Airfoil	24
3.1.5 Further Details on Boundary Layer	27
3.1.5.1 Background Considerations	27
3.1.5.2 Laminar Boundary Layer	27
3.1.5.3 Turbulent Boundary Layer	27
3.1.6 Production of Lift	28
3.1.7 Lift.....	30
3.1.7.1 Introduction	30
3.1.7.2 Airfoil Design.....	30
3.1.7.3 Two-Dimensional Testing.....	32
3.1.7.4 Aerodynamic Center	35
3.1.7.5 Mean Geometric Chord (M.G.C.)	35
3.1.7.6 Mean Aerodynamic Chord (M.A.C.)	36
3.1.7.7 Two-dimensional Wind Tunnel Data.....	37
3.1.7.8 Three-dimensional Flow.....	37
3.1.7.9.....	39
3.1.7.10 Flow Separation.....	39
3.1.7.11 High Lift Devices	40

- 3.1.7.11.1 Flaps 40
- 3.1.7.11.2 Boundary Layer Control 40
- 3.1.7.11.3 Practical Combinations 42
- 3.1.7.11.4 Practical Problems 43
- 3.1.8 Drag 44
 - 3.1.8.1 Introduction 44
 - 3.1.8.2 Components of Drag 44
 - 3.1.8.3 Real Fluid Flow 44
 - 3.1.8.4 Skin Friction Drag 45
 - 3.1.8.4.1 Boundary Layer Transition 47
 - 3.1.8.4.2 Reynolds Number 47
 - 3.1.8.4.3 Pressure Gradient 48
 - 3.1.8.4.4 Surface Roughness 49
 - 3.1.8.5 Pressure Drag 51
 - 3.1.8.5.1 Flow Separation 51
 - 3.1.8.5.2 Streamlining 52
 - 3.1.8.6 Interference Drag 54
 - 3.1.8.7 Induced Drag 56
 - 3.1.8.7.1 Wingtip Vortex Effects 58
 - 3.1.8.7.2 Induced Drag Coefficients 59
 - 3.1.8.7.3 Reduction of Induced Drag 60
 - 3.1.8.8 Drag Coefficients 65
- 3.1.9 References 65

3.1 Introduction

A sound understanding of the principles of subsonic aerodynamics is essential if the student is to comprehend the nuances of aircraft performance and of stability. This text, therefore, is based on the assumption that the student has had no prior instruction in aerodynamics and covers the basic concepts up to the level usually learned by military pilots during their training. Before it can be assumed that basic aerodynamics will mean anything, therefore, some words will be devoted to the atmosphere (especially as it is pertinent to flight test) and to the basic components of an aircraft.

3.1.1 The Atmosphere

3.1.1.1 Atmospheric Structure

Since our subject is aerodynamics, we will first make the assumption that air, or at least some gas, is basic to the discipline. The medium in which aircraft have been designed to travel is air and it is this medium which makes up the atmospheric spheres which surround our planet. The layer in which we live, termed the troposphere, is the one which will be of the most interest to us in our studies since the great majority of aviation takes place in this layer. As we climb we next encounter the stratosphere and a good many modern aircraft are capable of sustained flight in this region. Few atmospheric vehicles have ever ventured beyond the stratosphere; the X-15 flew through the next layer, the mesosphere, into the thermosphere but in these lower regions of space there ceased to be very much that was aerodynamic about the vehicle. The space shuttle, of course, traverses all the atmospheric strata but once again the study of ballistics and reaction control is more pertinent to vehicles operating at great altitudes. Probably the highest flying truly aerodynamic aircraft are the Lockheed SR-71 and the MIG-25, both of which can cruise well into the lower half of the stratosphere. Concorde, the highest flying passenger aircraft, is restricted to about 60,000 ft, an altitude which barely takes it out of the troposphere in some latitudes.

Figure 3.1 shows the atmospheric layers and gives typical heights for the various 'pauses' in the structure. It should be noted that the height of the tropopause (the only 'pause' which is of any real significance to our studies) varies with the seasons and with latitude. In effect, the tropopause is highest where the surface temperature is at its highest and the height of the tropopause varies typically from just below 30,000 ft to above 50,000 ft as one passes from polar to equatorial region.

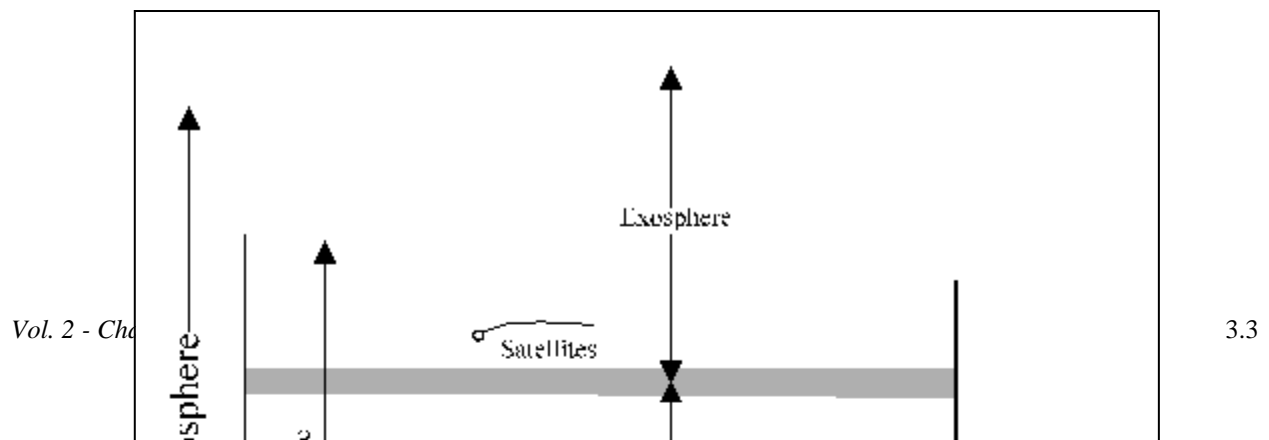


Figure 3.1: Atmospheric Structure.

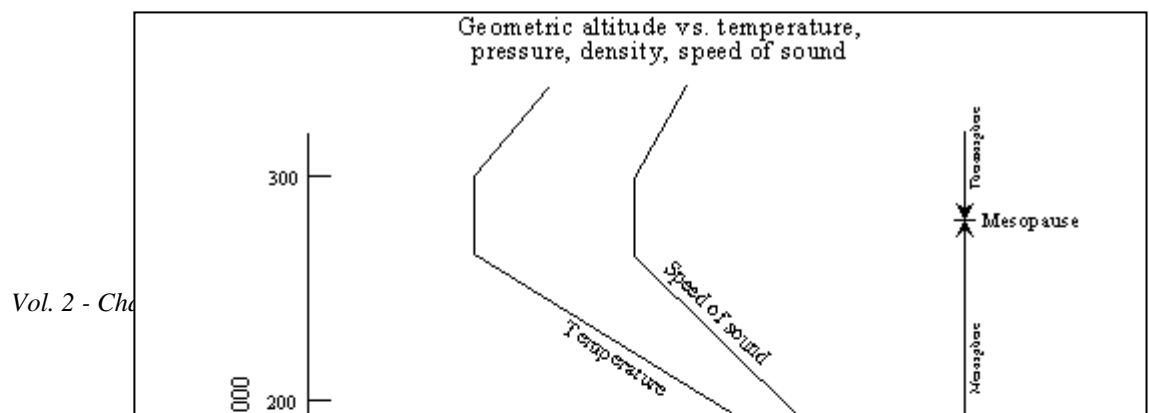


Figure 3.2: Atmospheric properties variation
Based on (1962) US Standard Atmosphere

3.1.1.2 ICAO Standard Atmosphere.

Because of diurnal, seasonal and random variations in the atmosphere, pressure, temperature and density will vary almost constantly at any given point in the atmosphere. These variations make the testing task complicated since many measurements can only be duplicated if similar conditions are found on successive flights. To simplify the problem, an internationally accepted standard atmosphere will be assumed and data will be corrected to accommodate any variation from these standards. Figure 3.2 illustrates the standard atmosphere and shows how density, pressure, temperature and speed of sound vary on the "standard day." It will be noted that, above 35 km above mean sea level (AMSL), there is little

atmosphere left since both pressure and density approximate zero. Temperature is assumed to vary at the temperature lapse rate $\lambda = -1.98^\circ\text{C}/1000$ ft altitude increase from a MSL standard of 15°C . At the tropopause, the temperature stabilizes at approximately -56°C and remains at that temperature for the remainder of the usable stratosphere. In reality, the temperature lapse rate with increasing altitude rarely even approximates this profile, especially in the lower layers. Another anomaly is that the temperature

will always continue to reduce right up to the tropopause; in consequence, upper atmosphere temperatures at the equator are usually lower than those at the poles.

3.1.1.3 Weather

An unpleasant feature of the troposphere, especially as far as aviation is concerned, is that all weather phenomena are contained therein. Figure 3.3 shows some of the features which are likely to occur within our test flying region. It has already been established that corrections can be made to our data to allow for temperature, pressure and density variations; it is small-scale movement of the atmosphere, in the form of turbulence, which is most disruptive in flight test. Figure 3.3 also shows a notional flight path as it might be affected by turbulence. It should be noted that the least turbulent area is over the sea; the water does not heat up from solar radiation so much as the land because currents are constantly mixing it. Unfortunately, many authorities will not allow flight testing over the sea in case something catastrophic occurs; in this case, the engineers will want to recover and examine the pieces.

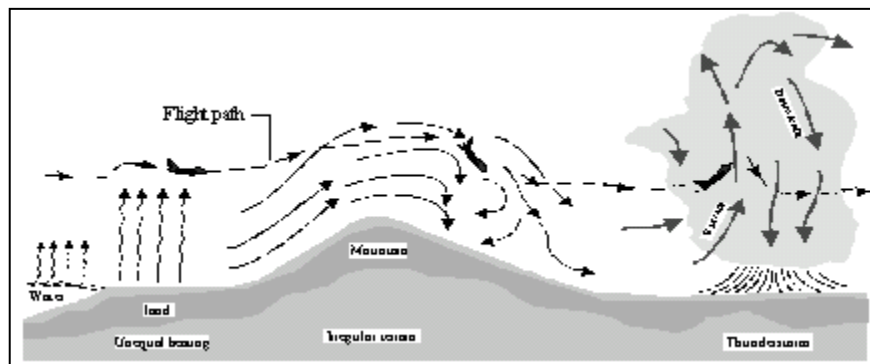


Figure 3.3 Weather effects on the atmosphere.

The land heats very rapidly in direct sunlight and convective turbulence is at its worst; in the desert during summer, however, there is insufficient moisture in the atmosphere to give this kind of signposting. The desert in summer, is likely to produce extensive convective turbulence any time after approximately 9 o'clock a.m.

Winds will also cause turbulence, particularly where changes in wind velocity and proximity to the surface mix air at various velocities. Mountains, therefore, are likely to cause significant turbulence. Another phenomenon associated with mountains is the large scale lifting of air on the windward side and large scale sinking on the leeward side. At least, such conditions will grossly distort performance data and at worst the subsidence of the air may be at a rate which exceeds the climb capability of the aircraft. If the winds are continuous and strong, a 'standing wave' may be established downwind of the mountains. Descending air hits the surface and is reflected back into the atmosphere only to be diverted earthward again to repeat the cycle. Such activity can continue for considerable distances downwind. A sure sign of the existence of a standing wave is a 'Lenticular' cloud; this is a streamline shaped cloud which forms in

the corner where the air turns back earthward. Lenticular clouds can occur at altitudes in excess of 50,000 ft.

A final weather phenomenon which should be avoided almost at all costs is the thunderstorm. Cumulonimbus clouds form when there is sufficient moisture, instability and some vigorous lifting; the resulting clouds will have a vertical development of a least 10,000 ft and perhaps as much as 70,000 ft. Enormously powerful vertical currents exist inside these clouds (10,000 ft/min vertical velocity up and down) and the areas in which the edges of up and down drafts mix are typified by some of the most severe turbulence which can be encountered anywhere. Such turbulence is demonstrably capable of destroying an aircraft. As if this were not enough, precipitation will circulate within the cloud, driven by the vertical drafts, and successive layers of ice can build hailstones at least the size of baseballs. The effect of such projectiles impinging on aircraft components can be catastrophic. But there is more to come. Static electricity can strike the aircraft and have highly detrimental effects on compasses and other navigational equipment; it can make entry and exit holes in aircraft structures; it can cause temporary blindness of the crew; and in the past it has been blamed for the ignition of fuel vapor in near-empty fuel tanks. Finally, when a downdraft eventually emerges from the base of a thunderstorm, the air will strike, and be diverted parallel to, the surface. This almost instantaneous change in wind velocity has been enough, in the past, to cause aircraft accidents. If this 'microburst' appears as a tailwind to a slow-flying aircraft, it can be enough to reduce the aircraft's airspeed to below its stalling speed. Thunderstorm effects are still not fully understood and the best advice must be to keep well away from them.

3.1.1.4 Drift

One effect of wind which must be understood is drift. It is best to think about wind as a general movement of an air mass relative to the surface rather than as a stream of air blowing between two air masses. Except for minor, short-term variations (like the microburst described above) whenever the aircraft is flying, it moves with the moving air mass in such a way that the only relative motion between aircraft and air mass is the aircraft's own forward velocity. All the 'relative wind' is therefore on the aircraft's nose. However, because the air mass is moving relative to the ground, the aircraft's movement relative to the surface will be the vector sum of its forward velocity and that of the air mass. As far as ground-oriented navigation is concerned, therefore, the aircraft does not necessarily go in the direction in which it is pointing; this phenomenon is known as drift. Figure 3.4 demonstrates the different ground related motion achieved by an aircraft when (a) it ignores the effect of a wind and when (b) it compensates for the effect. It must be noted that this effect is completely separate from sideslip. Sideslip β is when the velocity vector of the aircraft is laterally displaced from the aircraft's longitudinal datum; wind will only cause sideslip when the aircraft is moving on a fixed path over the surface and is, therefore, unable to move at the speed of the wind (i.e. on takeoff and landing ground rolls).

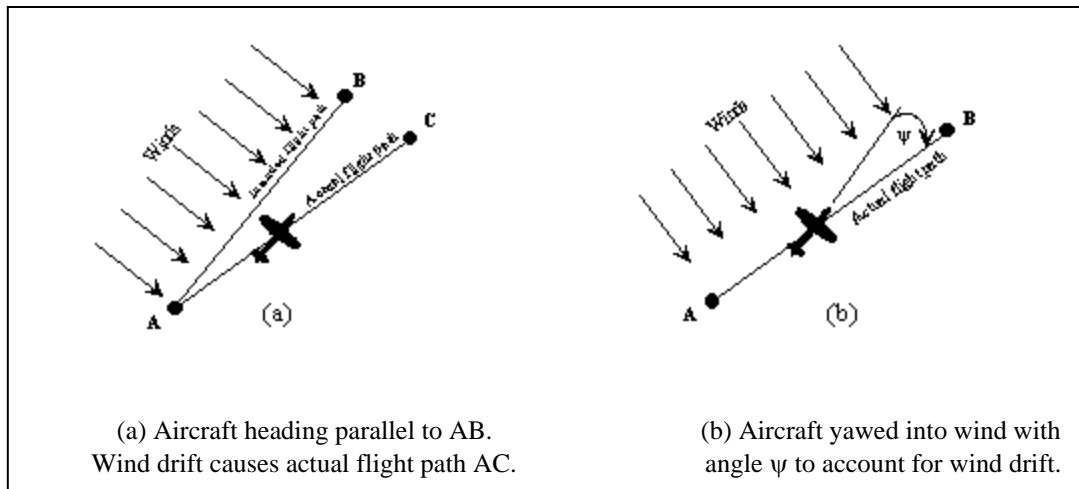


Figure 3.4 Effect of Winds

3.1.2 Aircraft Terminology

3.1.2.1 Introduction

The purpose of this text is not to graduate the student with a degree in aerodynamics but to give a basic explanation as a lead-in to the study of stability and performance. In consequence, the explanations may be simplified; any student wishing to learn more about aerodynamics may refer to a wide variety of excellent text books on the subject.

The first premise which must be accepted is that an aircraft moving through the air is subject to the same forces as if a stationary aircraft had air passed over it at the same speed. The basis of aerodynamics is, therefore, relative movement of aircraft and air; it is the observers viewpoint which is the only difference. The two phenomena which will be of most interest to us will be lift and drag, but before we go into the theory, it is necessary to ensure that the student is familiar with the terminology of aircraft.

3.1.2.2 Basic Terminology

Figure 3.5 shows the very basic components. The power plant moves the aircraft through the air, overcoming both inertia and drag. The fuselage contains the pilot, payload and, in many cases, fuel, the power-plants and other equipment. In Figure 3.5, it also provides the mounting point for the tail assembly or empennage. The surfaces of the tail assembly provide the forces both to balance the aircraft and to maneuver it in pitch and yaw; the latter function is achieved by movement of the control surfaces in a way which will be described. The wing or mainplane provides the lift for the entire aircraft and can also house fuel, equipment, engines and landing gear. Maneuvering in roll is achieved through wing-mounted control surfaces. By rolling the aircraft to a bank angle, the pilot is able to turn the aircraft.

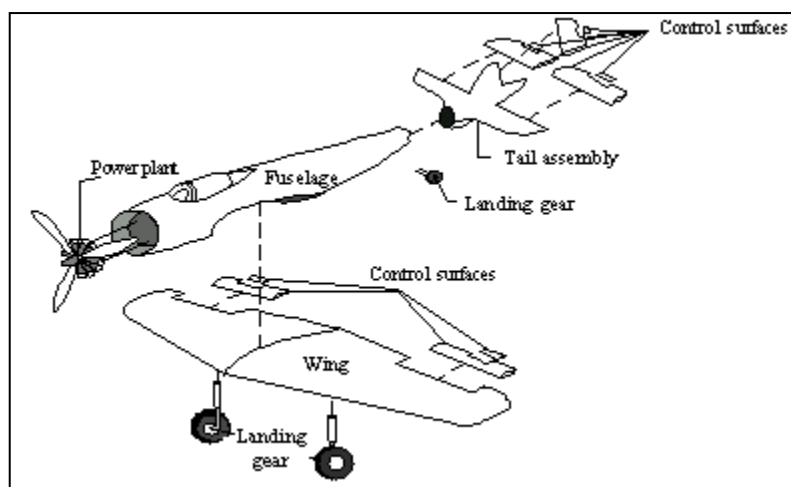


Figure 3.5 Basic Airplane Components.

3.1.2.3 Fuselage

Although the main function of the fuselage is to contain the aircraft's operators and payload, its function as an aerodynamic entity in its own right cannot be ignored. Figure 3.6 illustrates a number of fuselage designs and highlights the fact that the shape will be derived from the aircraft's task; the shape must, however, be aerodynamically acceptable since it will affect both drag and stability.

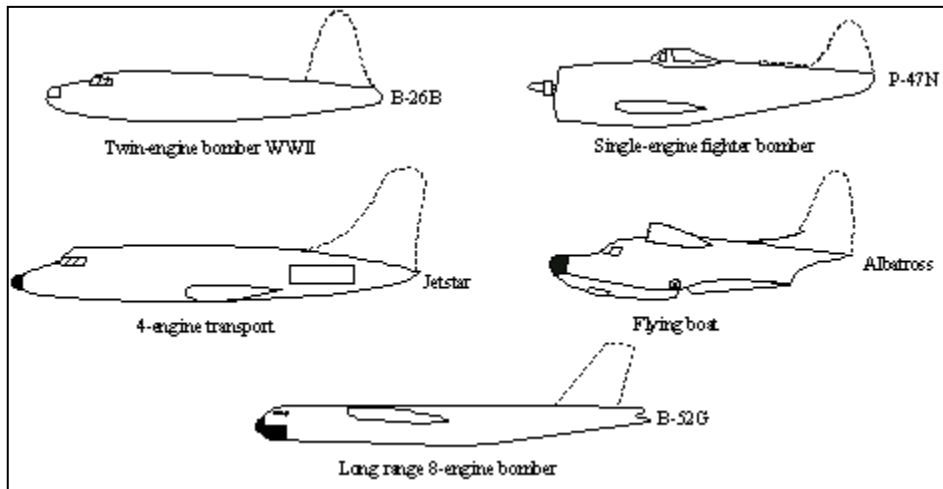


Figure 3.6 Various Fuselage Designs

3.1.2.4 Wings

The wing provides most of the lift required to support the entire aircraft. The shape of the wing's cross-section (the airfoil section), the plan form shape of the wing and the placement of the wing on the fuselage will affect the lift and drag characteristics of the wing and the stability of the aircraft. Figure 2.7 shows how the airfoil sections of wings have changed with the changing speed capabilities of aircraft. It is interesting to note that the current crop of ultra-light aircraft use an airfoil section very reminiscent of the Wright Brothers airplane.

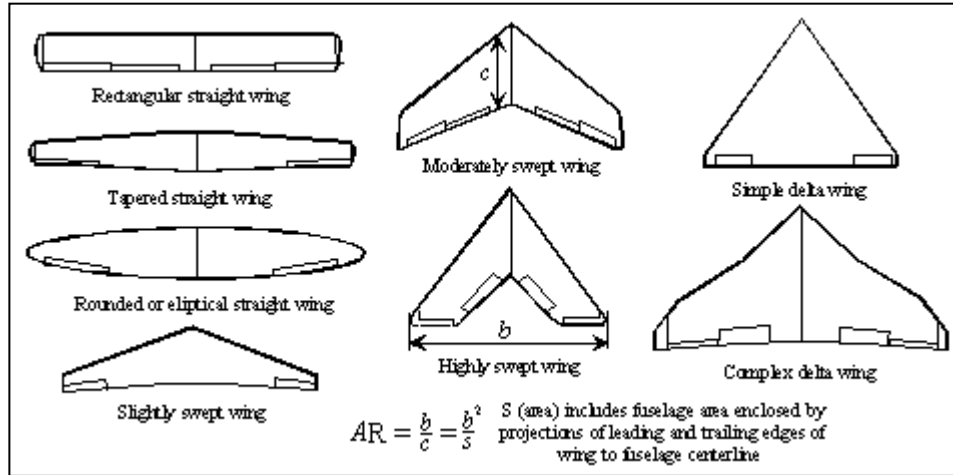


Figure 3.7 Wing Shapes

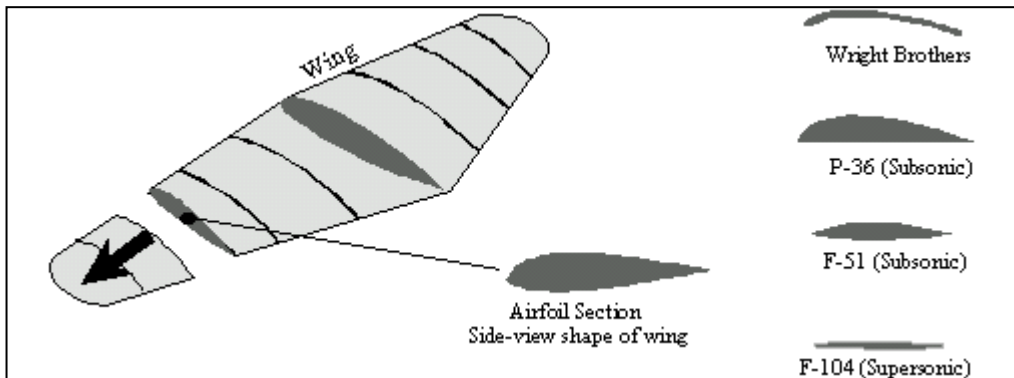


Figure 3.8 Examples of Wing Planform

Figure 3.8 illustrates the diversity of wing planforms which are used; the list is far from exhaustive. The shape will be dictated in part by the speed range in which the aircraft will operate, in part by the efficiency required of the wing and in part by the economics of production.

Figure 3.9 shows the possible wing positions relative to the fuselage. The lateral-directional stability requirements of the aircraft may well indicate one position or another although aircraft task (e.g.

high wing on many tactical transports) may be the deciding factor; aesthetics may well hold sway when all else fails.

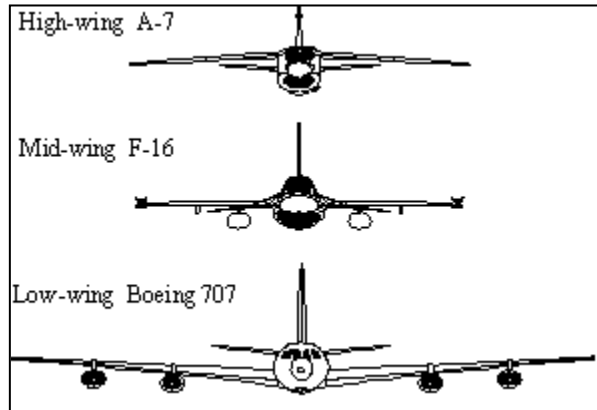


Figure 3.9 Examples of Wing Placements.

Unfavorable stability characteristics brought on by plan form shape and wing placement may well be corrected by applying either anhedral or dihedral. The mid-wing aircraft in Figure 3.9 exhibits slight anhedral; the wings appear to 'droop'. The low-wing aircraft shows marked dihedral; the wingtips are further from the ground than the wing roots.

While considering wing plan forms, it is convenient to define certain measurements. The span b is the distance from wing tip to wingtip. The chord c is the distance from the leading edge to the trailing edge normal to the span (i.e. parallel to the relative airflow). Aspect ratio is the relationship between span and chord and is expressed as b/c . However in most wings, c will vary with location throughout the span and so an average chord length must be used. It is better, therefore, to express aspect ratio as b^2/S where S is the wing area (span) (average chord).

3.1.2.5 Tail Assembly

The tail assembly is provided to increase the aircraft's vertical and horizontal surfaces aft of the center of gravity and hence improve stability. At the same time, these surfaces can be used, along with the hinged controls mounted on them, to provide pitching and yawing moments for maneuver and trim.

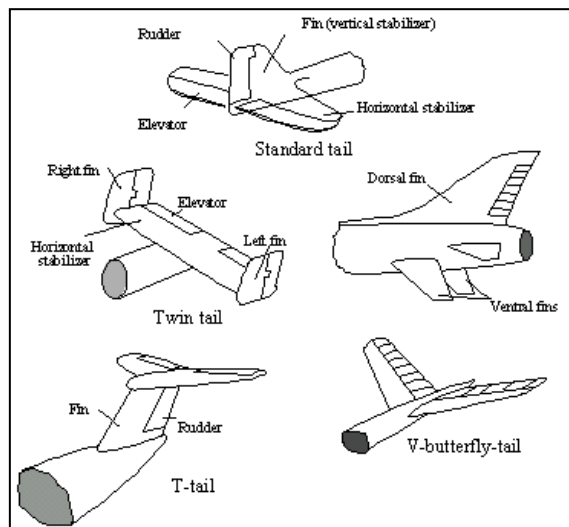


Figure 3.10 Tail Assembly Forms

Figure 3.10 depicts a selection of tail designs and names the various parts. The conventional arrangement is seen at the top of the figure. Center right is an adaptation, probably for a swept-wing aircraft whose fuselage, at high angles of attack, will shield the dorsal fin from the airflow; ventral fins are hence fitted to retain directional stability. The twin ventral fins of F-16 and F-14 help to fulfill a similar function. Twin fins like those at center left are common on larger aircraft, particularly multi-engine types. Placing the fins and rudders in the propeller slipstream improves the aircraft's directional control when an engine is lost.

Aircraft like the E2 Hawkeye and NASA's shuttle-carrying 747 have sprouted extra fins to replace the stability lost when a rotor-dome and the space shuttle respectively were mounted over their fuselages. The V-butterfly-tail design owes more to the manufacturer's desire to be distinctive than to aerodynamics. There is no demonstrable reduction in drag from the elimination of one entire surface and the need to 'mix' pitch and yaw control inputs to the remaining control surfaces adds complexity to a basically simple system. The T-tail has been favored by transport aircraft manufacturers in past years largely because it allows the mounting of engines on the aft fuselage (DC-9, Boeing 727). Aerodynamic advantages and disadvantages probably cancel each other out. The horizontal stabilizer end-plates the fin and, therefore, improves the effectiveness of the fin/rudder combination in the engine-out case. However, many T-tail aircraft suffer from deep stall characteristics caused by the horizontal stabilizer's being cloaked in turbulent air from the wing at the time when a nose-down pitching moment is urgently required; the design can, therefore, reduce the usable speed range of the aircraft and also add complexity in the form of a stick-pusher.

3.1.2.6 Primary Flying Controls

The theory behind control surfaces will be covered later in this text. The purpose of the flying controls is, of course, to allow the pilot to generate moments about all three aircraft axes and hence to maneuver the aircraft. In the great majority of cases, simple hinged surfaces on the trailing edge of the wing, horizontal and vertical stabilizers are used. In reversible systems, a further hinged surface called a control tab is connected to the trailing edge of the control surfaces to allow the pilot to trim out stick forces. As Figure 3.11 shows, the normal names for primary control surfaces are aileron (for roll control), rudder (for yaw control) and elevator (for pitch control). Many modern aircraft combine the functions of elevator and aileron into devices variously called tailerons or elevons.

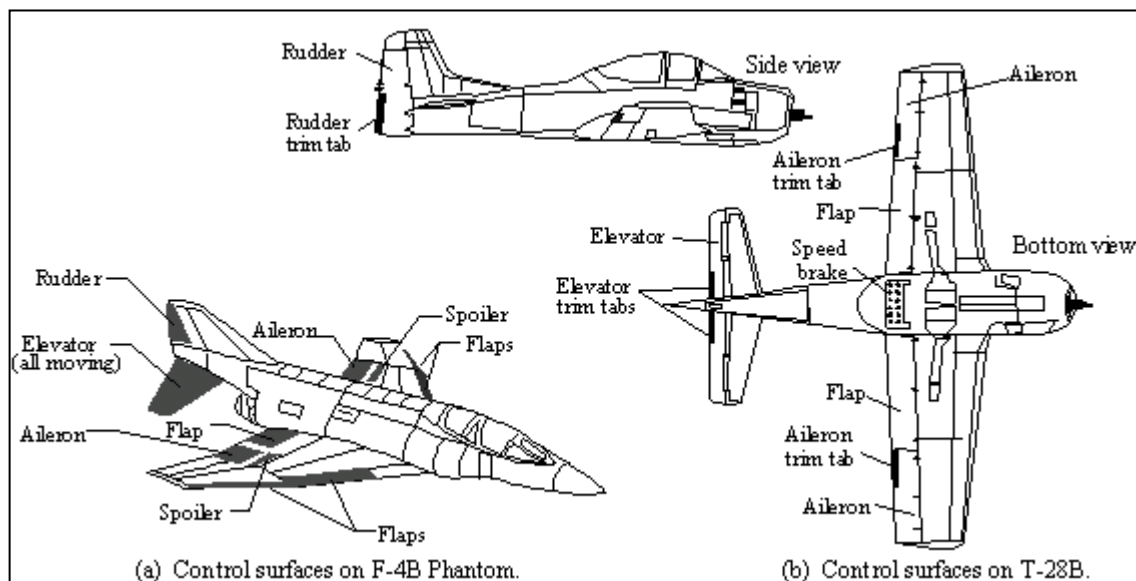


Figure 3.11 Main Control Surfaces

3.1.2.7 Secondary Controls

Secondary control surfaces like flaps, spoilers and speed brakes are not universal in application. Flaps are probably the most common secondary controls and they are used to increase lift during the takeoff phase and to increase both lift and drag during landing phase. Modern fighter aircraft like the F-16 also use flaps during other phases of flight to improve lift during maneuvering. The flaps may be on the trailing edge or a combination of leading and trailing edge; few aircraft have leading edge flaps alone. Figure 3.12 shows flap arrangements.

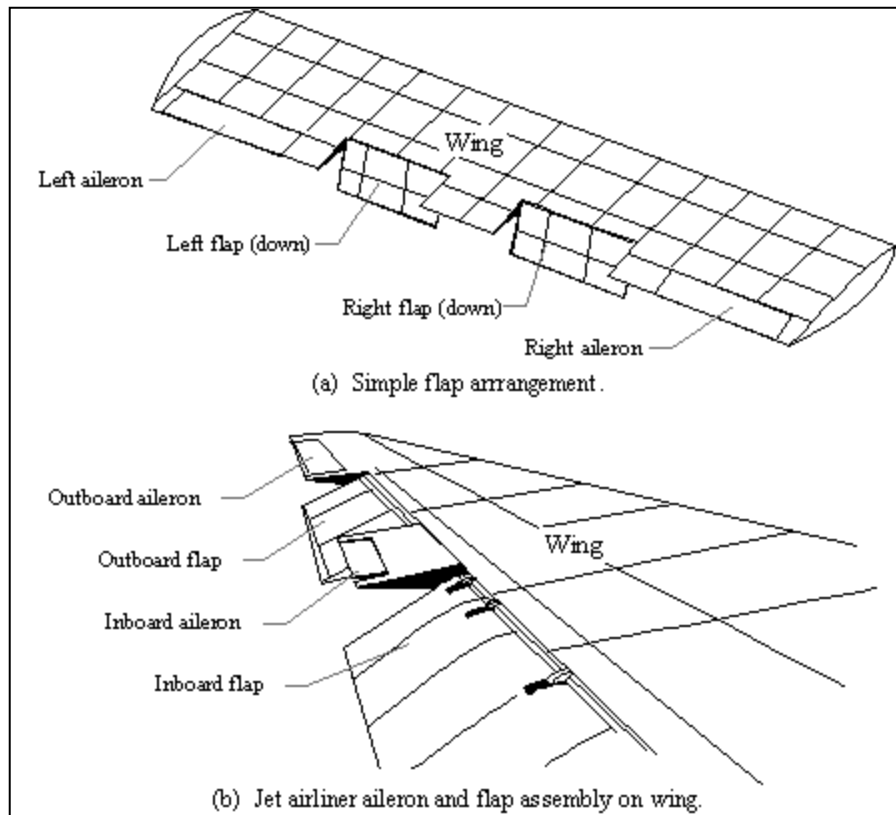


Figure 3.12 Flaps and Ailerons

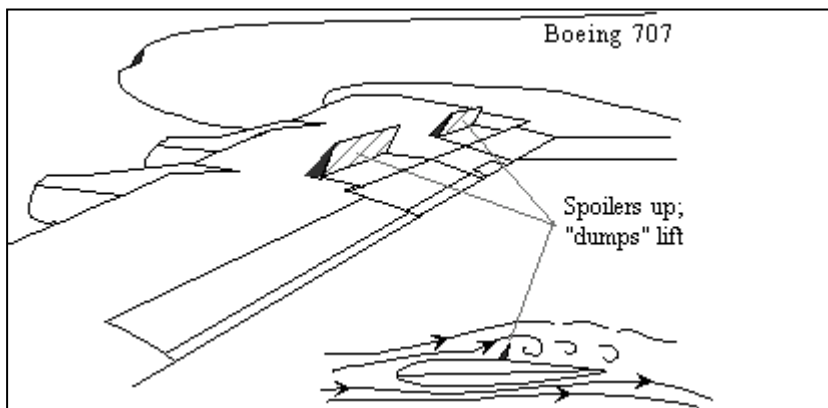


Figure 3.13 Use of Spoilers

Spoilers can be used in a number of ways. They can supplement or even replace primary roll controls by "spoiling" the flow over one wing and hence reduce lift over that wing. They can be used to increase drag both in flight (speedbrakes) or during the landing roll, putting more weight on the wheels and allowing heavier braking. They can be used from a semi-extended position to give direct control of the lift (controlled through the pilot's pitch or throttle inputs). Finally, because their deployment causes a nose-up pitching moment, their automatic extension may be used to recover the aircraft from a high-speed upset. Figure 3.13 depicts spoilers on a Boeing 707. In many modern wide-bodied transport there are up to 6 separate panels on each wing and various combinations of the panels are used to fulfill each of the functions listed above.

Speedbrakes are very common on military fast jets but, apart from spoilers, few appear on transport aircraft. Figure 3.14 shows a selection and highlights a transport aircraft which does not use spoilers; The Fokker F-28 and the BAe 146 both use the split rear fuselage approach. Because such airbrakes do not affect the airflow over the wing, they can safely be used to increase drag during an approach to landing.

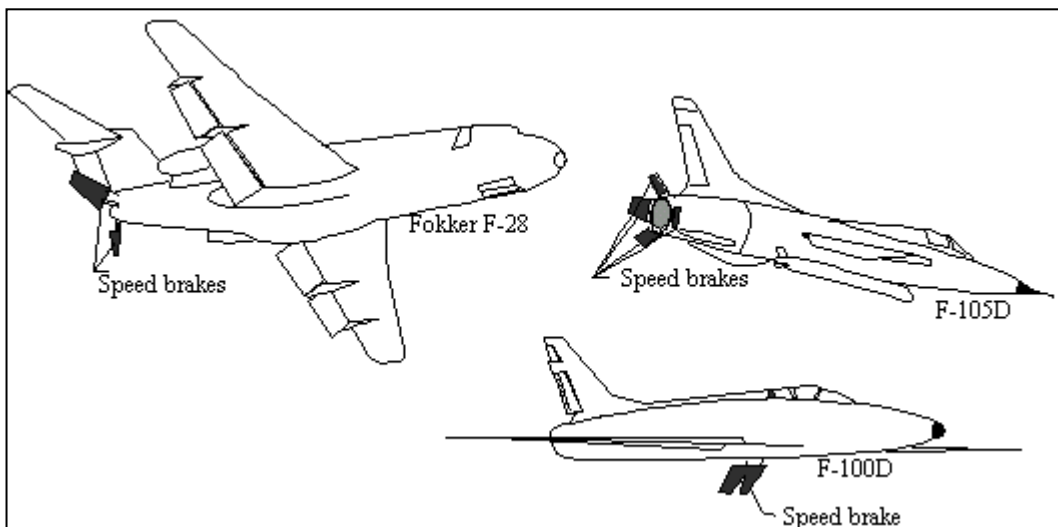


Figure 3.14 Dive (speed) Brake Arrangements.

Increasing the drag reduces the minimum drag speed and also allows a jet engine to work in the r.p.m. range where a large amount of thrust is rapidly available. Fighters have speedbrakes anywhere there is a spare surface. The F-105D shown is an unusual if not unique one. The F-100 installation resembles that on the F-111. The T-46 has a large surface which extend from the sides of the fuselage ahead of and below the horizontal stabilizer. The A-6 and S-3 employ split ailerons while the space shuttle orbiter has a split rudder. Anything which increases drag can be acceptable.

3.1.2.8 Landing Gear

The landing gear may not seem aerodynamically significant but a nosewheel placed well forward of the center of gravity can adversely affect lateral and directional stability. It is important, therefore, to ensure that stability tests are carried out with the gear down at some stage.

3.1.2.9 Powerplants

Powerplants are common to most aircraft; they produce thrust to accelerate the aircraft and to sustain it in unaccelerated flight by overcoming drag. The engine may also drive electrical, hydraulic and pneumatic power units.




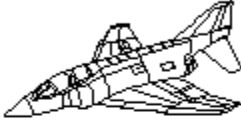




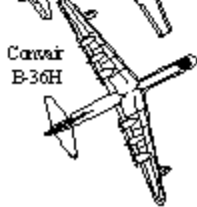
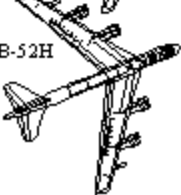
	Reciprocating or turbo-engine propellers	Jet engine
Single engine	 Kyushu J7W1 Shinden	 Heinkel He. 162 A-2
Twin engine	 Domier Do.335 A-1	 F-4B Phantom
Three engines	 SIAI Marchetti -79	 L-1011
Four engines	 Boeing B-29A Superfortress	 Boeing 707
Multi engine	 Convair B-36H	 B-52H

Figure 3.15 Power-Plant Placements

The main types in use today are reciprocating (driving a propeller or fan), turbo-propeller, turbojet, turbofan and, in very limited application, rockets. In order that the application of extra power does not induce any unwanted rotational motion of the aircraft, most modern fighters have their thrust lines very close to the center of gravity of the aircraft both laterally and vertically. As Figure 3.15 shows, it was not always possible to achieve this; it was very difficult to put more than one engine on the aircraft's centerline and many twin-engine fighters with horrendous asymmetric power characteristics were produced. Since larger aircraft do relatively little maneuvering, any suitable location can be used; however, the possibility of engine failure must be considered and the aircraft must be endowed with sufficient control to balance out the unbalanced moments during all phases of flight.

3.1.3 Aerodynamic Theory

3.1.3.1 Introduction

Figure 3.16 shows the forces acting on an aircraft in flight; of these forces, lift and drag are the direct result of the displacement of air by the aircraft's structure. In other words lift and drag are a result of aerodynamic action and it is these forces which will be considered in the remainder of this text.

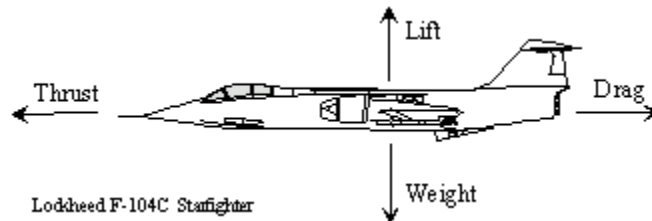


Figure 3.16 Forces on an Aircraft in Formal Flight

3.1.3.2 Simplifying Assumptions

Aerodynamics is a very complex subject which must make certain assumptions about the properties of air if any progress is to be made. Subsonic aerodynamics, our subject here, assumes that air is incompressible which eliminates the effect of density variation from the free stream density; in subsonic flight, the density changes brought about by the movement of the aircraft in the air are insignificant.

Basic subsonic aerodynamics also assumes that air is inviscid (i.e. has zero viscosity). While this assumption can be made for the majority of air flowing around an aircraft, recognition must be made of the air's viscosity if any understanding of practical aerodynamics is to be achieved.

3.1.3.3 Flow Visualization

In aerodynamics, it is important to be able to visualize the flow of air around the aircraft; there are two methods to be considered and both are illustrated in Figure 3.17.

In the Lagrangian approach (a) the position of one particle is plotted repeatedly as time passes. The line joining the points will be a record of the movement of the particle but there will be no guarantee that another particle will follow the same pathline since, as in the case in the diagram, the tides (external forces) may change. The Eulerian approach is to take a snapshot of the fluid which is relevant for that instant and shows the direction of movement of all particles in a particular streamline. Again, the "tides" may change things and the next snapshot may show different streamlines.

If the streamlines remain identical over the entire period for which the Lagrangian plot is being made, then the particle pathline will be identical to the relative streamline; such a case is termed "steady flow".

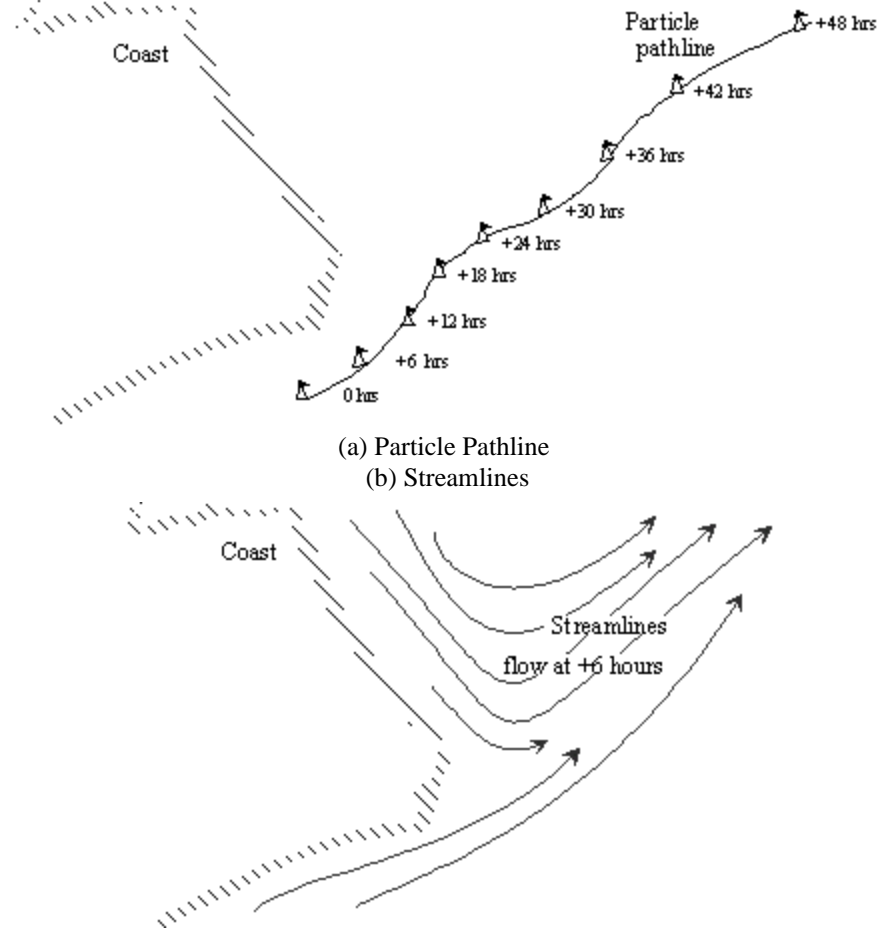
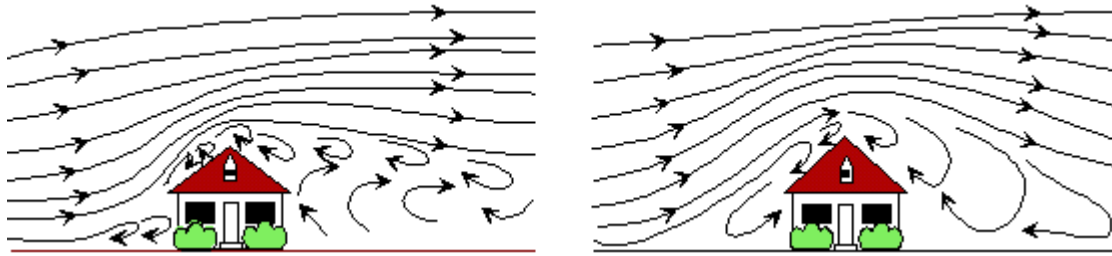


Figure 3.17 Flow Visualization

3.1.3.4 Unsteady Flow

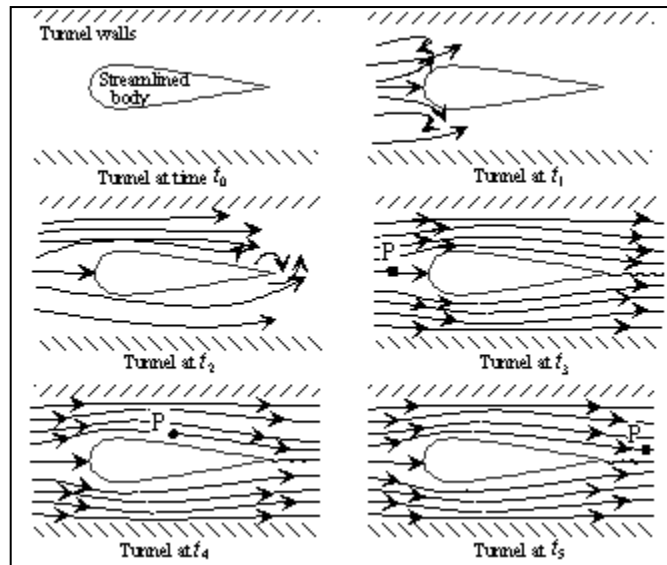
Unsteady flow is very common. The example of the ocean has already been used. Figure 3.18 is another example; in it you can see the changes in the flow pattern which have occurred over a brief delay. It is very difficult to predict such a flow field and so aerodynamic theory avoids calculations utilizing unsteady flow data. Perhaps the best example of unsteady flow is a turbulent wake which may well be unsteady but consistent, hence allowing steady data to be recorded. Although the flow in the wake, like any other unsteady flow, will be difficult to analyze mathematically, its effect on the airfoil may be consistent.

During the first stages of airfoil testing, when the wind tunnel is being used, unsteady flow will be achieved as air starts to flow in the tunnel. Only when the flow is steady, that is after the time when the pathline of point *P* follows a streamline, should data be taken. Many wind tunnel runs are brief and it is very important to separate the transient unsteady flow period from the steady period which follows if representative data are to be gathered.



(a) Streamlines at t_0 (b) Streamlines at time t_1

Figure 3.18 Unsteady Flow of Air about a House



Steady flow: Particle pathline = Streamline

Figure 3.19 Unsteady and Steady Flow

3.1.3.5 Rotational and Irrotational Flow

Having separated unsteady and steady flow, let us now consider rotational and irrotational flow. Figure 3.20 illustrates the differences and then relates the concept to flow around an airfoil section. In the diagram, the 'stars' represent paddlewheels which are immersed in the fluid. If the wheels translate without rotation (a) then the flow is irrotational; if the wheels also rotate, the flow is rotational (b). The final part of the diagram shows irrotational flow around an airfoil; this would still be the case even if the airfoil caused a large angular change of direction as with the airfoil at a high angle of attack. However, the diagram assumes that the fluid is ideal, that it has no viscosity. In reality, the flow close to the airfoil surface would be slowed owing to the air's viscosity and some of the flow would, therefore, be rotational.

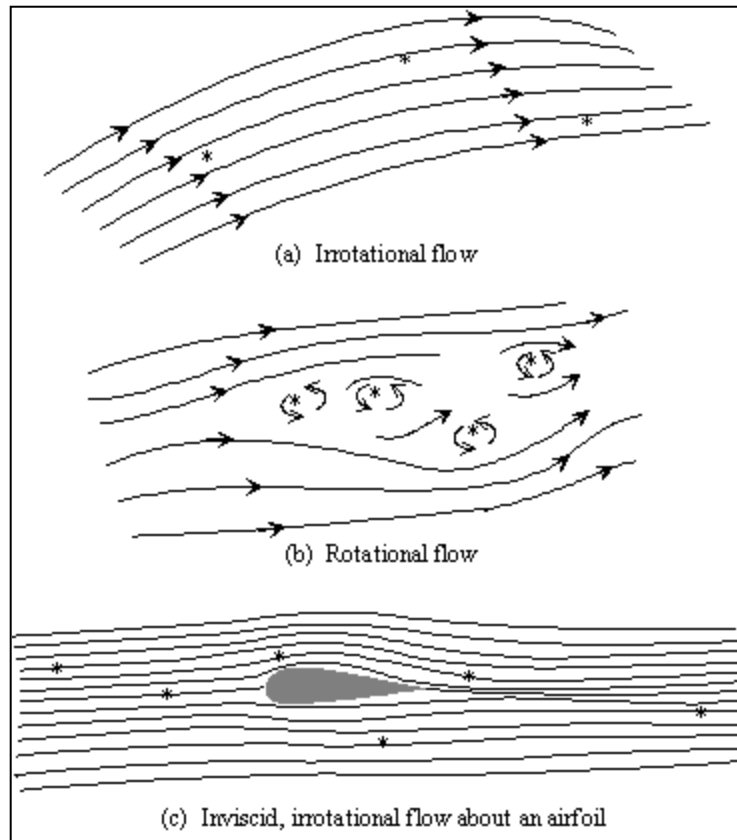


Figure 3.20 Rotational and Irrotational Flow

3.1.3.6 One-Dimensional Flow

To simplify understanding of the basic principles of Aerodynamics, we will assume that the air is both inviscid and incompressible. We can hence use the concept of one dimensional flow as illustrated in Figure 3.21. The air is considered to be a bundle of discrete streamtubes which make up the total flow of air. If one-dimensional flow is assumed, there will be no variation in velocity across the section of the flow; neither will there be any changes in density, temperature, pressure or any other flow property. As Figure 3.21(b) illustrates, such a flow is unlikely to exist in reality since the walls of the "containing tube" will reduce the velocity of the flow to zero at the surface owing to viscosity. However, the flow will closely approximate one-dimensional flow at the average velocity.

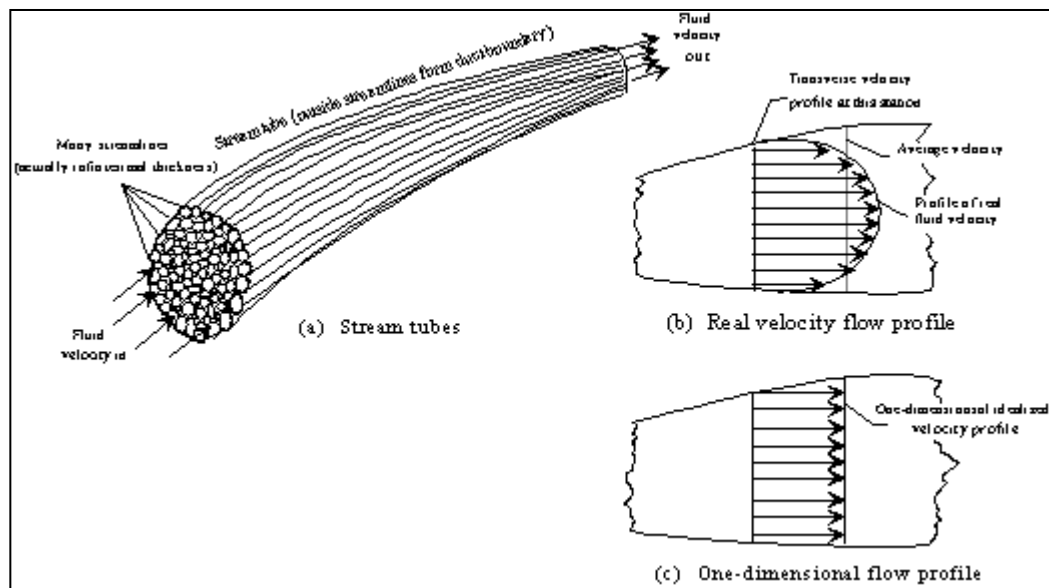


Figure 3.21 Stream tube concept.

Effects of Viscosity

The effects of viscosity on the characteristics of the flow past a solid contour are very important to illustrate the production of lift and drag of bi-dimensional and tri-dimensional bodies.

The boundary conditions of inviscid and viscous flow are respectively:

- Inviscid flow: $V_{\perp}|_{y=0} = 0$. The component of the velocity normal to the surface of the solid body is null. This corresponds physically to the flow being tangent to the body in any point.
- Viscous flow: $|\vec{v}|_{y=0} = 0$. The norm of the velocity vector at the surface of the solid body is null.

One of the fundamental boundary phenomena deriving from the viscosity of the flow and its boundary condition is that the norm of the velocity increases from zero, at the wall, to the local value in a portion of the flow of finite thickness.

We can further describe the effects of viscosity referring to the case of a flat plate in an asymptotic flow of velocity V_{∞} . Assuming the thickness of the particle corresponds to that in which the speed varies from zero to V_{∞} , the speed of the side in contact with the plate is zero, the speed of the upper side at distance dy

from the wall is V_∞ . The consequence is a distortion of the particle and a change of direction of its diagonals, with average non null rotation, or vorticity, as represented in Figure 3.22.

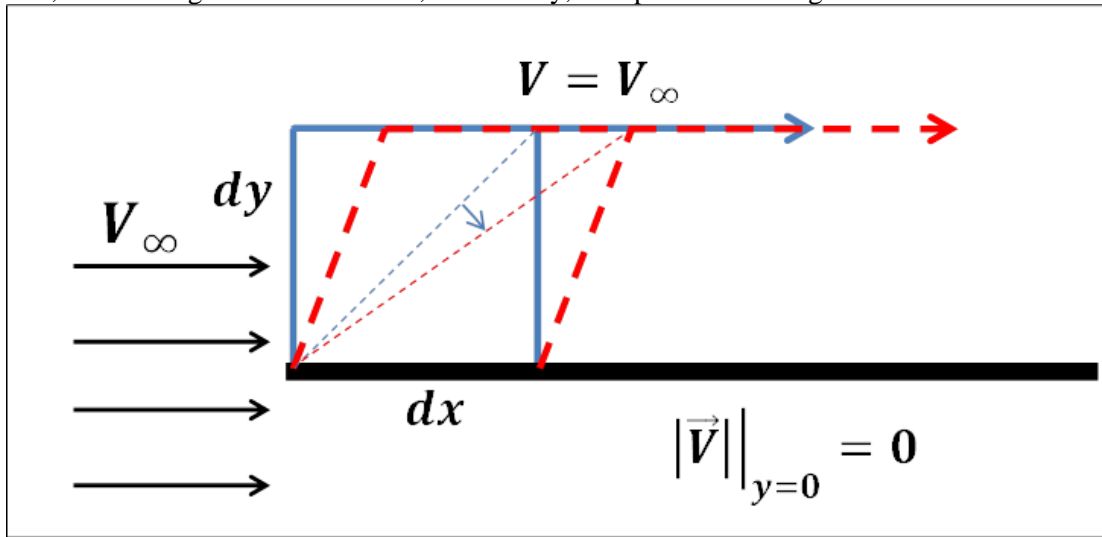


Figure 3.22: Conceptual explanation of vorticity generation.

This leads to see that with the start of the flow a layer of infinitesimal thickness is formed around the plate, in which vorticity is concentrated, called boundary layer.

The previous simplifying assumptions are not valid within the boundary layer. As a consequence, the flow can be conceptually divided into:

- Potential, in which the four assumptions described above are valid
- Boundary layer, in which the energy losses due to viscosity and the vorticity are not negligible

The definition “potential” derives from the fact that at any point in that portion of the flow, the velocity vector can be calculated as the gradient of a scalar function, called *velocity potential*.

Further explanation of the boundary layer and its interaction with the potential flow is provided in the next sections.

A notional representation of the two regions in which the flow around an airfoil can be divided into is provided in Figure 3.23.

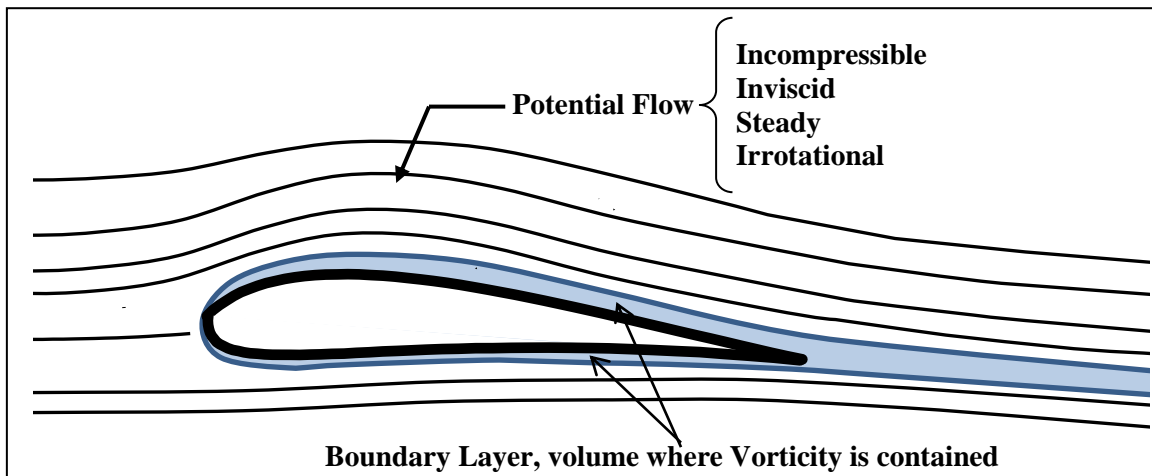


Figure 3.23: Potential flow and boundary layer.

3.1.3.7 Physical Laws

Now that all the simplifying assumptions have been stated, it is possible to examine the theories of lift and drag production. As in any other physical system, the laws of conservation of mass and of conservation of energy apply. If we consider a stream tube like the one in Figure 3.24(a), the law of conservation of mass will tell us that the mass flow rate past any point in that tube must be a constant. If the tube is constricted into what is called a Venturi tube, as in Figure 3.24, the mass flow rate through area A_2 must equal that through areas A_1 and A_3 . Mass flow rate, or mass flow per unit time, can be expressed as ρVA where ρ is the density, V the velocity and A the area.

Thus:

$$\rho_1 V_1 A_1 = \rho_2 V_2 A_2$$

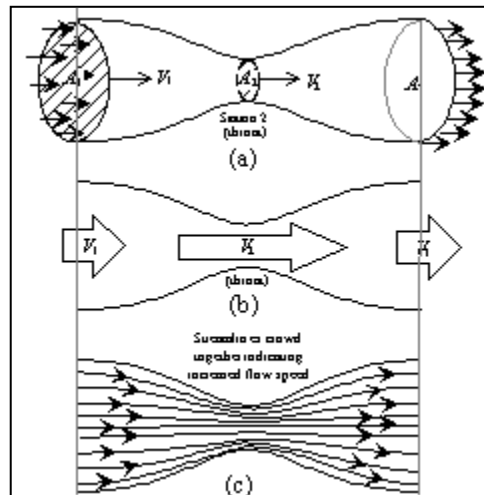


Figure 3.24: Venturi Tube and Continuity Principle.

Since we have already stated that the flow is incompressible and density ρ is constant,

$$V_1 A_1 = V_2 A_2 \quad \text{or} \quad V_2 = \frac{A_1}{A_2} \cdot V_1$$

Hence velocity at any given point in the tube is inversely proportional to the cross sectional area of the tube. As Figure 3.24 (c) shows, conventionally, a crowding together of the streamlines indicates an increased velocity.

We can apply the law of conservation of energy (usually called Bernoulli's Theorem in this context), to proceed in the development of the broad theory of production of lift. Bernoulli states that, in an ideal fluid, assumed to be:

- Incompressible
- Steady
- Irrotational
- Inviscid

the total energy will remain constant along the streamlines although the proportions of discrete energies may change.

For simplicity, let us consider that the flow possesses kinetic, pressure and potential energy caused by raising or lowering the flow as it passes the constriction in the Venturi tube. Because air has little weight, variation of potential energy is small and will be neglected; the energy in the flow can thus be considered made up of kinetic energy and pressure energy. We know that the kinetic energy of a flow particle, or a volume of the flow of mass m , $\frac{1}{2}mV^2$, will change since the flow velocity is increased at the throat of the Venturi tube. For the total energy to remain constant, an increase of kinetic energy

corresponds to a reduction of pressure energy. Considering energy per unit volume, which is pressure, we can see that the total energy corresponds to a pressure term that can be defined as *total pressure* (P_t). At any point total pressure has two components: kinetic energy per unit volume, or dynamic pressure $\frac{1}{2}\rho V^2$, and static pressure P_s . Referring back to the changes in energy in the Venturi tube, we can now say that dynamic pressure increases at the throat while static pressure reduces. If all points are considered, the following will emerge:

$$P_t = \frac{1}{2}\rho V^2 + P_s$$

where P_t is total pressure (or total energy) of the gas. This is the result of Bernoulli's Theorem and is true as long as energy is not added or subtracted (an ideal system satisfying the four assumptions listed above). In reality, energy is subtracted through friction. Referring to the previous subdivision of the flow past a solid contour, Bernoulli equation is not valid within the boundary layer, while it is valid in the potential flow.

3.1.4 Basic Lift Theory

3.1.4.1 Model of Vorticity around an Airfoil

The generation of lift can be explained considering the vorticity and its distribution in the field. The origin and the definition of the *starting vortex* and the corresponding *bound vortex* is the first step. Assuming to have a cambered airfoil in a fluid at rest and to start the fluid motion with an impulse, the initial transient of the flow field of motion around the airfoil is characterized by the formation of a vortex at the trailing edge, the *starting vortex*. The conceptual formation of the vortex is represented in Figure 3.25. After the transient, the *starting vortex* moves downstream with the flow, being connected with the flow around the airfoil by the wake. Vorticity is concentrated in the *starting vortex* which induces velocity and initially affects the flow field around the airfoil, noting that the net vorticity in the wake is zero. The velocity field induced by the *starting vortex* becomes negligible with the increase of its distance (10 to 15 chord lengths). The reason is that the speed induced by the vortex is directly proportional to its intensity, or circulation Γ , and inversely proportional to the distance from its core.

The vorticity initially contained in the flow was zero and it has to remain zero within a control volume which includes the airfoil and the *starting vortex*. This is formalized in the theorem of conservation of vorticity.

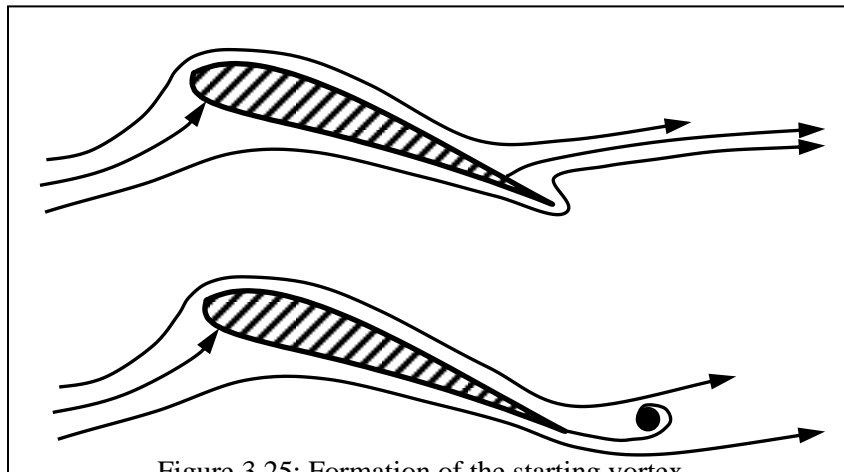


Figure 3.25: Formation of the starting vortex.

Counter clock-wise rotating vorticity is conventionally considered positive, so a positive circulation Γ^+ is assigned the *starting vortex*. To satisfy the conservation of general vorticity, a vortex with same

circulation and opposite sign must be contained within a control contour V which includes the airfoil and the *starting vortex*. This vortex is called the *bound vortex*, which can be thought to be centered on the airfoil. Figure 3.26 represents the *bound*, the *starting vortex* and the control contour V which includes both.

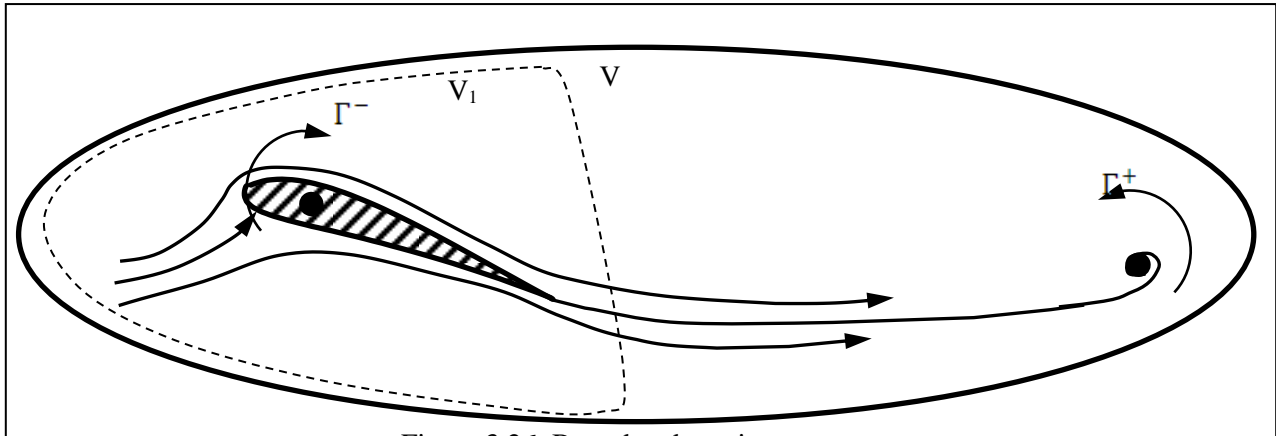


Figure 3.26: Bound and starting vortex.

As described before, when the distance of the *starting vortex* from the airfoil is around 15 chord lengths, its effect on the airfoil flow field is negligible. The flow field can then be adequately modeled by the composition of the asymptotic flow and of that induced by the *bound vortex*, contained in the contour V_1 . That of the concentrated *bound vortex* is a model which represents the vorticity distributed in the boundary layer, the region of the flow around the airfoil where non-zero net vorticity is contained.

It has to be noted that the formation of the starting and the bound vortex is possible when the flow is viscous, which means in presence of the viscous mechanism of separation of the flow from a solid contour.

Pressure Distribution

Based on the flow model described above, we now examine the effect of flow around an airfoil. Under a macroscopic standpoint, the velocity induced by the bound vortex produces acceleration of the flow on the upper part of the airfoil and deceleration on the lower part. The composition of the asymptotic and the induced velocity field leads to having one point on the airfoil in which velocity is zero. This point is intuitively placed in the front part of the airfoil and, for a given asymptotic speed, its location is a function of the *bound vortex* circulation, which depends on the airfoil geometric characteristics and the angle of attack. This point is called the stagnation point. Based on the description and the conceptual explanation of the flow components above, we can plot qualitatively the changes in velocity and pressure as a function of distance along the flow. The air is decelerated as it approaches the leading edge of the airfoil and in fact is stagnated at the stagnation point on the leading edge. Based on the Bernoulli theorem, since dynamic pressure is zero at that point, static pressure equals total pressure. From the stagnation point, the air gradually accelerates to a velocity above V_∞ (free stream velocity) until a maximum velocity is achieved at the "shoulder" of the airfoil; at this point the static pressure has fallen below P_∞ (free stream static pressure). From the shoulder, the airflow decelerates until, at the trailing edge, the static pressure equates ambient pressure P_∞ . The entire sequence is depicted in Figure 3.27: both the real and the ideal fluid case are represented, which differ qualitatively mainly at the trailing edge. The notional velocity and pressure profiles of the real fluid are depicted with the red dashed line.

It is fundamental to note that in the ideal case the requirement for the flow to leave the airfoil from the trailing edge imposes to have a streamline departing from the trailing edge itself. This corresponds to having a stagnation point at the trailing edge. This is called the *Kutta condition* and it is imposed to

reproduce the flow field of the real fluid, when dealing with the ideal one. It should be noted that the diagram shows a symmetrical airfoil with the airflow parallel to the chord (angle of attack = 0). In this case, therefore, there is no net lift since the flow field is symmetric. The mechanism of generation of the *starting vortex* is not present: the point of separation of the flow from the airfoil is unchanged from the initial transient to steady conditions and no boundary layer vorticity is shed in the flow at the start. As a consequence, the net circulation around the airfoil is zero and pressure variation is the same on both upper and lower surfaces.

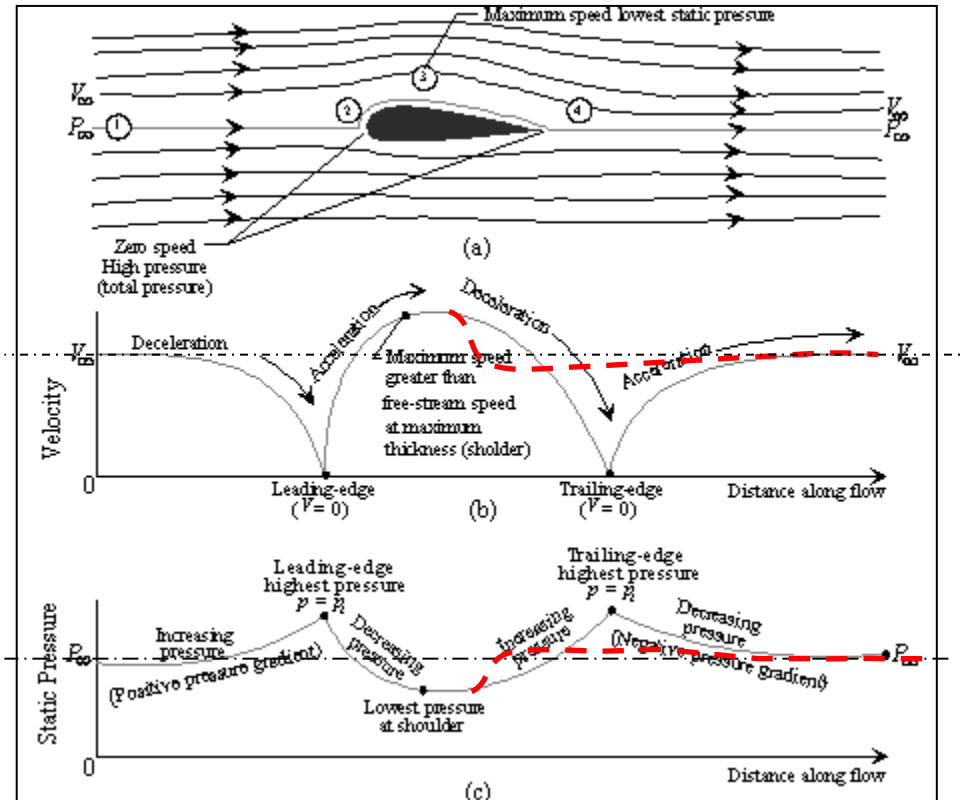


Figure 3.27: Fluid Flow About an Airfoil.

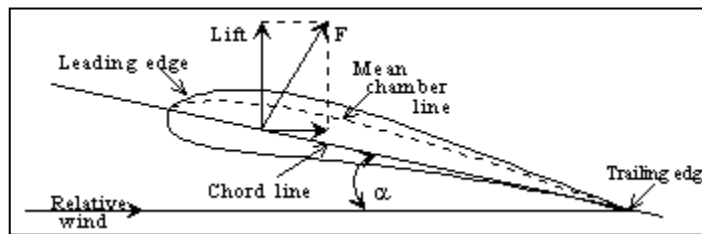


Figure 3.28: Airfoil Terminology

3.1.5 Further Details on Boundary Layer

3.1.5.1 Background Considerations

Since we are considering subsonic aerodynamics in this text, the assumption of incompressibility will be retained. Details about the effects of viscosity on the fluid-dynamic characteristics of the boundary layer, and in particular on its velocity and pressure profile, will now be considered.

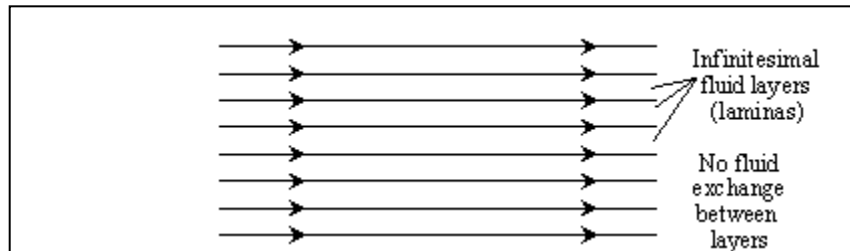


Figure 3.29 Basic Laminar Flow

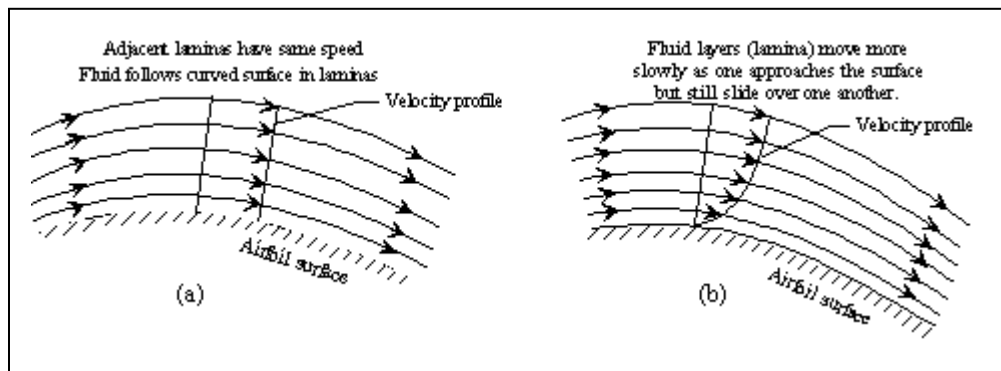


Figure 3.30 Laminar Flow Around an Airfoil: Ideal (a) and Real Fluid (b).

As described above, the major effect of viscosity is that, when moving air comes into contact with a stationary surface, the air touching the surface must also be stationary. Above the surface the velocity of the air gradually increases until it equals that of the free stream at that point. The layer in which this acceleration occurs is defined as the boundary layer and its nature affects the aerodynamic performance of the airfoil.

3.1.5.2 Laminar Boundary Layer

The boundary layer will be such that it can be considered to be infinitely thin layers or laminae, each of which is traveling at a slightly different velocity. There is no mixing between the laminae so the flow is smooth and the acceleration between airfoil surface and free stream is gradual and uniform. This type of layer is called a laminar flow boundary layer. Figure 3.29 shows a basic laminar flow while 3.30(a) and (b) compare laminar boundary layers in ideal and viscous flow respectively.

3.1.5.3 Turbulent Boundary Layer

The second type of boundary layer is one in which there is secondary, random velocity added to the general flow. Air moves freely between layers and air particles exchange energy such that fast-moving particles decelerate and slow-moving ones accelerate. One of the most important characteristics of this type of flow is that the general velocity close to the airfoil surface is higher than in laminar flow;

the outcome of such a change will be discussed later. This type of layer is called a turbulent boundary layer and is illustrated in Figure 3.31.

Outside the boundary layer, there is no velocity difference between the layers in the flow so the assumption of inviscid flow can be retained, simplifying the basic understanding of aerodynamics.

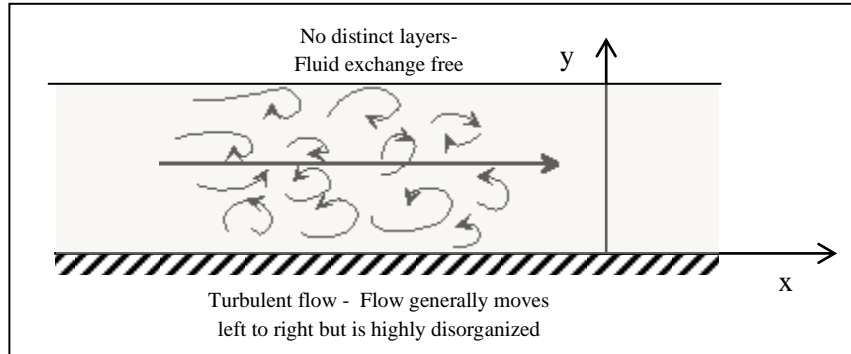


Figure 3.31 Turbulent Flow

A fundamental characteristic of the boundary layer is that for high Reynolds numbers and small perturbations the pressure variation along the normal to the contour in any point is negligible:

$$\frac{\partial P}{\partial y} \approx 0.$$

This is one of the most important results of the boundary layer theory, because it makes it possible to bind the pressure acting on the body with that on the outer limit of the boundary layer. This allows to derive the pressure distribution in the potential flow region by means of the Bernoulli equation and extend the results obtained at the limit of the boundary layer to the body itself.

3.1.6 Production of Lift

The concepts illustrated in the previous section of this chapter provide the foundations to describe the mechanism of production of lift. The previous case of the airfoil will be considered.

The viscosity of the flow allows for the development of the boundary layer around the airfoil, in which the flow velocity varies from zero at the wall to 99% of the flow field value at that point. This is the region of the flow in which vorticity is contained and significant energy losses due to friction take place, making it not possible to apply the Bernoulli equation. When the flow around the airfoil is started left to right, a significant amount of counter clock-wise vorticity is shed from the boundary layer into the flow domain. This vorticity is the *starting vortex*, which is washed away from the airfoil by the asymptotic flow. In order to have zero net total vorticity, a clock-wise rotating vortex centered in the airfoil has to develop simultaneously. This is the *bound vortex*. The velocity induced by the bound vortex is composed with the asymptotic flow, to form the flow field around the airfoil. The qualitative result is an increase of the velocity on the upper and a decrease on the lower part of the airfoil. Applying Bernoulli theorem to this flow, it results that lower pressures than asymptotic develop on the upper, and higher pressures on the lower part. The consequence is the production of a fluid-dynamic force, derived from the pressure distribution and the friction force, at an angle with the direction of the asymptotic flow. The normal component of this force is lift, the parallel component is drag.

A notional representation of the resulting pressure coefficient distribution is provided in Figure 3.32.

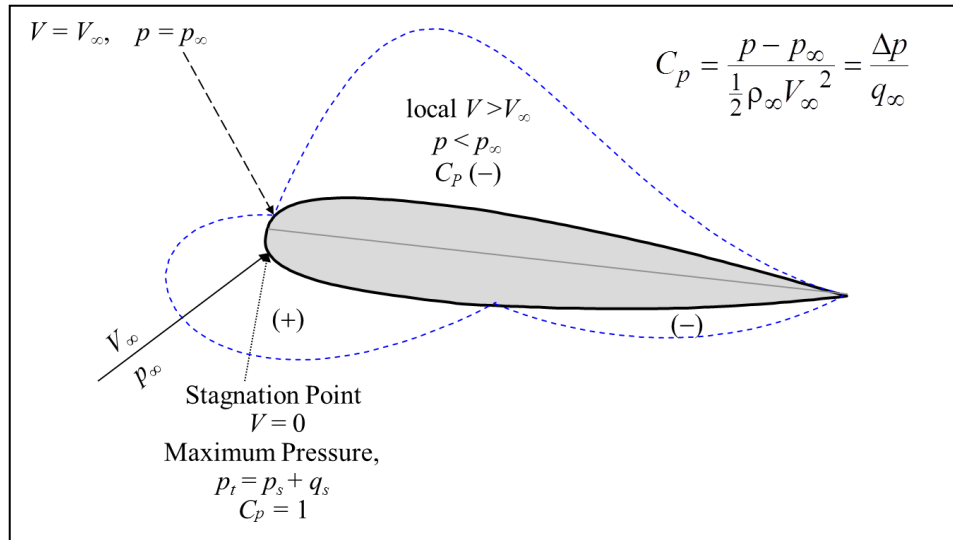


Figure 3.32: Pressure distribution around an airfoil.

It must be noted that no lift is produced without circulation, hence without viscosity.

As a side note, the relationship that binds circulation and asymptotic conditions in the production of lift from the Kutta-Joukowski theory is:

$$Lift = -\rho V_\infty \Gamma$$

Where Γ is the circulation around the airfoil. In the case presented above the circulation Γ is clock-wise and negative ($\Gamma < 0$), which corresponds to a positive lift.

A more general formulation of the expression above is:

$$\vec{F} = \rho \vec{V} \times \vec{\Gamma}.$$

3.1.7 Lift

3.1.7.1 Introduction

The purpose of any airfoil on an aircraft is to generate lift in some or all phases of flight. This section continues the study of lift production and examines the parameters which will change the available lift.

3.1.7.2 Airfoil Design

Scientists have known for more than 150 years that a curved surface would produce lift if an air stream was passed across it. Even a flat plate will produce lift if it is at an angle of attack to the flow, but the drag produced would be excessive in subsonic flight. So much data has been accumulated concerning the performance of particular types of airfoil that it is possible to design an airfoil for a set task using theoretical methods only. Figure 3.29 shows the sequence of operations for the design of an airfoil. First the chord length is fixed as a function of overall airfoil design. Next the curved camber line is added; it is this line which dictates the main lift characteristics of the airfoil. The thickness of the airfoil is governed by the strength required, the aircraft's operating envelope and the load (fuel, landing gear etc.) to be housed in the airfoil; equal thickness is added above and below the camber line to give the upper and lower surfaces.

In general, a thick, heavily cambered airfoil will give high lift and high drag at low speeds. Thin, sharp wings are used for high speed applications to minimize drag while giving enough lift at the higher speeds; at low speeds, the high angles of attack required to give sufficient lift will mean that the drag will be very high.

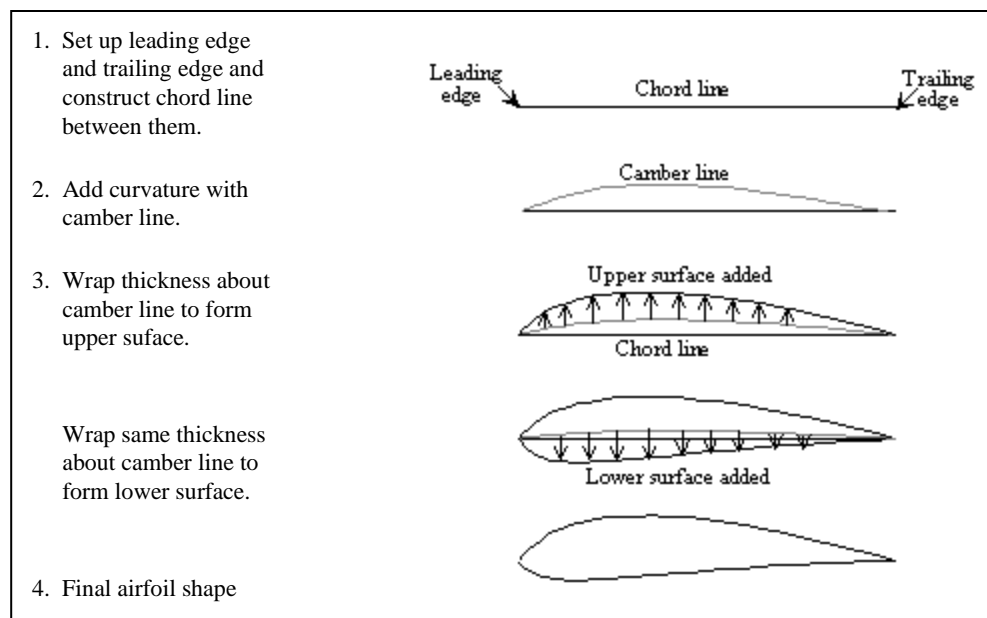


Figure 3.33 Geometric Construction of an Airfoil

Figures 3.30 and 3.31 show the varying shapes of airfoils and highlight some of the terminology used.

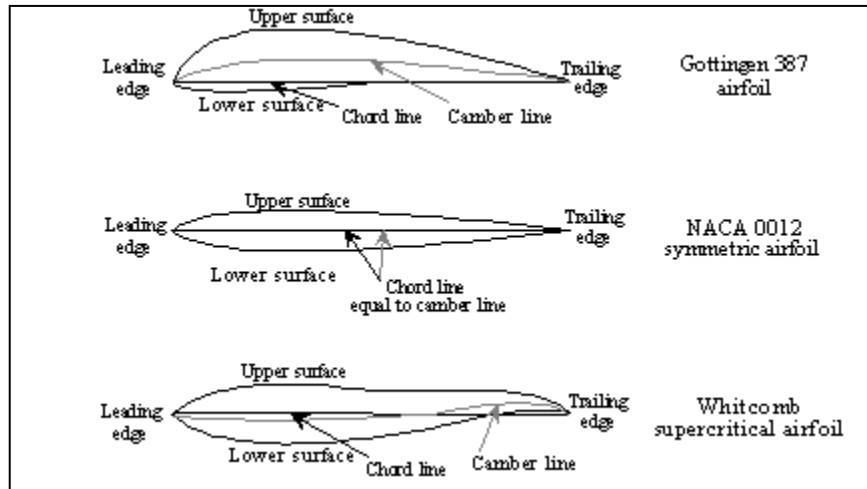


Figure 3.34 Airfoil Shapes

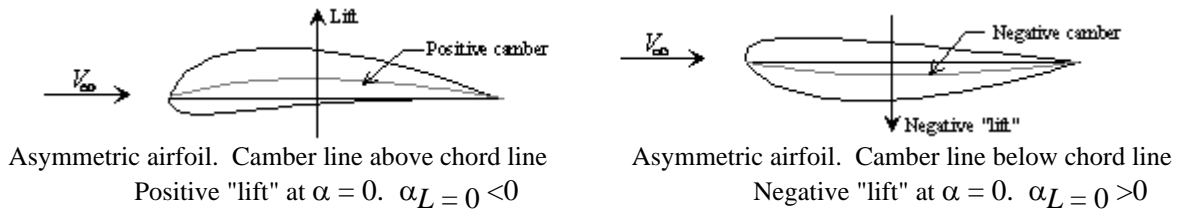
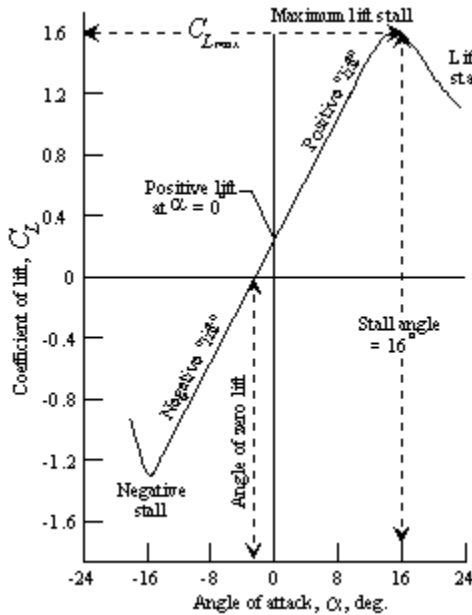


Figure 3.35 Airfoil Camber Line Variation

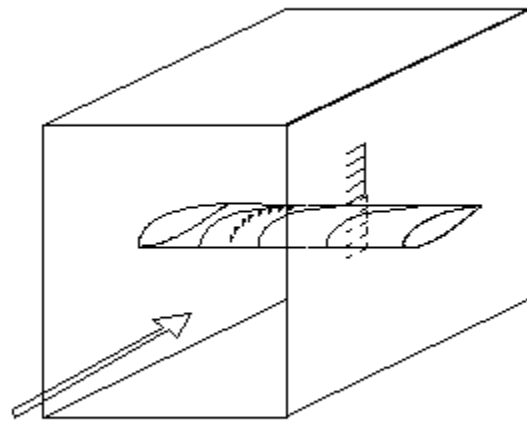
A fundamental property of an airfoil with positive camber is that, even at 0° angle of attack, lift will still be produced since the pressure distribution over the upper and lower surfaces is dissimilar. Figure 3.32 highlights the fact that a negative angle of attack will be required to generate zero lift; the figure also shows the general shape of the lift versus angle of attack graph.

3.1.7.3 Two-Dimensional Testing

Airfoils are manually tested in two-dimensional wind tunnels which effectively endplates the constant chord wing, Figure 3.33.



Lift Curves for a Cambered Airfoil
Figure 3.36



An Airfoil in a Two-dimensional Wind Tunnel
Figure 3.37

The pressure distribution around the airfoil is measured using a line of flush static ports in the airfoil and the drag of the airfoil is measured using an integrating total head rake behind the wing trailing edge. The pressures are measured in lb/ft^2 but are non-dimensionalized to a pressure coefficient form prior to plotting.

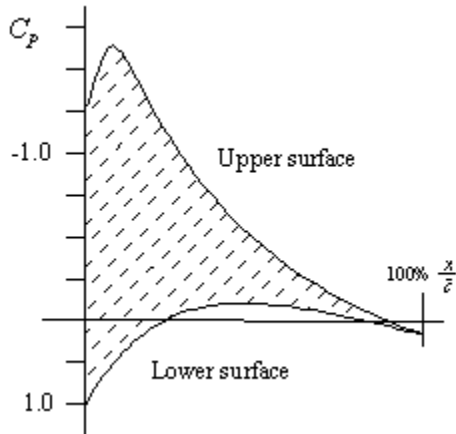
The pressure coefficient

$$C_p = \frac{p - p_\infty}{\frac{1}{2} \rho_\infty V_\infty^2} = \frac{\Delta p}{q_\infty}$$

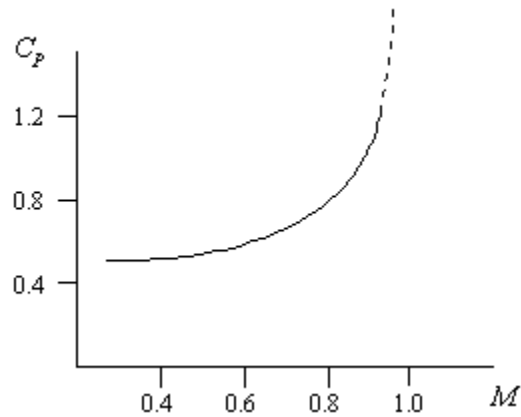
For example, if the wind tunnel pressure is = $2116 \text{ lb}/\text{ft}^2$ (sea level)
 the wind tunnel density is = $0.002377 \text{ lb sec}^2/\text{ft}^4$ (sea level)
 the wind tunnel velocity is = $400 \text{ ft}/\text{sec}$
 and the local pressure on the airfoil is measured as $1000 \text{ lb}/\text{ft}^2$ in our example

$$C_p = \frac{1000 - 2116}{\frac{1}{2} (0.002377)(400)^2} = -5.88$$

The pressure coefficients are then plotted against the chord line for the upper and lower surfaces as shown in Figure 3.38.



Pressure Distribution
Around an Airfoil
Figure 3.38



Effect of Compressibility
on Pressure Coefficients
Figure 3.39

Each pressure coefficient is a function of Mach number (compressibility) as shown in Figure 3.39.

C_{P_0} is the incompressible value of C_P at a Mach number of zero ($M = 0$). It can be seen from figure 3.39 that up to a Mach of about 0.3, C_P is unchanged or in other words, the pressures behave as though there is no compressibility effect. Above $M = 0.3$ C_P increases with Mach approximating the Prandtl-Glauert equation.

$$C_p = \frac{C_{p_0}}{\sqrt{1 - M_\infty^2}}$$

The region of compressible subsonic flow extends from $M = 0.3$ to M_{crit} . $Mach_{\text{crit}}$ is defined as the minimum freestream Mach number when the local flow at any point on the aircraft reaches the speed of sound. The Prandtl-Glauert equation is useful because it predicts how the C_P changes with Mach number. Because the C_P distribution is related to C_L for the entire wing, we have a way of predicting the lift (and drag) for any Mach number.

Resultant Aerodynamic Force

The integral of the pressure distribution (which is affected by the frictional & pressure drag forces) gives the resultant aerodynamic force (R.A.F.) which is located on the chord line at the center of pressure, (CP) Figure 3.40.

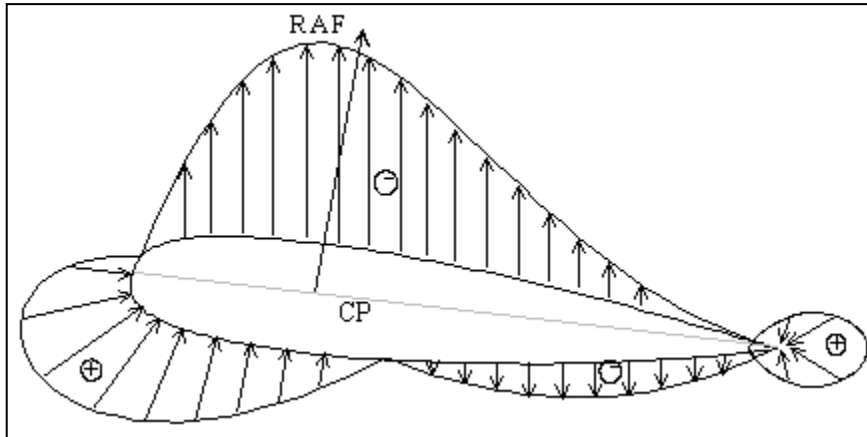


Figure 3.40 The Resultant Aerodynamic Force (R.A.F.)

The resultant aerodynamic force is resolved into two components; one normal to the freestream called lift and the other parallel to the freestream called drag.

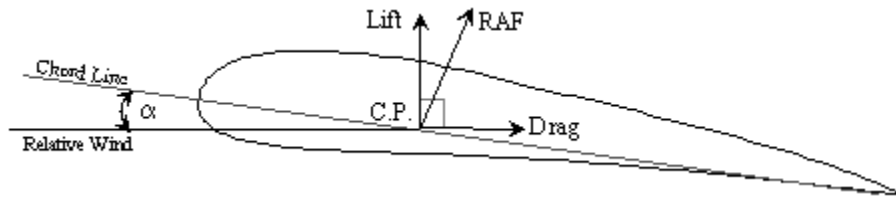


Figure 3.41 Definition of Lift and Drag

Because the pressure distribution changes with angle of attack, both the RAF and its center of pressure change. Figure 3.42 illustrates the change in lift, drag and CP.

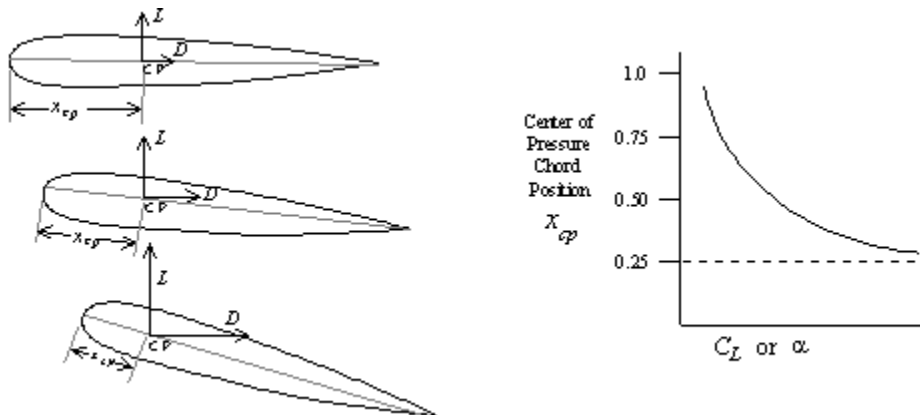


Figure 3.42 The Effects of Changes in Angle of Attack on Lift, Drag and Center of Pressure

3.1.7.4 Aerodynamic Center

Part of stability and control analysis involves determining the pitching moments generated by the wing. One component of this moment is that due to the lift acting at some distance along the chord. As an example, figure 3.42, shows that as AOA increases, the lift magnitude grows but the moment arm (x_{cp} , measured relative to the leading edge) decreases. With the reference point at the leading edge, the moment (product of arm and lift magnitude) changes with AOA. Instead of using the leading edge as the reference point, find another location which will balance the product of lift and arm so that it is constant, regardless of AOA. Such a reference point is termed the "aerodynamic center" and is used extensively in aircraft studies. The location of the a.c. is at approximately 25% MAC for all wings at subsonic conditions and at 50% MAC for wings in supersonic flow. Figure 3.43 illustrates how the parallel axis theorem is applied. The lift force acting through the CP is replaced with the same lift force acting through the aircraft and a constant moment. By referring pitching moments to this aircraft, this pitching moment is constant for all AOA, thereby simplifying stability and control analysis.

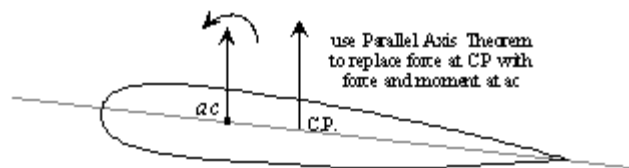


Figure 3.43 Concept of the Aerodynamic Center

3.1.7.5 Mean Geometric Chord (M.G.C.)

The aerodynamic center concept for an airfoil section works well for rectangular wings with no twist. Wings with sweep and different chord lengths as shown in Figure 3.40, can use the concept of a mean geometric chord which defines a mean chord line which represents the average lift of the entire wing. Determination of the M.G.C. is shown in Figure 3.40. The mean geometric chord gives reasonable results for untwisted wings with a constant airfoil section throughout the wing span.

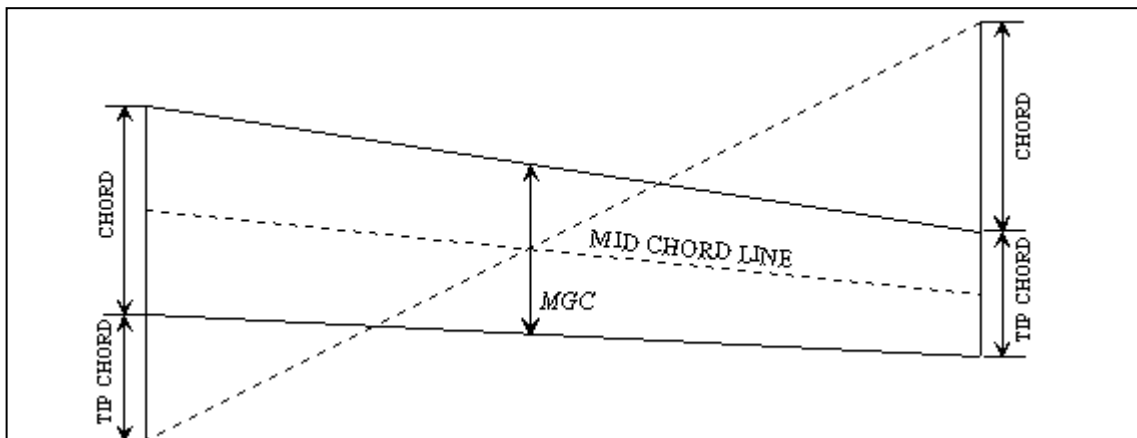
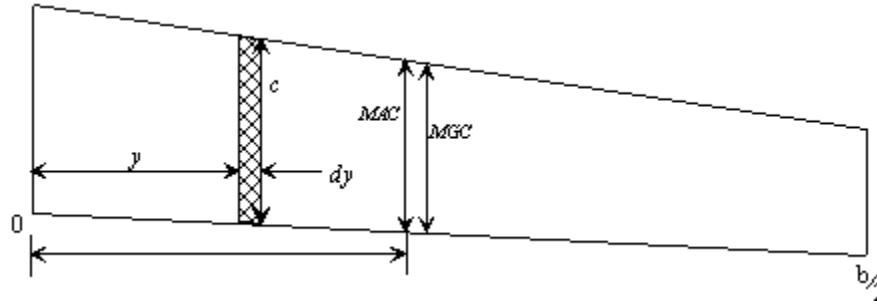


Figure 3.44 Mean Geometric Chord

3.1.7.6 Mean Aerodynamic Chord (M.A.C.)

If the airfoil section varies throughout the span or if the wing is twisted, then the mean geometric chord is not very useful and is replaced by the mean aerodynamic chord, which is often depicted as (MAC) in literature. The mean aerodynamic chord is the chordline on the wing that represents the average aerodynamic characteristics of the entire wing. A method of calculation of the mean aerodynamic chord is shown in Figure 3.45.



$$\bar{y} = \frac{\int_0^{b/2} \left(\frac{1}{2} \rho V^2 c dy C_{L\alpha} \cdot \alpha_y \right) y}{\int_0^{b/2} \left(\frac{1}{2} \rho V^2 c dy C_{L\alpha} \cdot \alpha \right)} = \text{location of MAC on span}$$

Figure 3.45 Mean Aerodynamic Chord

The length and location of the mean aerodynamic chord of a wing relative to the aircraft datum is very important in all longitudinal stability and control flight tests because it is assumed that all the lift of the wing is concentrated at the aerodynamic center of the mean aerodynamic chord.

Similarly, the lift on the horizontal tail is considered to be located at the aerodynamic center (a.c.) of the tail mean aerodynamic chord. The above approach of using M.A.C.'s and a.c.'s simplifies the longitudinal stability calculations of an aircraft. Figure 3.46 shows the M.A.C. for the F-15A as well as the location of the mean geometric chord. The weight vector location is the other main contributor to longitudinal stability and the center of gravity (c.g.) is determined as a percentage of the mean aerodynamic chord (%M.A.C.).

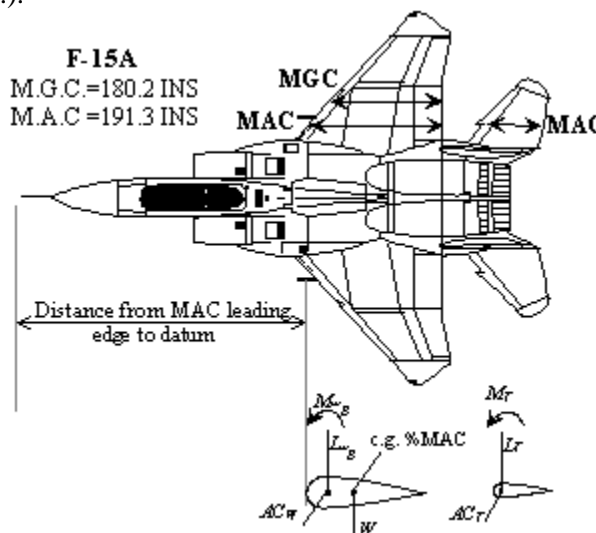


Figure 3.46 Location of M.A.C. and M.G.C. on F-15A Aircraft

On many aircraft the aircraft center of gravity is determined as a distance from the aircraft datum line which is often located on or near the nose of the aircraft. The British sometimes use the main spar (typically located at the 25% chord point) as the aircraft datum which means that moment arms are either (+) or (-). The center of gravity limits for acceptable controllability and stability, i.e. the forward and aft c.g. limits, are given in distances from the datum but they are more meaningful when given in percent of M.A.C. The c.g. limits for unaugmented aircraft are seldom less than 15% or more than 35% M.A.C.

3.1.7.7 Two-dimensional Wind Tunnel Data.

The data published on airfoils are obtained from two-dimensional wind tunnels as shown in Figure 3.36. The pressure data are integrated around the airfoil at each angle of attack to get lift coefficients and the wake rake data are used to determine the drag coefficients. The resulting data are plotted in Figure 3.47.

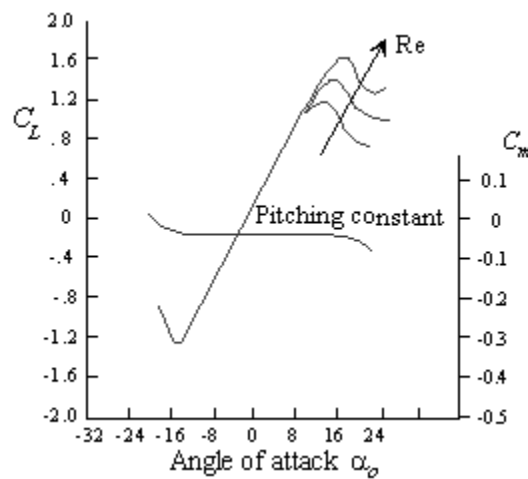


Figure 3.47 Airfoil Characteristics

3.1.7.8 Three-dimensional Flow

The end plated two-dimensional airfoil data as shown in Figure 3.47 must be modified when applied to a finite (three-dimensional) wing. This is necessary because the combination of pressure flow & freestream flow generate a wingtip vortex (Figure 3.48). This vortex creates a large flow field that decreases the average AOA that the wing encounters. Figure 3.49 shows the variations in $C_L \sim \alpha$ curves brought about by the transition from two-dimensional to three-dimensional flow. It shows that a finite span wing requires more freestream AOA to achieve a given C_L . This $\Delta\alpha$ is, in fact, the amount of downwash generated by the wingtip vortex.

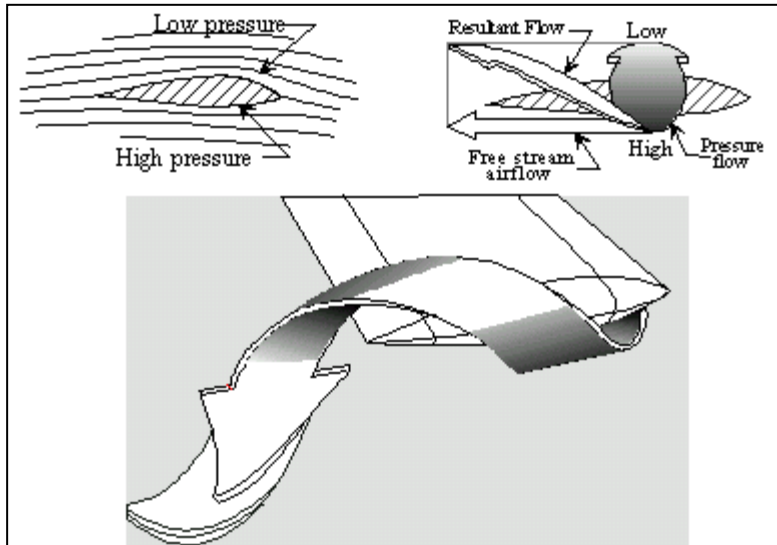


Figure 3.48 Wing Tip Vortex Formations

Note that although the zero lift angle of attack remains the same, there is a decrease in the lift curve slope $C_{L\alpha}$ with a decrease in aspect ratio AR . The maximum lift coefficient C_{Lmax} decreases with a decrease in aspect ratio but the angle of attack associated with C_{Lmax} increases. The lift curve slope of an infinite wing (a_o) can be corrected to " a " for a finite wing using the equation in Figure 3.49. This is expected to be adequate for simplified analyses.

Industry standard is to test in the wind tunnel scaled models of the whole aircraft, with the capability to deflect the primary, secondary control surfaces, landing gear deployment, external stores. An aerodynamic model of the aircraft is developed from these tests, based on which the required in-depth analyses are conducted to validate or improve the aerodynamic design, model the pitot-static system measurements, predict the aerodynamic loads, design the control laws. This ultimately allows authorization of the aircraft to fly. Aircraft design is based on high fidelity wind tunnel testing.

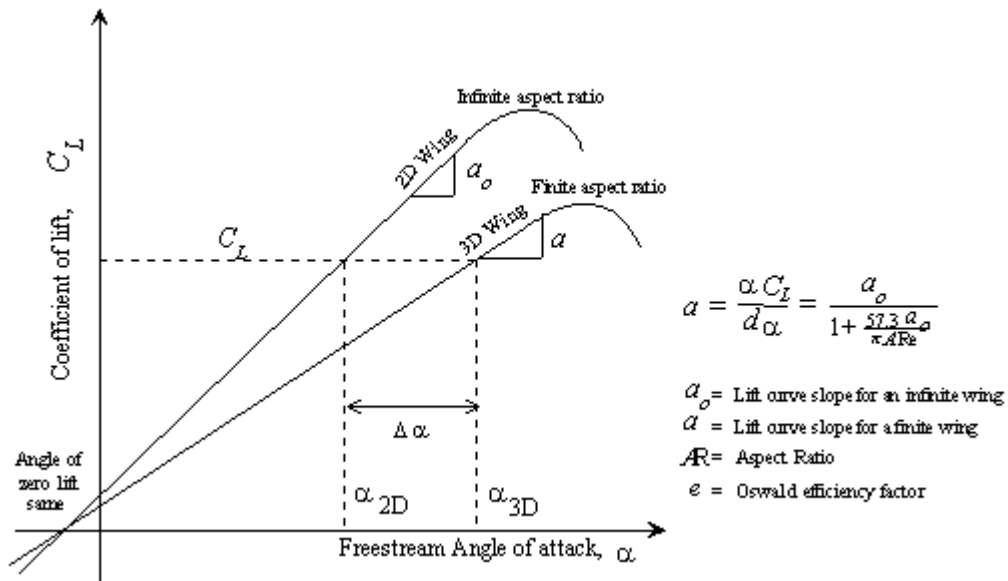


Figure 3.49 Three-Dimensional Flow Effects on Lift

3.1.7.9

3.1.7.10 Flow Separation

Figure 3.50 shows how the coefficient of lift, C_L , increases with increasing angle of attack. The slope of the section of the curve is largely a function of the camber of the airfoil while the maximum C_L achieved is also dependent upon Reynolds number, surface roughness and Mach number. The cause of the reduction in increase in C_L as $C_{L\max}$ is approached, is the start of separation of the boundary layer from the upper surface of the airfoil.

Figure 3.50 shows the progressive forward movement of the separation point with increasing angle of attack, α . As the point moves forward, the free stream experiences, in effect, a reduction in camber since the stream does not penetrate the turbulent wake. The reasons for the separation are twofold. First, since the boundary layer is moving over a stationary surface, some of the layer's energy will be expended in frictional heating.

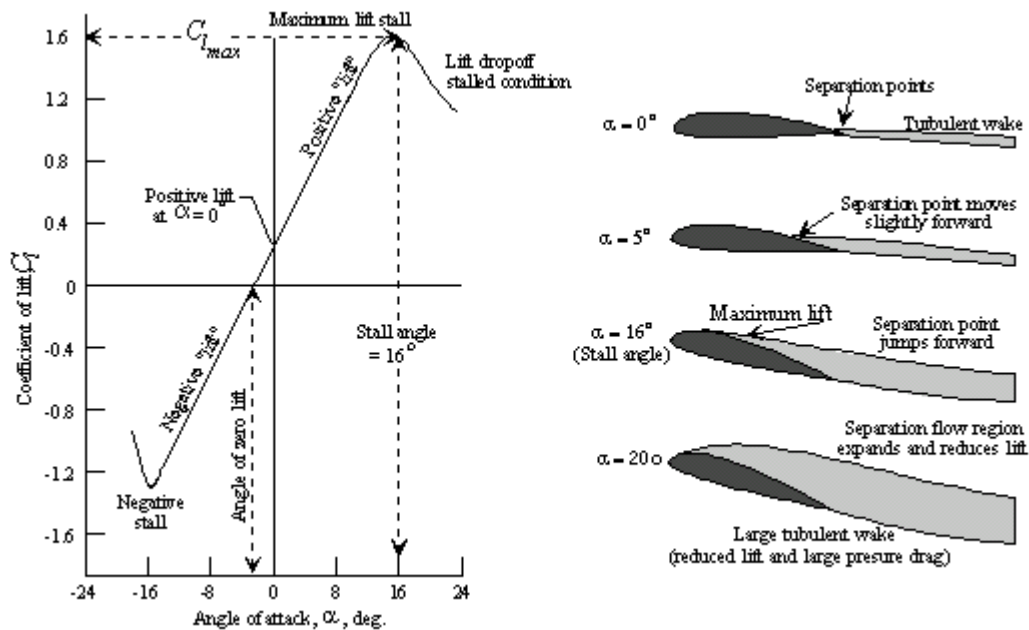


Figure 3.50 Stall Formation

Frictional losses will be the main cause of the separation of the laminar layer; this separation will cause the transition into turbulent flow which will reattach to the upper surface of the airfoil as a turbulent boundary layer. Because the velocity profile of the turbulent layer is steep, the frictional losses will be even greater following reattachment. The second cause of energy loss from the boundary layer is the pressure envelope being created by the airfoil. From the leading edge stagnation point to the 'shoulder' of the airfoil, where pressure is at its lowest, the boundary layer will experience a favorable pressure gradient, i.e., the pressure will be reducing and encouraging the flow along. Once past the shoulder, the

layer will experience an adverse pressure gradient and will expend energy in overcoming this. Eventually, the layer will have insufficient energy to remain attached to the surface and will separate into a turbulent wake. The static pressure in the wake will be close to free stream static pressure, so lift will be lost. As α increases, the 'shoulder' position moves progressively forward, advancing the start of the adverse pressure gradient, thus causing earlier separation of the flow.

Another alternative is that when the laminar boundary layer separates prior to turbulent transition, the layer has insufficient energy even after transition to reattach. Such a circumstance causes a rapid loss of lift and the possibility of undesirable stalling characteristics.

3.1.7.11 High Lift Devices

The following paragraphs illustrate the devices which can be used to delay the stall and, therefore, allow the use of lower takeoff and landing speeds. In general, high-lift devices will be retractable since they generate drag (see later) as well as lift. The manufacturer will want to endow his product with efficient, high-speed cruising performance as well as good low-speed characteristics and so the high speed and low speed configurations may be radically different.

3.1.7.11.1 Flaps

The basic high-lift device, common to most types of aircraft is the trailing edge flap. Figure 3.47 shows how a 'plain flap' operates. Plain flap operation is, of course, the principle used by ailerons, elevators and rudders, the principle being that deflection of the surface increases the camber of the airfoil and therefore increases lift at the existing angle of attack and velocity. In the diagram its operation can be compared with the split flap, the slotted flap and the Fowler flap. It will be seen from the accompanying curves that the first two are similar in performance; the slight differences can be attributed to the retention of attached flow to the fixed upper surface of the split flap installation.

The slotted flap allows the pressure differential between upper and lower surfaces to generate a flow through the slot ahead of the flap. Because the slot is convergent, the air is accelerated and is introduced, tangential to the flap upper surface, into the boundary layer and delays separation. The Fowler flap not only increases the camber but also the surface area of the wing thereby changing both the C_L and S terms in the lift equation. When extended, the Fowler may also be slotted, taking advantage of this form of boundary layer control (*BLC*) and hence, as the $C_{L\alpha}$ curves show, giving the biggest boost to C_L .

3.1.7.11.2 Boundary Layer Control

The control of the boundary layer mentioned in relation to slotted flaps above is an alternative to increasing camber as a means of achieving lower stall speeds. Instead of increasing C_L throughout the range of angle of attack (see effect of flap on C_L in Figure 3.51), *BLC* extends the existing curve to higher values of C_{Lmax} by delaying separation. The simplest form of *BLC* is the slot which has already been mentioned; however, slots are not necessarily associated with flaps.

A simple fixed slot close to the leading edge of an airfoil will introduce high energy flow into the boundary layer at an early stage. Such an arrangement may be required if the basic airfoil has a small radius leading edge. A slightly more complex arrangement is the movable slat which can be faired part of the basic airfoil or can move to open a slot close to the leading edge. Automatic slats are easily engineered. The slot will be spring-loaded open and when α and dynamic pressure reach the required

values, the stagnation pressure at the stagnation point will close the slat and hold the slat in until an increase in α or a reduction in dynamic pressure necessitate its opening.

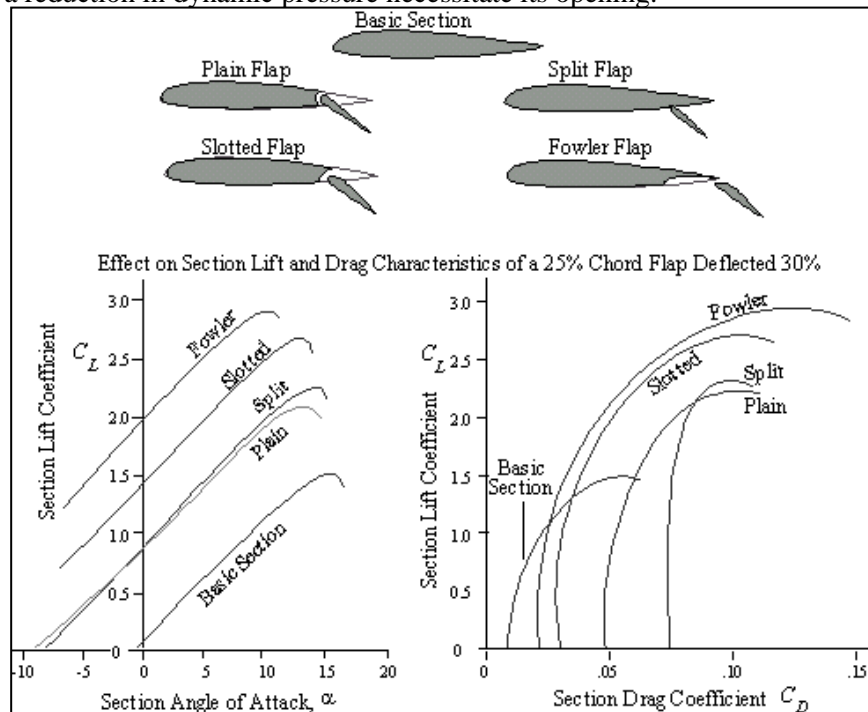


Figure 3.51 Flap Configurations

An alternative and potentially very cheap method of controlling the boundary layer to prevent sharp leading edge separation is to encourage the laminar boundary layer to separate sooner. The base cause of the undesirable 'instant' separation is that once the laminar layer detaches to transition to turbulent flow, it has insufficient energy to reattach even after transition. If the layer were made to detach while its energy level was higher then it might achieve reattachment. Such 'persuasion' might be simply achieved by making the leading edge rough; sandpaper-like surfaces have proved successful in the past. Another option is to attach a span-wise wire or metal bead strip along the leading edge to "trip" the laminar layer into separation. A final innovative method is to detect the characteristic pressure pulses present in the transition areas using microphones. The pulses are then amplified and fed to speakers along the leading edge of the airfoil. This acoustic method excites the boundary layer into transitioning into turbulent form by placing the characteristic pulses into the more energetic layer.

Another form of *BLC* is upper surface suction. A vacuum chamber is built into the wing and tappings from the chamber to the upper surface are made. The tappings may simply be a large number of small holes; in future applications, modern materials which make the upper surface porous are likely to be used. The vacuum draws the low-energy layers of the boundary layer down from the surface and allows them to be replaced with higher energy air from closer to the free stream, delaying boundary layer separation by substantial amounts. Figure 3.52 shows the *BLC* arrangement and the changes in $C_{L\alpha}$ which they achieve.

A good example of *BLC* suction was the US Army XV-11 which used nearly a million tiny holes in the wings and forward fuselage as the air inlet for the turboprop engine.

An equally complex and costly method of boundary layer control is upper surface blowing. High pressure air is ducted through slots tangential to the airfoils upper surface and adds energy to the boundary layer. The slots can be at any point along the chord length depending where critical separation is taking place. Blowing flaps is particularly popular since separation is most likely to occur where there is a large change in camber. While the theory of slots and of upper surface blowing is similar, it is, of course, possible to inject far more energy into the boundary layer from powered blowing than when simply relying on aerodynamic pressure differential. The technique has been particularly popular on carrier-borne aircraft.

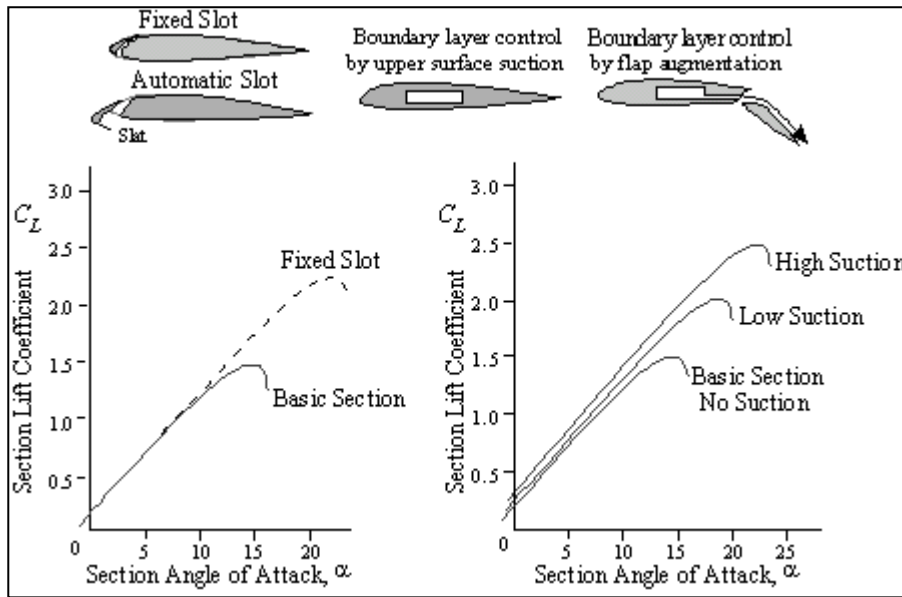


Figure 3.52 Effects of Slots and Boundary Layer Control

3.1.7.11.3 Practical Combinations

It is commercial pressure demanding high-speed, efficient cruise and a high degree of takeoff and landing flexibility which has driven the development of the most complex high lift devices. In practice, modern airliners use combinations of leading and trailing edge devices and of camber variation, surface area and *BLC*. Figure 3.53 shows a typical airfoil section. The Kruger flaps at the leading edge are hinged at what becomes their trailing edge and in high speed flight they fit flush into the lower surface of the airfoil. Their deployment increases camber and, in this case, also introduces a slot near the leading edge. Other variants are unslotted. In this case, once the stagnation point moves aft of the Kruger flap leading edge, a buildup of pressure occurs which eventually simulates a large leading edge radius and helps to prevent separation. The trailing edge flap in Figure 3.53 is a double-slotted Fowler type. In this case camber and surface area are both increased and two *BLC* slots are opened.



Figure 3.53: Slotted Kruger and Fowler Flap.

Figure 3.54 shows the high lift devices used on the Boeing 737 and the leading and trailing edges of the MD11's wing respectively. The Boeing boasts triple slotted flaps which reduce the aircraft stalling speed by up to 30%. The Douglas aircraft has positions which are optimized for takeoff and landing cases and the complexity need not end here.

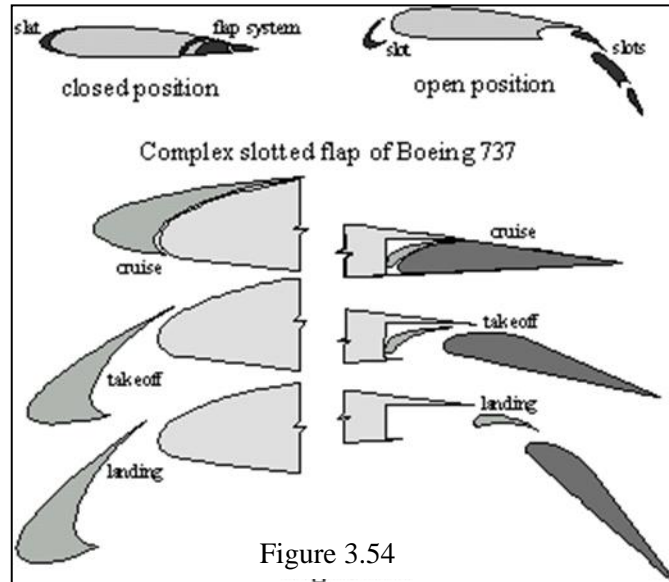


Figure 3.54

Operation of leading edge devices may not be equal over the entire span; it is common for a different setting to be used ahead of the aileron to improve roll control. Flap retraction may lock the ailerons in the neutral position leaving the pilot reliant on the small, high-speed ailerons and spoilers for roll control.

When flaps are extended, ailerons may themselves take on the form of flaps by 'drooping' from the neutral position. Many combinations are used and it seems certain that not all combinations have been tried. The mission adaptive wing on the AFTI F-111 used a smooth, flexible structure that changed camber to provide optimum performance and gust alleviation. NASA research with the augmentor wing Buffalo and the QSTOL aircraft are examples of powered lift. The Boeing YC-14 used ducted engine efflux to attain extremely high values of C_L and the Douglas YC-15 had engine exhausts directed into slotted flaps.

3.1.7.11.4 Practical Problems

Reference to Figure 3.52 will show that leading edge devices, particularly slots, only achieve extra lift by increasing α . To increase α , the aircraft must fly more nose high to achieve the same flight path. This highlights a problem encountered by some airliners. If the trailing edge flaps fail to deploy, the aircraft may be unable to decelerate to its usual margin over the stall ($1.3V_s$ for the approach case) because the geometry of the aircraft will bring the rear fuselage into contact with the runway before the wheels touch. This limitation made the rear fuselage engine mounting with its aft mounted wing and landing gear very popular. Conversely, if the leading edge devices fail, the pilot may be unable to use full trailing edge flap without a risk of landing the aircraft nosewheel first. Variations in flap/slat settings have startling effects on the pilot's perception of the landing maneuver.

Clearly, lift is the property which the airfoil surfaces on an aircraft are designed to provide. Unfortunately, production of lift must be paid for and the price of lift is drag. It is drag which will concern us for the remaining paragraphs in this text.

3.1.8 Drag

3.1.8.1 Introduction

The manufacturer's prime objective in providing his aircraft with engines is to give the pilot the ability to add energy in the form of increased speed and altitude. Unfortunately, the fact that the aircraft moves through a viscous fluid and produces lift with a finite length wing, generating drag, means that the aircraft must use its engines constantly simply to maintain its energy level. In the absence of drag, once the aircraft had climbed to height and accelerated to cruising speed, the engines could be reduced to zero thrust like a spacecraft; but for aircraft this will never be. To produce lift, an aircraft will always produce drag; even ballistic missiles which do not rely on aerodynamic lift produce drag! In truth, drag has its advantages; without it, the aircraft would have to expend energy to slow down which would make the approach to landing interesting to say the least. Drag, then, is an important characteristic and the next few paragraphs will examine it in detail.

3.1.8.2 Components of Drag

Figure 3.55 itemizes the components which make up total aircraft drag. Total drag is the only one which can be measured, and that indirectly, in flight. By obtaining a range of readings across a spectrum of C_L values, it is possible to extrapolate and find the parasite drag element; parasite drag is the drag in incompressible flow which is not reliant upon lift. It is the zero-lift drag. Induced drag is the drag created by lift and falls to zero when lift is zero. Induced drag is at its highest when C_L is highest. Wave drag, sometimes called Mach drag, is a result of compressibility and its cause and effect will not be discussed here.

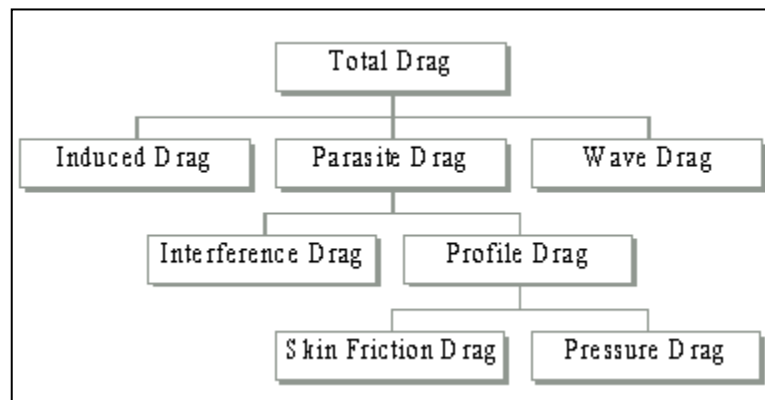


Figure 3.55 Components of total drag

3.1.8.3 Real Fluid Flow

Before starting to look at the individual components of drag, it is convenient to recap the properties of real fluid flow around an airfoil. Figure 3.56 shows typical flow around an airfoil and highlights the effects of the fluid's viscosity. The first effect is that there is a boundary layer. The next is that the boundary layer loses energy, becomes thicker and eventually transitions from laminar flow into turbulent flow. Eventually even the high-energy boundary layer loses energy. This happens because the adverse pressure and friction are continually combating the downstream velocity, eventually reversing it. With the flow moving downstream at one point along the chord and upstream at another point, it will

collide and separate from the airfoil's surface, causing a premature pressure recovery over the surface and generating a turbulent wake.

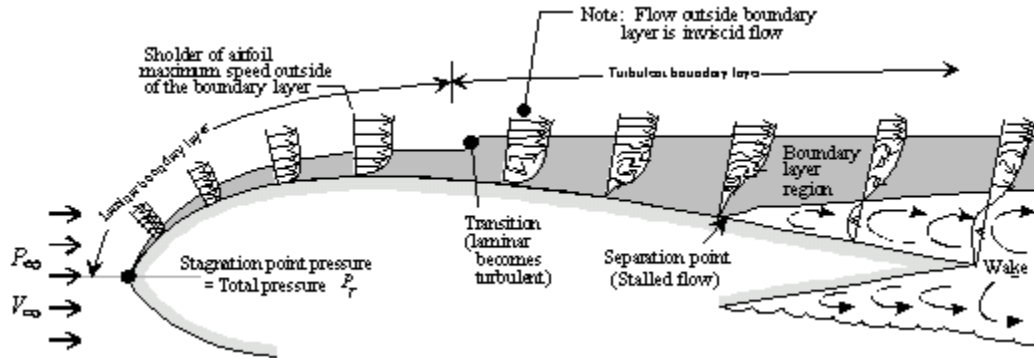


Figure 3.56

3.1.8.4 Skin Friction Drag

The first component of profile drag which we shall consider is skin friction. Figure 3.57 compares the forces acting on an airfoil at rest and those acting on an airfoil moving through an ideal fluid. As seen in Figure 3.27, we have already discussed how the motion produces changes in the static pressure (arrows marked P); we must now look at the shear forces being produced by the viscosity of the fluid and its proximity to the airfoil surface.

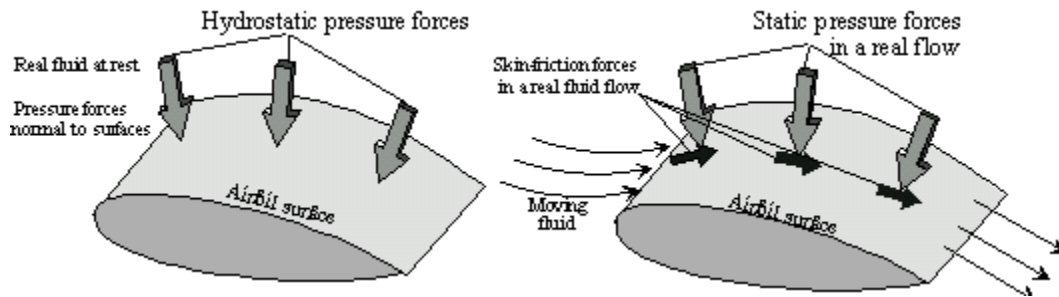


Figure 3.57 Pressure and Viscous Forces

Figure 3.57 compares ideal and real (i.e. inviscid and viscous in this subsonic application) flow by showing the differences between the flows over a flat plate parallel to the airflow. The boundary layer in the ideal fluid has the same kinetic energy and the same pressure energy as the free stream. In reality, however, the fluid's viscosity causes the flow in contact with the surface to be reduced to zero and subsequent layers above the surface are travelling at progressively higher velocity until, at the same stage, the free stream velocity is achieved. Because the layers of air are travelling at different velocities and because the air has viscosity, frictional forces are generated between the airfoil surface and the free stream. The accumulation of these forces is known as skin friction drag.

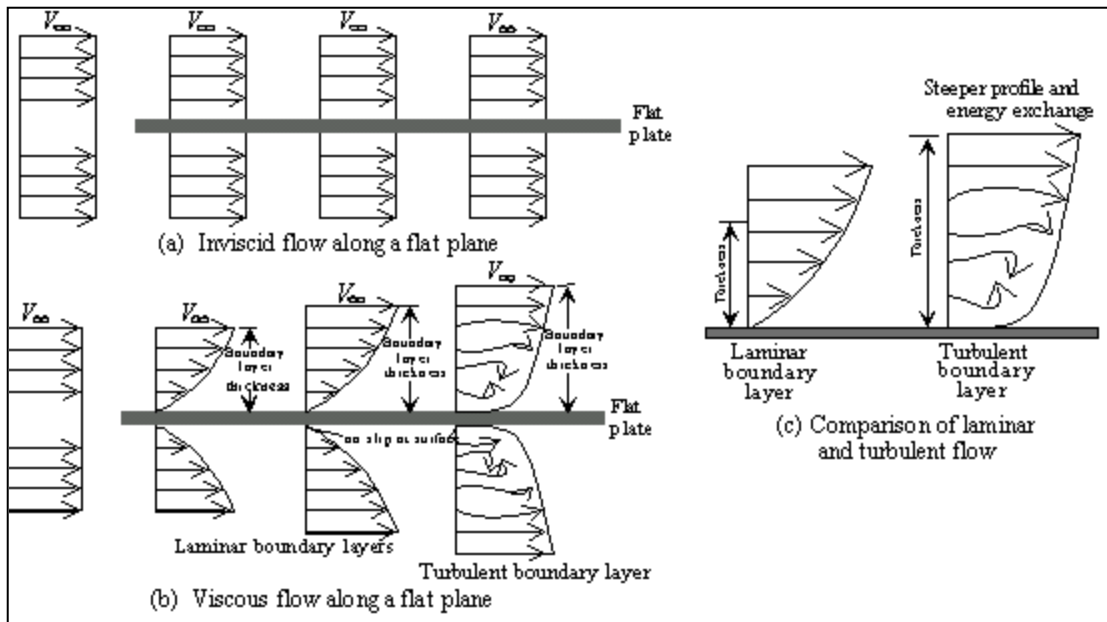


Figure 3.58 The Causes of Skin Friction Drag

The magnitude of the force will be a function of the velocity gradient (i.e. the change of velocity between adjacent layers). Because a turbulent boundary layer has higher energy air close to the airfoil surface, its velocity profile is steeper and so a turbulent boundary layer produces more drag than a laminar boundary layer; the ratio is typically 7:1. It should be noted that a boundary layer can be less than a centimeter thick; in that distance, the air must change from static with respect to the surface to a relative velocity in the order of hundreds of feet per second.

The thickness of a boundary layer is about 1% of the distance the flow has traveled along a surface. This is why jet engine inlet splitter plates or inboard intake lips are located a few inches from the fuselage side. (i.e. F-4, F-111, F-15, F-16, F-22)

It is not surprising, therefore, that large frictional forces are produced. Also, of course, the effect applies to the entire aircraft, not simply to the airfoils, so skin friction can be a large contributor to drag.

3.1.8.4.1 Boundary Layer Transition

The transition from laminar flow with low drag and low energy to turbulent flow which has high skin friction drag and high energy is a function of Reynolds number, pressure gradient and surface roughness.

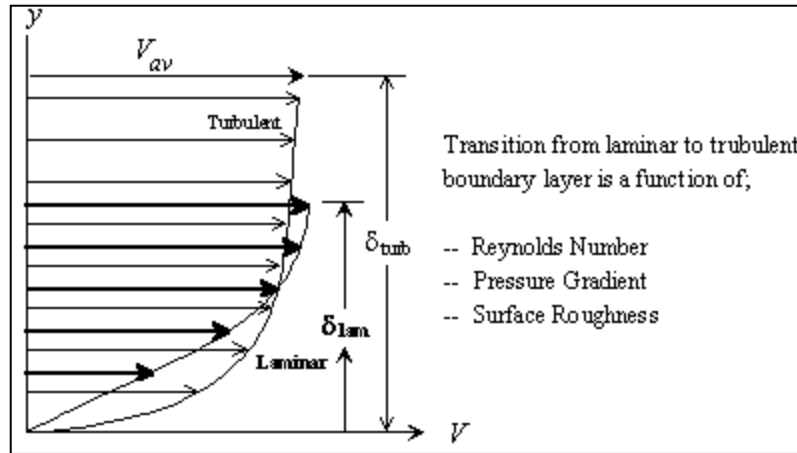


Figure 3.59 Comparison of Laminar and Turbulent Boundary Layer Mean Velocity Profile

3.1.8.4.2 Reynolds Number

Dr Reynolds, in 1894 at the University of Manchester in England, proved the importance of Reynolds number in the transition from laminar to turbulent flow. The series of experiments with water in pipes showed that when the Reynolds number was less than 2100, the flow in the pipe was always laminar and when greater than 40,000 the flow was always turbulent.

$$Re = \frac{\rho V l}{\mu}$$

where ρ = density

V = velocity

l = representative length along the flow

μ = coefficient of viscosity

At Reynolds number between 2100 and 40,000 the flow was a mixture of laminar and turbulent flow. Figure 3.56 shows a schematic of Reynolds pipe experiments. For aircraft, a Reynolds number of about 1,000,000 defines the transition from laminar flow. Inspection of this figure shows that the local Reynolds number (Re_x) at the leading edge of a surface is zero, but can grow rapidly as the flow moves

along the length of the surface. If a surface is long enough, any flow can become turbulent due to Re only. Pressure gradient and surface roughness can "trip" the boundary layer into turbulence sooner.

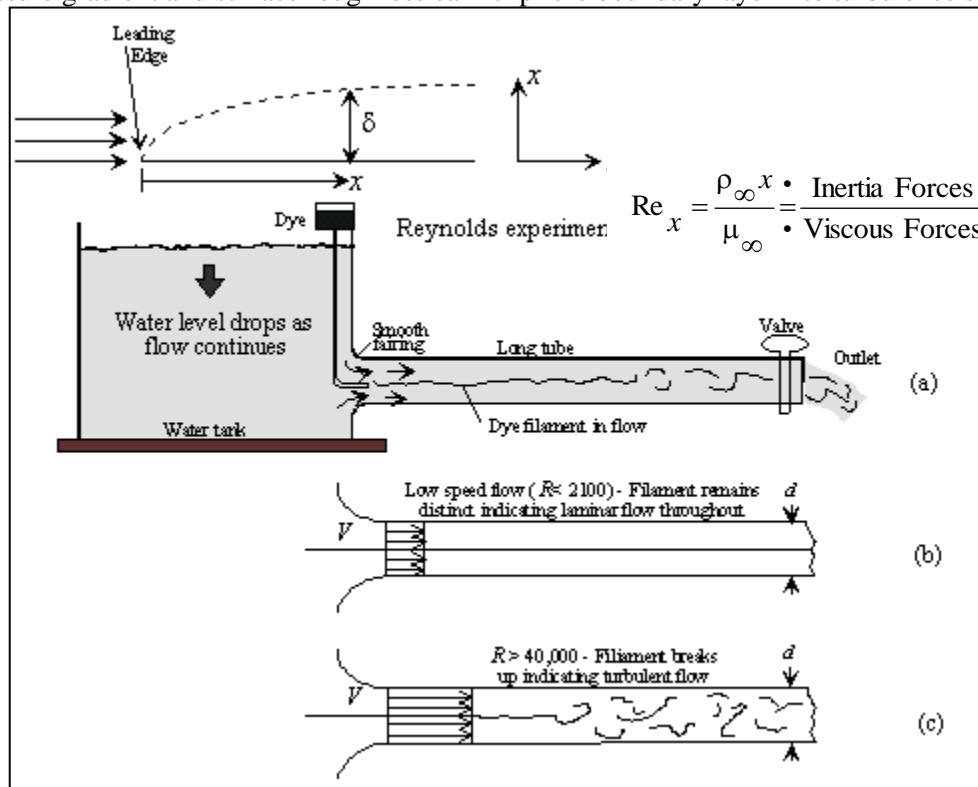


Figure 3.60 The Effect of Reynolds Number of Transition

3.1.8.4.3 Pressure Gradient

The highest pressure on a wing is on the leading edge at the stagnation point where the flow velocity is zero. From the stagnation point to the maximum velocity point on the airfoil, the flow accelerates in the favorable pressure gradient. In a favorable pressure gradient, the boundary layer gains energy and will tend to remain laminar. From the lowest pressure point on the airfoil to the trailing edge on the upper surface the local static pressure increases generating an adverse pressure gradient. Advancing against an adverse pressure gradient is similar to coasting uphill and the boundary layer loses energy. The low energy laminar boundary layer momentarily separates from the surface and reattaches as a turbulent boundary layer. The turbulent boundary layer has more skin friction drag but also more energy due to the intermixing of the shear layers and will remain attached in an adverse pressure gradient for a longer period of time than the low energy laminar boundary layer.

Since transition from laminar to turbulent flow in the boundary occurs shortly after the minimum pressure point on an airfoil it would appear reasonable to design airfoils so that the minimum pressure

point occurs as far aft as possible. Figure 3.61 shows the pressure distribution around two different airfoil sections.

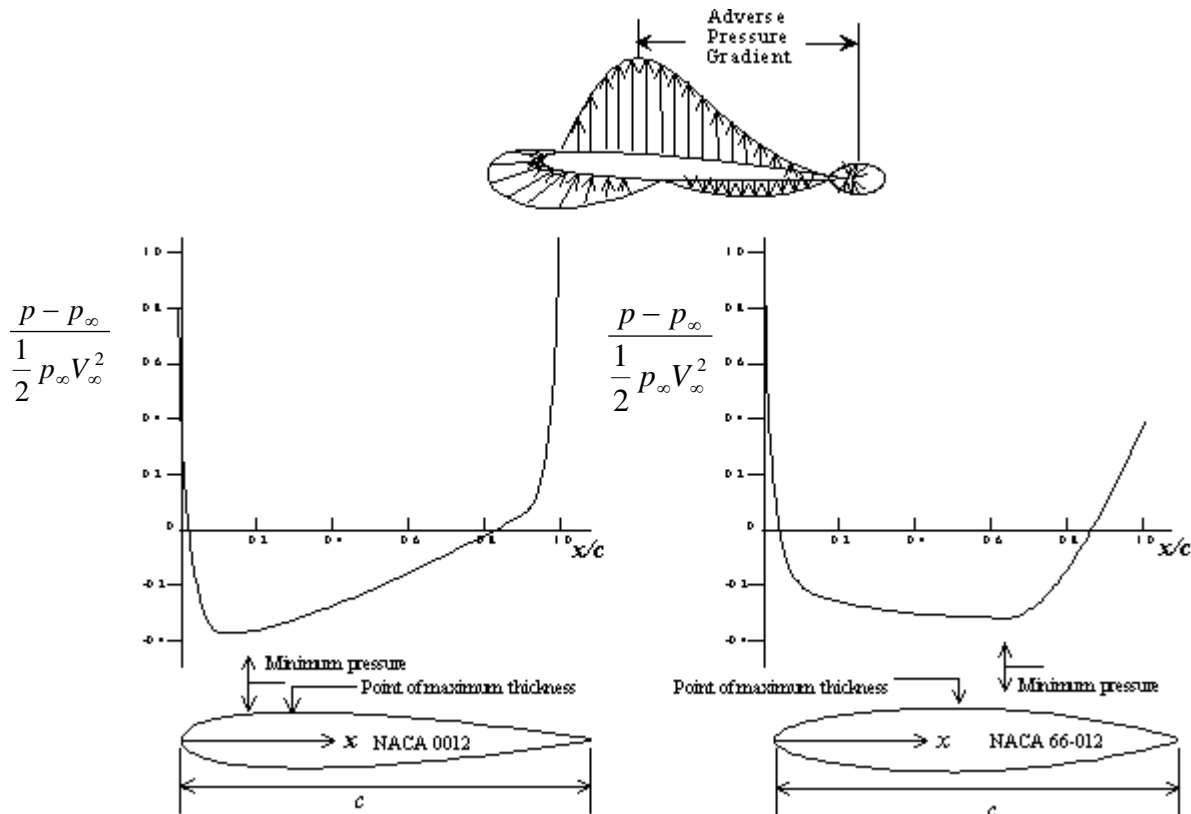


Figure 3.61 Pressure Gradients of Airfoils

The NACA 0012 airfoil section has a minimum pressure point at approximately 20% chord whereas the NACA 66-012 airfoil has a minimum pressure point at a approximately 60% chord. From a pressure gradient viewpoint only, the NACA 66-012 airfoil should have approximately three times more laminar flow than the NACA 0012 airfoil resulting in significantly lower skin friction drag. Unfortunately, such a "laminar flow" wing is expensive to build and very sensitive to any sort of surface defect.

3.1.8.4.4 Surface Roughness

Surface roughness will have a profound effect on the transition from laminar to turbulent flow as can be seen from Figure 3.62. As surface roughness increases, the transition will occur closer to the leading edge resulting in higher skin friction drag. Round head rivet and fuel caps are prime examples of turbulence producers. Insects that impale themselves in the leading edge of wings (the insect belt is close to the surface of the earth), promote transition and generate turbulent wedges trailing aft from the insect.

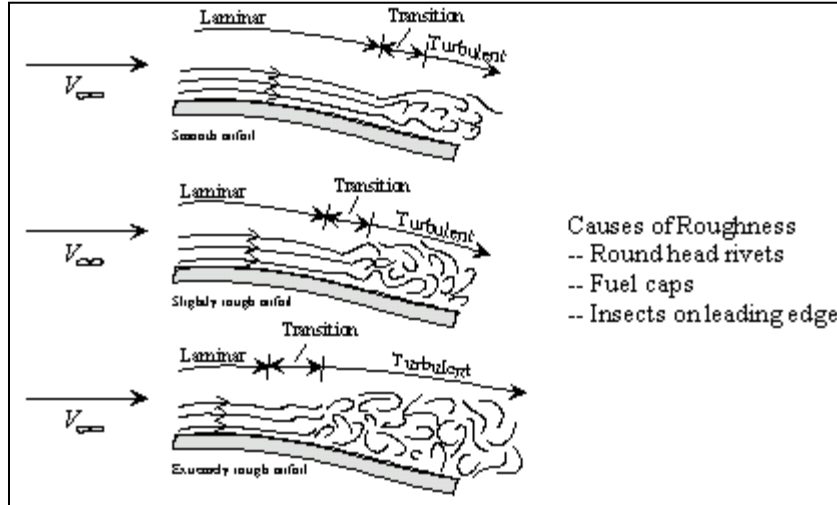


Figure 3.62 Effect of Surface Roughness in the Boundary Layer Transition

Whether caused by Re , pressure gradient or surface roughness, the effect of transition from laminar to turbulent flow on the skin friction coefficient of drag is shown in Figure 3.62. At low Reynolds numbers of about 10^6 , turbulence increases the C_f by a factor of five. Approximate equations for estimating the skin friction coefficients for both laminar and turbulent flow are also shown in Figure 3.63.

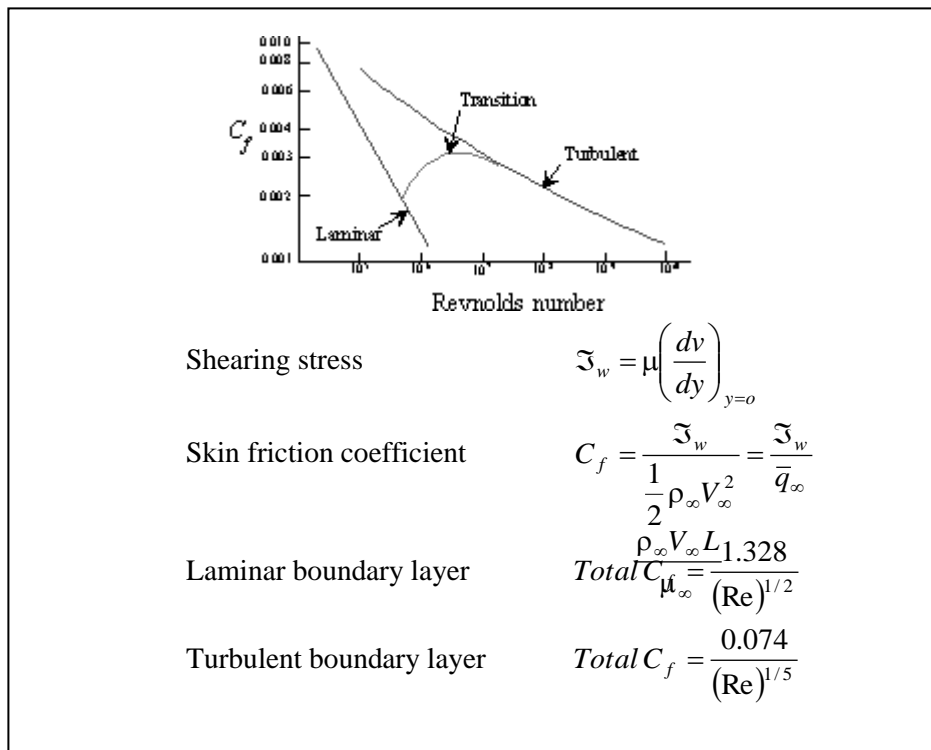


Figure 3.63 Skin Friction Coefficients as a Function of Reynolds Number

3.1.8.5 Pressure Drag

The other component of profile drag is pressure drag. If Figure 3.64 is compared with Figure 3.28, the effects of the fluid's viscosity will be clearly seen. In approaching the leading edge of the airfoil, there is little difference between ideal and real fluid flow. In reality it is even possible to realize almost theoretical stagnation pressure. Soon after the flow around the airfoil starts, however, reality begins to diverge from ideal theory. The losses to friction in the boundary layer mean that the lowest pressure is never realized and, once separation occurs, there is a sudden jump in static pressure over the airfoil up to near freestream static pressure. In consequence, since there is no stagnation point at the trailing edge, total pressure will not be reached and a pressure differential will exist between leading and trailing edges. This pressure differential multiplied by a representative cross-sectional area related to airfoil thickness will produce a retarding force called pressure drag.

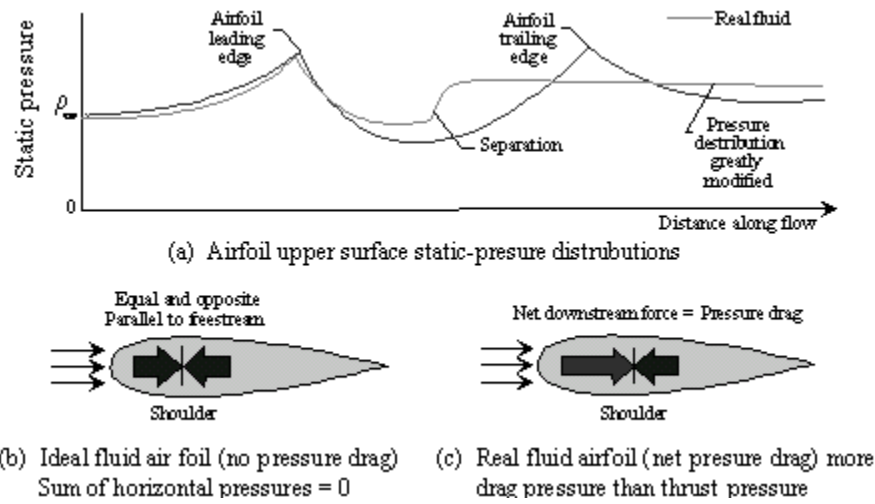


Figure 3.64 Real Fluid Effects on an Airfoil

3.1.8.5.1 Flow Separation

The boundary layer will lose energy in an adverse pressure gradient and will eventually reach the condition of having insufficient energy to fight the pressure gradient and will separate from the airfoil surface. When the flow separates, the wake size increases and the pressure drag increases significantly. The pressure in separated flow quickly reaches static pressure and with the total pressure at the stagnation on the front of the airfoil the pressure drag is maximum. The pressure drag is essentially proportional to the size of the wake behind the body.

Figure 3.65 shows the effect of separated flow on the pressure distribution around an airfoil and it is obvious that separated flow causes a dramatic loss of lift and a severe increase in drag.

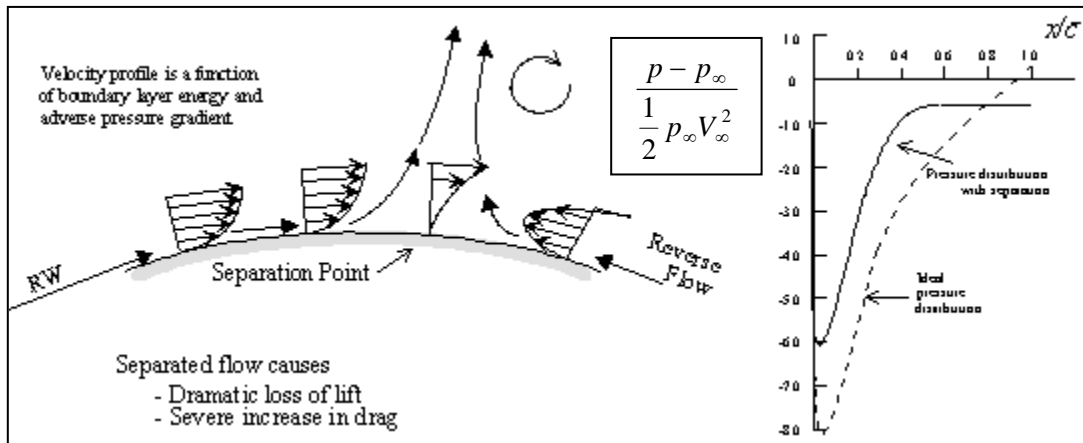


Figure 3.65 Flow Separation Effects on Pressure Distribution

The minimum drag condition for any aircraft occurs when the separated flow is eliminated and the surface is smooth to maximize the region of laminar flow. Therefore if an aircraft does not meet its performance requirements, rather than blame the engine, it would be a good idea to completely tuft the aircraft, fly in the cruise condition and using a chase aircraft with a photographer look for separated flow on the aircraft. If separated flow is found, then some sort of aerodynamic contouring must be performed to eliminate the separated flow.

3.1.8.5.2 Streamlining

Skin friction is a function of the surface area wetted by the airstream and any increase in surface area will increase this component of drag. Pressure drag is a function of the size of the wake behind an object in an airstream; it can be reduced by streamlining the object in order to delay separation of the flow. A side effect of streamlining is an increase in the wetted area and hence the skin friction, so it is important to ensure that a net reduction in drag is actually achieved when adding streamlining. Figure 3.66 compares the drag coefficients of various shapes which are immersed in the same airstream. The first three shapes even have the same Reynolds number because they have the same frontal area.

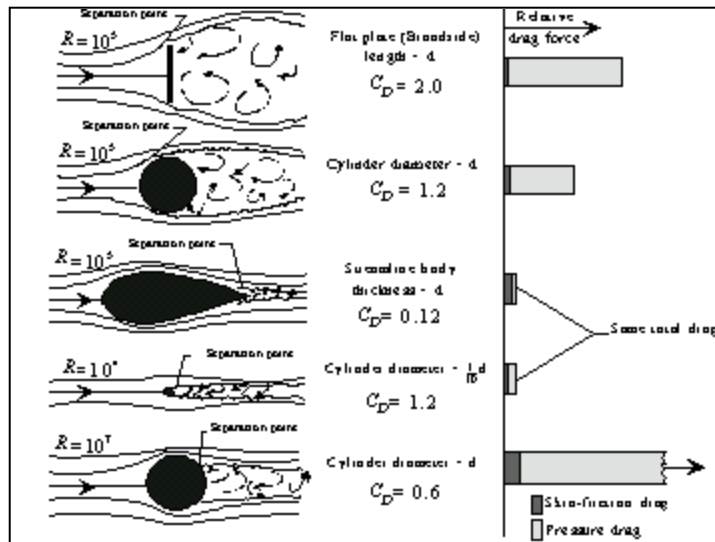


Figure 3.66 Drag Coefficients of Various Bodies

The flat plate has almost no skin friction drag because the flow is attached to the plate only at the edge. The plate does, however, generate a strong, turbulent wake, so pressure drag is very high. Because a flat plate normal to the airstream creates so much drag, one might think that aerodynamicists would avoid such additions to aircraft. Examination of the *NTPS Dove* will reveal an antenna on the nosewheel door which is an effective flat plate normal to the relative wind when the landing gear is raised.

If a cylindrical cross-section is used instead of a flat plate, the airflow stays attached to the surface almost to the shoulder producing more skin friction drag but reducing the strength of the wake and, therefore, the pressure drag. The diagram shows that the total drag is 40% lower than that of the flat plate.

Proper streamlining of the same basic diameter reduces the total drag to 6% of the flat plate drag. The skin friction component is almost four times as large as in the flat plate's friction but, because the flow stays attached for almost all of the surface area of the streamlined shape, the wake and, therefore, the pressure drag, are minimized.

Perhaps the most startling revelation in Figure 3.66 is that the small cylinder generates the same amount of drag as the streamlined shape. The Reynolds number changes only because of the dimensional change; all the airflow parameters remain the same as in the three previous examples. The drag coefficient, C_D , is ten times that for the streamlined shape and since the dimensional term is one tenth that of the shape, the cross-sections have equal total drag. The small cylinder might be the size of an unfaired landing gear leg, a pitot head mast or an antenna, so it cannot be assumed that "small" additions to an aircraft will be insignificant in terms of drag increments.

The final diagram shows the large cylinder again but operating in an airflow with one hundred times the velocity of the earlier examples. Because the added velocity makes the boundary layer more energetic, the flow remains attached to the cylinder past the "shoulder" producing a smaller wake. It might be expected, therefore, that the pressure drag would be less than in the second example but, of course, this is not the case. The stagnation pressure is a function of V^2 and is thus much higher while the pressure in the wake is almost independent of the free stream velocity (i.e. close to the free stream static pressure). So, although the wake cross-section is smaller, the pressure differential is much larger, generating higher pressure drag. The skin friction drag element is also larger, firstly because the wetted

area is larger and also because the boundary layer has a higher velocity profile. The significant factor in the final diagram is the drag coefficient, C_D , which is only 50% of that realized by the same cylinder in a slower moving airstream. If the airflow could be induced to stay attached when $R_N = 10^5$ to the same degree it does when $R_N = 10^7$, then the total drag would be halved. One method of achieving prolonged attachment would be to induce separation of the laminar boundary layer at a stage when it had sufficient energy to reattach to the cylinder following transition to turbulent flow. Surface roughness might achieve this. In fact this is the principle used in dimpling golf balls. If the golf ball were smooth its drag would be higher and it would not fly so far, Figure 3.67.

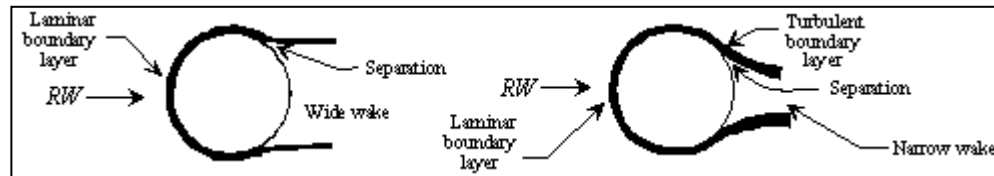


Figure 3.67 Drag Reduction Due to Boundary Layer Transitions

The sum of skin friction and pressure drag is called "profile" drag because all factors are determined from the side view of the object in question.

3.1.8.6 Interference Drag

Each component of an aircraft which is exposed to the airflow will produce drag. If these drag elements are measured and totaled, the result will be a drag which is less than that realized if the drag of the total aircraft is measured. The difference is called interference drag and is caused by the interaction of flows around various parts of the aircraft. Corners like those usually found between horizontal and vertical stabilizers and between wings and fuselage are the main culprits but any small addition to the basic airframe will also contribute. The interaction of the airflows will be the type of disturbance which promotes separation; transition may thus occur early increasing skin friction and wake formation may also be early increasing pressure drag. The effect of interference drag may be insidious. Flight testing at the start of an aircraft's life will lead to a C_D for the basic aircraft. Additions to the aircraft during its life (e.g. antennas, electro-optical sensors, weapons, pylons) will have their drag components measured before installation and the change in C_D will be allowed for in the performance manuals. Because a complete performance flight test program is extremely costly, it is unlikely that the true increase in C_D will be measured and the aircraft may reach retirement with a C_D considerably higher than the estimated data show. Figure 3.68 shows the type of changes which were made and indeed are still made during an aircraft's operational life; the aircraft depicted is a TBF Avenger of WWII vintage.

Condition	Airplane Configuration	C_D at $C_L = 0.254$	Reference Condition (see column 1)	ΔC_D
1	Airplane completely sealed and faired.	0.0183	---	---
2	Flat plate removed from nose.	0.0189	1	0.0006
3	Seals removed from flapped-cowling air exits.	0.0199	2	0.001
4	Seals removed from cowling-flap hinge-line gaps.	0.0203	3	0.0004
5	Exhaust stacks replaced.	0.0211	4	0.0008
6	Canopy fairing removed, turret leaks sealed.	0.0222	5	0.0011
7	Tail wheel and arresting-hook openings uncovered.	0.0223	6	0.0001
8	Aerial, mast, and trailing antenna tube installed.	0.0227	7	0.0004
9	Canopy and turret leak seals removed.	0.023	8	0.0003
10	Leak seals removed from shock strut, cover plate, and wing-fold axis.	0.0231	9	0.0004
11	Seak seals removed from bomb-bay doors and miscellaneous leak seals removed.	0.0234	10	0.0002
12	Fairings over catapult hooks removed.	0.0237	11	0.0001
13	Wheel-well cover plates removed.	0.0251	12	0.0014
14	Seals removed from tail-surface gaps.	0.026	13	0.0009
15	Plates over wing-tip slot openings removed. Airplane in service condition.	0.0264	14	0.0004
Total Drag Change				0.0081

Figure 3.68 Small Item Influence on Total Airplane Drag

Not all additions to aircraft external structure will increase drag; the type of filleting shown in Figure 3.69 can actually reduce drag by minimizing the interference between wing and fuselage flows and modern aircraft like F-16 blend the wing and fuselage together minimizing this component of interference drag.

Unfortunately, it is difficult to predict the effects of interference analytically and so wind tunnel and flight test measurement must be used to ensure that minimization of this drag is effective.

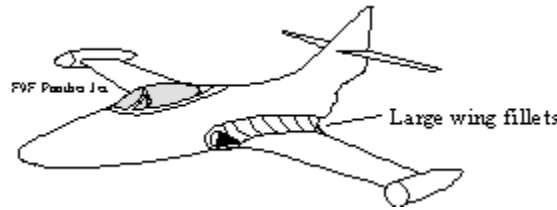


Figure 3.69 Wing Fillets

3.1.8.7 Induced Drag

So far we have only considered profile and interference drag, the components which make up parasite drag. A more descriptive term is zero-lift drag because this drag will be present even when no lift is being produced by the airfoil. We must now look at the second major component of the aircraft's total drag, induced drag. Again a more descriptive term is lift-induced drag, adequately describing the source of this component.

You will recall that the major difference between two-dimensional and three-dimensional flows was described in Figures 3.48 and 3.49 on three-dimensional flow. The result, as far as lift was concerned, was a reduction in C_L across the board. The 3-D effects also influence drag. Figure 3.70 shows how the main feature of 3-D flow comes about.

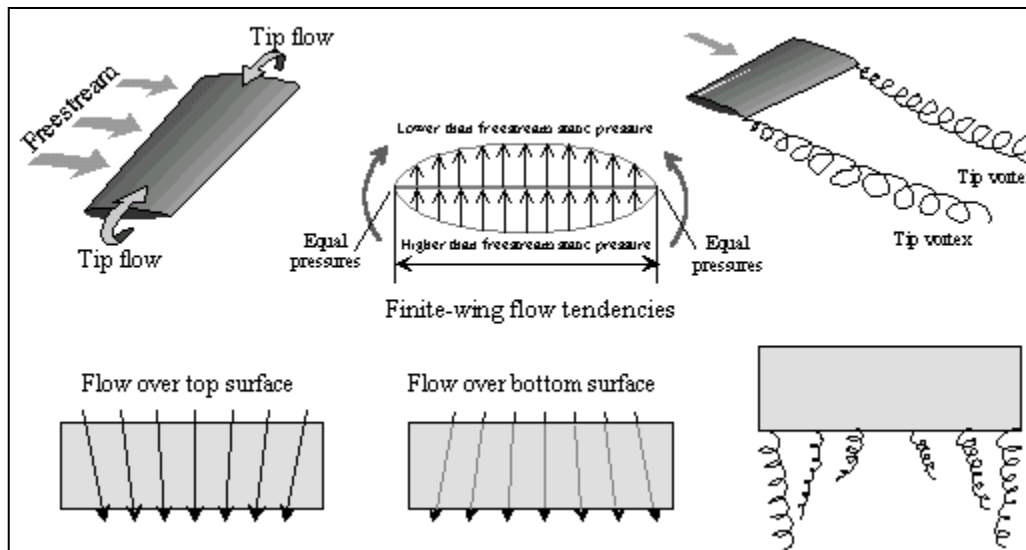


Figure 3.70 Formation of Wingtip Vortices

The pressure differential causes flow around the wingtips adding a spanwise component to the total flow around the airfoil. A vortex is formed at the wingtip by the addition of the free stream flow and the rotational flow around the tip. Further vortices form when the slightly inward flowing air from the upper surface interacts with the slightly outward flowing air from the lower surface at the trailing edge; these subsidiary vortices merge into the wingtip vortices a short distance downstream and the strong vortices so formed persist for considerable distances behind the aircraft.

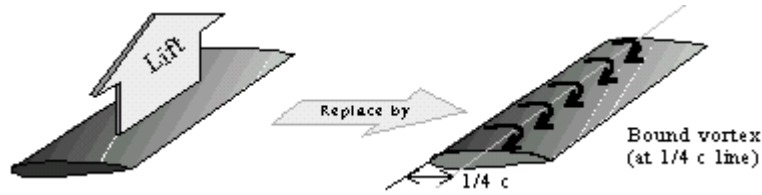


Figure 3.71

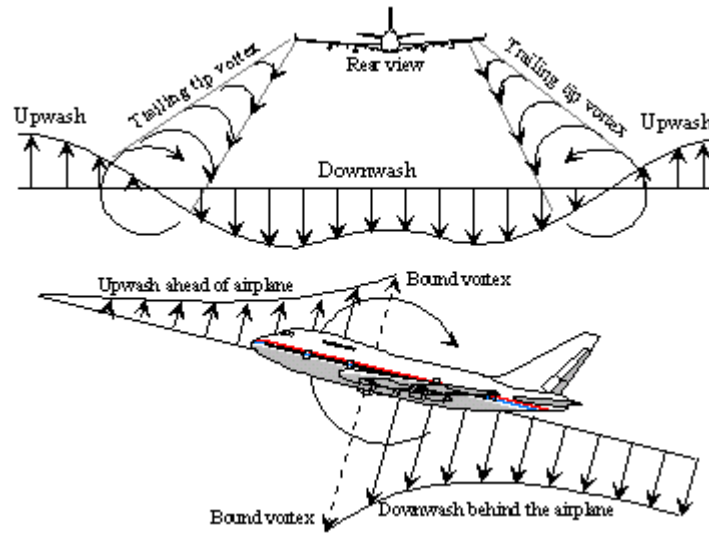


Figure 3.72 Effect of Wingtip Vortices on Downwash

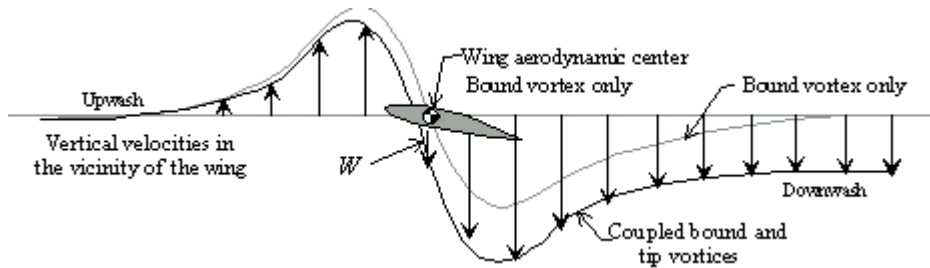


Figure 3.73 Tip Vortex Effect on Downwash Distribution

Airflow around an airfoil can be considered to be a combination of the free stream and spanwise vortex, called the bound vortex, centered at the aerodynamic center (Figure 3.72). The bound vortex adds an upward component to the relative wind ahead of the wing (upwash) and a downward component astern it (downwash). For a 2D wing, the net upwash at the aerodynamic center is zero and, since this is the point through which the lift force is considered to act, the lift vector will be normal to the freestream, Figure 3.68.

However, as Figure 3.74 shows, the wingtip vortices add downwash between the wing tips and therefore distort the upwash/downwash distribution forward along the airfoil's chord resulting in a net downwash at the aerodynamic center. The strength of the vortex will increase as the pressure differential between upper and lower surfaces C_L increases. The increased vertical component will increase this net downwash at the aerodynamic center. Also, if the pressure differential remains the same but the relative wind velocity reduces, the downwash angle will again increase, effectively increasing the downwash at the aerodynamic center.

Now, because lift is the vector acting through the aerodynamic center, perpendicular to the relative wind, and because the local relative wind at the aerodynamic center is the vector sum of the freestream and the downwash component, the resultant local lift vector will not be perpendicular to the freestream relative wind (i.e. the direction of motion of the aircraft). The local lift force vector will be tilted backward. The component of this vector that is parallel to the freestream relative wind resists aircraft motion. This component is *induced drag*. Figure 3.74 shows the vectors associated with the production of induced drag. From the facts stated above, it should be clear that induced drag increases as speed is reduced and also as angle of attack is increased at a constant velocity.

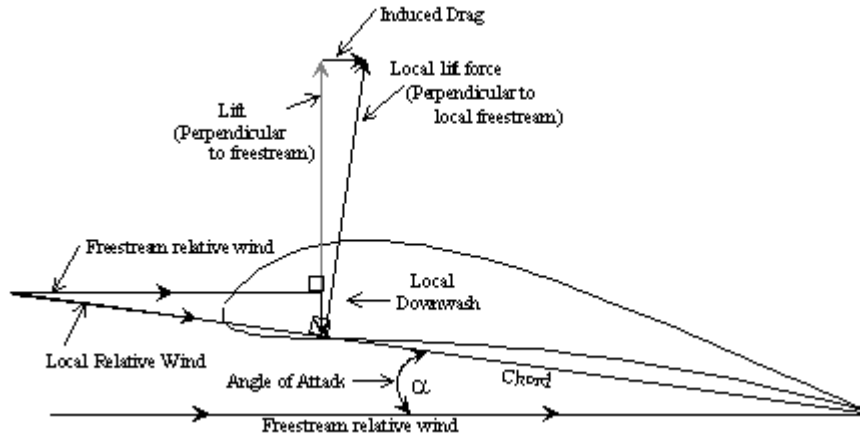


Figure 3.74 Induced drag

Induced drag may, therefore, be a limiting factor for transport aircraft which are required to achieve minimum climb gradients at low speed and also for fighter types which may need the ability to maintain speed during high g combat maneuvering.

3.1.8.7.1 Wingtip Vortex Effects

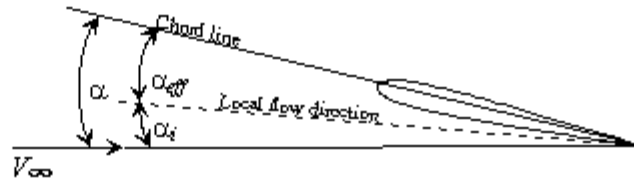
The wingtip vortex that causes induced drag is not limited to the generating aircraft. The strength of the vortices may be such that other aircraft flying into the vortex may be significantly affected by it. In particular, an aircraft entering the vortex along its axis may lack the roll control power to overcome the rotational effects of the vortex. Because the vortices are more energetic when the host aircraft is at low speed and at high weight, the greatest danger arises during the takeoff and landing phases where the disturbed aircraft's chances of recovery are at their lowest. Since the advent of the wide bodied transport, more stringent limitations have been applied on the spacing of following aircraft. This has not prevented all "wake turbulence" accidents, however.

A further effect is most significant to tanker/receiver operations during in-flight refueling. Not only does the receiver have to cope with the rotational problems outlined above but in most cases it must

contend with the downwash field astern the tanker. The effect of flying in the downwash is to reduce the effective angle of attack of the receiver. To maintain position, the angle of attack must be increased, so increasing drag and power requirements. A C-130, refueling from a wide body tanker (KC10, Tristar), needs 100% more power in the refuel position than when flying in the free stream at the same speed and altitude.

3.1.8.7.2 Induced Drag Coefficients

The induced drag is caused by the downwash induced at the aerodynamic center. This downwash is caused by the vortex distribution due to the trailing vortex system behind the aircraft. The induced angle as shown in Figure 3.75, is a function of the spanwise downwash and lift distribution.



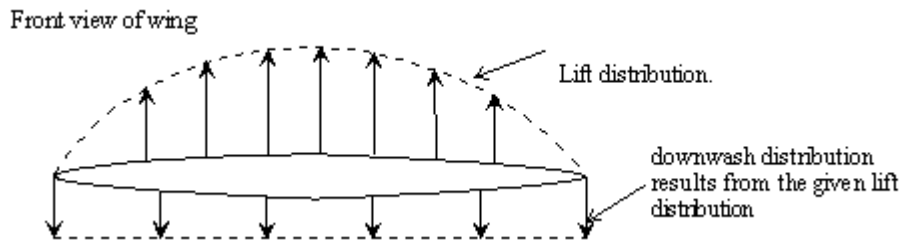
The induced Angle

$$\alpha_i = f(\text{distribution of downwash along wing span})$$

$$= f(\text{distribution of lift along span})$$

Figure 3.75 Definition of Induced Angle

An elliptical lift distribution produces a uniform downwash distribution as shown in Figure 3.76. This is normally obtained with an elliptical shaped plan form wing as was used in many World War II fighter aircraft. A drawback of an elliptical wing is that at high angles of attack the flow will separate evenly along the trailing edge resulting in poor stall characteristics and early loss of roll control.



For a constant downwash distribution

$$\alpha_i = \frac{C_L}{\pi AR}$$

Figure 3.76 Elliptical Lift Distribution

The induced angle α_i at the aerodynamic center of a wing with a constant downwash distribution is given by:

$$\alpha_i = \frac{C_L}{\pi AR}$$

For small angles, the induced drag $D_i = Lift \alpha_i = L \alpha_i$

$$\therefore D_i = L \left(\frac{C_L}{\pi AR} \right) \quad \text{where} \quad L = qSC_L$$

$$\therefore D_i = qSC_L \left(\frac{C_L}{\pi AR} \right) = qS \frac{C_L^2}{\pi AR}$$

$$\text{However,} \quad C_{D_i} = \frac{D_i}{qS} = \frac{C_L^2}{\pi AR} = \quad \text{The induced Drag Coefficient}$$

For other than elliptical wings a "span efficiency factor e " also known as "Oswald Efficiency Factor" is defined such that $e = 1$ for perfect downwash distribution elliptical wings and less than one for other wings. Therefore for real aircraft:

$$C_{D_i} = \frac{C_L^2}{\pi AR e}$$

3.1.8.7.3 Reduction of Induced Drag

Induced drag is inversely proportional to the aspect ratio of the airfoil (i.e. span^2 area). To test this fact with an infinite wing it will be seen that the aspect ratio is infinity and, so, induced drag is zero. On an infinite wing there are no wing tips and, therefore, no wingtip vortices and, therefore, no induced drag. By increasing the airfoil's aspect ratio, we can effectively reduce induced drag. Figure 3.77 shows an aircraft whose wingspan is doubled without changing the wing area. The modified wing has only 25% of the induced drag of the original and, since induced drag represents around 70% of the aircraft's total drag in the takeoff and landing phases, the reduction is particularly significant. Of course, it may not be structurally practical to produce such a wing; gliders, however, have aspect ratios in the region of 35:1.

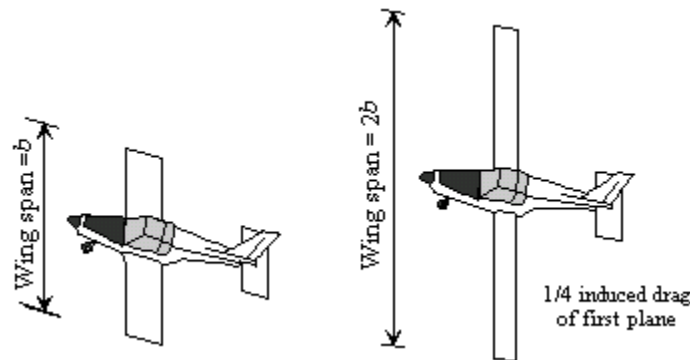


Figure 3.77 Wing- Span Effect on Induced Drag for Airplanes Having Same Wing Area, Same Lift Coefficient, and Same Dynamic Pressure

The effect of increasing aspect ratio is to reduce the average downwash because the wingtips are further apart. The measure of how much wingtip flow exists on a wing of given aspect ratio is the Oswald Efficiency (e) which is governed by the shape of the wing. The magnitude of induced drag is inversely proportional to e , so the larger the value of e (max $e = 1$), the more efficient is the wing.

One of the simplest methods of increasing e on an existing wing is to put end plates on the wingtips to inhibit the flow. Figure 3.77 shows the type of installation which may be used. Tip tanks or such things as tip-mounted missiles will have a similar effect. This idea works particularly well if the designer can meet two requirements at the same time. Examples include carrying needed stores, or combining winglets with vertical fins/rudders.

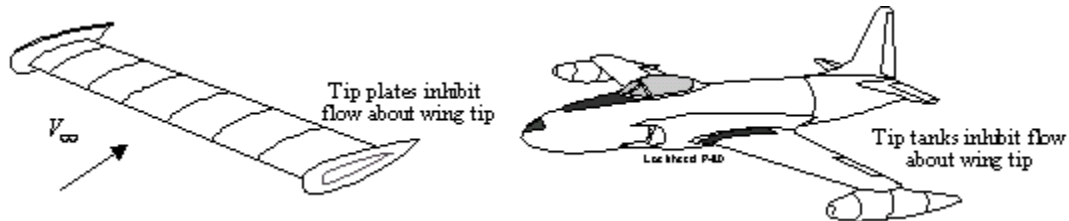


Figure 3.77 End Plates in Theory and Practice

Another method of improving e of an existing wing is to add "winglets". These devices give some endplating and also increase the effective aspect ratio of the wing. Many designs have been tried and many have fallen short of their theoretical gains. Development still continues, however, and Figure 3.78 shows the design for the Douglas MD11 wide body transport.

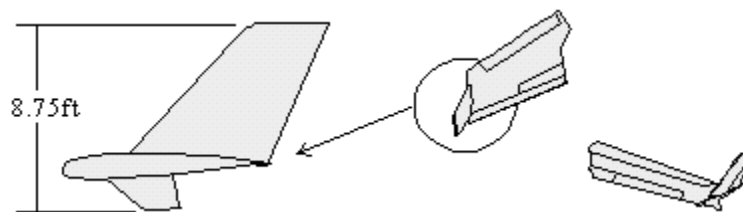


Figure 3.78 MD11 Winglet Installation.

Winglets are considered 'current' technology yet there is nothing new about them. F.W. Lancaster patented endplates for wings in 1897. M.M. Munk performed intensive work on partial endplating of wings in 1921 and the data are shown in Figure 3.76. Munk's data shows that the induced drag will be minimized by using the endplates as span extensions rather than endplates. Therefore the only reason to put winglets on an aircraft rather than an increase in span is because of a restriction in span due to hangarage or parking bay limitations. An increase in span will increase the bending moment at the wing root but so will the winglets which are cambered on the inside and produce a lift towards the fuselage parallel to the wing. If a winglet is generating lift, it would be better to use the lift to reduce stall speeds or increase the weight of the aircraft rather than reduce the induced drag. Nevertheless, with span restrictions, winglets will reduce the induced drag as shown by Whitcomb's experiments. The data point is shown in Figure 3.78.

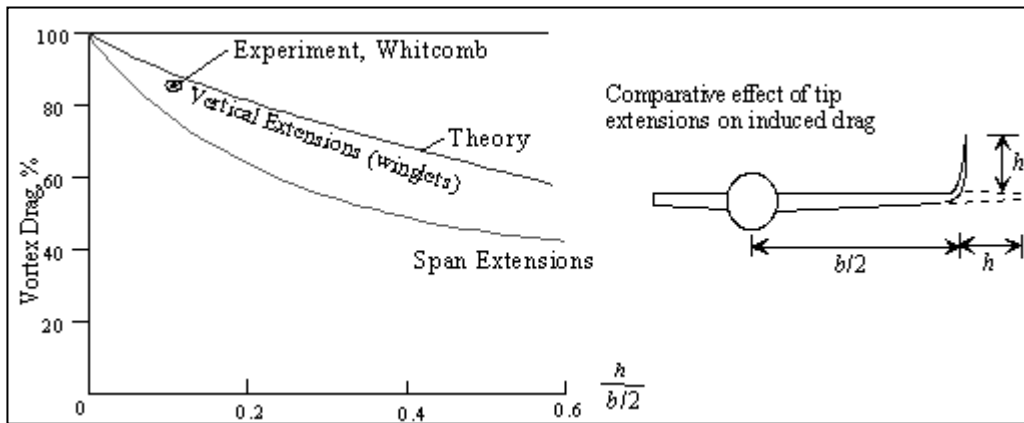


Figure 3.78 Reduction in Reduced Drag due to Partial Endplating.

C. Cone in 1962 performed wind tunnel experiments on non-planar wings, Figure 3.79, which showed that curving a wing upwards resulted in a reduction in drag. Soaring birds have understood this phenomena for a long time.

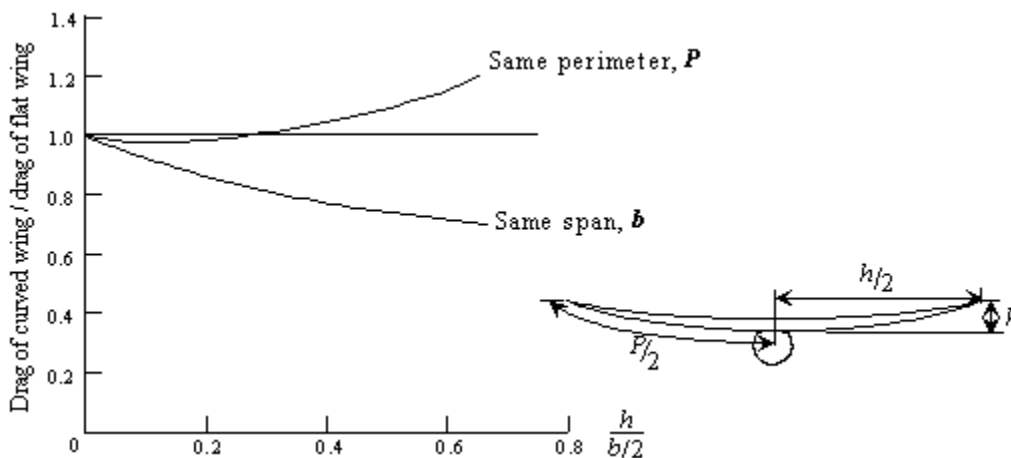


Figure 3.79 Reduction in Drag Due to Non-Planar Wings

Quite apart from these "cut and try" modifications, there are ways of optimizing e at the design stage of the airfoil. Before looking at these methods, it is necessary to define the terms "twist" and "taper" in a wing. The airfoil section may vary in three distinct ways along a wing. Firstly, the chord length may vary. Next, the shape (camber, thickness to chord ratio) of the airfoil section may change and finally the incidence angle may vary, changing the angle of attack.

Figure 3.80(a) shows a wing tapered in both planform and thickness while 80(b) shows a wing tapering in thickness only.

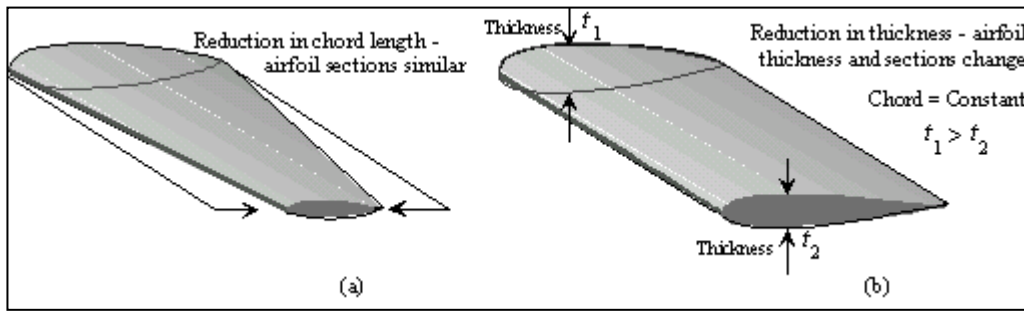


Figure 3.80 Planform and Thickness Taper

The wing may be "twisted" both geometrically and aerodynamically. In geometrical twist, the angle of incidence changes while in aerodynamic twist the airfoil section is changed, changing the characteristics of the wing. Figure 3.79 gives examples of both methods and shows the terminology used.

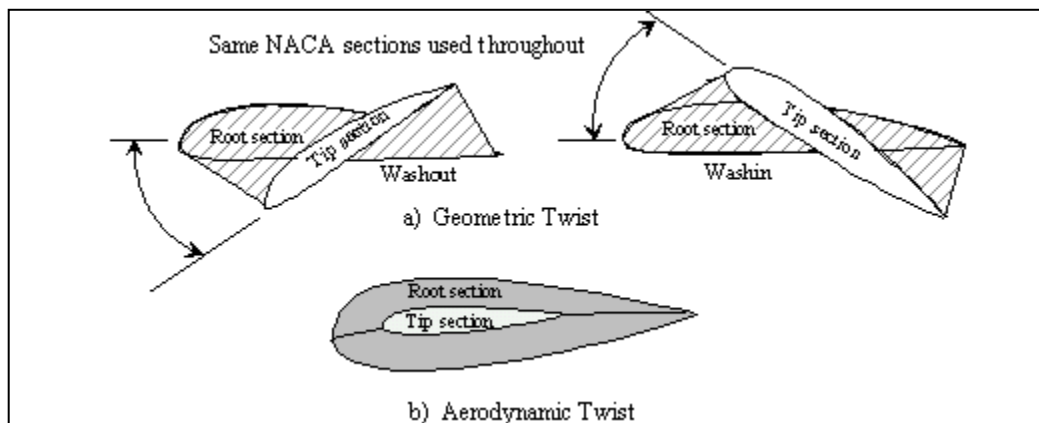


Figure 3.81 Airfoil Twisting

The best value of e theoretically achievable is 1 and this factor is realized when a spanwise, elliptical distribution of lift is achieved. The object of taper and twist, therefore, is to achieve elliptical distribution.

The wing used on the Spitfire achieved high efficiency by making the wing itself elliptical in plan but the wing was expensive to produce and would not be suitable for swept wing applications. Figure 3.81 shows the elegant shape of this airfoil. General Aviation manufacturers prefer the low-cost rectangular wing and surprisingly enough this planform achieves reasonable values of e . Figure 3.82 shows how wing tip shape may be improved to increase the efficiency of such an airfoil.

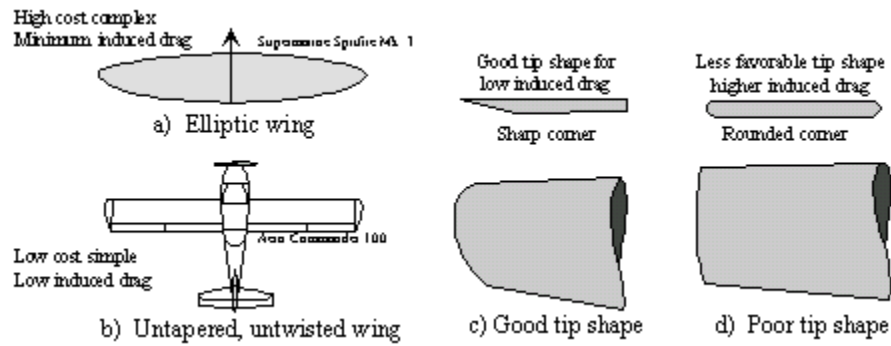


Figure 3.82 Elliptical Lift Distribution

Although taper and twist can both be used to attain elliptical lift distribution, the designer must also consider the requirements of stalling characteristics which might be adversely affected.

The spiroid wing tip, designed by Dr. Louis Gratzer, former Boeing Chief of Aerodynamics show promise in reducing fuel consumption in cruise by 6% to 10%. The closed surface loop design is said to eliminate the concentrated wingtip vortex, which represents almost 50% of aircraft induced drag generated during cruise flight. Figure 3.83 shows the installation of spiroid wing tips on a Gulfstream 2 test bed aircraft. Initial tests have indicated a 10% fuel saving in cruise as well as improved stability and climb performance.

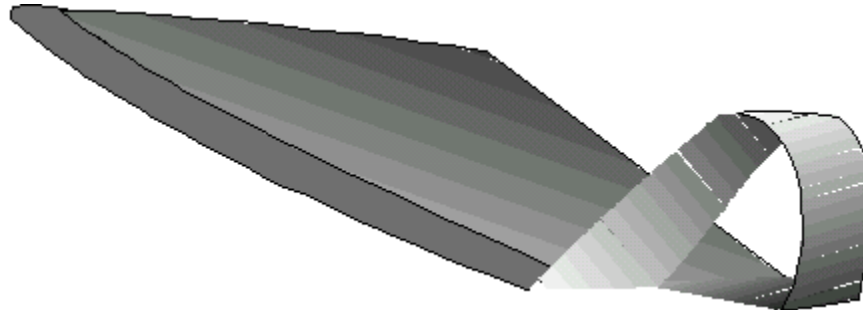


Figure 3.83 Spiroid Wingtips Mounted on the Gulfstream 2 Aircraft

3.1.8.8 Drag Coefficients

We have now examined all the elements which make up total drag in incompressible aerodynamics. Just as C_L was defined as follows:

$$C_L = \frac{L}{\frac{1}{2}\rho V^2 S}$$

The coefficient of drag, C_D , can also be similarly defined:

$$C_D = \frac{D}{\frac{1}{2}\rho V^2 S}$$

where: D = total aircraft drag
 ρ = free stream density
 V = free stream velocity
 S = wing area

3.1.9 References

3.1 Roberts, Sean C., *Light Aircraft Performance*, Flight Research Inc., Mojave CA, September 1981

3.2 *Flying Qualities Flight Testing of Light Aircraft*, Flight Research Inc., Mojave CA, July 1982

Volume 2 – Aerodynamics for Flight Testers

Chapter 4

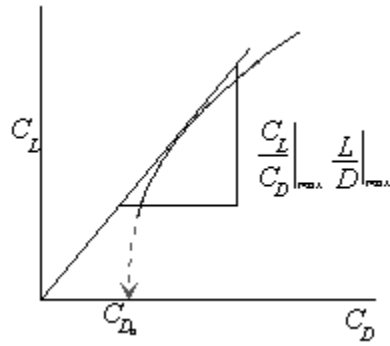
Drag Polar

Table of Contents

4.1 Introduction.....	2
4.2 The Glider.....	3
4.3 Jet Aircraft.....	5
4.3.1 Maximum Endurance.....	7
4.3.2 Maximum Range.....	8
4.3.3 Effect of Head Winds or Tail Winds on Range.....	8
4.3.4 Effect of Aircraft Weight on Endurance and Range.....	9
4.3.5 Effect of Configuration Changes.....	10
4.3.6 Effect of Altitude Changes.....	12
4.4 Propeller Aircraft.....	13
4.4.1 Effect of Weight on Endurance and Range.....	16
4.4.2 Configuration Changes.....	17
4.4.3 Effect of Altitude.....	18
4.5 Drag Polar Corrections.....	19
4.5.1 Cambered Airfoils.....	19
4.5.2 Flow Separation.....	22
4.5.3 Mach Number.....	22
4.5.4 Reynolds Number.....	23
4.5.5 Trim Drag.....	25
4.5.6 Slipstream Drag.....	26
4.6 References.....	27

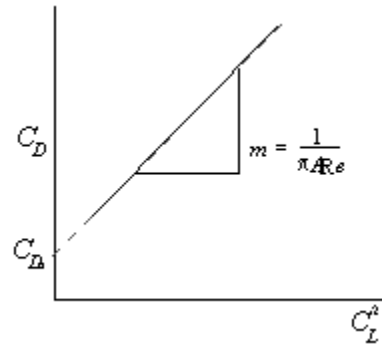
4.1 Introduction

The drag polar defines the aerodynamic lift and drag characteristics of an aircraft provided the basic assumptions of the drag polar are valid within the cruise range of angle of attack and below the critical Mach Number. The drag polar is a plot of the non-dimensional lift coefficient C_L versus the non-dimensional drag coefficient, C_D , of an aircraft and is shown in Figure 4.1.



Aircraft Drag Polar

Figure 4.1



Linear Plot of the Lift and Drag Characteristics of an Aircraft

Figure 4.2

The lift coefficient C_L is the total lift (L) divided by the dynamic pressure q and the aircraft wing reference area S . The drag coefficient is the total aircraft drag divided by qS . Therefore:

$$C_L = \frac{L}{\frac{1}{2}\rho V^2 S} = \frac{L}{qS}, C_D = \frac{D}{\frac{1}{2}\rho V^2 S} = \frac{D}{qS} \tag{4.1}$$

The relationship between C_D and C_L for an aircraft cruising in level, unaccelerated flight at a speed below the aircraft critical Mach Number is:

$$C_D = C_{D_o} + \frac{C_L^2}{\pi AR e} = C_{D_o} + C_{D_i} \tag{4.1}$$

where C_{D_o} is the parasitic drag coefficient and C_{D_i} is the induced drag coefficient which is equal to $\frac{C_L^2}{\pi AR e}$. In some texts, C_{D_o} is used to define the parasitic drag of the wing alone while C_{D_p} is used to define the parasitic drag of the complete aircraft. This text defines $C_{D_o} = C_{D_p}$ = total parasitic drag coefficient.

AR is the aspect ratio of the wing and is equal to the span squared divided by the wing area; note that the wing area includes that area inside the fuselage defined by the projection of the wing leading and trailing edges to the center line of the aircraft. e is the Oswald efficiency factor which accounts for changes in both parasitic drag and the wing's induced drag as angle of attack increases.

The plot of C_L vs C_D as shown in Figure 4.1 is a parabola. The extrapolation of the curve to $C_L=0$ is difficult; however, if the drag polar is plotted in the form of C_D versus C_L^2 as shown in Figure 4.2, the result is a straight line. The slope of the straight line in Figure 4.2 is equal to $\frac{1}{\pi AR e}$ and the intercept of the straight line with the ordinate gives C_{D_0} . The curve of C_D versus C_L^2 will be a straight line unless the angle of attack of the aircraft approaches the stall angle and flow separation occurs on the wings causing an increase in parasitic drag; this results in an increase in C_{D_0} which violates the basic premise that C_{D_0} is independent of angle of attack or lift coefficient.

4.2 The Glider

Most gliders are very aerodynamically efficient aircraft that are designed for either maximum cross-country speed or for minimum sink. The competitive sailplanes that are designed for cross-country competition are the most interesting. Figure 4.3 shows a typical sailplane in still air gliding flight, descending at a constant velocity and a constant descent angle (γ).

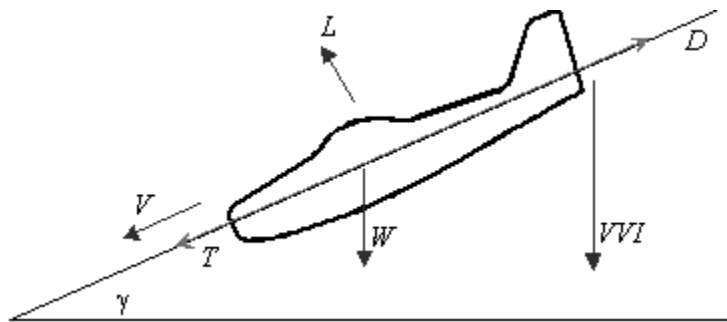


Figure 4.3 A Sailplane in Gliding Flight

Since the freestream velocity is constant, the sailplane is not accelerating nor decelerating and the forces are in equilibrium where:

$$\begin{aligned} T + W \sin \gamma &= D \\ L &= W \cos \gamma \end{aligned} \quad (4.3)$$

The only thrust of a glider is the component of weight down the glidepath, therefore:

$$\begin{aligned} W \sin \gamma &= D \\ W \cos \gamma &= L \end{aligned} \quad (4.4)$$

To determine the drag polar of a glider, the aircraft is flown at a constant velocity and the rate of descent measured by timing altitude changes with time. Once the true sink rate (VVI) is known and the true freestream velocity (V) is found, then the descent angle can be computed using

$$\gamma = \sin^{-1} \frac{VVI}{V} \quad (4.5)$$

$$\text{then } C_D = \frac{W \sin \gamma}{1/2\rho V^2 S} \quad \text{and} \quad C_L = \frac{W \cos \gamma}{1/2\rho V^2 S} \quad (4.6)$$

which gives one point on the drag polar. The process is repeated at different freestream velocities until the complete drag polar as shown in Figure 4.4 is defined.

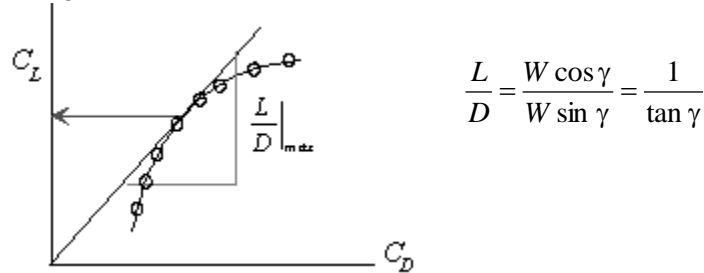


Figure 4.4 Drag Polar of a Sailplane

The $\left|\frac{L}{D}\right|_{\max}$ of the glider is the slope of the tangent from the origin to the curve in Figure 4.4. The condition for maximum L/D would correspond to the minimum descent angle (γ) and therefore to the best range condition in still air. Since the glider uses the component of weight down the glidepath as thrust, then to increase the performance of the glider, it is necessary to increase the weight. If weight is added internally with no external modifications, then is the same and the drag polar as shown in Figure 4.4 would still apply to the glider with the increased weight. To achieve the same $\left|\frac{L}{D}\right|_{\max}$ as the unmodified glider, the heavier glider must fly at the same C_L . Since $C_L = \frac{W \cos \gamma}{1/2\rho V^2 S}$ and ρ_0 , γ and S are constant, then an increase in weight (W) the velocity must also be increased such that the C_L for max (L/D) is the same. Since $C_L = f(W/V^2)$ then if the weight is doubled to increase cross-country cruising speed then the indicated velocity must be increased by a factor of $\sqrt{2}$ or 41%.

The increase in aircraft velocity also gives an increase in Reynolds Number of the glider which generally results in a slight decrease in drag and a subsequent increase in (L/D). Note that the glide range, represented by the lift-to-drag ratio, is *independent of aircraft weight*. The disadvantages of increasing the weight of the glider are a reduced ability of the structure to withstand normal acceleration or gust loading and a larger turning radius due to the increase in velocity. The larger turning radius is a problem when trying to stay in thermals to climb and in most cases can only be accomplished by using wing flaps so that the thermalling speed can be reduced. The minimum sink conditions of the glider are also increased; towards the end of the active thermal day, the ballast may have to be jettisoned to extend the time aloft. The ballast is usually carried in water tanks in the wings.

The max L/D ratio occurs at the maximum slope of the C_D vs C_L curve. Since the drag polar is $C_D = C_{D_0} + \frac{C_L^2}{\pi A R e}$ [Equation (4.1)] then, to find the conditions of $(L/D)_{\max}$, the above equation can be

divided by C_L and the ratio of C_D / C_L is differentiated with respect to C_L and equated to zero for maximum or minimum, i.e.,

$$\frac{C_D}{C_L} = C_{D_o} C_L^{-1} + \frac{1}{\pi A R e} C_L$$

$$\frac{d\left(\frac{C_D}{C_L}\right)}{dC_L} = -C_{D_o} C_L^{-2} + \frac{1}{\pi A R e} = 0$$

multiply through by C_L^2

$$-C_{D_o} + \frac{C_L^2}{\pi A R e} = 0$$

ie.,
$$C_{D_o} = \frac{C_L^2}{\pi A R e} = C_{D_i} \quad (4.7)$$

Therefore, for $\left(\frac{L}{D}\right)_{\max}$ for a glider, the parasitic drag must equal the induced drag. The condition for *minimum drag* is determined as follows:

$$Drag = q S C_D = q S \left(C_{D_o} + \frac{C_L^2}{\pi A R e} \right) = q S C_{D_o} + \frac{q S}{\pi A R e} \cdot \frac{W^2}{q^2 S^2} \quad (4.8)$$

$$D = q S C_{D_o} + \frac{W^2}{\pi A R e q S}$$

$$\frac{dD}{dq} = S C_{D_o} + \frac{W^2}{\pi A R e S} (-q^{-2}) = 0 \text{ for max or min}$$

dividing through by S gives:

$$C_{D_o} - \frac{1}{\pi A R e} \frac{W^2}{q^2 S^2} = 0$$

$$\boxed{\therefore C_{D_o} = \frac{C_L^2}{\pi A R e} = C_{D_i} \text{ for minimum drag}} \quad (4.9)$$

4.3 Jet Aircraft

The engine(s) in a jet aircraft produce a thrust. In level unaccelerated flight assuming small angles, Figure 4.5 depicts the basic force balance.

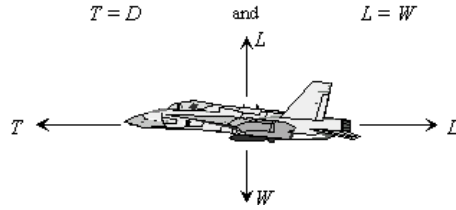


Figure 4.5 Jet Aircraft

Since the thrust equals the drag and the lift equals the weight, then

$$C_L = W/qS \quad \text{and} \quad C_D = T/qS$$

and the drag polar when cruising below the critical Mach number (M_{crit}) is:

$$C_D = C_{D_o} + \frac{C_L^2}{\pi A R e}$$

The conditions for *minimum drag* are found as follows:

$$D = qS C_{D_o} + \frac{qS}{\pi A R e} \cdot \frac{W^2}{q^2 S^2} = qS C_{D_o} + \frac{W^2}{\pi A R e} \cdot \frac{1}{qS} \quad (4.10)$$

$$\frac{dD}{dq} = S C_{D_o} + \frac{W^2}{\pi A R e S} (-q^{-2}) = 0 \text{ for max or min}$$

dividing by S gives:

$$C_{D_o} - \frac{1}{\pi A R e} \cdot \frac{W^2}{q^2 S^2} = 0$$

$$C_{D_o} = \frac{C_L^2}{\pi A R e} \quad (4.11)$$

Or, the parasitic drag equals the induced drag for minimum total drag. A plot of drag for a typical aircraft is shown in Figure 4.6.

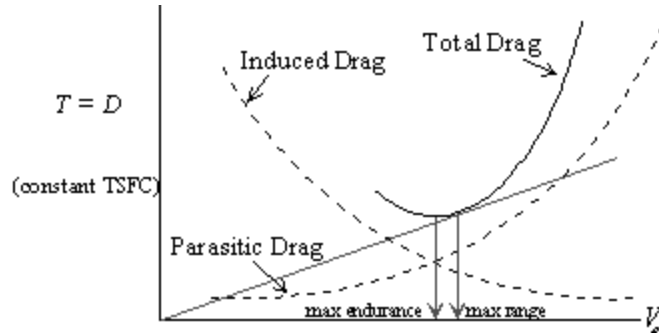


Figure 4.6 Drag of any Aircraft, Fuel Flow for a Jet Aircraft

4.3.1 Maximum Endurance

The velocity for minimum drag, where the induced drag equals the parasitic drag is shown in Figure 4.6. Recall that the drag equals the thrust for a jet aircraft in cruise. If it is assumed that the thrust specific fuel consumption of the engines (TSFC) is constant (fuel flow per pound of thrust is constant) then minimum drag corresponds to minimum fuel consumption (\dot{w}_f). Furthermore, the velocity for minimum drag (V_{MD}) corresponds to the velocity for minimum fuel flow and the velocity for maximum aircraft endurance. It can also be shown that the conditions for minimum drag corresponds to the conditions for maximum *Lift to Drag* ratio.

$$\text{If} \quad D = qSC_D$$

$$\text{and} \quad L = qSC_L$$

$$\therefore \frac{D}{L} = \frac{C_D}{C_L} = \frac{C_{D_o} + \frac{C_L^2}{\pi A R e}}{C_L} = \frac{C_{D_o}}{C_L} + \frac{C_L}{\pi A R e}$$

$$\text{Also:} \quad \frac{d\left(\frac{D}{L}\right)}{dC_L} = \frac{-C_{D_o}}{C_L^2} + \frac{1}{\pi A R e} = 0 \text{ for max or min}$$

$$\therefore C_{D_o} = \frac{C_L^2}{\pi A R e} = C_{D_o} \text{ for jet maximum endurance} \quad (4.12)$$

Therefore, for a jet aircraft, maximum endurance corresponds to the conditions for minimum drag which also corresponds for maximum (L/D) ratio.

4.3.2 Maximum Range

The conditions for maximum range is to maximize the "forward velocity / fuel flow" ratio or the minimize the " fuel flow / forward velocity" ratio. Since it has been assumed that the fuel flow (\dot{w}_f) is directly proportional to thrust (which is equal to drag in cruising flight) then the ratios:

$$\left(\frac{\dot{w}_f}{V}\right), \left(\frac{D}{V}\right) \text{ must be minimized for maximum range}$$

$$\frac{D}{V} = \frac{\frac{1}{2}\rho V^2 S}{V} \left[C_{D_o} + \frac{C_L^2}{\pi A R e} \right] = \frac{1}{2}\rho V S C_{D_o} + \frac{W^2}{\pi A R e \frac{1}{2}\rho V^3 S}$$

$$\therefore \frac{d \frac{D}{V}}{dV} = \frac{1}{2}\rho S C_{D_o} + \frac{W^2}{\pi A R e \frac{1}{2}\rho S} \left(-\frac{3}{V^4} \right) = 0 \text{ for max or min}$$

Dividing by $\frac{1}{2}\rho S$ gives:

$$C_{D_o} - \frac{3}{\pi A R e} \cdot \frac{W^2}{\left(\frac{1}{2}\rho V^2 S\right)^2} = 0$$

or

$$C_{D_o} - 3 \frac{C_L^2}{\pi A R e} = 0$$

$$\boxed{C_{D_o} = 3C_{D_i} \text{ for jet aircraft maximum range}} \tag{4.13}$$

Therefore, for maximum range, the parasitic drag equals three times the induced drag. This condition for maximum range can also be determined graphically as shown in Figure 4.6, by drawing the tangent to the curve from the origin. The tangent point is the condition for maximum range.

In the summary, for a jet aircraft:

For maximum endurance $C_{D_o} = C_{D_i}$

and for maximum range $C_{D_o} = 3C_{D_i}$

4.3.3 Effect of Head Winds or Tail Winds on Range

Figure 4.7 shows the thrust required curve for any aircraft in level cruise flight. For a jet aircraft with constant TSFC, the figure shows conditions for maximum still air range.

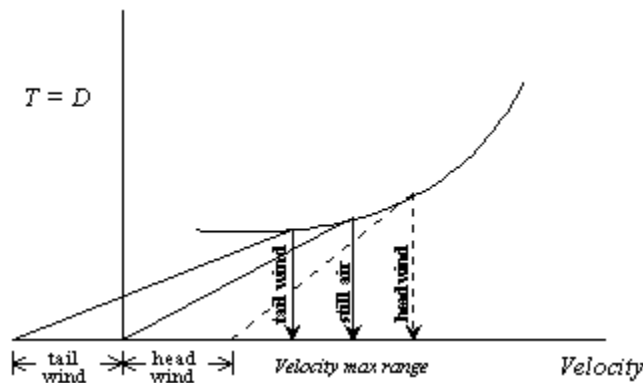


Figure 4.7 Effects of Winds on Range

To find the velocity for maximum range when flying against a head wind, the origin along abscissa is moved to the right by an amount equal to the head wind velocity. The tangent to the curve from this new origin will define the point for maximum range in a head wind. A similar process is used to find the velocity for maximum range when flying with a tail wind, but the origin is now moved left along the abscissa. As seen from Figure 4.7, it is necessary to fly faster than the best still air range speed when flying into a head wind and to fly slower when flying with a tail wind.

4.3.4 Effect of Aircraft Weight on Endurance and Range

Aircraft weight has no effect on parasitic drag, i.e., C_{D_0} is constant for all angles of attack above the stall buffet angle and below the speed for critical Mach Number. The induced drag is a function of lift coefficient squared. Therefore, the induced drag is a function of weight squared but is only significant when C_L is high (which is at low airspeeds). Note that:

$$D = \frac{1}{2} \rho V^2 S \left[C_{D_0} + \frac{C_L^2}{\pi A R e} \right]$$

$$D = \frac{1}{2} \rho V^2 S C_{D_0} + \frac{\frac{1}{2} \rho V^2 S}{\pi A R e} \cdot \frac{W^2}{\left(\frac{1}{2} \rho V^2 S \right)^2}$$

$$D = \frac{1}{2} \rho V^2 S C_{D_0} + \frac{1}{\pi A R e} \cdot \frac{W^2}{\frac{1}{2} \rho V^2 S}$$

$$D = K_1 V^2 + K_2 \left(\frac{W^2}{V^2} \right) \quad (4.14)$$

Therefore, plots of parasitic drag (D_0) and induced drag (D_i) are shown plotted in Figure 4.8. Plots of total drag (D) are shown in Figure 4.9 at various values of aircraft weight. Figure 4.9 shows that as the aircraft weight increases, the speeds for minimum drag and for maximum range also increase.

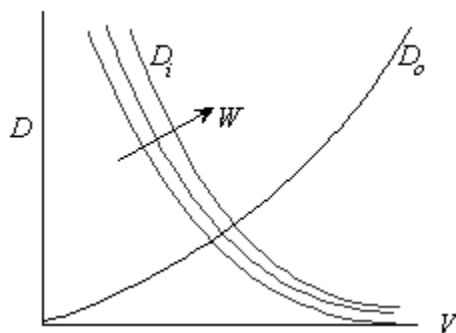
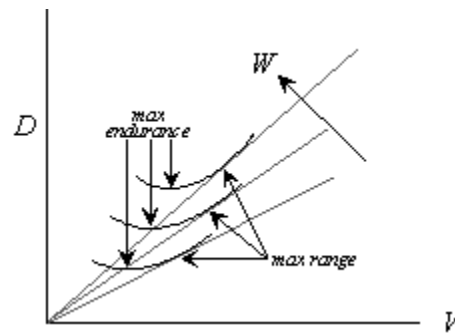
Figure 4.8 D_0 & D_i at Various Weights

Figure 4.9 Total Drag at Various Weights

For maximum *endurance*:

$$C_{D_o} = C_{D_i} = K_2 \left(\frac{W_1^2}{V_1^4} \right) = K_2 \left(\frac{W_2^2}{V_2^4} \right)$$

$$\therefore V_2 = \left(\frac{W_2}{W_1} \right)^{\frac{1}{2}} V_1 \quad (4.15)$$

Therefore, if V_1 corresponds to the speed for maximum endurance at a weight of W_1 then V_2 will be the speed for maximum endurance at a weight of W_2 .

For maximum *range*:

$$C_{D_o} = 3C_{D_i} = 3K_2 \left(\frac{W_1^2}{V_1^4} \right) = 3K_2 \left(\frac{W_2^2}{V_2^4} \right)$$

$$\therefore V_2 = \left(\frac{W_2}{W_1} \right)^{\frac{1}{2}} V_1 \quad (4.16)$$

Similarly, assuming that V_1 corresponds to the speed for maximum range at W_1 then V_2 is the speed for maximum range at W_2 .

4.3.5 Effect of Configuration Changes

Fighter/bomber aircraft with external weapons have changes in the drag count which directly affects the parasitic drag coefficient. Drag counts can be defined in various ways; one way is that each drag count increases C_{D_o} by one ten-thousandth's i.e., (0.0001). The effect of parasitic drag changes on range and endurance speeds are important for air-to-ground attack aircraft since these can yield considerable changes in speed going to the target loaded with weapons and returning clean.

For maximum endurance $C_{D_o} = C_{D_i}$

$$C_{D_{o1}} = K_2 \left(\frac{W_1^2}{V_1^4} \right) \text{ and } C_{D_{o2}} = K_2 \left(\frac{W_2^2}{V_2^4} \right)$$

assuming that C_{D_i} is changed but the weight remains unchanged:

$$\therefore \frac{C_{D_{o1}}}{C_{D_{o2}}} = \frac{W_1^2}{V_1^4} \frac{V_2^4}{W_2^2} = \left(\frac{V_2}{V_1} \right)^4$$

or
$$V_2 = \left(\frac{C_{D_{o1}}}{C_{D_{o2}}} \right)^{\frac{1}{4}} V_1 \tag{4.17}$$

For example, if V_1 is 300 kts with a total drag count of 2000 which is the clean aircraft, then the speed for the aircraft with a total drag count of 3000 is:

$$V_2 = \left(\frac{2000}{3000} \right)^{\frac{1}{4}} 300$$

$$V_2 = 271 \text{ kts}$$

The range speeds operate in a similar manner as the endurance speed. The rule is that the optimum range speed is slower when the aircraft has increased drag - assuming no weight change. This is illustrated in Figures 4.10 and 4.11.

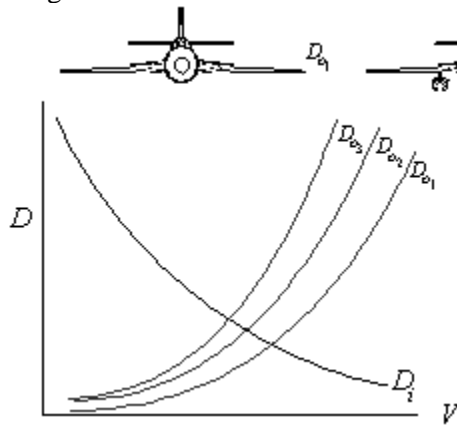


Figure 4.10 Parasitic Drag Changes

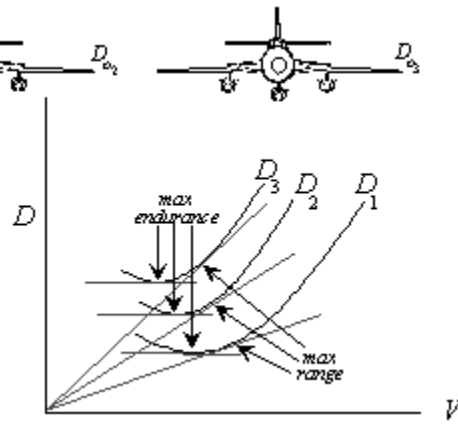


Figure 4.11 Total Drag Changes

If the weight of the aircraft is also changed at the same time that the external drag is changed then,

$$V_2 = \left(\frac{C_{D_{o1}}}{C_{D_{o2}}} \right)^{\frac{1}{4}} \left(\frac{W_2}{W_1} \right)^{\frac{1}{2}} V_1 \tag{4.18}$$

Where $C_{D_{o2}}$ is the new parasitic drag data of the aircraft at the new weight W_2 . Note that as the weight is increased, the speed for best range increases drag is increased with stores, the speed for best range decreases.

4.3.6 Effect of Altitude Changes

Since the drag of a jet aircraft equals the thrust generated by the engine(s) in unaccelerated cruise flight, then:

$$T = D = \frac{1}{2} \rho_o V_e^2 S C_D$$

where ρ_o is standard day sea level density and V_e is the equivalent airspeed.

If it is assumed that the specific fuel consumption of the engines is constant, then drag is directly proportional to fuel flow (\dot{w}_f). Plots of drag or (\dot{w}_f) versus true airspeed (V_e) are shown in Figure 4.12.

True airspeed is $\frac{V_e}{\sqrt{\sigma}}$ where σ is the density ratio ρ/ρ_o .

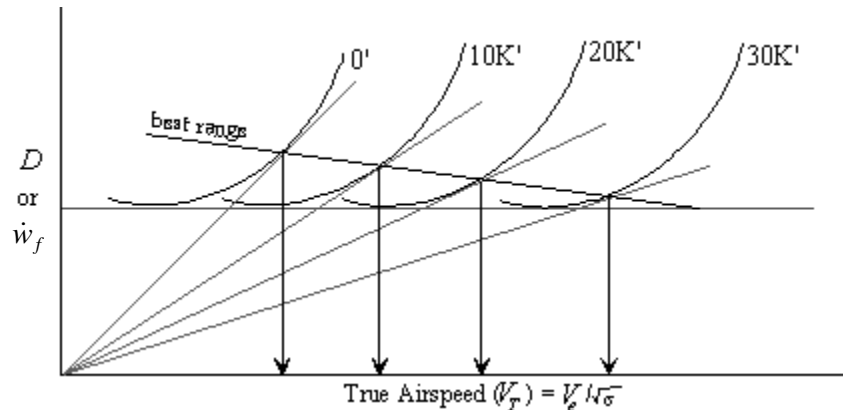


Figure 4.12 Effect Altitude on Jet Aircraft Drag

The equation above shows that if an aircraft cruises at a constant V_e , below the critical Mach number, the drag will remain unchanged, regardless of altitude. The true airspeed however, will increase since:

$$V_T = \frac{V_e}{\sqrt{\sigma}}$$

and $\sqrt{\sigma}$ decreases with an increase in altitude. The "thrust required" curves of a jet aircraft move to the right (as a function of $\frac{1}{\sqrt{\sigma}}$) with an increase in altitude. The maximum range is the condition defined by the maximum number of nautical miles per pound of fuel, which is the tangent to the thrust required curve from the origin, as shown in Figure 4.12.

The range at sea level is proportional to V_0/D_0 ; at 10,000 ft, V_{10}/D_{10} , etc... It can be seen that the range of a jet aircraft increases with altitude because the true airspeed is increasing with altitude and the thrust required for maximum range condition is decreasing with an increase in altitude. Interestingly enough, the endurance of a jet aircraft is not affected by altitude but the range is dramatically increased with an increase in altitude. Note that this analysis is based entirely on the drag polar. Realistic engine characteristics are not taken into consideration (turbines are actually more efficient at colder temperatures).

4.4 Propeller Aircraft

A propeller aircraft also generates a thrust which is equal and opposite to the drag of the aircraft (in unaccelerated flight). The difference is that the fuel flow of a prop-driven aircraft is related to the engine's power output, not its thrust explicitly. The engine generates a brake horsepower (*BHP*) for a reciprocating engine or a shaft horsepower (*SHP*) for a turbo-propeller aircraft. This shaft horsepower is converted to a thrust horsepower (*THP*) by means of a propeller which has a propeller efficiency, η . Therefore:

$$THP = \eta(SHP)$$

$$THP = \frac{(\text{Thrust})(\text{True Velocity})}{550} = \frac{TV_T}{550} = \frac{T \frac{V_e}{\sqrt{\sigma}}}{550}$$

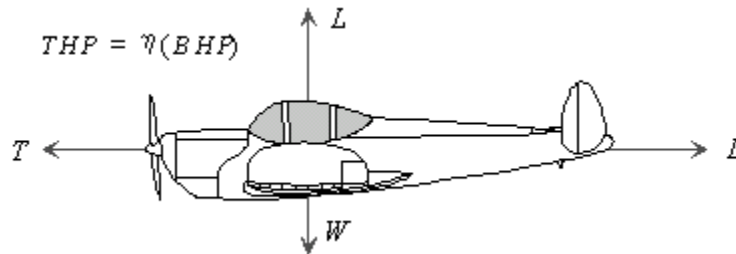


Figure 4.13 Cruise Conditions for a Propeller Aircraft

The *BHP* or the *SHP* output of an engine is a function of *RPM*, boost pressure or manifold pressure, altitude, temperature etc. . . Propeller efficiency η is a function of the propeller power loading coefficient C_P and propeller advance ratio V_T/ND where V_T is the true velocity, N is the rotational speed and D is the diameter of the propeller. To determine the thrust developed by an engine propeller combination, it is necessary to know the horsepower output of the engine, the propeller efficiency η and the true velocity V_T . Therefore:

$$\text{Thrust } (T) = \frac{(SHP)\eta 550}{V_T}$$

Since the Thrust (T) equals the drag in level unaccelerated flight, then:

$$\begin{aligned} \text{Thrust HP } (THP) &= \frac{(\text{drag})V_T}{550} \\ THP &= \frac{V_T}{550} \left[\frac{1}{2} \rho_o V_e^2 S C_D \right] = \frac{\frac{V_e}{\sqrt{\sigma}}}{550} \left[\frac{1}{2} \rho_o V_e^2 S C_D \right] \\ THP &= \frac{\frac{1}{2} \rho_o S V_e^3}{550 \sqrt{\sigma}} \left[C_{D_o} + \frac{C_L^2}{\pi A Re} \right] \end{aligned}$$

$$\text{Brakes HP or Shaft HP} = \frac{THP}{\eta}$$

$$\therefore BHP_{req} = \frac{\frac{1}{2}\rho_o S V_e^3}{\eta 550 \sqrt{\sigma}} \left[C_{D_o} + \frac{C_L^2}{\pi A R e} \right]$$

Since $C_L = \frac{W}{\frac{1}{2}\rho_o V_e^2 S}$ then:

$$BHP_{req} = \frac{\frac{1}{2}\rho_o S}{550\eta\sqrt{\sigma}} C_{D_o} V_e^3 + \frac{\frac{1}{2}\rho_o S}{550\eta\sqrt{\sigma}} \frac{V_e^3}{\pi A R e} \left(\frac{W}{\frac{1}{2}\rho_o V_e^2 S} \right)^2$$

letting $k_1 = \frac{\frac{1}{2}\rho_o S}{550\eta} C_{D_o}$ gives:

$$BHP_{req} = K_1 \frac{V_e^3}{\sqrt{\sigma}} + \frac{W^2}{\frac{1}{2}\rho_o V_e S} \cdot \frac{1}{550\eta\sqrt{\sigma}\pi A R e}$$

letting $k_2 = \frac{1}{\frac{1}{2}\rho_o S 550\eta \pi A R e}$ gives:

$$BHP_{req} = K_1 \frac{V_e^3}{\sqrt{\sigma}} + K_2 \frac{W^2}{\sqrt{\sigma} V_e} \quad (4.19)$$

The above equations indicate that the parasitic power required increases as a function of the velocity *cubed* and the induced power only decreases as a linear function of $1/V_e$ as shown in Figure 4.14.

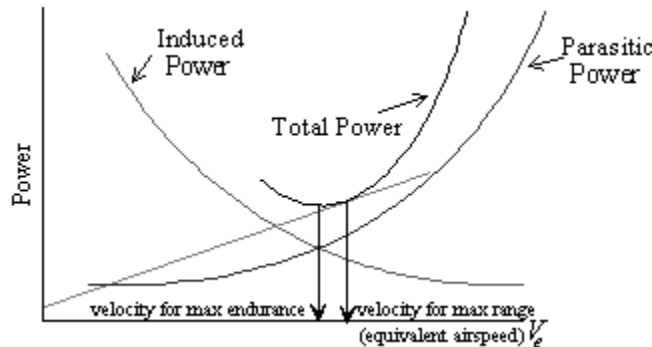


Figure 4.14 Parasitic and Induced Power

To find the conditions for minimum power assuming that:

$$BHP_{req} = K_1 \frac{V_e^3}{\sqrt{\sigma}} + K_2 \frac{W^2}{\sqrt{\sigma} V_e}$$

$$\begin{aligned} \frac{d(BHP)}{dV_e} &= \frac{3K_1}{\sqrt{\sigma}} V_e^2 + \frac{K_2 W^2}{\sqrt{\sigma}} \left(\frac{-1}{V_e^2} \right) = 0 \text{ for min or max} \\ \therefore \frac{3K_1}{\sqrt{\sigma}} V_e^2 &= \frac{K_2 W^2}{\sqrt{\sigma}} \frac{1}{V_e^2} \end{aligned}$$

Dividing through by V_e^2 gives:

$$\frac{3K_1}{\sqrt{\sigma}} = \frac{K_2 W^2}{\sqrt{\sigma}} \frac{1}{V_e^4}$$

Substituting values for K_1, K_2

$$\frac{3}{\sqrt{\sigma}} \frac{\frac{1}{2} \rho_o S C_{D_o}}{550 \eta} = \frac{W^2}{\sqrt{\sigma} V_e^4} \left(\frac{1}{\frac{1}{2} \rho_o S 550 \eta \pi A R e} \right)$$

dividing through by $\frac{\frac{1}{2} \rho_o S}{\sqrt{\sigma} 550 \eta}$ gives:

$$3C_{D_o} = \frac{1}{\pi A R e} \left(\frac{W}{\frac{1}{2} \rho_o V_e^2 S} \right)^2 = \frac{C_L^2}{\pi A R e} = C_{D_i} \quad (4.20)$$

$$\boxed{C_{D_i} = 3C_{D_o} \text{ for minimum power}}$$

Therefore, the conditions for minimum power are that the parasitic drag coefficient equals one third the induced drag coefficient. If it is assumed that the specific fuel consumption of the engine(s) is constant (fuel flow per HP is constant) then the condition for minimum power corresponds to the conditions for minimum fuel flow and therefore the conditions for maximum endurance.

$$\therefore \text{For maximum endurance for a propeller aircraft: } C_{D_o} = \frac{1}{3} C_{D_i} \quad (4.21)$$

For maximum range it is necessary to maximize the true velocity/fuel flow ratio or to minimize the \dot{w}_f / V_T ratio. This corresponds to minimizing (BHP/V_T) ratio for a propeller aircraft with a constant specific fuel consumption.

$$\frac{BHP_{req}}{V_T} = \left[K_1 \frac{V_e^3}{\sqrt{\sigma}} + K_2 \frac{W^2}{\sqrt{\sigma} V_e} \right]$$

but $V_T = \frac{V_e}{\sqrt{\sigma}}$

therefore

$$\frac{BHP_{req}}{V_T} = K_1 V_e^2 + K_2 \frac{W^2}{V_e^2}$$

$$\frac{d\left(\frac{BHP_{req}}{V_T}\right)}{dV_e} = 2K_1V_e + K_2W^2(-2V_e^{-3}) = 0 \text{ for max or min}$$

$$\therefore 2K_1V_e = \frac{2K_2W^2}{V_e^3}$$

$$(2)\frac{\frac{1}{2}\rho_oSC_{D_o}}{550\eta} \cdot V_e = (2)\frac{W^2}{V_e^3} + \frac{1}{\frac{1}{2}\rho_oS 550\eta \pi AR e}$$

Canceling terms and dividing by $\frac{1}{2}\rho_oV_eS$ gives:

$$C_{D_o} = \frac{W^2}{\frac{1}{2}\rho_oV_e^2S} \cdot \frac{1}{\pi AR e} = \frac{C_L^2}{\pi AR e} = C_{D_i}$$

$$\boxed{C_{D_i} = C_{D_o} \text{ for propeller aircraft maximum range}} \tag{4.22}$$

Therefore the conditions for maximum range of a propeller aircraft are when the parasitic drag coefficient C_{D_o} equals the induced drag coefficient. Note that this is the same as the conditions for maximum endurance for a jet aircraft. Also from previous analysis, the condition where $C_{D_i} = C_{D_o}$ corresponds to the conditions for $\left(\frac{L}{D}\right)_{max}$.

4.4.1 Effect of Weight on Endurance and Range

The maximum endurance condition for propeller aircraft is when $C_{D_o} = \frac{1}{3}C_{D_i}$ and the maximum range condition for a propeller aircraft is when $C_{D_o} = C_{D_i}$. If W_1 is the weight of the aircraft when the best endurance speed is V_1 then,

$$\begin{aligned} C_{D_o} &= \frac{1}{3} \frac{C_L^2}{\pi AR e} \frac{1}{3} \pi AR e \cdot \frac{W^2}{\left(\frac{1}{2}\rho_oV_e^2S\right)^2} \\ &= \frac{1}{3} K_1 \left(\frac{W_1^2}{V_{e1}^4}\right) = \frac{1}{3} K_2 \left(\frac{W_2^2}{V_{e2}^4}\right) \\ V_{e2} &= \left(\frac{W_2}{W_1}\right)^{\frac{1}{2}} V_{e1} \end{aligned} \tag{4.23}$$

where V_{e2} is the speed for maximum endurance at the new weight of W_2 . The same analysis can be done for the maximum range condition as shown in Figure 4.15.

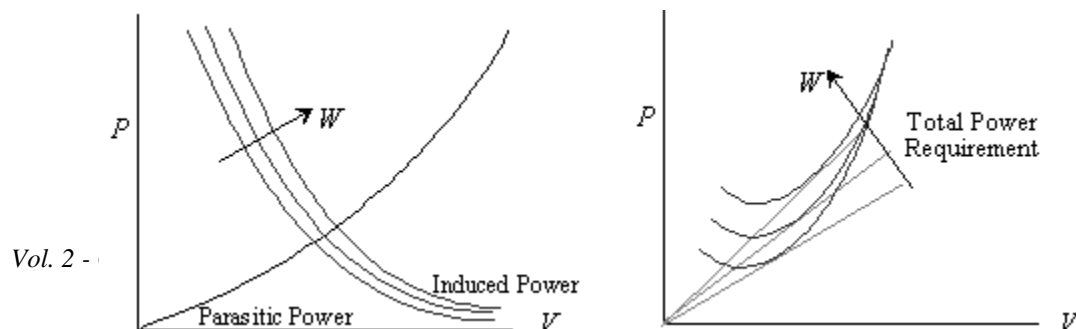


Figure 4.15 Effect of Weight on Power Required

4.4.2 Configuration Changes

If $C_{D_{o1}}$ is the parasitic drag of the clean aircraft and V_1 is the velocity for maximum endurance at a weight of W_1 and since:

$$C_{D_{o1}} = \frac{1}{3} C_{D_i} = \frac{1}{3} K_2 \left(\frac{W_1^2}{V_1^4} \right)$$

and

$$C_{D_{o2}} = \frac{1}{3} C_{D_i} = \frac{1}{3} K_2 \left(\frac{W_{21}^2}{V_{21}^4} \right)$$

then

$$\frac{C_{D_{o1}}}{C_{D_{o2}}} = \frac{W_1^2}{V_1^4} \cdot \frac{V_2^4}{W_2^2}$$

and

$$V_2 = \left(\frac{C_{D_{o1}}}{C_{D_{o2}}} \right)^{\frac{1}{4}} \left(\frac{W_2}{W_1} \right)^{\frac{1}{2}} V_1 \tag{4.24}$$

Where $C_{D_{o2}}$ is the new parasitic drag coefficient at a new aircraft weight W_2 and V_1 is the speed for maximum endurance at the original weight (W_1) and drag coefficient ($C_{D_{o1}}$).

The speed for best range operate exactly in the same fashion and are:

$$V_2 = \left(\frac{C_{D_{o1}}}{C_{D_{o2}}} \right)^{\frac{1}{4}} \left(\frac{W_2}{W_1} \right)^{\frac{1}{2}} V_1 \tag{4.25}$$

where V_1 is the best range speed at a weight W_1 and a parasitic drag $C_{D_{o1}}$ of and the subscript '2' denotes conditions for maximum range at the new weight and drag. The effect changing only the parasitic drag is shown in Figure 4.16.

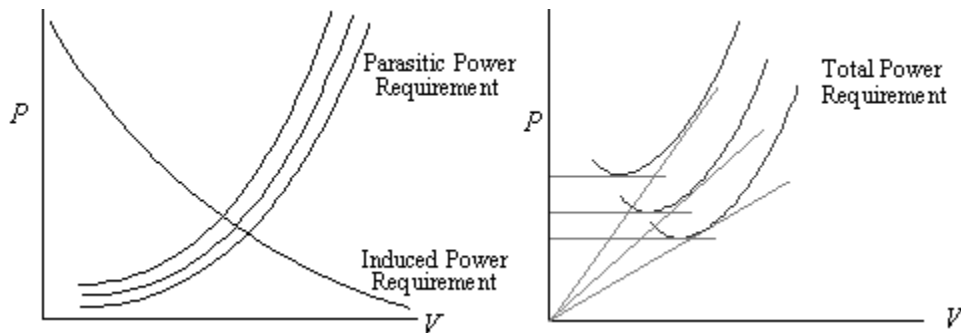


Figure 4.16 Effect of Configuration Change

4.4.3 Effect of Altitude

Since the $(BHP)_{req}$ to fly a propeller aircraft is equal to:

$$(BHP)_{req} = \frac{(Thrust)_{req} V_T}{550\eta} = \frac{V_e}{550\eta} \cdot \frac{1}{2} \rho_o V_e^2 S C_D$$

then:

$$(BHP)_{req} = K_1 \frac{V_e^3}{\sqrt{\sigma}} + K_2 \frac{W^2}{\sqrt{\sigma} V_e} \tag{4.26}$$

The cubic relationship between power and velocity is often a great surprise to aircraft modifiers who put larger engines in existing airframes; doubling the speed takes approximately eight times the power. A plot of $(BHP)_{req}$ versus V_T is shown in Figure 4.17.

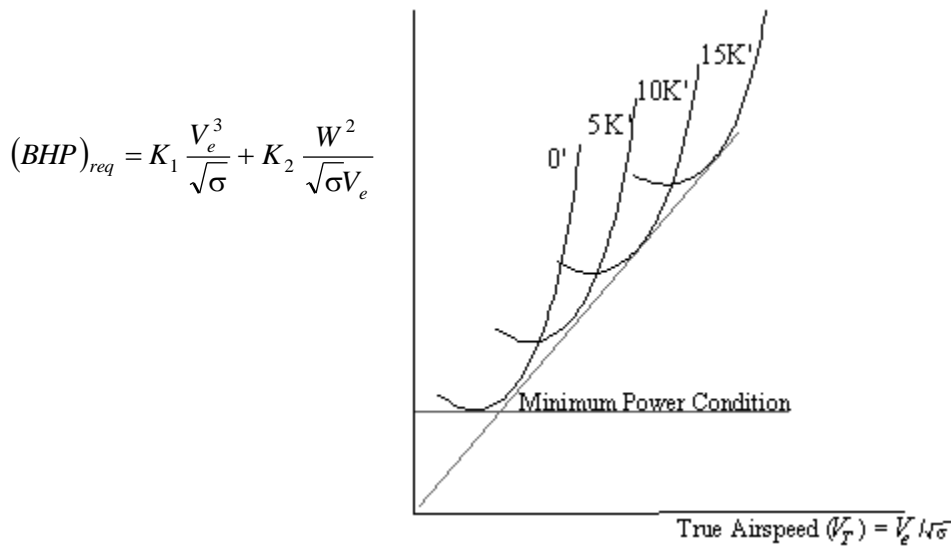


Figure 4.17 Power Required as a Function of Altitude for Propeller Aircraft

Since the power required increases as a function of $\frac{1}{\sqrt{\sigma}}$ and the true velocity of the abscissa increases as $\frac{1}{\sqrt{\sigma}}$, then, as altitude increases, both the power required and the true velocity increase in the same proportion. From Figure 4.17, it is obvious that the flight conditions for minimum power occurs at sea level. Also seen is that altitude has no effect on range since the ratio of true velocity to power required a constant with altitude. Although altitude has no effect on the maximum range of an aircraft, altitude will have a considerable effect on the time en route. The higher the propeller aircraft can operate (and still have the power available for the best range condition), the faster it will fly and achieve

minimum time en route. Minimum time en route is important if operating cost of the aircraft per hour is considered. Mandatory reduction in altitude due to weather or mission will have no effect on the maximum range.

4.5 Drag Polar Corrections

The previous discussion presents the utility of drag polars as they relate to aircraft performance. Although the characteristics are dominated by the parasitic and induced drag, there are more sophisticated methods used to adjust the basic drag polar developed above to provide a more comprehensive model. Basic corrections to the model can be made to account for wing camber and separating flow effects. Beyond this, as many as five other factors can alter the drag polar for any given configuration. The most important adjustment is related to the aircraft Mach number and is required for aircraft that fly into the transonic region. The second most important adjustment is due to changes in Reynolds number and is significant for aircraft that fly at altitudes above about 20,000 feet. A less important correction could be made for the effects of trim drag. Propeller-driven aircraft have an additional correction due to the slipstream.

Finally, sometime corrections are applied for aircraft bending at high load factor and/or high dynamic pressure. If accomplished at all, this correction due to structural bending is predicted by the manufacturer. These corrections may take the form of a matrix of ΔC_D values at various q and N_Z . These corrections are insignificant for relatively rigid aircraft. Flight testers can check predictions by flying at appropriate levels of load factor and airspeed. The other corrections are addressed below.

4.5.1 Cambered Airfoils

The drag polar model developed previously assumes that the drag is a minimum at zero C_L . This describes a wing with no camber. A wing *with* camber will create some lift even though the angle of attack is zero and the only way to create zero lift is to rotate the wing nose-down to some negative angle of attack. At this condition, however, the wing will actually have more drag than at zero α . The drag polar of a cambered wing may be illustrated as shown in Figure 4.18. The same effect shown below appears for an uncambered wing if it is mounted with some angle of incidence.

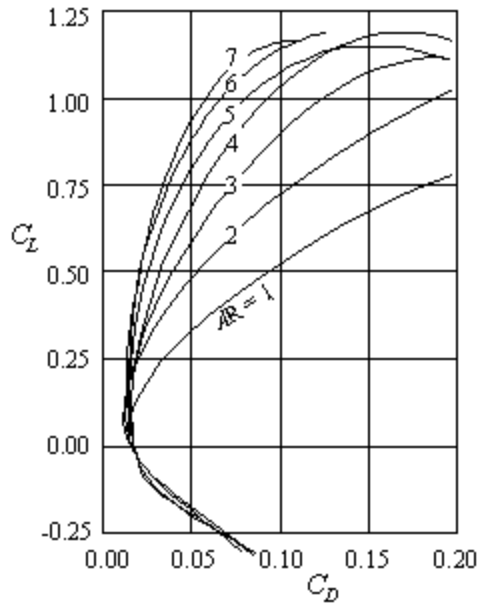


Figure 4.18 Drag Polar for Wing with Camber or Incidence Angle

The minimum drag for a cambered airfoil occurs at some low positive value of C_L . If this wing is attached to a fuselage (with zero incidence angle), then as the complete unit rotates nose-down, the drag increases even more as the fuselage also adds drag as it deviates from its most streamlined orientation. If this wing is mounted at some positive angle of incidence, then the α for minimum drag will be higher than that for the wing in isolation but lower than that for the fuselage in isolation (Figure 4.19). As the complete aircraft rotates slightly nose-down from this minimum drag orientation, the increased body drag overcomes the decrease in wing drag.

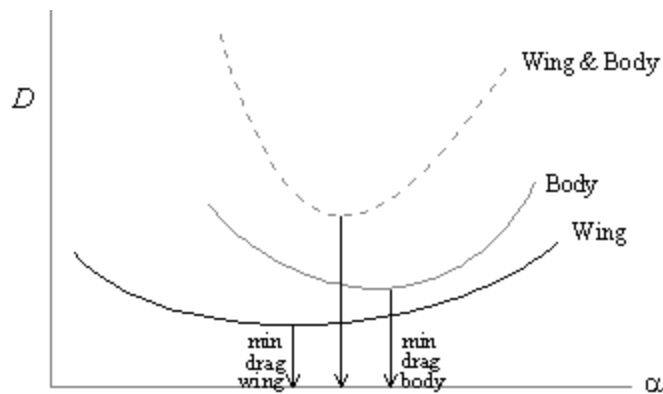


Figure 4.19 Parasitic Drag for Body and Wing at Various Angles of Attack

If a cambered wing is mounted with a negative angle of incidence, then it is possible that the α for zero lift nearly corresponds to the α for minimum drag. Although such a layout would simplify the drag polar, it is not beneficial to performance. The best configuration for a transport aircraft is one where the fuselage is oriented to create the least parasitic drag when the wing is lifting at its most efficient condition (i.e., maximum aircraft C_L/C_D).

To thoroughly model the drag polar of an aircraft with any combination of wing camber and incidence, recognize that the induced drag is a function of the lift coefficient above the minimum drag $C_{L_{min}}$,

$$C_D = C_{D_{min}} + \frac{(C_L - C_{L_{min}})^2}{\pi A R e}$$

The linearized plot of the above drag polar would look similar to the simplified polars developed earlier. Recall that if there is no camber or angle of incidence, extrapolating the drag curve to $C_L = 0$ would yield the parasitic drag C_{D_o} . For most aircraft, extrapolation yields an effective parasitic drag coefficient $C_{D_{pe}}$, Figure 4.20. $C_{D_{pe}}$ is somewhat artificial because the drag is never really that low but is still useful because it allows the same simple modeling of the drag polar used in the earlier discussion. Its perfectly accurate to assume $C_{D_{pe}} = C_{D_o}$ as long as $C_L > C_{L_{min}}$. In fact, it is common practice to ignore the drag difference at very low values of C_L since aircraft do not sustain flight at these conditions. The error of the simplified model becomes apparent only when dealing with aircraft flying near zero-lift conditions.

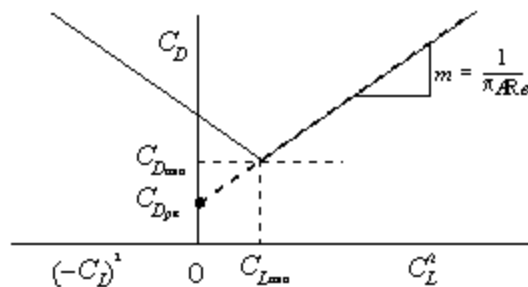


Figure 4.20 Linearized Drag Polar for Wing with Camber or Incidence

Figure 4.20 shows how the actual drag coefficient increases if below $C_{L_{min}}$. $C_{L_{min}}$ can be determined from flight test using the rollercoaster flight test technique or from wind tunnel data. Typical values for $C_{L_{min}}$ were 0.05 for the General Dynamics/Lockheed F-16 and 0.2 for the Republic A-10.

4.5.2 Flow Separation

As an aircraft approaches stall, the flow begins to separate and the drag increases more than that normally described by the induced drag term $C_{D_i} = \frac{C_L^2}{\pi AR e}$. Above a certain break-point C_L , the induced drag is further increased by some factor k_2 . The complete drag polar equation accounting for both a cambered airfoil and separating flow can be written as:

$$C_D = C_{D_{\min}} + \frac{(C_L - C_{L_{\min}})^2}{\pi AR e} + k_2 (C_L - C_{L_{\text{break}}})$$

Both k_2 and $C_{L_{\text{break}}}$ can be set to match flight test data. The last term above is not used if the lift coefficient is below $C_{L_{\text{break}}}$.

Because the effects of camber and flow separation cause the drag polar to deviate from the purely parabolic shape discussed originally, it then follows that some of the “optimum performance” equations developed earlier are also less valid. These equations include 4.7, 4.9, 4.12, 4.13, 4.20 and 4.22

4.5.3 Mach Number

The critical Mach number occurs once flow becomes supersonic somewhere on the aircraft. As soon as this happens, shock waves form and their attendant drag increase strengthens with the shockwave. Figure 4.21 shows that changes to the drag polar can be modeled according to constant values for Mach number. This is logical since shock wave formation is directly related to Mach number for a given shape.

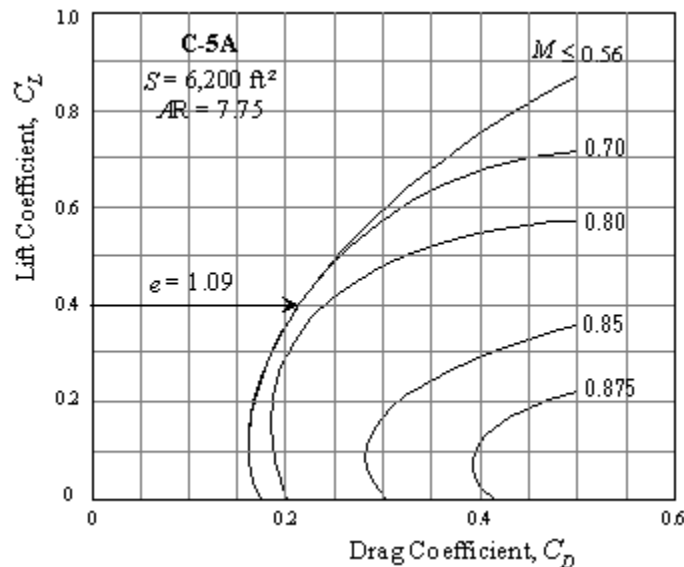


Figure 4.21 Drag Polar for the USAF C-5 Cargo aircraft

Shapes that are streamlined and have a high fineness ratio are less affected than shapes that are blunt and not streamlined. This is illustrated in Figure 4.22 for a multirole fighter aircraft flying with no external stores and again with multiple external stores. Note the more dramatic high-Mach drag penalty for the configuration with stores.

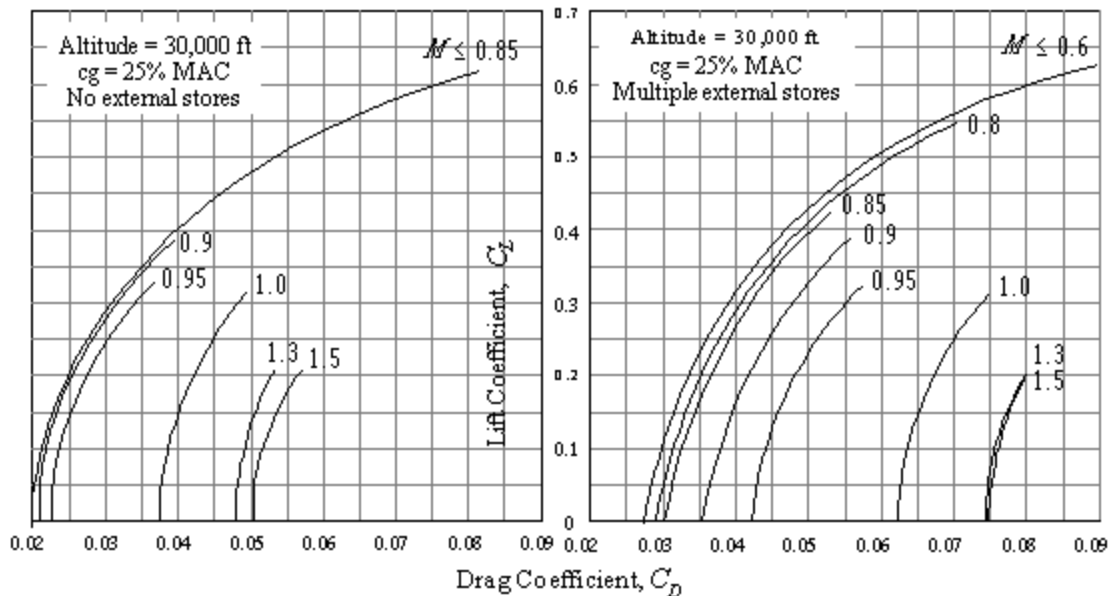


Figure 4.22 Drag Polars for Multirole Fighter Bomber

As a general rule, jet transport aircraft tend to show a drag rise above 0.6 or 0.7 Mach number, while clean fighter-types may not get a drag rise until about 0.9 Mach number. The latest jets developed for executive transport cruise at the edge of drag divergence at about 0.92 Mach number.

4.5.4 Reynolds Number

As developed in dimensional analysis, the force coefficients on an object immersed in a fluid flow are affected by the object's shape & orientation as well as the flow's dynamic pressure, compressibility (i.e. Mach effects) and Reynolds number. Reynolds number R_e equals $\rho V l / \mu$ where ρ is the flow density, V is flow velocity, μ is the viscosity of the fluid, and l is the distance the flow has traveled along the surface. From this definition, it is apparent that the Reynolds number of an aircraft in flight changes with altitude, velocity, and ambient temperature (which affect both density and viscosity to a small degree). It is also apparent that the Reynolds number changes as the flow progresses along any surface. This change in "local R_e " contributes to the boundary layer changing from laminar to turbulent

conditions. For aircraft, this transition occurs when the local R_e reaches about 1 million. Except for especially small vehicles that fly slow (such as high altitude remotely piloted vehicles), the majority of boundary layer flow against the skin of an aircraft is turbulent.

When discussing the overall R_e of an aircraft or one of its components, it is common to use a characteristic length such as the wing or tail chord or the fuselage length. This overall R_e is used to describe the correction to drag polars. Essentially, the only Reynolds number effect is a **decrease in skin friction drag coefficient (c_f) as R_e increases**. This principle does not apply as the flow transitions to turbulent flow which has higher drag along with its higher R_e . If the boundary layer is laminar, then $c_{f_i} = 1.326 R_n^{-0.5}$. If the boundary layer is turbulent, then $c_{f_i} = 0.455 \{\log R_n\}^{-2.58}$ (Prandtl-Schlichting relationship). The subscript i denotes the incompressible flow value.

The total skin friction drag = $q c_f S_w$ where S_w is the actual exposed or "wetted" area of the surface under consideration. Because each component of an aircraft has a different length along the flow, each component will have its own characteristic R_e . This means that the drag polar corrections due to R_e will be different for the wing, fuselage, horizontal & vertical tails and other components with their leading edges exposed to the freestream. The total correction is the sum of individual corrections.

Considering the parameters that comprise Reynolds number, flight testers can view R_e effects as a decrease in drag coefficient as an aircraft accelerates to higher speed (at some constant altitude). More commonly, however, we view it as an altitude effect (at some specific Mach number). If an aircraft's drag polar is accurately determined at one altitude, then corrections to this polar can be made for other altitudes. In a similar fashion, data collected at two different altitudes can be corrected to some common altitude for comparison purposes. It is common practice to use a "heart of the envelope" value for the reference Reynolds number.

The correction to the drag polar is expressed in term of ΔC_D and is determined as follows:

1. At the test condition, determine the characteristic R_e for each component of the aircraft (wing, fuselage, fin, etc.). A convenient method for calculating R_e comes from Sutherland's Law:

$$R_e = 7.101 \times 10^6 M \left[\frac{\delta}{\theta^2} \left[\frac{T + 110}{398.15} \right] \right] l \text{ (use } T \text{ in Kelvin)}$$

2. Use the Prandtl-Schlichting relationship to calculate c_{f_i} for each component.
3. For each component, correct to compressible friction coefficient: $c_f = c_{f_i} \left\{ 1 + 0.15 M^2 \right\}^{-0.58}$ for turbulent boundary layers (or $c_f = c_{f_i} \left\{ 1 + 0.1305 M^2 \right\}^{-0.12}$ for laminar boundary layers).
4. Repeat steps 1-3 for the desired reference or standard flight condition.
5. For each component, calculate the change in drag = $\Delta c_f q S_w = \left\{ c_{f_{ref}} - c_{f_{test}} \right\} q S_w$
6. The change in total drag coefficient is the sum of changes in component drag divided by $q S$:

$$\Delta C_D = \frac{\Sigma \Delta c_f q S_w}{q S} = \frac{\Sigma [\Delta c_f S_w]}{S}$$

4.5.5 Trim Drag

If an aircraft's cg is located so that the horizontal tail or canard is not lifting, then the only drag created is that due to its parasitic drag. If the surface does create lift, whether upwards or downwards, then it will also create its own induced drag. If this surface lifts downwards, then the main wing must compensate by lifting more upwards, thereby creating even more induced drag. If the tail or canard lifts upward, then the wing's lifting requirement is slightly reduced and so is the wing's induced drag.

Careful placement of an aircraft's cg can ensure that both surfaces lift upwards, but this might cause problems. For tailed aircraft, the aft cg location required may yield unsatisfactory stability. For canard aircraft, the downwash created by the canard disturbs the flow and efficiency over the main wing. For both types of aircraft, the smaller lifting surface is less efficient and creates more drag-per-lift than the main wing, so it does little good for the smaller surface to create large amounts of upward lift.

The total change in drag due to changes in cg only are called trim drag corrections. The common practice is to evaluate an aircraft at some typical cg location and adjust the drag polar to show the effect of cg movement from this baseline or "reference" condition.

A development of trim drag estimation is outlined in reference 4.4 for an aircraft with geometry shown in Figure 4.23.

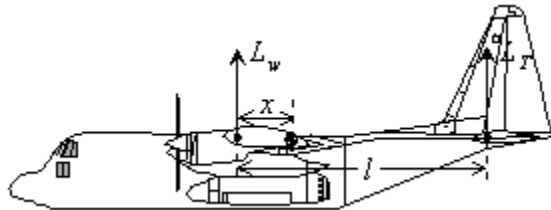


Figure 4.23 Model for Trim Drag Development

The change in induced drag from cg location x_0 to x_1 is:

$$\Delta C_{D_{trim}} = \frac{W^2}{\pi q^2 S b^2 e} \left\{ \frac{2}{l W} [x_0 - x_1] + \frac{1}{l^2} \left[1 + \frac{S}{S_t} \frac{e}{e_t} \left(\frac{b}{b_t} \right)^2 \right] [x_0^2 - x_1^2] \right\}$$

The fractional change in drag is

$$\frac{\Delta C_{D_{trim}}}{C_{D_i}} = \frac{x}{l} \left[\frac{x}{l} \left(\frac{b}{b_t} \right)^2 \frac{e}{e_t} - 2 \right]$$

This equation is illustrated in Figure 4.24 to show the effect of x/l on trim drag for various combinations of $\left[\left(\frac{b}{b_t} \right)^2 \frac{e}{e_t} \right]$.

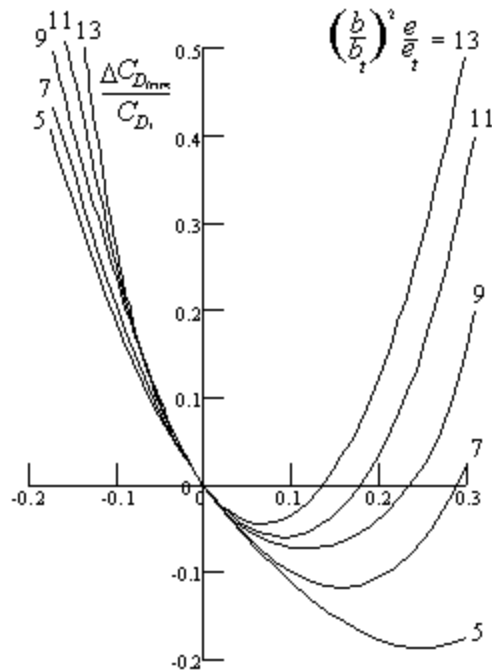


Figure 4.24 Effect of cg Position on Trim Drag

Typical values are $b/b_t = 3$ and $e=e_t$. Note that a small negative drag increment can be obtained with a cg slightly aft of the aircraft's aerodynamic center. Because of limitations on the cg range of most aircraft, the trim drag is usually less than 1-2% of the total aircraft drag. Sometimes this small difference is not measurable.

4.5.6 Slipstream Drag

Propeller-driven aircraft create a "scrubbing drag" on the surfaces exposed to the propwash. This can appear as either increased drag or as decreased engine or propeller efficiency, depending on drag bookkeeping + methods. A propeller manufacturer might perform carefully instrumented measurements to determine a prop's exact efficiency in an isolated environment (i.e. no body interference). The same

can be done by the engine manufacturer. At the same time, aerodynamicists might perform wind tunnel tests or even propless glider-style testing to determine the exact drag of the basic airframe.

All of the above data can be assembled to predict the horsepower required to fly at any flight condition. Typically, however, it appears as though one of the measurements must be wrong since the aircraft needs more power than predicted for that given flight condition. Assuming correct information for the prop, engine and airframe, the extra power requirement is due to the propwash. This "slipstream" or "scrubbing" drag is caused by the higher airflow velocity along the surfaces exposed to the slipstream.

Scrubbing drag is a function of the propwash velocity, which is a function of the propeller's thrust. Wind tunnels can be used to estimate the prop thrust effect. This correction might be shown as a series of drag polars, one for each value of thrust coefficient.

4.6 References

- 4.1 U.S.A.F. Test Pilot School, *Performance Theory and Flight Test Techniques*, Edwards AFB, 1979
- 4.2 Hurt, Hugh H., *Aerodynamics for Naval Aviators*, University of Southern California, Los Angeles, CA, 1959.
- 4.3 Roskam, Jan Dr., *Airplane Design, Part VI*, Roskam Aviation and Engineering Corp. 1990.
- 4.4 McCormick, Barnes W., *Aerodynamics, Aeronautics, and Flight Mechanics*, Wiley & Sons, 1979.
- 4.5 Stinton, Darryl, *The Design of the Aeroplane*, BSP Professional Books, Oxford, 1983.

Volume 2 – Aerodynamics for Flight Testers

Chapter 5

Transonic Aerodynamics

Table of Contents

5.1 Introduction.....	2
5.2 Compressibility.....	2
5.3 Mach Number.....	3
5.4 Critical Mach Number.....	4
5.5 Wave Drag.....	5
5.6 Shock Waves.....	6
5.7 Sonic Booms.....	7
5.8 Design Methods for Delaying or Reducing Mach Drag.....	8
5.8.1 Thin Airfoils.....	9
5.8.2 Wing Sweep.....	10
5.8.3 Low Aspect Ratio.....	13
5.9 Area Ruling.....	13
5.10 Supercritical Wing.....	15
5.11 References.....	16

5.1 Introduction

The difference between subsonic and transonic aerodynamics is the way we treat density. In subsonic aerodynamics we made the simplifying assumption that the flow was incompressible; that is, that density remained constant throughout the flow field. Incompressible flow is obviously a myth. Anyone who has blown up a bicycle tire is aware of the compressible nature of air. If air were actually incompressible, then the speed of sound would be infinite, which is also clearly incorrect. But the assumption was used for two reasons: it made the equations easier to solve, and it gave good predictions for early, slow moving aircraft. One way to see how the equations were made easier is to look at the equation for mass flow rate, which must remain constant in steady flow through a varying area streamtube as shown in Figure 5.1:

$$\rho_1 V_1 A_1 = \rho_2 V_2 A_2$$

or the velocity at station 2 is just

$$V_2 = \frac{\rho_1}{\rho_2} \frac{A_1}{A_2} V_1$$

By assuming density doesn't change, we can simplify the relationship:

$$V_2 = \frac{A_1}{A_2} V_1,$$

and we have the velocity throughout the streamtube knowing only the entrance velocity and how the area changes in the streamtube. This allows us to calculate static and dynamic pressure throughout the streamtube using Bernoulli's equation, from which we can determine all the aerodynamic forces.

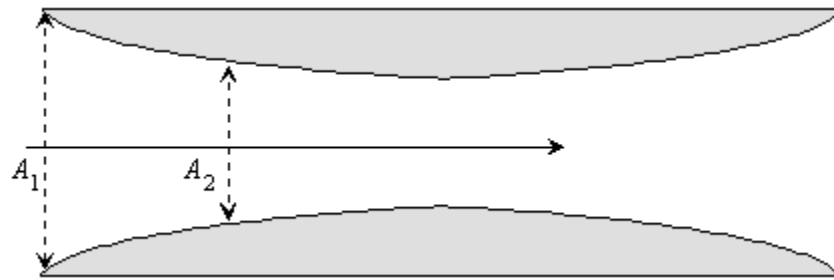


Figure 5.1 Varying Area Streamtube

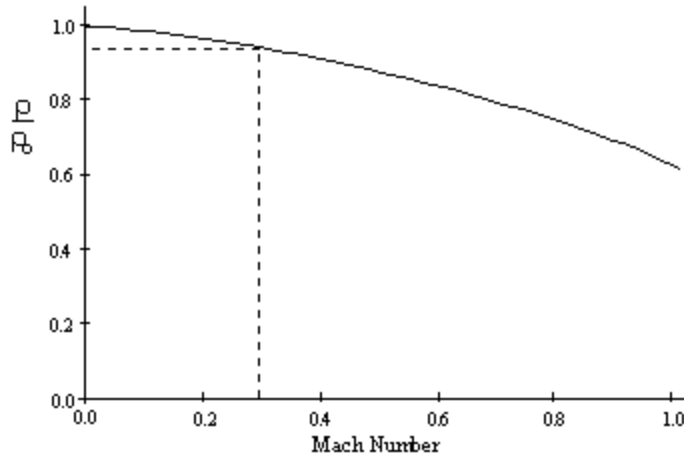
5.2 Compressibility

The results of incompressible flow theory worked well for aircraft through the 1920's. But as aircraft began to fly faster, the results were less capable of predicting actual aircraft performance. This is because air is a compressible fluid and the error in assuming that it was incompressible was low at slow speeds, but as speeds increased, so did the errors. Figure 5.2 shows how density changes with Mach number. At speeds up to about Mach 0.3, there is less than a 5% error in assuming that density was a

constant. Given the accuracy of most aeronautical experiments before 1930, this error could easily be considered negligible.

Figure 5.2 Density Change of Air with Speed

But at Mach numbers above 0.3, the errors resulting from an incompressible flow assumption



became too large. In 1928, Herman Glauert, a British aerodynamicist, published a paper with a proof for a compressibility correction factor first proposed by a German, Ludwig Prandtl. The purpose of the correction factor was to allow aircraft designers to continue using the basic incompressible equations with a small modification. This correction was to multiply the pressure coefficient (which affects lift, drag, etc.) as follows:

$$C_{P_{compressible}} = \frac{1}{\sqrt{1-M^2}} \times C_{P_{incompressible}}$$

This is called the Prandtl-Glauert compressibility correction factor. The correction worked well up to a point. At Mach numbers close to 1.0, this correction factor would lead to infinite nondimensional coefficients - one source of the "sound barrier" myth in the 1940's. Thus there is an upper limit to how far the Prandtl-Glauert correction factor can be applied. It is generally considered to give reasonable results up to speeds of approximately Mach 0.7.

5.3 Mach Number

The regions of applicability and the correction factor are both expressed in terms of Mach number, a common term, but what exactly is it? In 1887, a German physicist, Ernst Mach, published a paper on supersonic shock waves. In the paper he pointed out the importance of the flow velocity relative to the speed of sound. Later in 1929, a Swiss engineer, Jacob Ackeret, introduced the term "Mach Number" in honor of Ernst Mach and defined it as the ratio of the speed of the flow to the speed of the sound in the fluid, usually denoted by a .

$$M = \frac{V}{a}$$

Unlike some of the other nondimensional numbers used by aerodynamicists, this is not just a convenient way of avoiding messy units. The magnitude of the Mach number has real physical significance. The ratio tells how fast the fluid is moving relative to sound waves, which are nothing more than pressure disturbances. Thus if the static pressure changes due to the presence of a cambered airfoil, then that pressure disturbance will travel upstream at the speed of sound. If the flow is moving at a significant fraction of the speed of sound, the pressure change will have less influence upstream.

Thus at low subsonic Mach numbers, the flow ahead is warned of an approaching body and the flow can adjust gradually and go smoothly around the body. Once Mach one is reached or exceeded, the upstream flow has no warning of the approaching body and so it must adjust abruptly. This abrupt adjustment of the flow is a discontinuity called a shock wave. Figure 5.3 shows how Mach number affects pressure disturbance propagation.

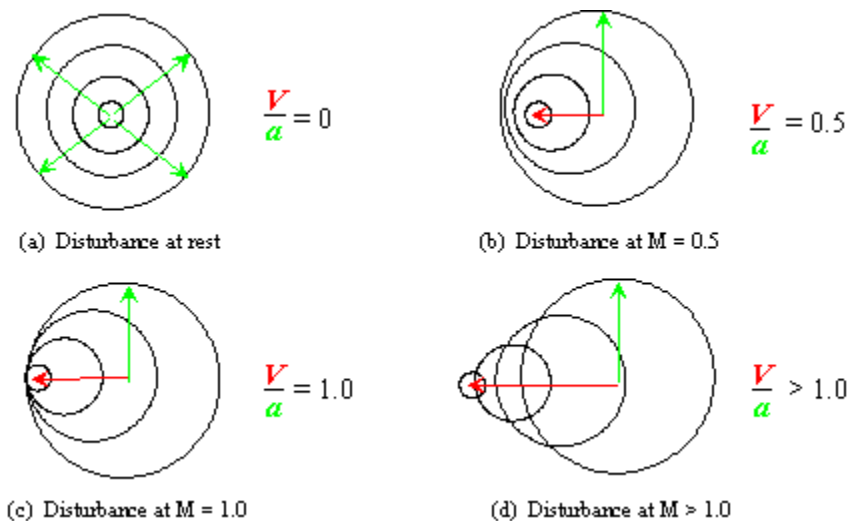


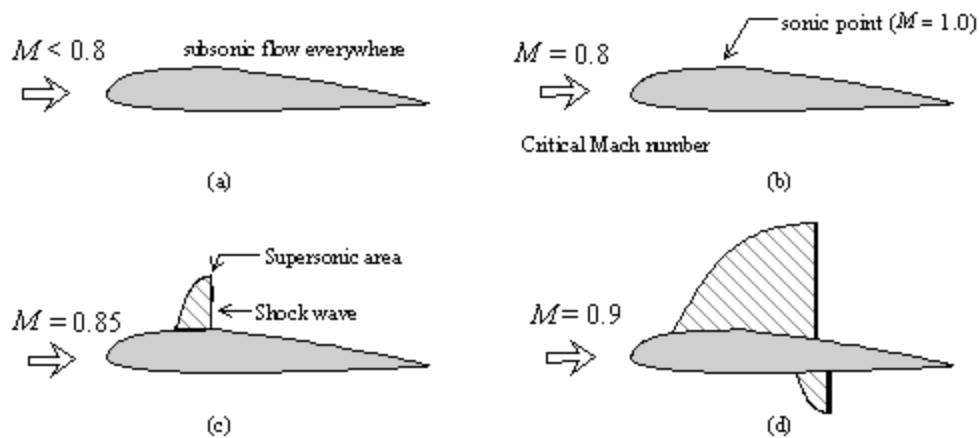
Figure 5.3 Mach Number's Influence on Pressure Propagation

5.4 Critical Mach Number

The critical Mach number (M_{CRIT}) is the freestream Mach number at which some portion of the flow around an airfoil or other part of an aircraft first reaches sonic velocity. Suppose a wing is at some low speed and the flow over the entire wing is subsonic (see Figure 5.4a). The wing as a whole is at one speed, but the flow accelerates as it moves over the wing's camber, resulting in a higher local speed on the upper surface. If the highest speed on the wing is still below Mach 1.0, then the wing is below M_{CRIT} . As the aircraft accelerates to a higher speed, so does the flow over the highest camber point. At some freestream speed less than Mach 1.0, the flow over the highest camber point will reach Mach 1.0. The

freestream speed at which this first occurs is the critical Mach number, shown as $M = 0.8$ in Figure 5.4b. The critical Mach number for a specific airfoil depends on the wing shape and angle of attack. At speeds slightly above the critical Mach number, the point of sonic flow will grow to a region of supersonic flow (Figure 5.4c). Pressure changes downstream of the supersonic region move forward towards the supersonic area but can progress no further and thus form a pressure discontinuity called a shockwave. As the airflow passes through this shock wave it experiences almost instantaneous changes in pressure, temperature and density; in giving up this energy, the airflow is decelerated abruptly from supersonic to subsonic velocity. A rapid change in velocity requires a large force. This force opposes the motion of the wing through the air, thus it is a form of drag, called wave drag or Mach drag. At higher subsonic freestream Mach numbers the supersonic area grows larger, the shock wave gets bigger, and a second area begins on the lower surface. All of this produces more wave drag.

Figure 5.4 Shock Wave Formation at the Critical Mach Number



5.5 Wave Drag

In purely subsonic flow we divided drag into two major components: parasitic drag and induced drag. Parasite drag was due to skin friction, frontal area, and interference between various parts of the vehicle. Induced drag was the drag due to producing lift. The new drag source above M_{CRIT} doesn't fit into either of these categories. See Figure 5.5.

Wave drag has two major components. The first part occurs only in the transonic regime. As the supersonic area begins to grow on the upper surface of the wing (Fig.5.4c) the shock wave at the end of the area can trigger flow separation. This is called *shock-induced separation*. The cause and its effects on flying qualities is described more fully in Chapter 6 Volume 4. However, in general, pressure increases dramatically through the shock and this increase in static pressure aft of the shock can trigger separation. This new region of separated flow will cause additional pressure drag.

The second part of wave drag is the major contributor to the drag increase. The shock wave is very thin; a discontinuity in the flow. Across this very short region, the flow abruptly slows. This large velocity change over a short distance (or short time in a moving reference system) requires a large force to oppose the velocity decrease, as was stated earlier. This force is the major part of wave drag.

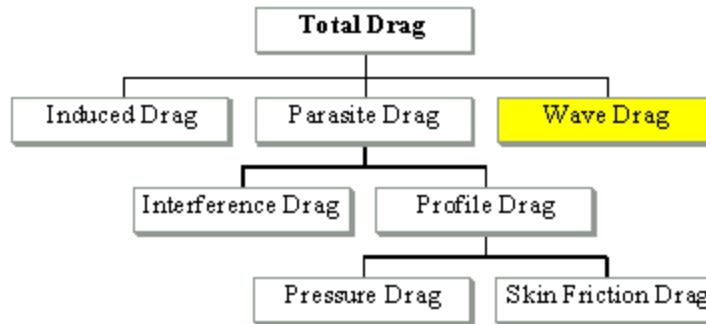


Figure 5.5 Aircraft Drag Components

5.6 Shock Waves

As we have already seen, the principal component of wave drag is due to slowing the flow through a shock wave. In the transonic regime, normal shock waves develop on the upper and lower surface of the wing. By normal, we imply that the shock wave is perpendicular to the flow direction. Normal shocks slow the flow more dramatically than oblique shocks. Oblique shocks develop on the leading and trailing edge of wings that have accelerated to completely supersonic speeds. See Figure 5.6.

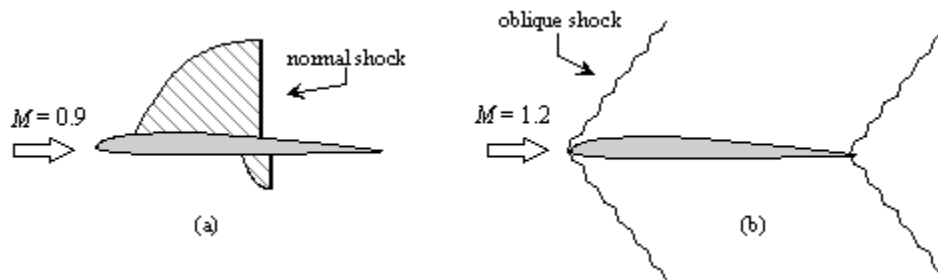


Figure 5.6 Normal and Oblique Shock Waves

Both types of shocks slow the flow, but at transonic speeds the deceleration is bigger and so the drag increment is larger. The increment of drag coefficient at transonic speeds can be seen in Figure 5.7. Drag coefficient is plotted at a constant lift coefficient. Thus both parasite and induced drag coefficient components are constant. The increase is simply the delta due to wave drag.

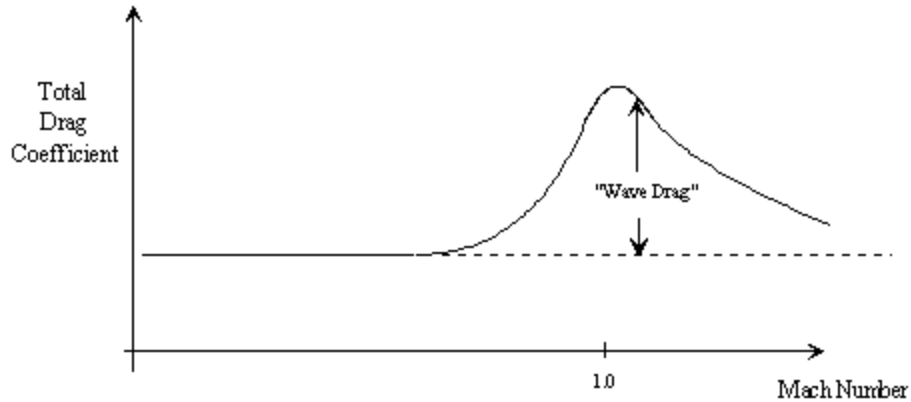


Figure 5.7 Wave Drag Increment

In Figure 5.7 the drag diverges from the subsonic constant value (at a given lift coefficient) at a speed below Mach one. The point at which drag increases, sometimes called the *drag-divergence* Mach number, is just above M_{CRIT} . As stated earlier, the oblique shocks at fully supersonic speeds give less drag increase than the multiple normal shocks near Mach one, so the total drag coefficient actually decreases at higher speeds. This does not mean that total drag goes down, just the drag coefficient. When the drag coefficient is multiplied by the dynamic pressure ($1/2 \rho V^2$), total drag still increases, but at a slower rate. The peak in the drag coefficient curve is one source of the sound barrier myth popularized by the press in the 1940's. Adding to the sound barrier concerns was the fact that early drag data from aircraft approaching the speed of sound fell along a curve that closely matched Prandtl and Glauert's approximations which predicted that at Mach one the drag would be infinite! But knowledgeable aerodynamicists realized that supersonic speeds were routinely achieved by rifle bullets and thus the drag might be large but not infinite. In fact, in his 1887 paper, Ernst Mach published photographs showing the shock waves produced by a supersonic bullet. While the designers of the Bell X-1, the first airplane to exceed Mach one, knew the drag couldn't be infinite, they didn't know how large it might become. They therefore took a conservative approach and chose a proven design. The nose shape of the X-1 was the same as a 0.50 caliber bullet.

5.7 Sonic Booms

Sonic booms are the result of shock waves. When the flow abruptly slows through a shock wave the static pressure dramatically increases over a very short distance. The thickness of the shock wave is on the order of the average distance individual atoms travel between collisions, approximately 10^{-6} meters. When the pressure changes this abruptly it produces a large overpressure which is heard on the ground as a boom. The magnitude of the overpressure is a function of several things, including:

1. Mach number of the vehicle. The higher the Mach number the greater the velocity changes and hence the greater the pressure change.

2. Wing/body shape. Very thin wings tend to produce less strong, oblique shock waves rather than a strong normal shock. Thus thin wings develop less overpressure and a smaller sonic boom.
3. Distance from the source is a key factor in the magnitude of the overpressure felt at the surface. Thus increasing either height or lateral offset will reduce the size of the boom. For this reason, except in specially designated areas, supersonic flight in the United States is restricted to altitudes above 30,000 ft.

The sonic boom on the ground is felt as the pressure change due to the shock as it is dragged across the surface as shown in Figure 5.8. A frequent misconception is that the boom only occurs as a result of the aircraft initially exceeding the speed of sound. While shocks formed in transonic flight can be quite loud due to the numerous normal shocks, a sonic boom will be heard by everyone in the path of an aircraft traveling at speeds above Mach one. On rare occasions, a dramatically increased overpressure can occur when the supersonic aircraft turns. If you envision the overpressure area as a cone being dragged behind the aircraft, when the source of the overpressure turns, the overpressures generated can pile up at one location on the ground. This is called a focused shock and can result in very high local overpressures.

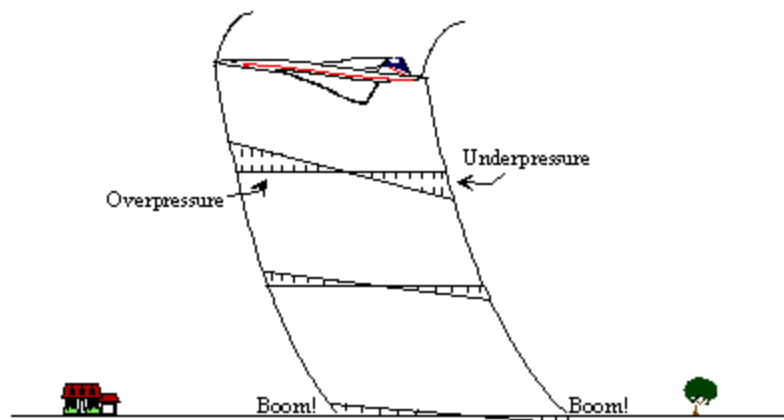


Figure 5.8 Sonic Booms

5.8 Design Methods for Delaying or Reducing Mach Drag

The remainder of this chapter will focus on design methods used to minimize the effect of shock waves on the performance of the aircraft. This can be done by either increasing M_{CRIT} and thus avoiding shock waves at higher and higher subsonic speeds, or by reducing the effects of the shock waves once M_{CRIT} has been exceeded. The design methods to be covered include:

1. Thin airfoils.
2. Swept wings.
3. Low aspect ratio.
4. Area ruling.
5. Supercritical wing design.

5.8.1 Thin Airfoils

Most supersonic airfoils are very thin. That is, the maximum thickness to chord length ratio (t/c) is small compared to subsonic wing designs. Typical variations are shown in Figure 5.9

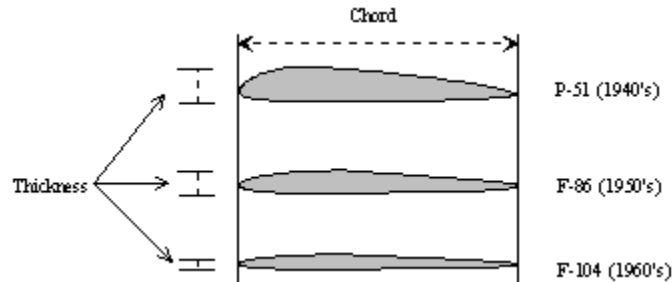


Figure 5.9 Thickness to Chord Ratio Definition

It has been found that the wave drag coefficient is approximately proportional to the square of the thickness to chord ratio. This is due to two causes. First, a small t/c means that the flow is sped up less as it passes over the wing resulting in a delayed M_{CRIT} and less delta velocity once M_{CRIT} has been exceeded. Secondly, weaker oblique shocks form once the wing is entirely supersonic due to less turning angle for the supersonic flow required at the leading edge. The delay in the drag divergence Mach number and the reduction of drag coefficient transonically is shown for two airfoils in Figure 5.10.

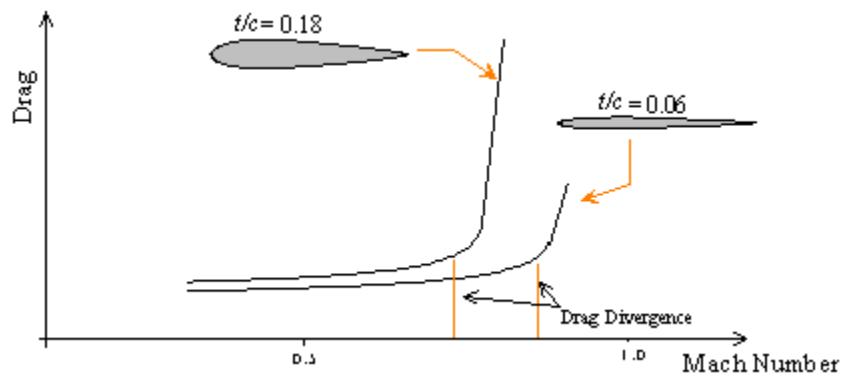


Figure 5.10 Mach Drag Increase is Delayed for Thin Wings

The obvious benefits of thin wings for transonic and supersonic flight are offset by some drawbacks. First the minimal camber produces less lift at subsonic speeds, requiring high angle of attack and/or high speeds for landing. Secondly, the internal space in the wing does not allow a truss-like construction, resulting in a heavier structure than for thicker wing. And finally, the wing allows no room for fuel, landing gear, or in extreme cases, not even for flap and aileron actuators, which end up being mounted externally.

5.8.2 Wing Sweep

The first examples of wing sweep were seen in some German aircraft during World War II following the prediction by Adolf Busemann that sweeping the wing back would delay and reduce the effects of compressibility. There are two ways to illustrate how wing sweep affects the critical Mach number and the speed at which the drag begins to rise. First, sweeping the wing effectively decreases the thickness to chord ratio as shown in Figure 5.11. With the wing swept, the flow goes over a longer distance from leading to trailing edge (chord length), the maximum camber thickness is unchanged by sweeping, and so the t/c is smaller, resulting in delayed and reduced Mach drag as discussed above under thin wings.

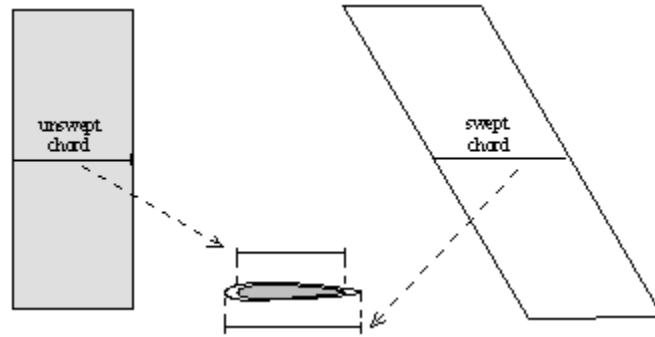


Figure 5.11 Sweeping Wings Decreases Thickness to Chord Ratio

A second way to understand the benefit of swept wings in transonic flight is to realize that only the normal component of the freestream flow is accelerated over the wing. The wing is not cambered from root to tip, only from leading to trailing edge. Thus only the component of the flow normal to the leading edge is accelerated over the wing. As shown in Figure 5.12, if the wing is swept aft by an angle, L , then the flow normal to the leading edge is moving at a speed equal to $V_{\infty} \cos(L)$. If M_{crit} was 0.8 Mach for an unswept wing, the new M_{crit} for the same wing cross-section swept 30° would be 0.8 Mach divided by the cosine of 30° , or 0.92 Mach. But this is only the theoretical effect and practical increases will be slightly less.

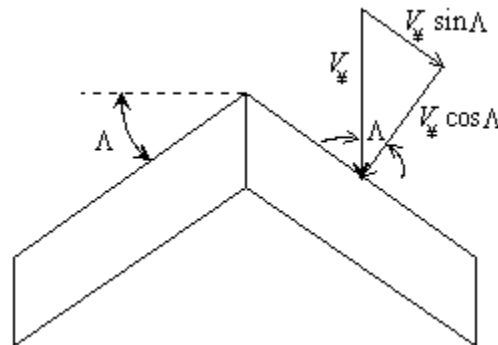


Figure 5.12 Wing Sweep Angle

Sweeping the wings aft thus delays the drag divergence Mach number. Typical data can be seen in Figure 5.13. A second effect of sweeping the wings is to reduce the peak magnitude of the drag coefficient in the transonic range, which can also be seen in the same figure. This reduced maximum drag coefficient is the result of fewer normal shocks as the aircraft transitions from subsonic through transonic to reach the fully supersonic region. That is, since M_{crit} is higher, there is a smaller speed range between subsonic flow throughout and the fully supersonic case. As you can also see, the Mach number at the maximum drag coefficient point increases with wing sweep angle. It appears from the figure that the drag divergence Mach number increases to supersonic speeds. This is just the theoretical result assuming simply that only the normal component is affected by the wing. But in the real world with fuselages and interference effects, the value of M_{crit} and drag divergence is always less than 1.0.

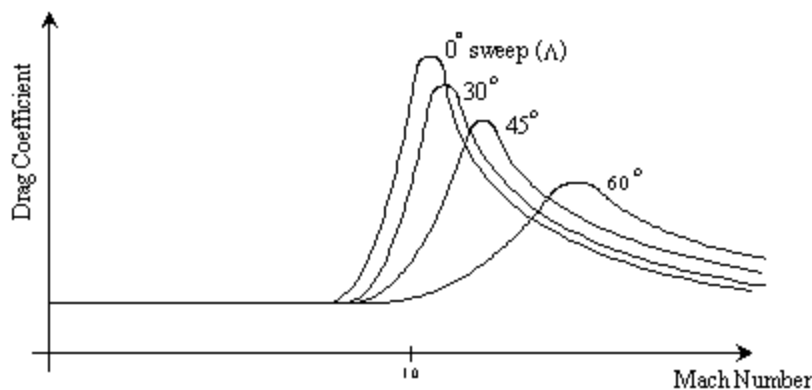


Figure 5.13 Theoretical Wave Drag Variation with Wing Sweep Angle

Swept wings, like thin wings, have disadvantages. Since only the normal component of the flow is accelerated, less pressure change is developed and so lift is less at the same angle of attack as compared to a straight wing (see Figure 5.14).

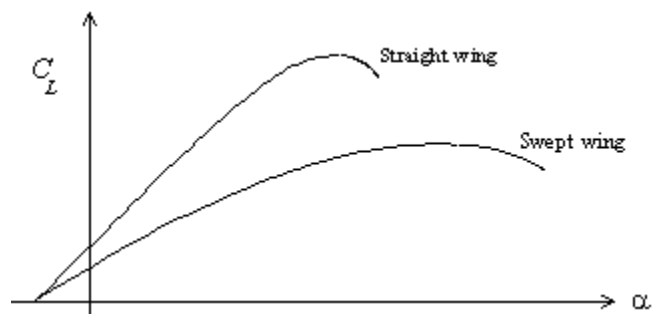


Figure 5.14 Swept Wings Produce Less Lift than Straight Wings at the Same AOA

At very high speeds, the design condition for a swept wing, the decrease in lift coefficient is not a major problem since $L = qSC_L$ and q (dynamic pressure) is a function of V^2 . But all planes have to takeoff and land. High speeds during takeoff and landing increase both runway required and risk. Swept

wing airplanes minimize the speed increases in two principal ways. First, wing area (S) can be increased which will offset the reduction in C_L . This is commonly done by simply filling in the area between the swept wing and the fuselage, making a delta wing. Secondly, the wing can be made to pivot, allowing the wing to be swept at high speeds and straight at low speeds. The additional weight and complexity of this variable sweep must be traded off against the performance advantages during the design process. Examples are shown in Figure 5.15.

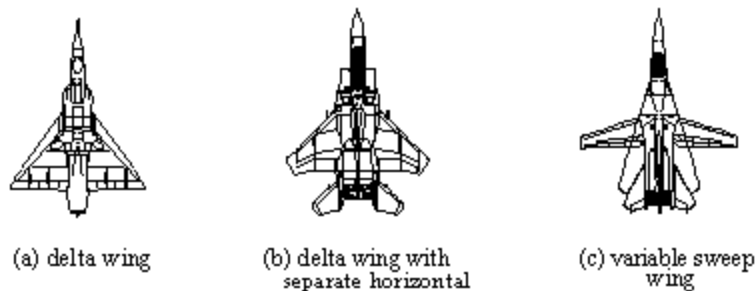


Figure 5.15 Swept Wing Design Variations

Either aft or forward wing sweep would be equally effective in delaying M_{crit} and reducing the peak wave drag coefficient. Forward swept wings would be more desirable for two reasons. First, aft swept wings generally produce adverse stall characteristics, as we will discuss in Chapter 11 Volume 3, Stalls - Theory and Flight Test. Secondly, forward swept wings are more efficient at cruise angles of attack since the fuselage acts as an end plate for the spanwise flow which is in an inboard direction.

The reason that forward swept wings are not in general use is due to structural considerations, specifically wing divergence. When a swept wing bends due to aerodynamic loads, it also twists. For an aft swept wing, bending will produce a twist that decreases the angle of attack slightly, which reduces the forcing function. On a forward swept wing the opposite occurs. That is, when a large aerodynamic force bends a forward swept wing upward it produces an upward twist in the leading edge, which increases the angle of attack, increasing the forcing function. Unless the wing is made rigid enough, divergence (a euphemism for breaking) can occur. The added weight to achieve the necessary rigidity has been prohibitive until the advent of composite structures. The X-29 demonstrated the feasibility of building a forward swept wing with "aeroelastically tailored" composite structures. By aeroelastic tailoring it is meant that the wing strength is increased in torsional rigidity without making the entire wing more rigid and thus heavier. Figure 5.16 illustrates the wing divergence problem. Other problems with forward swept wings include RADAR cross section for military applications and public acceptance for civilian applications.

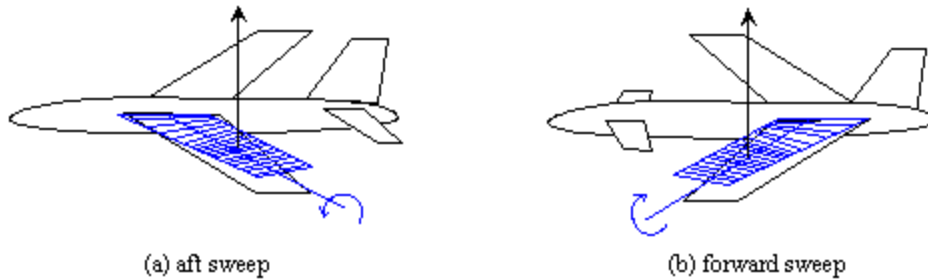


Figure 5.16 Wing Divergence of Forward Swept Wings

5.8.3 Low Aspect Ratio

Recalling from Chapter 3, Subsonic Aerodynamics, a wing's aspect ratio is defined as the ratio of the span squared to the wing area (b^2/S). High aspect wings are more efficient than low aspect wings at subsonic speeds. Transonically, low aspect wings are better. Figure 5.17 shows how M_{crit} varies with aspect ratio. For aspect ratios below approximately 4, there is a significant increase in M_{crit} . The F-104 is probably the most extreme example of transonic optimization by reducing aspect ratio; it has an AR of only 2.45. Even the F-4's AR is only 2.78, but the much larger wing area makes it less obvious.

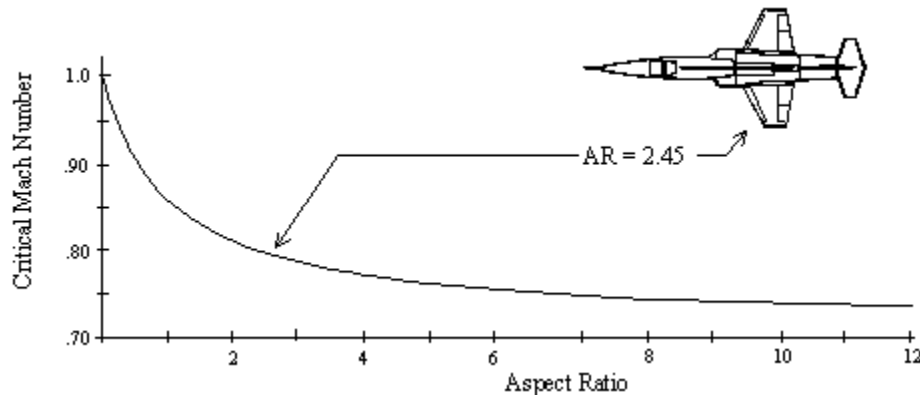


Figure 5.17 Decreasing Aspect Ratio Increases Critical Mach Number

The major drawback of low aspect ratio is in the low speed and high angle of attack areas where induced drag becomes a problem since $C_{D_i} = C_L^2 / (ARe)$. Also causing problems is the lower C_{Lmax} available at low aspect ratios, requiring higher takeoff and landing speeds.

5.9 Area Ruling

In the mid-1950's, an aeronautical engineer at the NACA Langley Aeronautical Laboratory, Richard T. Whitcomb, experimented with different shaped aircraft to determine the preferred shape for minimum transonic drag. He empirically determined (by using a file on balsa wood models) that the transonic drag was a linear function of the rate of change of cross-sectional area from nose to tail:

$$C_{D_M} = f\left(\frac{dA}{dx}\right)$$

where $A(x)$ is the area of a slice of the aircraft at a distance x from the nose, perpendicular to the x , or longitudinal, axis. Thus the peak transonic drag would be minimized by making the cross-sectional area vary smoothly from nose to tail. This concept was first applied to the Convair YF-102. At the trailing edge of the large delta wing on the YF-102, the cross-sectional area decreased abruptly, giving a large value of dA/dx , and thus a large value of wave drag near Mach one. Using Whitcomb's findings, the engineers at Convair redesigned the fuselage to give it a "coke bottle" shape. This reduced the abrupt decrease in dA/dx which reduced the transonic drag and allowed the YF-102 to exceed Mach one in level flight. Figure 5.18 illustrates the use of area rule.

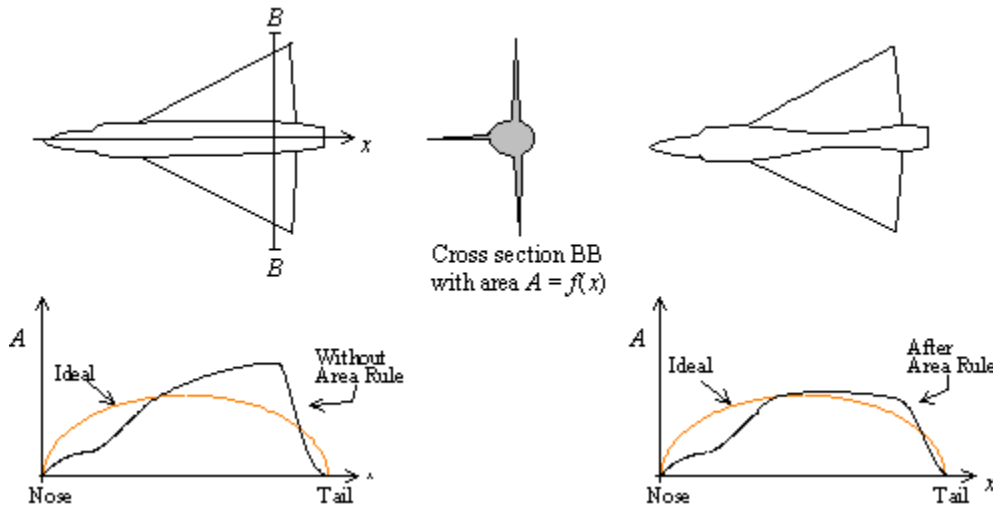


Figure 5.18 Area Ruling of YF-102

In the 1970's, aerodynamicists caught up with Whitcomb's empirical findings and showed that the wave drag was a function of the rate of variation of the intersecting area between the aircraft and a cone with a half angle of the Mach wave angle. The Mach wave angle is a function only of the Mach number as shown in Figure 5.19. It is defined as $\mu = \sin^{-1} \frac{1}{M}$. Regions in front of the Mach wave angle are not influenced by the approaching pressure disturbance and are said to be in the "zone of silence."

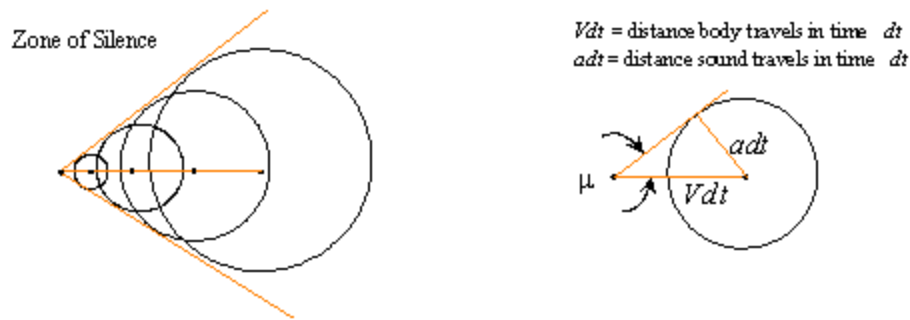


Figure 5.19 Mach Wave Angle

The Mach wave angle for $M = 1.0$ is 90° , so the 90° cross-sectional area is the correct variable to smooth for minimizing drag at Mach one, as Whitcomb correctly suggested. But at higher Mach numbers, a different smoothing technique is required. One of the design considerations for the YF-22 was minimizing wave drag at Mach 1.6 (the design condition) by smoothing the area variation along a cone with a half angle of $\mu = \sin^{-1} \frac{1}{1.6} = 39^\circ$.

5.10 Supercritical Wing

Whitcomb didn't stop there and in 1965 was responsible for the second major breakthrough in transonic airplane design since 1945, the supercritical wing. In analyzing the causes of drag rise in the transonic region, Whitcomb realized that the velocity profile over a conventionally cambered airfoil resulted in a peak velocity at approximately 25% mean aerodynamic chord (MAC). After that point the flow would continue to gradually slow back towards the original free stream velocity. The resulting pressure profile on the wing is shown in Figure 5.20(a). Changing the upper surface so that it would be flatter and thus produce lower peak velocity (delaying M_{CRIT}) would reduce the camber and the total lift. Increasing the reflex in the lower surface near the trailing edge restores the camber and total lift while retaining a lower peak velocity on the upper surface as shown in Figure 5.20(b).

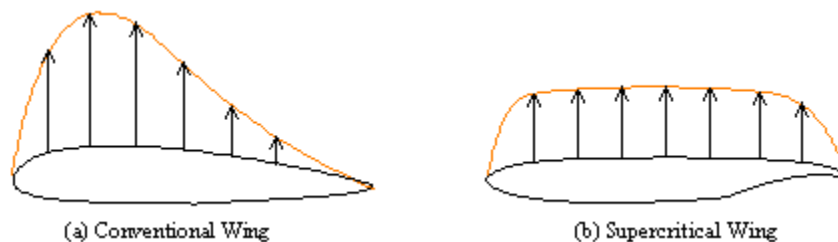


Figure 5.20 Supercritical Wing Design

This velocity profile change allows the aircraft to fly faster before the flow reaches Mach one on the upper surface. A second, and more significant, benefit is that once M_{crit} is exceeded, the resulting

shock wave on the upper surface is weaker due to the lower supersonic Mach numbers there. This gives less wave drag at speeds above M_{CRIT} , hence the term "supercritical." The analysis appeared sound, wind tunnel tests showed promise, and so a flight experiment was planned. In the past, many promising ideas were unable to fulfill expectations when put to a test in the actual flight environment. But the supercritical wing that NASA flew on a modified F-8 confirmed predictions. Supercritical wings are now being used in a variety of aircraft including the Boeing 757 and 767 as well as the latest model Lear jets. The decrease in drag rise can be exploited in two different ways as shown in Figure 5.21. You can either cruise at a 15% higher speed at the same drag or you can use a 58% thicker wing. Use of a thicker wing has several advantages. For the same strength, structural weight can be reduced by using truss like internal structure, resulting in better economy in manufacture and during flight. Also the larger volume allows more fuel to be carried internally and makes it easier to accommodate the landing gear. Finally, this thicker airfoil would give more lift at low speeds, allowing a lower speed during takeoff and landing.

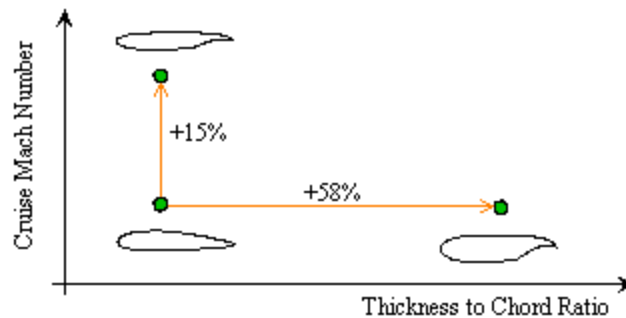


Figure 5.21 Supercritical Wing Advantages

5.11 References

- 5.1 Anderson, J. D., Jr., *Fundamentals of Aerodynamics, 2nd. ed.*, New York: McGraw-Hill, Inc., 1991.
- 5.2 *Aerodynamics for Pilots*, ATC Pamphlet 51-3, July 1979.
- 5.3 Hurt, H. H., Jr., *Aerodynamics for Naval Aviation*, NAVWEPS OD-8DT-80, Office of the Chief of Naval Operations Aviation Training Division, U. S. Navy, 1960.
- 5.4 NACA Report 1135, *Equations, Tables, and Charts for Compressible Flow*, Ames Research Staff, Ames Aeronautical Laboratory, Moffett Field, CA.
- 5.5 *Aircraft Performance*, Vol. 1, Chapter 6, "Supersonic Aerodynamics", USAF Test Pilot School, June, 1987.
- 5.6 Liepmann and Rochko, *Gas Dynamics*

Volume 2 – Aerodynamics for Flight Testers

Chapter 6

Supersonic Aerodynamics

Table of Contents

6.1 Introduction.....	3
6.2 Types of Ideal Gases.....	3
6.3 Aerodynamic Consideration of Compressible Flow.....	3
6.4 One-Dimensional Flow Approximation.....	4
6.5 Total (Stagnation) Properties.....	5
6.5.1 Total Temperature.....	5
6.5.2 Total Pressure.....	7
6.5.3 Total Density.....	7
6.5.4 Mathematical Relationships for Total Properties.....	7
6.6 Speed of Sound.....	8
6.7 Mach.....	9
6.8 Two-Dimensional Propagation of Sound Waves.....	9
6.8.1 Mach Angles.....	10
6.8.2 Activity Envelope.....	11
6.9 Classification of Speed Ranges.....	11
6.10 Isentropic Flow.....	11
6.11 Flow in Convergent-Divergent Streamtubes.....	14
6.11.1 Flow at the Throat.....	17
6.11.2 Mass Flow in a Choked Streamtube.....	19
6.11.3 Local Sonic Conditions.....	19
6.11.4 M^*	20
6.11.5 Area Ratio.....	21
6.12 Normal Shock Waves.....	21
6.12.1 Normal Shock Equations.....	21
6.12.2 Normal Shock Summary.....	22
6.13 Supersonic Pitot Tube.....	22
6.14 Oblique Shock Waves.....	23
6.14.1 Oblique Shock Relations.....	25
6.14.2 Minimum and Maximum Wave Angle.....	26
6.14.3 Relation between θ and δ	26
6.14.4 Mach Lines.....	28
6.15 Isentropic Compression.....	28
6.16 Isentropic Expansion.....	29
6.17 Interaction of Wave Forms.....	33
6.18 Two-Dimensional Supersonic Airfoils.....	34
6.19 Pressure Coefficient for Two-Dimensional Supersonic Airfoils and Infinite Wings.....	35
6.20 Thin Wing Theory.....	36
6.21 Supersonic Flow In Three Dimensions.....	38
6.22 Three-Dimensional Supersonic Wings.....	39
6.23 Transonic Flow Regime.....	40
6.23.1 Thickness.....	41

6.23.2 Supercritical Airfoils	42
6.23.3 Wing Sweep.....	43
6.23.4 Fuselage Shape and Area Rule	45
6.23.5 Transonic and Supersonic Control Surfaces.....	46
6.24 Summary	47
6.25 Problems	48
6.26 Answers.....	53
6.27 Bibliography	54

6.1 Introduction

Some of the basic concepts of Aerodynamics and Thermodynamics have previously been covered. These related to determination of the fluid flow around various shapes and the resultant forces acting upon the shapes. Fluids previously studied were assumed to be incompressible. This assumption reduced the number of variables involved and allowed relatively simple solutions to previously complex sets of equations. (This is an everyday activity of the engineer, but care must be taken to make sure the assumptions made to provide an idealized solution to a physical system are still valid if the idealized solution is applied to a different physical system.)

Incompressible flow is a myth. However, for low speed air ($M < 0.3$) the idealized incompressible-, flow solution was accurate enough. This was the case for aerodynamics up to the late 1930s. But as speed increased, so did the requirements for new idealized solutions to physical systems using different assumptions. In this chapter, the assumption of incompressible flow will be dropped, and the flow field will be considered compressible. Results obtained from the study of compressible fluids will then be applied to transonic and supersonic flow situations.

6.2 Types of Ideal Gases

A real gas is a compressible, viscous, elastic, non-homogeneous, and chemically active fluid, and the physical principles governing its behavior are not understood ' completely enough to permit the exact mathematical formulation of a general flow problem. Even if it were possible, the resulting equations would defy solution. Utilizing reasonable assumptions which, can be verified by experiment, specific physical systems can be described by equation, and the necessary properties determined.

The use of three different, idealized fluids has been found acceptable for solving fluid dynamic problems involving subsonic, transonic, and supersonic flows. In each idealized fluid, the fluid is assumed to be homogeneous and non-chemically reacting. The assumption of a homogeneous fluid is acceptable until the mean free path between gas molecules becomes a significant fraction of the size of the object being studied. The assumption of a non-chemically reacting gas is good up to fairly significant temperatures.

A perfect fluid is one which is incompressible, inelastic, and non-viscous. The perfect fluid assumption gives reasonable results when analyzing flow outside of a boundary layer at less than $M = 0.7$.

An incompressible, inelastic viscous fluid differs from a perfect fluid because of viscosity. This fluid assumption gives reasonable results for flow at less than $M = 0.7$ inside a boundary layer and in wakes behind an object.

A compressible, non-viscous, elastic fluid will be used in this chapter. This fluid assumption provides reasonable results for flow outside of the boundary layer up to hypersonic speeds ($Mach = 5$). Elasticity is defined as the change in pressure per unit change in specific volume and accounts for the finite propagation of a sound wave.

Analysis of a viscous, compressible fluid is very complex and relies heavily on experimental evidence for confirmation of the theory. Hypersonic flow requires the consideration of a viscous, compressible, nonhomogeneous dissociated, and chemically active fluid. It can be seen that the complexity of this analysis is much greater than subsonic and supersonic flow analysis.

6.3 Aerodynamic Consideration of Compressible Flow

Aerodynamics is concerned with the changes in pressure that occur over bodies of various sizes and shapes and the causes and effects of these changes. A large part of early aerodynamic research was based on the assumption of a non-viscous, inelastic, incompressible fluid. The assumption of incompressible, inelastic flow was acceptable at low speeds where a small change in pressure caused virtually no change in the density of the fluid. The assumption of a non-viscous fluid was acceptable as long as the viscous effects were restricted to the vicinity of the surface (in the boundary layer).

With the advent of high speed flight, these assumptions had to be reconsidered. The inelastic flow assumption implies that pressure variations are instantaneously felt everywhere in the fluid. In reality, they are transmitted at a finite speed, the speed of sound.

As the velocity of an aircraft approaches some sizeable fraction of the speed of sound (one half or more), the results obtained from incompressible flow relations are found to be significantly in error due to the effects of compressibility.

Viscous effects and boundary layers can be omitted from this discussion by studying the flow on an object outside of the boundary layer.

Flow is defined as being compressible when a change in pressure is accompanied by a change in density, and the amount of compressibility depends on the velocity of the fluid flow. All gaseous flow is compressible, and even the so-called incompressible flow experiences some degree of compression. In the incompressible case, the velocity is so low that the change in density is insignificant compared to the change in pressure.

The introduction of a new variable, density, in aerodynamic problems requires the introduction of an equation of state and other thermodynamic relations to describe the changes in pressure, density, and temperature. The study of compressible flow combines the science of fluid mechanics and thermodynamics.

The general solution of a compressible flow problem consists of finding three unknown velocity components and three density and pressure changes with respect to the space coordinates x , y , and z . The mathematical complexity of this solution obscures many of the fundamental concepts of compressible flow which are quite clear when the flow is analyzed in one or two dimensions. In this chapter, fluid flow equations will be developed for one-dimensional flow, and then modification necessary to use the equations for two-dimensional flow will be discussed.

6.4 One-Dimensional Flow Approximation

One-dimensional flow generally implies straight line or linear motion; however, it need not be this restrictive. The equations of "one-dimensional" fluid flow can apply to flow through a passage in which the cross-section varies slowly so that components of velocity normal to the primary direction of flow can be considered negligible. For instance, flow in a curved channel can be considered one-dimensional as long as the radius of curvature is large compared to the length of the segment of channel that is under consideration. The channel need not be constant in area as long as the divergence or convergence is small compared with the distance along the channel.

The channel may either be bounded by physical boundaries such as the walls of a pipe or wind tunnel or by streamlines such as those surrounding an airfoil in flight.

The compressible flow equations which relate the flow velocity to the pressure, temperature, and density are obtained from three fundamental conservation principles and the equation of state for the fluid in question.

1. Conservation of mass
2. Conservation of momentum
3. Conservation of Energy
4. Equation of State

The assumptions that are made when first developing the compressible flow relations are: the flow is steady, one-dimensional, non-viscous, adiabatic, and the fluid conforms to the equation of state for a perfect gas. As restrictive as these assumptions may seem, they do not seriously limit the validity of the resulting equations.

The one-dimensional assumption can be extended to other than linear motion with certain restrictions, and viscosity can be ignored when flow is examined outside of a boundary layer. The adiabatic assumption can be justified by the fact that the temperature gradients, which are the driving potential for the transfer of heat in a flow, are small, causing the heat transfer, dq , to be small or negligible. The perfect gas assumption is good for air up to moderately high temperatures.

Under these assumptions, the conservation equations and equation of state may be written

Conservation of Mass: (Continuity Equation)

$$\dot{m} = \rho VA = \text{constant} \quad (6.1)$$

Applying the product rule of differentials and dividing by ρVA gives

$$\frac{d\rho}{\rho} + \frac{dV}{V} + \frac{dA}{A} = 0 \quad (6.2)$$

Conservation of Momentum: (Momentum Equation)

$$dP + \rho V dV = 0 \quad (6.3)$$

Conservation of Energy: (First Law of Thermodynamics)

$$dQ - dw = dE \quad (6.4)$$

Equation of State: (Thermally Perfect Gas)

$$P = \rho R T \quad (6.5)$$

Before deriving the compressible flow equations, the concepts of total properties, speed of sound, Mach, and sound wave propagation must be studied in detail.

The speed of sound is a fundamental parameter in compressible flow theory and is the speed at which small disturbances (sound waves) propagate through a compressible fluid.

Mach is the most important parameter in compressible flow theory, since it compares the speed of sound in a fluid (a significant measure of compressibility effects) and the speed at which the fluid is flowing.

6.5 Total (Stagnation) Properties

Temperature, density, and pressure are normally thought of as static properties of a gas. Since we will be dealing entirely with a flowing gas, it becomes convenient to define a new temperature, density, and pressure to include a velocity component. We will find that not only does it simplify calculation, but, under certain conditions, it is more convenient to measure the total values of temperature, density, and pressure than the static values and velocities.

6.5.1 Total Temperature

Consider the restricted steady flow energy equation from Derivation F.4 in Appendix F.

$$h + \frac{V^2}{2} = \text{constant}$$

The kinetic energy term may be combined with enthalpy to form a new term, total enthalpy, h_t

$$h_t \equiv h + \frac{V^2}{2} = \text{constant} \quad (6.6)$$

Consider a calorically perfect gas, then

$$h = C_p T$$

$$h = C_p T + \frac{V^2}{2} = C_p \left[T + \frac{V^2}{2C_p} \right] \quad (6.7)$$

$$h_T = C_p T_T \quad (6.8)$$

where $T_T \equiv T + V^2/2C_p$ and is called the total or stagnation temperature. Thus the total temperature at a given point in a flow is that temperature that would exist if the flow were slowed down adiabatically to zero velocity. Physically this means in a flowing gas the molecules have superimposed on their random motion the directed motion of the flow. The kinetic energy of the directed motion is the cause of the difference between static and total temperature. If, in some manner, the velocity of the airstream is reduced to zero adiabatically, and in the absence of shaft work, the resulting static temperature of the gas becomes equal to the total temperature of the flowing fluid. This will be true whether the "slowing down" process occurs reversibly or irreversibly. Therefore, a thermometer fixed with respect to the duct will measure total temperature (neglecting heat transfer effects) because it reduces the velocity of a small portion of the stream to zero.

Although the same final temperature T_T is attained whether the slowing down process is reversible or irreversible, the pressure and density finally reached will vary with the degree of irreversibility associated with the slowing down process. For pressure this may be illustrated as follows: in Figure 6-1, imagine the flowing gas at station (1) to be brought to rest adiabatically by means of a duct diverging (dashed lines) to an extremely large area (X) where the flow velocity, in the limit, is zero. If the diverging duct is frictionless, the slowing down process from (1) to (X) is isentropic and is shown as the vertical line from (1) to (2) on the temperature-entropy (T - S) diagram. If the diverging duct is frictional, the slowing down process from (1) to (X) is irreversible but adiabatic (hence, $ds = 0$) and is shown by the line of increasing entropy, (1) to (3), on the T - S diagram.

The final temperature attained at (2) and at (3) is the same; since by the First Law of Thermodynamics written between station (1) and (X) for each of these processes,

$$C_p T_1 + \frac{V^2}{2} = C_p T_2 \quad (\text{frictionless process}) \quad (6.9)$$

$$C_p T_1 + \frac{V^2}{2} = C_p T_3 \quad (\text{frictional process}) \quad (6.10)$$

However $P_b < P_C$

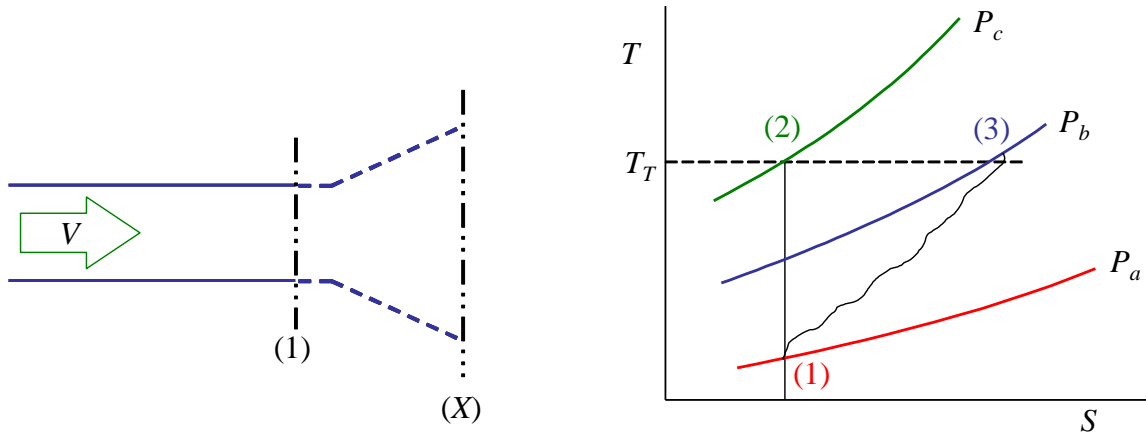


Figure 6.1 Total Pressure and Density for Reversible and Irreversible Processes

6.5.2 Total Pressure

The total pressure of a flowing gas is defined as the pressure obtained when the gas is brought to rest isentropically. Thus the pressure corresponding to state (2) on the T-S plot in Figure 6.1 is the total pressure of the gas in state (1), hence $P_{(2)} = P_c = P_T$. The pressure measured by a pitot tube placed in a subsonic flowing gas at any given station corresponds very closely to the total pressure of the gas at that station since the slowing down process preceding the pitot tube is basically isentropic.

6.5.3 Total Density

Total density of a flowing gas is defined similarly to pressure as the density obtained when the gas is brought to rest isentropically.

6.5.4 Mathematical Relationships for Total Properties

By use of the perfect gas law and the equation of state for an isentropic process

$$P\rho^{-\gamma} = \text{constant} \quad (6.11)$$

The following relationships between static and total values of pressure, density, and temperature can be developed

$$\frac{P_T}{P} = \left(\frac{T_T}{T}\right)^{\frac{\gamma}{\gamma-1}} \quad (6.12)$$

$$\frac{\rho_T}{\rho} = \left(\frac{T_T}{T}\right)^{\frac{1}{\gamma-1}} \quad (6.13)$$

Since total properties are constant throughout an isentropic flow and are easily measured, they are useful and convenient tools when evaluating the changes in compressible fluid flow. The subscripts *o*, *t*, or *T* are used to denote total properties. In this text, "*T*" is used.

6.6 Speed of Sound

The quantity $a = \sqrt{\frac{dP}{d\rho}}$ (6.14)

is called the speed of sound or acoustic speed since it is the speed with which sound waves propagate through a fluid. Equation 6.14 is derived for a nonviscous fluid; therefore, it is only valid for small disturbances which do not create any shear forces in the fluid. (Derivation F.1 in Appendix F.)

Sound waves are, by definition, "small"; the criterion being that the velocity gradients in a fluid, dV , due to the pressure disturbances, are so small that they create negligible shear or friction forces, and that

$$a \gg dv$$

It follows that the motion of a sound wave through a fluid is an isentropic phenomenon ($ds = 0$), since it does not disturb the "disorder" of the fluid, i.e., the dP , $d\rho$, and dT in the fluid caused by the passage of a sound wave are very small. In reality, the size of an audible sound wave is so small that the entropy increase near the wave is negligible, and Equation 6.14 is quite accurate for computing the speed of sound wave propagation.

Rewriting Equation 6.14 in terms of a^2 gives a pressure-density relationship for a fluid which may be used to eliminate the pressure term in the momentum equation

$$dP + \rho V dV = 0 \quad (6.3)$$

$$a^2 d\rho + \rho V dV = 0 \quad (6.15)$$

Equation 6.15 is important for later derivation of compressible flow relations, and the inference of isentropic conditions must be remembered when using it.

If $P = P(\rho, S)$

Then $dP = \frac{\partial P}{\partial s} ds + \frac{\partial P}{\partial \rho} d\rho$

and the substitution for $d\rho$ in the momentum equation cannot be made as conveniently. If the flow conditions are isentropic, $ds = 0$, then

$$\frac{dP}{d\rho} = \frac{\partial P}{\partial \rho}$$

and dP can be eliminated from the momentum equation. Since an isentropic process has been assumed, Equation 6.14 should be correctly written as

$$a = \sqrt{\left(\frac{\partial P}{\partial \rho}\right)_{ds=0}}$$

The speed of sound may be evaluated for a perfect gas from the conservation of energy equation and the equation of state. The relationship between P and ρ evaluated for an isentropic process is

$$\frac{P}{\rho^\gamma} = \text{constant} \quad (6.11)$$

Taking the natural log of this equation and differentiating

$$\ln P - \gamma \ln \rho = \ln c$$

$$\frac{dP}{P} - \gamma \frac{d\rho}{\rho} = 0$$

or $\frac{dP}{d\rho} = \gamma \frac{P}{\rho}$ (6.16)

Substituting $\rho = \frac{P}{RT}$ (Equation of State)

$$\frac{dP}{d\rho} = a^2 = \gamma RT$$

or

$$a = \sqrt{\gamma RT} \quad (6.17)$$

Thus the speed of sound is a function of temperature only.

A "cookbook" equation for the speed of sound at a local air temperature is

$$a \text{ (knots)} = 29\sqrt{T(^{\circ}R)} \quad (6.18)$$

or

$$a \text{ (ft/sec)} = 49\sqrt{T(^{\circ}R)} \quad (6.18a)$$

6.7 Mach

The Mach is defined as the ratio of a flow velocity to a speed of sound.

$$M = \frac{V}{a} \quad (6.19)$$

If the Mach is defined in terms of a local speed of sound, it is called the local Mach. The Mach may be defined in terms of the speed of sound at some given point in the flow, i.e., the ratio of an aircraft velocity to the speed of sound based on the ambient temperature (as opposed to local temperature). When the local Mach is used, it will be written without a subscript.

For flow in channels, ducts, and nozzles, it is sometimes more convenient to reference the Mach to a specific place in the flow. When this is done, the Mach is written with a subscript or a superscript, i.e.,

$$M_T = \frac{V}{a_T} \text{ or } M^{\bullet} = \frac{V}{a^{\bullet}}$$

where a_T is the speed of sound at the stagnation temperature, T_T .

a^{\bullet} is the speed of sound at local sonic conditions.

The concept of the local sonic conditions will be discussed later in this chapter.

Rewriting Equation 6.19 as

$$M^2 = \frac{V^2}{a^2} = \frac{V^2}{\gamma RT}$$

it can be seen that V^2 is a measure of the directed or kinetic energy of the fluid flow and that the temperature term in the denominator is a measure of the internal or random thermal energy of the fluid.

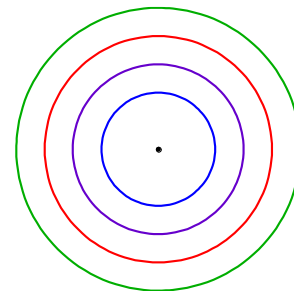
This interpretation points out the two disadvantages of using Mach in flow descriptions:

1. Mach is proportional to the velocity of the flow and also to a temperature.
2. Mach tends toward infinity as the flow velocity increases.

These limitations will become apparent when working with hypersonic fluid flow or at extreme altitudes where the fluid is no longer a continuous medium.

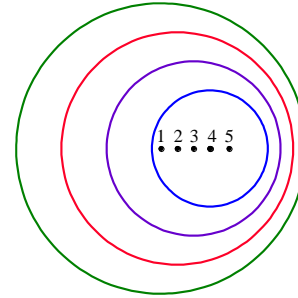
6.8 Two-Dimensional Propagation of Sound Waves

Sound waves are a series of alternate compression and rarefaction pressure pulses such as might be caused by a tuning fork. They are propagated or transmitted in all directions in a fluid at a given speed proportional to the temperature of the fluid. If the disturbance which is causing sound waves is motionless in the fluid, these waves appear to radiate out from the disturbance in a series of concentric rings like ripples on a pond as in Figure 6.2a.



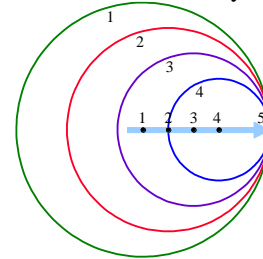
a. Stationary Source

If the disturbance is moving in the fluid, the wave pattern is quite different since each wave is emitted from a different point in the fluid. For example, if the disturbance is traveling at some speed which is less than the speed of sound in the fluid, the wave pattern is distorted as shown in Figure 6.2b. In this case, the sound wave outruns the disturbance, forming a series of circles one inside the other, but with different centers.



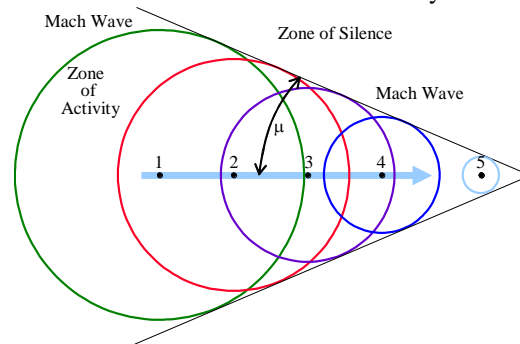
b. Source Moving at Subsonic Velocity

If the disturbance travels at exactly the speed of sound, the wave front and the disturbance travel together, forming the pattern shown in Figure 6.2c. Each successive wave reinforces the next wave, forming a wave front. This is a sound wave front, which is, by definition, isentropic.



c. Source Moving at Sonic Velocity

If the disturbance travels at greater than sonic velocity, it outruns the wave patterns which radiate out from the point where they were emitted, forming an oblique wavefront trailing behind the disturbance (Figure 6.2d).



d. Source Moving at Supersonic Velocity

Figure 6.2 Sound Wave Propagation from a Point Source

6.8.1 Mach Angles

This isentropic wave front (Figure 6.2d) is analogous to the oblique shock wave, and the angle between the wave front and the direction of the disturbance's motion is called the Mach wave angle or Mach angle, μ .

In the paragraph "Oblique Shock Waves," it will be shown that μ is the smallest possible wave angle for any pressure disturbance. It is the angle of a zero strength shock wave (an isentropic shock wave) which is nothing more than a sound wave.

The triangle formed by the Mach angle is called the Mach cone, and from the geometry of the Mach cone it can be seen that

$$\sin \mu = \frac{a}{V} \frac{dt}{dt} = \frac{a}{V} = \frac{1}{M}$$

where dt is a given time interval, and

$$\text{Mach Angle} = \mu = \sin^{-1} \frac{1}{M} \tag{6.20}$$

6.8.2 Activity Envelope

The real significance of the propagation of sound waves relative to the speed of the disturbance is the envelope they describe. It can be seen that sound waves or pressure disturbances are not transmitted upstream when the Mach is equal to or greater than one.

The pattern of Figure 6.2(d) illustrates the three rules of supersonic flow given by Von Karman in 1947 in the Tenth Wright Brothers Lecture. These rules are based on the assumption of small disturbances. They are qualitatively applicable, however, to large disturbances.

- a. The rule of forbidden signals. The effect of pressure changes produced by a body moving at a speed faster than sound cannot reach points ahead of the body.
- b. The zone of activity and zone of silence. All effects produced by a body moving at a supersonic speed are contained within the zone of activity bounded by the Mach cone extending downstream from the body. Conversely, any arbitrary point in a supersonic stream can be affected only by disturbances emanating from source points lying on or within a cone of the vertex angle μ extending upstream from the point considered. The region outside of the zone of activity is called the zone of silence.
- c. The rule of concentrated action. The effects produced by the motion of an object at supersonic speeds are concentrated along the Mach lines. Extrapolating this rule to large disturbances, we can observe its qualitative application in the concentration of effects along a shock wave accompanying a body at supersonic speeds.

6.9 Classification of Speed Ranges

It is clear that there are at least two basic speed ranges to be considered: subsonic speeds where the Mach is less than one and supersonic speeds where the Mach is greater than one. When describing the aerodynamics of an aircraft, a range is found extending from high subsonic speeds to low supersonic speeds which is not described by either the subsonic or supersonic flow equations. This is the transonic speed range.

The local flow over an aircraft in transonic flight is part subsonic and part supersonic. The interaction between the two types of flow causes aerodynamic phenomena which have characteristics of neither subsonic nor supersonic flow. These phenomena begin at the critical Mach and continue until the flow on the aircraft is completely supersonic. This range is from about Mach 0.8 to 1.2.

Since the transonic range is difficult (in some cases impossible) to describe mathematically, it will be discussed after more knowledge is gained about supersonic flow.

Extremely low velocities are studied as incompressible flow, and extremely high velocities typify hypersonic flow, which is of current interest to space scientists concerned with orbital and re-entry velocities.

The hypersonic speed range is considered to begin at Mach 5.0, but some hypersonic characteristics appear at speeds as low as Mach 3.5. Hypersonic flow is characterized by high temperatures which cause ionization, gaseous dissociation and recombination, extreme wave angles, boundary layer interaction, and high heat transfer rates.

6.10 Isentropic Flow

The isentropic flow process was defined as being both adiabatic and reversible. These conditions are very nearly met in one-dimensional, nonviscous, shock-free flow where both the cross-sectional area of the streamtube and the flow direction are constant or change very slowly. The nonviscous assumption is extremely important when flow in a channel is considered, since boundary layer interaction causes irreversible changes in flow properties.

The isentropic flow assumptions, while seemingly quite restrictive, are very useful when evaluating one-dimensional flow conditions existing outside of a boundary layer and between shock waves. Special

relationships will be derived later in this chapter for evaluating the changes occurring because of shock waves.

Valuable insight into a great number of real aerodynamic and fluid flow problems can be gained from the ability to predict isentropic changes and changes caused by shock waves in supersonic flow. A few of the isentropic flow equations will be derived from the one-dimensional, conservation equations. Many others can be derived when needed or may be found in most texts on supersonic aerodynamics and fluid dynamics.

Since the stagnation properties P_T , ρ_T , and T_T can be experimentally measured or calculated from energy concepts at any place in an isentropic flow, it is useful to obtain relationships between these stagnation properties and the free stream properties of the flow in terms of Mach, that is,

$$\frac{P_T}{P}, \frac{\rho_T}{\rho}, \frac{T_T}{T} = f(M)$$

Using Equation 6.7 which was developed for adiabatic flow

$$h_T = C_p T + \frac{V^2}{2} \quad (6.7)$$

$$C_p T_T = C_p T + \frac{V^2}{2} \quad (6.21)$$

To write Equation 6.21 in terms of Mach, where $M^2 = V^2 / \gamma RT$ divide the equation by $C_p T$

$$\begin{aligned}\frac{T_T}{T} &= 1 + \frac{V^2}{2C_p T} \\ &= 1 + \left[\frac{V^2}{2C_p T} \right] \left[\frac{RC_v}{RC_v} \right] \\ &= 1 + \left[\frac{R}{2C_v} \right] \left[\frac{V^2}{\gamma RT} \right]\end{aligned}$$

but $\frac{R}{C_v} = \gamma - 1$ since $R = C_p - C_v$ and $\gamma = C_p / C_v$

therefore,
$$\frac{T_T}{T} = 1 + \frac{\gamma - 1}{2} M^2 \quad (6.22)$$

This is a very important equation relating stagnation temperature to free stream temperature in terms of flow Mach for an adiabatic flow process. Notice that the flow does not have to be isentropic for this equation to be valid. This equation should be recognized as the one used to determine the ambient air temperature, T_a , from flight test data

$$\frac{T_{ic}}{T_a} = 1 + \frac{k_t(\gamma - 1)M^2}{2} \quad (6.23)$$

where k_t is a recovery factor that describes the efficiency of the adiabatic flow process between the ambient air and the temperature probe. The two equations are identical when the recovery factor, k_t , is equal to one, i.e., the probe is perfectly insulated from the ambient air.

To obtain an expression for P_T/P as a function of Mach use Equation 6.12

$$\frac{P_T}{P} = \left[\frac{T_T}{T} \right]^{\frac{\gamma}{\gamma-1}} \quad (6.12)$$

Substituting Equation 6.22 into this equation,

$$\frac{P_T}{P} = \left[1 + \frac{\gamma - 1}{2} M^2 \right]^{\frac{\gamma}{\gamma-1}} \quad (6.24)$$

Substituting Equation 6.22 into Equation 6.13,

$$\frac{\rho_T}{\rho} = \left[1 + \frac{\gamma - 1}{2} M^2 \right]^{\frac{1}{\gamma-1}} \quad (6.25)$$

It should be noted that it is not necessary for the stagnation properties to actually exist at some point in the flow to write the equations relating them to the free stream pressure, density, and temperature. It is only necessary to assume that the flow at some given point could be slowed isentropically to zero velocity.

It was previously stated that the stagnation properties remained constant throughout an isentropic flow. The proof of this statement begins with the fact that temperature is a direct measure of the internal energy of a flow.

The internal energy of an adiabatic flow is constant since no heat is exchanged with the surroundings. If an adiabatic flow is slowed isentropically to zero velocity, the stagnation temperature measured would be a constant throughout the flow.

If viscous or other irreversible effects were present in the adiabatic flow, the stagnation temperature would still remain constant since no heat is exchanged with the surroundings. The presence of viscous

and irreversible effects means that some of the kinetic energy of the flow is converted to thermal energy, but the stagnation temperature of the flow remains constant for reasons stated.

By integrating the entropy relation, rearranging terms, and evaluating at stagnation conditions

$$S_T = \ln \left[\left(\frac{T_T}{P_T} \right)^{\frac{\gamma}{\gamma-1}} \right] + \ln c$$

It can be seen that P_T is constant in isentropic flow, since S_T and T_T are constant. From the equation of state, $P_T = \rho_T R T_T$, it can be seen that ρ_T is also constant in isentropic flow.

Because P_T , ρ_T , and T_T are all constants in isentropic flow, the ratio of free stream conditions at two different stations in the flow may be obtained by taking a ratio of stagnation properties evaluated at the two stations, i.e.,

$$\frac{P_1 / P_{T_1}}{P_2 / P_{T_2}} = P_1 / P_2$$

Resulting temperature, pressure and density ratios are shown below.

$$\frac{T_1}{T_2} = \frac{1 + \frac{\gamma-1}{2} M_2^2}{1 + \frac{\gamma-1}{2} M_1^2} \quad (6.26)$$

$$\frac{P_1}{P_2} = \left[\frac{1 + \frac{\gamma-1}{2} M_2^2}{1 + \frac{\gamma-1}{2} M_1^2} \right]^{\frac{\gamma}{\gamma-1}} \quad (6.27)$$

$$\frac{\rho_1}{\rho_2} = \left[\frac{1 + \frac{\gamma-1}{2} M_2^2}{1 + \frac{\gamma-1}{2} M_1^2} \right]^{\frac{\gamma}{\gamma-1}} \quad (6.28)$$

Values of P/P_T , ρ/ρ_T , and T/T_T are tabulated versus Mach (at $\gamma = 1.4$ for air) in the appendices of most thermodynamics books. The same quantities are plotted versus Mach in Reference 6.4.

Since Mach is a quantity that may be measured in the flow problem and stagnation properties are constant in isentropic flow, use of these charts and graphs simplifies the work required to calculate P , ρ , and T at a given station in the flow.

6.11 Flow in Convergent-Divergent Streamtubes

Understanding the characteristics of a compressible fluid flowing through a streamtube is very important in supersonic aerodynamics. If viscous effects are to be neglected in the streamtube, the boundary layer streamline may be used as the streamtube boundary. For this discussion a streamtube is defined as any convergent or divergent section bounded either by physical walls or by streamlines as shown in Figure 6.3. Such a streamtube might be formed by the

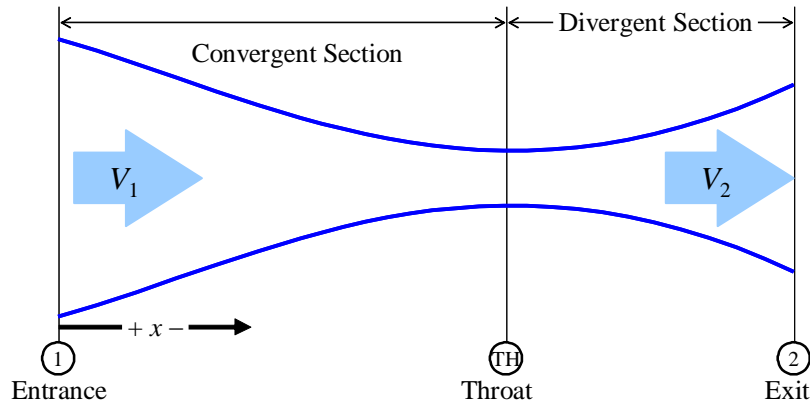


Figure 6.3 Convergent Divergent Streamtube

inlet or exhaust duct of a jet aircraft or between converging and diverging streamlines as the air flows over the surface of the aircraft. Also, a supersonic wind tunnel uses convergent-divergent designs to obtain Mach greater than one in the test section.

Compressible flow through a convergent-divergent streamtube is quite different from the classical flow of an incompressible fluid through a venturi. At low velocities, the flow situation is almost identical to the venturi, but at high velocities the change in density causes a complete reversal of the low velocity trends.

Consider steady, nonviscous, compressible, isentropic flow in the streamtube shown in Figure 6.3. In steady flow, the mass entering at Station 1 is equal to the mass leaving at Station 2, and the continuity equation may be used to describe the flow conditions

$$\frac{d\rho}{\rho} + \frac{dV}{V} + \frac{dA}{A} = 0 \quad (6.2)$$

Substituting the definition of the speed of sound into the momentum equation as done in Equation 6.15 yields

$$a^2 d\rho + \rho V dV = 0 \quad (6.15)$$

or

$$\frac{d\rho}{\rho} = -\frac{V dV}{a^2}$$

Multiplying the right side by $\frac{V}{V}$

$$\frac{d\rho}{\rho} = -M^2 \frac{dV}{V} \quad (6.29)$$

and substituting this into the continuity equation above gives

$$-M^2 \frac{dV}{V} + \frac{dV}{V} + \frac{dA}{A} = 0$$

or

$$\frac{dA}{A} = (M^2 - 1) \frac{dV}{V} \quad (6.30)$$

Equation 6.30 describes the flow situation caused by compressible fluid flow in streamtubes. Defining a diverging streamtube as having a positive dA , i.e., an increasing area in the direction of the flow, and a converging streamtube as having a negative dA , the following conclusions can be drawn:

1. When the Mach is less than 1, a diverging streamtube causes a decrease in velocity, and a converging streamtube causes an increase in velocity.
2. When the Mach is greater than 1, a diverging nozzle causes an increase in velocity, and a converging nozzle causes a decrease in velocity.

3. When the Mach is 1, dA must be zero.

Examining Equation 6.29 may give a physical understanding of what happens to subsonic or supersonic, compressible flow in a streamtube.

$$\frac{d\rho}{\rho} = -M^2 \frac{dV}{V} \quad (6.30)$$

It can be seen that for Mach less than 1, a small change in velocity results in a proportionately smaller change in density.

For air flowing at Mach of 0.3, 0.9, 1, and 2, consider the density effects caused by an arbitrary 10% increase in velocity ($dV/V = 10\%$).

At

$$M = 0.3; \quad \frac{d\rho}{\rho} = -0.9\%$$

$$M = 0.9; \quad \frac{d\rho}{\rho} = -8.1\%$$

$$M = 1; \quad \frac{d\rho}{\rho} = -10\%$$

$$M = 2; \quad \frac{d\rho}{\rho} = -40\%$$

Notice that for all Mach, an increase in velocity results in a decrease in density. The magnitude of the density change is proportional to the Mach squared; consequently, as the Mach increases, the change in density becomes more pronounced.

It is interesting to note that Equation 6.29 indicates the validity of the incompressible flow assumption. It shows that at low Mach, a change in velocity results in a very small change in density, and as the Mach increases, the assumption becomes poorer, until at Mach 1, the change in velocity is of the same magnitude as the change in density.

To complete the picture, an equation must be obtained relating density change to area change as a function of Mach. If in the derivation of Equation 6.30 the value of dV/V had been substituted instead of dp/p , the following relation would have been obtained

$$\frac{dA}{A} = \left[\frac{1}{M^2} - 1 \right] \frac{d\rho}{\rho} \quad (6.31)$$

In the preceding discussion, it was found that for subsonic and supersonic Mach the density always decreased for increased velocity. This leads to the question, what shape is required to produce this decrease in density and increase in velocity? From Equation 6.31 it can be seen that for subsonic speed ($M < 1$), a decrease in density (and an increase in velocity) is caused by a converging duct (negative dA). That is, the factor $(1/M^2 - 1)$ is positive for subsonic speeds. Supersonic, this factor is negative; therefore, a diverging duct (positive dA) causes a decrease in density (and a corresponding increase in velocity).

Qualitatively speaking, the decrease in density is a second order effect and can usually be neglected for flow at low Mach because a reduction in area creates only a proportional increase in velocity. At high subsonic speeds, the reduction in density becomes more significant, but the density still is able to decrease fast enough to allow the velocity to increase as the fluid flows into a converging duct. At supersonic speeds, the density does not decrease fast enough in a converging section; therefore the nozzle must diverge to further reduce the density and allow an increase in velocity.

Only the case of accelerating flow has been considered, but it is obvious that the reverse of the described conditions is also true. That is, a subsonic stream is slowed down by a diverging section, and a supersonic stream is slowed down by a converging section. The general conclusions of the convergent-divergent streamtube problem may be summarized as shown in Figure 6.4.

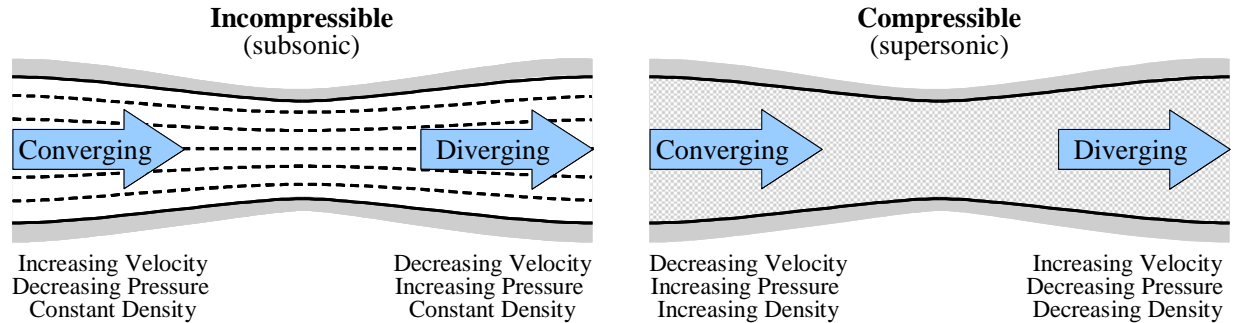


Figure 6.4 Comparison of Compressible and Incompressible Flow through a Closed Tube (6.2:205)

6.11.1 Flow at the Throat

The flow in a convergent-divergent streamtube has been discussed at some length, but now the specific flow characteristics at the throat of the streamtube must be studied.

The minimum cross-sectional area of a convergent-divergent streamtube is called the throat, and at this section, the derivative $dA/dx = 0$, or $dA = 0$. Two conditions can exist at the throat since dA is zero. Either dV and/or $(M^2 - 1)$ must equal zero to satisfy Equation 6.30.

The first condition, $dV = 0$, is characteristic of flow in a subsonic streamtube in which the fluid accelerates to a maximum subsonic speed at the throat and then decelerates again in the divergent section. It is also characteristic of supersonic flow which decelerates in the converging section, reaching a lower supersonic or exactly sonic velocity at the throat and then accelerates again in the divergent section.

The second condition, $(M^2 - 1) = 0$, is characteristic of what is called choked flow. It occurs when $M = 1$ at the throat. This condition exists whenever the flow is accelerated from subsonic to supersonic speeds by a nozzle or when flow is decelerated from supersonic to subsonic speeds by a diffuser. By definition, a nozzle accelerates flow, while a diffuser decelerates flow.

Flow through a streamtube is caused by a pressure differential between the inlet and exit. Increasing the inlet pressure or lowering the exit pressure causes an increase in the flow velocity and the mass flow rate. Since the maximum subsonic velocity occurs at the throat, sonic velocity ($M = 1$) is attained first at the throat, and further reduction in exit pressure will not increase the velocity at this point. This may be seen by considering the mechanism which causes a change in the mass flow rate and the flow velocity in the convergent-divergent streamtube (Figure 6.5).

If the exit pressure is exactly equal to the inlet pressure, no flow will occur. There are three critical values of exit pressure for a given inlet pressure. Between pressure equilibrium and first critical pressure, the flow will accelerate in the convergent portion of the streamtube and then decelerate through the diverging portion, remaining subsonic throughout. This is called the venturi regime. If the pressure is reduced to the first critical pressure at the exit, the flow will accelerate through the convergent portion, reach sonic velocity at the throat, and then decelerate back to a subsonic value. Once sonic conditions have been attained at the throat, further reductions in exit pressure will not affect what happens' upstream of the throat. The maximum mass flow rate has been achieved for that inlet pressure, and the streamtube is said to be choked. Further reduction in exit pressure beyond the first critical point will produce a normal shock somewhere in the divergent portion of the streamtube until the second critical pressure is reached. At the second critical pressure, a normal shock stands at the exit plane. Further reduction in exit pressure beyond the second critical value will produce oblique shocks or a combination oblique-normal shock outside the streamtube as shown in Figure 6.6a. This is called the overexpanded condition, indicating that the streamtube is too long, and will occur until reaching the third critical pressure. The third critical value is the only pressure for which no shocks occur anywhere in the streamtube flow field, and supersonic flow is maintained downstream of the throat. This is the on-design condition. Further reduction in pressure below the third critical valve is an underexpanded condition, indicating the streamtube is too short, and expansion fans will form outside the streamtube as illustrated in Figure 6.6b.

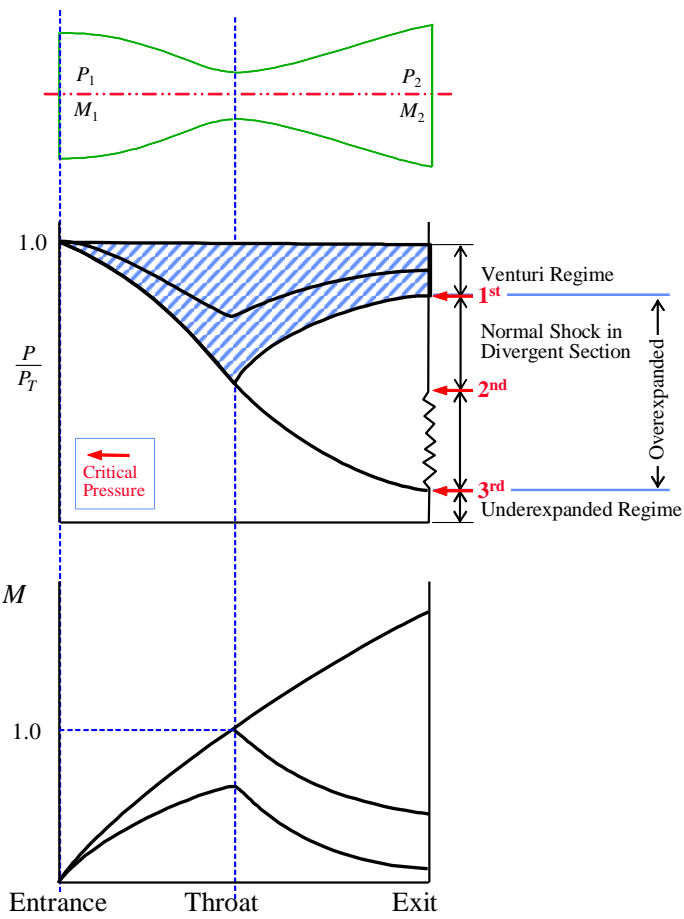


Figure 6.5 Pressure and Mach Variation through a Converging-Diverging Streamtube

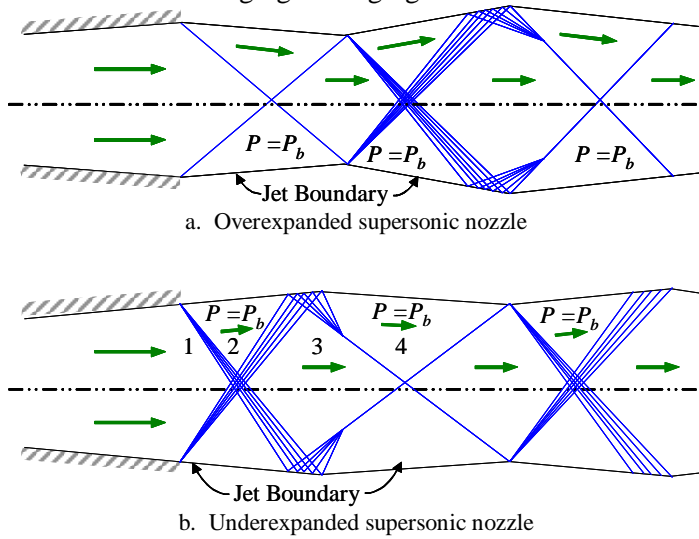


Figure 6.6 Pressure Adjustment Outside a Nozzle or Streamtube

6.11.2 Mass Flow in a Choked Streamtube

The mass flow rate of a gas ($\dot{m} = \rho VA$) increases with increasing pressure differential between the entrance and exit of a subsonic, converging-diverging streamtube until sonic velocity is attained in the throat. When sonic velocity is reached, it has been shown that the velocity and density at the throat are fixed; consequently the mass flow rate, m , is fixed or the streamtube is choked. Sonic velocity is the maximum velocity that can occur in the throat; therefore it fixes the maximum mass flow through the streamtube for given entrance conditions.

This should not be interpreted to mean that a choked streamtube is passing the maximum mass flow for the streamtube; it is passing the maximum mass flow for given entrance conditions. Since the streamtube was assumed isentropic, this is the same as saying a choked streamtube is passing the maximum mass flow for given stagnation conditions.

A choked streamtube makes an excellent metering device for gaseous fluids. By adjusting the stagnation or entrance conditions, the exact mass flow can be measured and calculated. In reality, a well designed metering streamtube passes within 2 - 3% of the mass flow calculated for an isentropic streamtube.

An equation for the mass flow rate through an isentropic streamtube can be derived by substituting appropriate values into $\dot{m} = \rho VA$:

$$\dot{m} = \frac{P_T}{\sqrt{T_T}} A \sqrt{\frac{\gamma}{R}} \frac{M}{\left[1 + \frac{\gamma-1}{2} M^2\right]^{\left[\frac{\gamma+1}{2(\gamma-1)}\right]}} \quad (6.32)$$

If the streamline is choked, $M = 1$ and $A = A_{throat} = A^*$:

$$\dot{m} = \frac{P_T}{\sqrt{T_T}} A_{throat} \sqrt{\frac{\gamma}{R}} \left[1 + \frac{\gamma-1}{2}\right]^{\left[\frac{-\gamma+1}{2(\gamma-1)}\right]} \quad (6.33)$$

6.11.3 Local Sonic Conditions

When a streamline is choked, specific values for P , ρ , T , A , etc., are determined at the throat. These unique values are designated with a superscript, *, and are written P^* , ρ^* , T^* , A^* , etc. The concept of the local sonic area, A^* , where $M = 1$, is similar to the stagnation condition concept. Both refer to flow conditions at some specific Mach, i.e., $M = 1$ for local sonic conditions and $M = 0$ for stagnation conditions.

It is not necessary for the flow to be actually at Mach 1 to define the local sonic values. To determine local sonic conditions at some point in a flow, it has to be assumed that the area of the channel could be varied to the value A^* . When this is done, the prevailing conditions at the section with area A^* are local sonic conditions.

For instance, in an isentropic flow, A^* can be imagined at any point, that is, the channel can be reduced in area to that which would reduce a supersonic stream to Mach 1 or increase a subsonic stream to Mach 1. Properties at local sonic conditions in an isentropic flow may be conveniently evaluated in terms of stagnation conditions, which are usually known or easily measured. The general procedure is to evaluate the identities

$$p^* = \frac{P_T}{P^*}; \rho^* = \frac{\rho_T}{\rho^*}; T^* = \frac{T_T}{T^*}$$

using Equation 6.24

$$\frac{P_T}{P} = \left[1 + \frac{\gamma - 1}{2} M^2 \right]^{\frac{\gamma}{\gamma - 1}} \quad (6.24)$$

and that local sonic conditions are defined where $M = 1$, gives

$$\frac{P_T}{P^*} = \left[1 + \frac{\gamma - 1}{2} \right]^{\frac{\gamma}{\gamma - 1}}$$

and

$$p^* = \frac{P_T}{\left[1 + \frac{\gamma - 1}{2} \right]^{\frac{\gamma}{\gamma - 1}}} \quad (6.34)$$

The p^* and T^* can be easily derived, and for air, $\gamma = 1.4$, the local sonic properties as a function of stagnation properties are

$$P^* = P_T (0.528) \quad (6.35)$$

$$\rho^* = \rho_T (0.634) \quad (6.36)$$

$$T^* = T_T (0.833) \quad (6.37)$$

6.11.4 M^*

The concept of local sonic conditions allows a dimensionless parameter M^* to be defined. Mach, M , is a very convenient parameter but has the disadvantages listed in the paragraph, "Mach."

Often it is convenient to work with the parameter M^* , which is the flow velocity V , divided by a^* , the speed of sound at local sonic conditions.

$$M^* = \frac{V}{a^*}$$

It should be noted immediately that M^* does not mean Mach at a place where $M = 1$ like all other starred quantities but is defined by Equation 6.38.

Unique relations between M and M^* can be derived for adiabatic flow using the definition of M^* and the energy equation for a perfect gas (refer to Appendix F, Derivation F.5)

$$M^{*2} = \frac{\frac{\gamma + 1}{2} M^2}{1 + \frac{\gamma - 1}{2} M^2} \quad (6.39)$$

$$M^2 = \frac{\frac{2}{\gamma + 1} M^{*2}}{1 - \frac{\gamma - 1}{\gamma + 1} M^{*2}} \quad (6.40)$$

From these two equations it can be seen that M^* is a simple index of when the flow is subsonic and when the flow is supersonic, i.e.:

when

$$M < 1; \quad M^* < 1$$

$$M > 1; \quad M^* > 1$$

$$M = 1; \quad M^* = 1$$

$$M = 0; \quad M^* = 0$$

$$M = \infty; \quad M^* = \sqrt{\frac{\gamma + 1}{\gamma - 1}} = \sqrt{6} \text{ (for air)}$$

Equation 6.39 is tabulated in Reference 6.4, and if M^* is known, then M can be found or vice versa.

6.11.5 Area Ratio

Just as it is convenient to work with dimensionless parameters p/p_T , etc., it is convenient to use a dimensionless area ratio, A/A^* . Equating Equation 6.32 and 6.33, this parameter is found to be

$$\frac{A}{A^*} = \frac{1}{M} \left[\left(\frac{2}{\gamma+1} \right) \left(1 + \frac{\gamma-1}{2} \right) \right]^{\frac{\gamma+1}{2(\gamma-1)}} \quad (6.41)$$

and is always greater than one. For a given value of A/A^* , there are always two values of M , one for subsonic flow and the other for supersonic flow.

6.12 Normal Shock Waves

Shock waves are observed as a discontinuity between supersonic and subsonic flow. The flow passes from supersonic to subsonic speeds in an extremely short distance which is of the order of magnitude of the mean free path of the molecules in the flow. The kinetic energy of the supersonic, upstream molecules is instantaneously converted to pressure-volume (pv) and thermal energy.

Experimental studies of normal shocks in supersonic wind tunnels show fivefold pressure increases and threefold velocity decreases behind the shock. These changes occur in a distance too small to be measured on a photographic plate, but theoretical calculations and experimental measurements indicate a distance of the order of 10^{-5} inches.

Because changes due to a normal shock occur in such a short distance, the changes are highly irreversible, and a shock wave is not isentropic. Two valid assumptions made when studying normal shocks are that:

1. The flow through a shock is adiabatic.
2. The shock is very thin and has a constant cross-sectional area between the front and rear face.

With these two assumptions and the conservation equations (see "OneDimensional Flow Approximation"), the changes in flow properties caused by a shock can be derived as functions of M_1 , i.e., P_2/P_1 , ρ_2/ρ_1 , T_2/T_1 , M_2 . These derivations are conceptually simple but involve lengthy mathematical equation juggling which is carried out in most textbooks on compressible flow; therefore only the results of the derivations will be listed (refer to Appendix F, Derivation F.6).

A pictorial representation of a normal shock and the change in flow properties across the shock is shown in Figure 6.7.

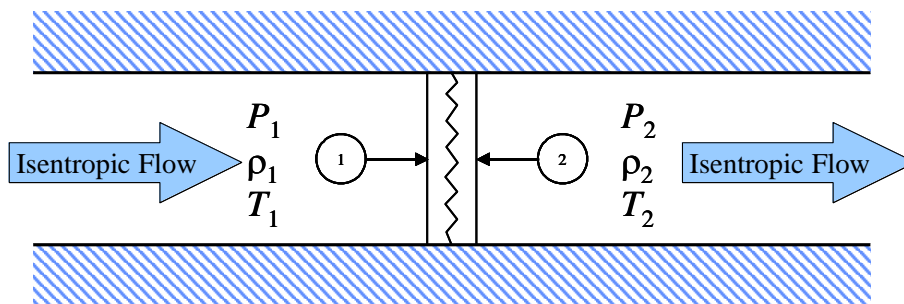


Figure 6.7. Flow Properties in the Vicinity of a Normal Shock

6.12.1 Normal Shock Equations

The notation used to describe the flow situation must be established before listing the normal shock equations. For these relations, the following assumptions were made:

1. All property changes occur in a constant area
2. Flow across the shock is adiabatic
3. Flow upstream and downstream of the shock is isentropic

$$\frac{P_2}{P_1} = \frac{1 - \gamma + 2\gamma M_1^2}{1 + \gamma} \tag{6.42}$$

$$\frac{\rho_2}{\rho_1} = \left[\frac{2 + (\gamma - 1)M_1^2}{(\gamma + 1)M_1^2} \right]^{-1} \tag{6.43}$$

$$\frac{T_2}{T_1} = \left[\frac{1 - \gamma + 2\gamma M_1^2}{1 + \gamma} \right] \left[\frac{2 + (\gamma - 1)M_1^2}{(1 + \gamma)(M_1^2)} \right] \tag{6.44}$$

$$M_2^2 = \frac{M_1^2 + \frac{2}{\gamma - 1}}{\frac{2\gamma}{\gamma - 1} M_1^2 - 1} \tag{6.45}$$

Values of P_2/P_1 , ρ_2/ρ_1 , T_2/T_1 and M_2 are tabulated versus Mach, M_1 , (at $\gamma = 1.4$ for air) in the appendices of most thermodynamic books. The same quantities are plotted versus Mach in Reference 6.4.

6.12.2 Normal Shock Summary

A shock wave is an extremely thin discontinuity which forms between supersonic and subsonic flow. The shock wave is an adiabatic process with no stagnation temperature loss across it, but as can be shown by entropy considerations, there is an accompanying stagnation pressure loss.

Supersonic flow always exists upstream of a shock wave, and the upstream stagnation pressure is greater than the downstream stagnation pressure.

General flow properties can be compared and tabulated as

$V_1 > V_2$	$s_1 < s_2$
$T_{T_1} = T_{T_2}$	$\rho_1 < \rho_2$
$P_{T_1} > P_{T_2}$	$M_1 > M_2$
$\rho_{T_1} > \rho_{T_2}$	$a_1 > a_2$
$T_1 < T_2$	$a^*_1 = a^*_2$
$P_1 < P_2$	$M^*_1 = M^*_2$
$A^*_1 = A^*_2$	

6.13 Supersonic Pitot Tube

The loss in stagnation pressure across a normal shock affects the stagnation pressures sensed by aircraft pitot static systems (Figure 6.8).

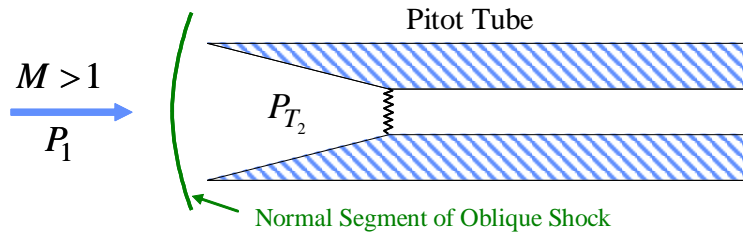


Figure 6.8 Pitot Tube in Supersonic Flow

To determine Mach from free stream static pressure and stagnation pressure behind a normal shock standing in front of a pitot tube, the Rayleigh Pitot Relation is often used

$$\frac{P_{T_2}}{P_1} = \frac{\left(\frac{\gamma+1}{2} M_1^2\right)^{\frac{\gamma}{\gamma-1}}}{\left(\frac{2\gamma}{\gamma+1} M_1^2 - \frac{\gamma-1}{\gamma+1}\right)^{\frac{1}{\gamma-1}}} \quad (6.46)$$

By measuring P_1 and P_{T_2} , M_1 , can be determined, and in many compressible flow textbooks, these values are plotted versus M_1 , for $\gamma_{\text{air}} = 1.4$.

When using Equation 6.46, the free stream static pressure must be measured in front of the shock wave. This is a very difficult procedure for an aircraft in supersonic flight. Experiments have proven that if the static source is approximately ten pitot tube diameters behind the shock wave, the static pressure measured is quite close to free stream static pressure.

On the pitot booms of supersonic aircraft, static pressure measuring holes will be found at varying distances from the end of the boom. The location of these holes usually has been determined experimentally to produce the closest approximation of free stream static pressure in supersonic flight.

6.14 Oblique Shock Waves

In the last paragraph on normal shocks, shock wave theory was presented, and the thermodynamic and kinematic changes that occurred when the flow traversed a normal shock were studied. Next, the changes that occur when flow passes through an oblique shock must be considered.

A normal shock is a special form of a pressure discontinuity in a fluid. In general, the discontinuities observed experimentally are inclined to the free stream velocity and are called oblique shocks.

Oblique shocks occur in supersonic flow because continuous compression waves caused by a concave, curved surface in the flow tend to merge, forming an oblique discontinuity at a finite distance from the surface.

When flow is forced to change direction suddenly at a sharp concave corner, an attached, oblique shock forms at the corner.

Oblique shocks occur in almost all supersonic flow situations of practical interest, but the mere existence of supersonic flow does not imply that there must be shock waves somewhere in the flow.

Developing the relations between the fluid properties on the two sides of an oblique shock is not as formidable a task as it might seem, because many of the normal shock equations with a slight modification apply equally well to oblique shocks.

Suppose a stationary observer sees the flow at Station 1 suddenly decelerate and compress to the conditions at Station 2 because it has traversed a normal shock wave (Figure 6.9).

Next, imagine that the observer moves along the shock wave in a downward direction with a velocity V_r . The moving observer would see a flow situation in which the shock is inclined to the free stream flow and in which the flow undergoes a sudden change in direction when it crosses the shock (Figure 6.10).

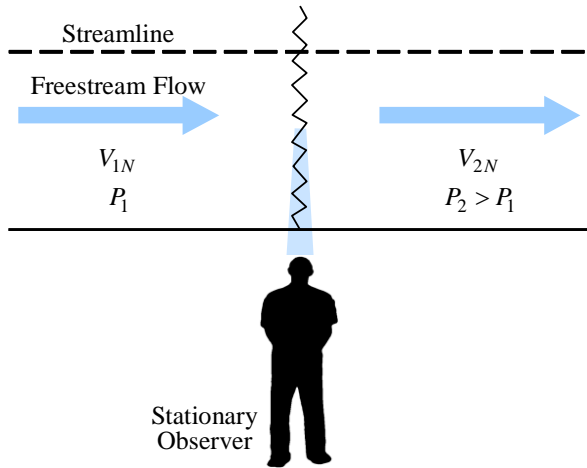


Figure 6.9 Shock Process as seen by Stationary Observer

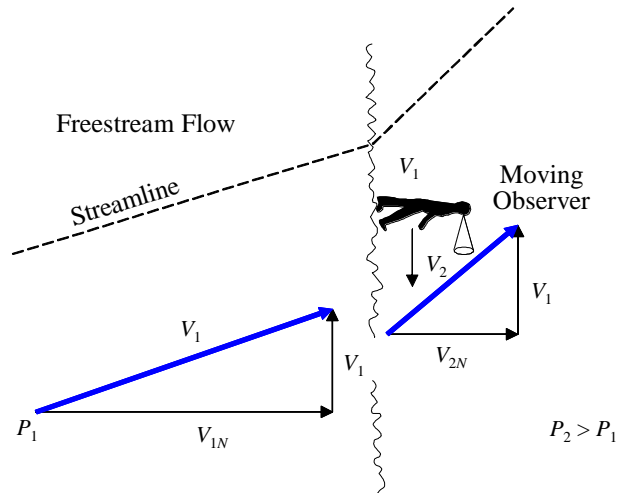


Figure 6.10 Shock Process as seen by Moving Observer

The oblique flow pattern constructed in this manner has equal tangential velocity components, V_t , on both sides of the shock. By placing a solid wall along one of the streamlines in Figure 6.10 and rotating the picture so that incoming velocity, V_1 , is horizontal, the supersonic flow situation in the neighborhood of a concave corner is described (Figure 6.11).

By imparting a uniform velocity to the flow field along any shock, a straight segment of an oblique shock may be transformed into a normal shock.

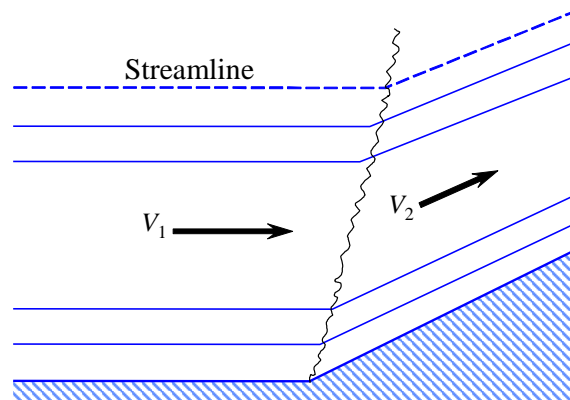


Figure 6.11 Supersonic Flow Into a Corner

To fix this concept, consider the falling rain in Figure 6.12.

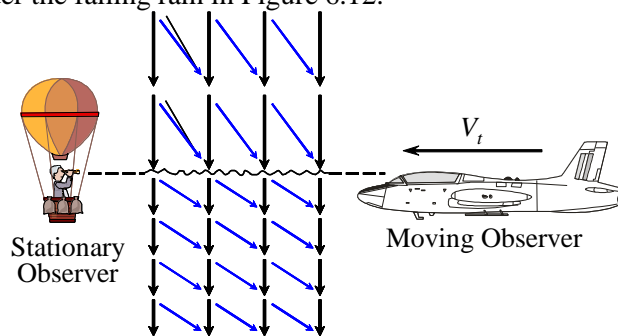


Figure 6.12 Analogy to Aid Understanding of Oblique Shocks

Relative to an observer at rest, the rain is falling vertically. Relative to an observer moving perpendicular to the rainfall, the rain is descending at an angle.

Let the rain be slowed down instantaneously at some altitude. An observer in a balloon at this altitude sees the rain falling vertically and slowing down at this level as shown by the single lines in Figure 6.12. The pilot of an aircraft traveling with a horizontal velocity V_t at this altitude sees the path of the raindrops as though they were being deflected as they pass through this level (double lines in Figure 6.12). The pilot's observation is also correct, for relative to the aircraft the drops are being deflected. Essentially, the velocity of the aircraft has been superimposed upon the changing velocity of the raindrops.

A careful comparison of Figures 6.9 and 6.10 will show that the thermodynamic properties of P , ρ , T , a , and s are unchanged by the motion of the observer. On the other hand, V_1 , M_1 , p_{T1} , and T_T are altered when the observer's motion V_T is superimposed on the normal shock flow situation.

The magnitude of V_T is arbitrary and depends upon the angle the oblique shock makes with the horizontal streamline in front of the shock and the velocity of the approaching flow. This presents an additional degree of freedom in the oblique shock relations.

An additional degree of freedom means that although only one independent parameter, i.e., approach Mach, M_1 , is required for normal shock relations, two independent parameters are required for oblique shock relations, i.e., M_1 and wave angle, θ .

6.14.1 Oblique Shock Relations

Since a shock appears to be normal or oblique depending upon the relative motion of the observer, the differences between normal and oblique shocks can be explained in geometric terms.

The flow orientation, flow notation, and angle descriptions used when modifying the normal shock equations are shown in Figure 6.13.

The number of degrees the flow must turn due to the concave corner is called the turning angle or wedge angle, δ . The angle the oblique shock makes with the incoming (upstream) streamlines is called the shock wave angle, θ .

Conditions upstream of the oblique shock have the subscript 1, and conditions downstream have the subscript 2.

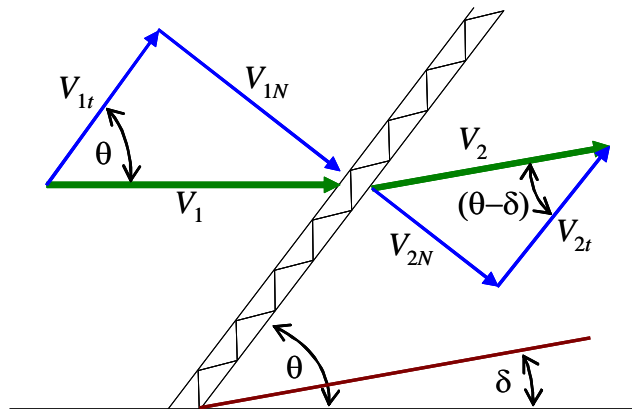


Figure 6.13 Analysis of Velocity Components Across an Oblique Shock

From this figure, it can be seen

$$M_{1N} = M_1 \sin \theta \quad (6.47)$$

where

M_{1N} = Flow Mach in front of a normal shock

M_1 = Flow Mach in front of an oblique shock

Consequently, all of the normal shock equations can be modified to apply to oblique shocks by substituting $M_1 \sin \theta$ everywhere M_1 appears. The oblique shock equations are

$$\frac{P_2}{P_1} = \frac{1 - \gamma + 2\gamma M_1^2 \sin^2 \theta}{1 + \gamma} \quad (6.48)$$

$$\frac{\rho_2}{\rho_1} = \left[\frac{2 + (\gamma - 1)M_1^2 \sin^2 \theta}{(\gamma + 1)M_1^2 \sin^2 \theta} \right]^{-1} \quad (6.49)$$

$$\frac{T_2}{T_1} = \left[\frac{2\gamma}{\gamma+1} M_1^2 \sin^2 \theta - \frac{\gamma-1}{\gamma+1} \right] \left[\frac{\gamma-1}{\gamma+1} + \frac{2}{(\gamma+1)M_1^2 \sin^2 \theta} \right] \quad (6.50)$$

$$M_2^2 \sin^2(\theta - \delta) = \frac{M_1^2 \sin^2 \theta + \frac{2}{\gamma-1}}{\frac{2\gamma}{\gamma-1} M_1^2 \sin^2 \theta - 1} \quad (6.51)$$

$$\frac{P_{T_2}}{P_{T_1}} = \left\{ \frac{1}{\left[\frac{\gamma-1}{\gamma+1} + \frac{2}{(\gamma+1)M_1^2 \sin^2 \theta} \right]^\gamma \left[\frac{2\gamma}{\gamma+1} M_1^2 \sin^2 \theta - \frac{\gamma-1}{\gamma+1} \right]} \right\}^{\frac{1}{\gamma-1}} \quad (6.52)$$

6.14.2 Minimum and Maximum Wave Angle

In the normal shock analysis, it was found that a shock can only occur when the free stream Mach is greater than one. The same is true for oblique shocks; the free stream Mach component normal to the shock must be greater than one.

The minimum wave angle for a given free stream Mach of $M_1 > 1$ can be found from Equation 6.47

$$M_{1N} = M_1 \sin \theta = 1$$

or
$$\theta_{(\min)} = \sin^{-1} \frac{1}{M_1} \quad (6.53)$$

Notice that the minimum oblique shock wave angle, $\theta_{(\min)}$, for the given free stream Mach, M_1 , is the same as the Mach angle, μ , (Equation 6.20) formed by an isentropic pressure disturbance traveling at $M > 1$.

This shows that an oblique shock wave at minimum wave angle to the free stream flow is a zero strength or isentropic shock.

The maximum oblique shock wave angle for a given free stream Mach is 90°. This is the limiting case and is a normal shock.

6.14.3 Relation between θ and δ

From Figure 6.13

$$\tan \theta = \frac{V_{1N}}{V_{1t}}$$

$$\tan(\theta - \delta) = \frac{V_{2N}}{V_{2t}}$$

Eliminating V_{1t} from these equations, then using the continuity equation, Equation 6.49, and a great amount of algebraic and trigonometric manipulation:

$$\frac{\tan(\theta - \delta)}{\tan \theta} = \frac{(\gamma-1)M_1^2 \sin^2 \theta + 2}{(\gamma+1)M_1^2 \sin^2 \theta} \quad (6.54)$$

For a given M_1 , Equation 6.54 is an implicit relation between θ and δ . It may be rewritten to show the dependence of δ explicitly (after much trigonometric manipulation).

$$\tan \delta = 2 \cot \theta \frac{M_1^2 \sin^2 \theta - 1}{M_1^2 (\gamma + \cos^2 \theta) + 2} \quad (6.55)$$

This equation may be solved for various combinations of Mach, M_1 , and wave angle, θ , and plotted as in Figure 6.14.

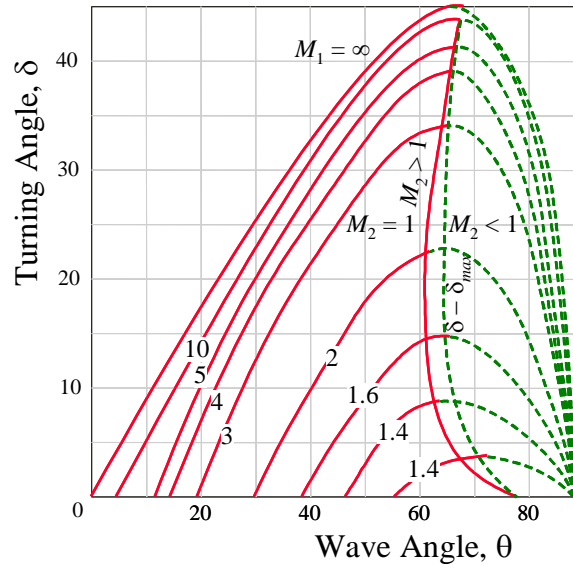


Figure 6.14 Turning Angle as a Function of Wave Angle for Flow through an Oblique Shock

Careful study of this figure will reveal several points of great interest when analyzing the flow through an oblique shock wave.

The existence of a maximum and minimum wave angle is verified- by the fact that Equation 6.55 becomes zero at $\theta = \pi/2$ and at $\theta = \sin^{-1} 1/M_1$.

The turning angle, δ , has a maximum value for a given value of M_1 . Turning angles larger than this maximum angle cause the oblique shock to detach from the surface at the concave corner. If δ is less than δ_{max} , an attached oblique shock will form.

There are two possible oblique shock solutions for a given turning angle, δ , and a given M_1 . The weak shock solution is represented by the solid lines in Figure 6.14, and the strong shock solution by the dotted lines.

The strong shock solution (the oblique shock with the greater wave angle) is characterized by subsonic flow downstream of the shock and by large energy losses in the shock. As a general rule, systems in nature tend to minimize their losses; therefore the weak shock occurs more frequently. However, there is no known mathematical law which predicts the type of shock that will occur for a given free stream Mach and a given turning angle.

The locus of points for which the Mach behind the shock, M_2 is equal to one is also plotted. It can be seen that the Mach downstream of a weak shock is usually supersonic, but in a small region (cross-hatched) near δ_{max} for a given free stream Mach, the Mach downstream of a weak shock can be subsonic.

The wave angle, θ , is generally the unknown quantity in analytical work and is conventionally plotted versus M_1 for different turning angles, δ (Figure 6.15).

From this figure, three important points can be noted:

1. There is a minimum allowable flow Mach for a given turning angle, below which the oblique shock will detach from the surface.
2. The wave angle of a weak shock decreases with increased free stream Mach, while the wave angle of a strong shock increases (approaching 90°) with increasing Mach.
3. For a given free stream Mach, the wave angle θ approaches the mach angle as δ is decreased.

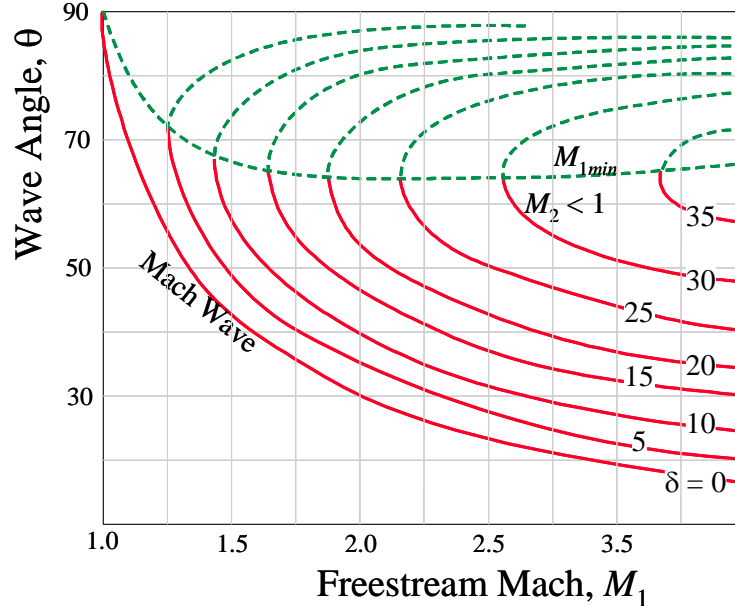


Figure 6.15 Wave Angle as a Function of Mach for Flow through an Oblique Shock

Because of the complexity of the equations for normal and oblique shock waves, it is common practice to use tables or charts of their solutions when solving a compressible flow problem. An excellent set of charts is in Reference 6.4.

6.14.4 Mach Lines

Considering that portion of Figure 6.14 where $M_2 > 1$, a decrease in turning angle δ corresponds to a decrease in wave angle θ . When δ becomes zero, θ reaches the limiting value given by Equation 6.53 which was previously shown to be the Mach angle μ (Equation 6.20).

$$\theta_{\min} = \sin^{-1} \frac{1}{M_1} = \mu \quad (6.53)$$

Analyzing the strength of the oblique shock formed at zero turning angle, with the oblique shock relations, Equations 6.48 through 6.52, it can be seen that the so-called "shock" has zero strength, or that no physical discontinuity in the supersonic flow exists.

For any point in a supersonic flow, there is a characteristic angle associated with the Mach of the flow at that point. This angle is the Mach angle μ . Lines drawn at an inclination of μ at a point in the flow are called Mach lines or sometimes Mach waves.

6.15 Isentropic Compression

A shock wave compresses supersonic flow by increasing the pressure and density of the fluid in a very short but finite distance. A simple method to compress supersonic flow is to deflect the flow boundary into the flow through an angle, thereby creating an oblique shock wave through which the flow must pass.

By dividing the total boundary deflection into several small segments of $\Delta \delta$, the compression can be visualized as occurring through several successive oblique shocks which divide the flow field near the boundary into segments of uniform flow (Figure 6.16).

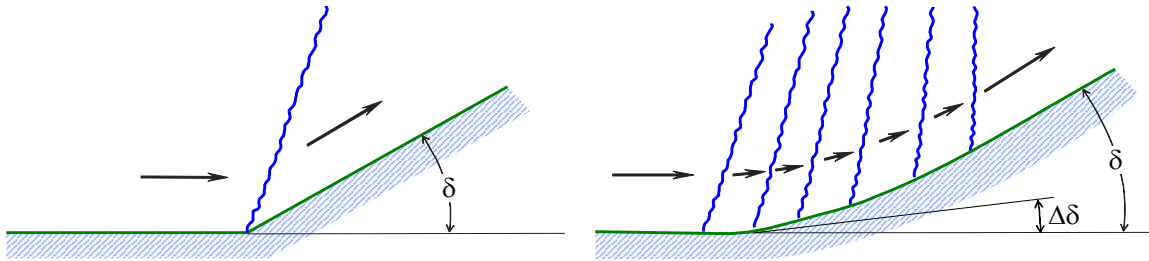


Figure 6.16 Isentropic Compression

In each region between oblique shocks, the supersonic flow is independent of the regions upstream and downstream, making it possible to analyze the flow field region by region.

Using the approximate equation for weak shocks to compare the one shock compression to the multi-shock compression, it can be shown that for each wave

$$\Delta P \approx \Delta \delta$$

$$\Delta S \approx (\Delta \delta)^3$$

If there are n segments being considered in the complete turning angle then

$$\delta = n \Delta \delta$$

and

$$\Delta P_{total} \approx n \Delta \delta \approx \delta$$

$$\begin{aligned} \Delta S_{total} &\approx n (\Delta \delta)^3 \approx n \Delta \delta (\Delta \delta)^2 \\ &\approx \delta (\Delta \delta^2) \end{aligned}$$

Thus, if a large number of weak waves cause the compression, the entropy increase is reduced drastically compared to a one shock compression for the same total turning angle.

By making $\Delta \delta$ smaller and smaller, a smooth turn with $\Delta \delta \rightarrow 0$ is created in the limit, the entropy increase becomes zero, and the compression can be considered isentropic.

This limiting process produces the following results:

1. The oblique shocks approach zero strength and become straight Mach lines.
2. Each region of uniform flow approaches the width of a Mach line; thus on each Mach line the flow inclination and Mach are constant.
3. The flow upstream of each Mach line is not affected by downstream changes in the wall.
4. The approximate equations for changes in properties across weak waves may be written in differential form, i.e., ΔP becomes dP .

The above discussion considers flow near the boundary of the supersonic flow field. Farther away from the wall, due to the convergence of Mach lines, the flow is no longer isentropic, and the Mach lines converge, forming an oblique shock wave.

6.16 Isentropic Expansion

When the boundary of a supersonic flow is deflected into the flow, the flow is compressed. If the deflection is abrupt, an oblique shock wave forms in the corner. If the deflection is smooth, an isentropic analysis of the compression may be performed.

/What happens when the boundary is deflected away from the supersonic flow? If a single oblique shock wave formed and the flow expanded through it, this would require that the normal component of velocity after the shock be greater than the normal component of velocity ahead of this shock, i.e., an increase in velocity through the shock (Figure 6.17). This is in direct violation of the second law of thermodynamics

because it demands a decrease in entropy (refer to Appendix F, Derivation F.7), even though the equations of motion are satisfied.

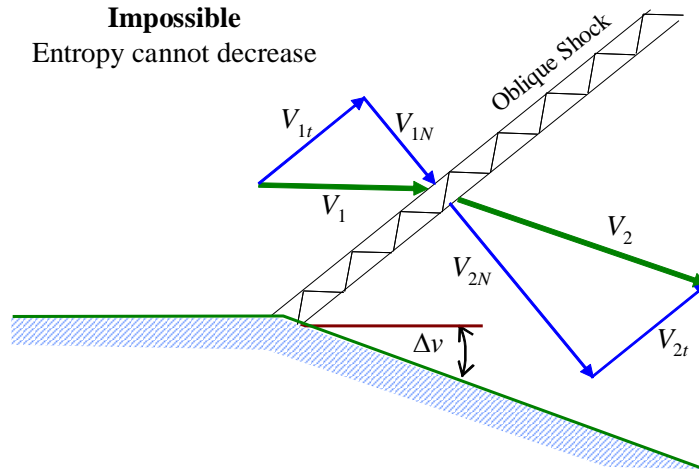


Figure 6.17 Impossibility of Shock Formation Flow Turning away from Itself

Actually, the same nonlinear effect that makes Mach lines converge in a compression makes the Mach lines diverge in an expansion, and the supersonic expansion is an isentropic phenomenon throughout.

Consider the expansion of supersonic flow caused by the boundary deflection Δv in Figure 6.18a.

If P_2 is less than P_1 , the disturbances from the lower pressure will be transmitted out into the stream. The pressure P_2 will not be transmitted upstream since the flow is supersonic, and it will only be felt as far upstream as the Mach line extending out from the corner into the flow.

When the flow passes this Mach line, it will sense the lower pressure and will tend to turn and accelerate because of the pressure differential. Associated with the flow velocity increase is a pressure decrease which changes the flow properties immediately following the Mach line and consequently defines a new Mach line upstream of which the influence of P_2 cannot be felt. Hence, the flow gradually increases velocity and changes direction through an infinite number of these Mach lines, forming a fan shaped array referred to as a "Prandtl-Meyer expansion fan" as shown in Figure 6.18b.

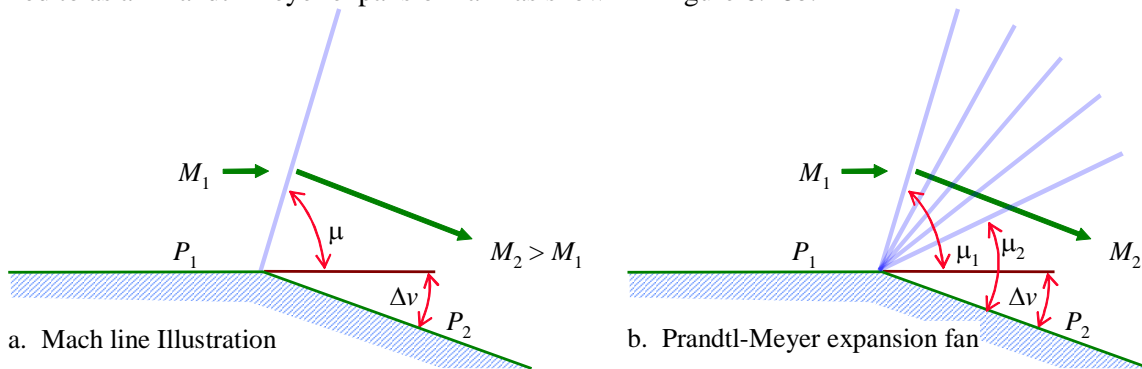


Figure 6.18 Supersonic Flow around a Corner

As the Mach increases through the first line and the pressure decreases, the approach of subsequent pressure signals is altered slightly by the increased Mach, thus causing the next Mach wave to be more inclined to the free stream. The Mach angle calculated for the last Mach line is that calculated from the final Mach, M_2 , after the turn.

Supersonic expansion occurs not only at abrupt corners but also on smooth surfaces. In this case, the fan is distributed over the entire curve as shown in Figure 6.19.

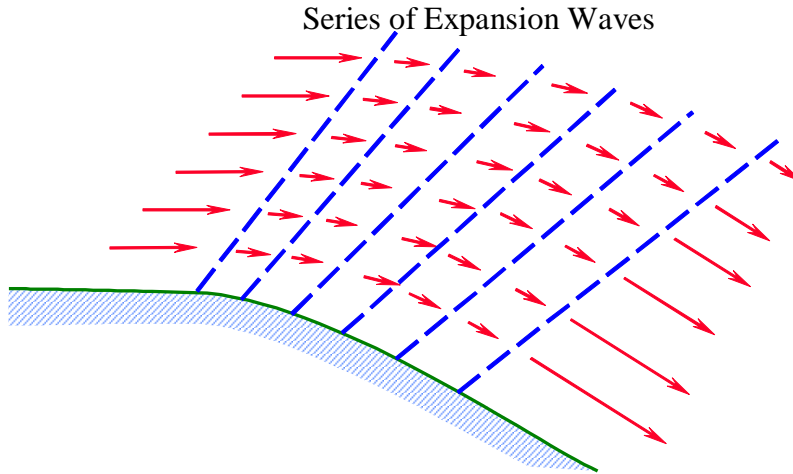


Figure 6.19 Supersonic Flow around a Smooth Corner

Further insight into the reason for the finite distance required to accelerate the flow around the corner might be gained from a physical interpretation of the acceleration itself. An instantaneous change in velocity and direction around the corner would mean that there was an infinite acceleration for a given mass of fluid. But from Newton's law, $F=ma$, an infinite acceleration requires an infinite force or pressure gradient, and no such source of energy is present; therefore the acceleration cannot be instantaneous.

The equation

$$\frac{\Delta V}{V} = + \frac{\Delta v}{\sqrt{M_1^2 - 1}} \quad (6.56)$$

is an approximate expression relating the velocity change through an isentropic Mach wave to incoming Mach, M_1 , and expansion angle, Δv . Derivation of this equation is tedious and will be omitted. It may be found in many aerodynamic textbooks on supersonic flow.

For small values of Δv and ΔV , Equation 6.56 may be written in differential form

$$+ dv = \sqrt{M^2 - 1} \frac{dV}{V}$$

and integrated

$$+ v + cont = \int \sqrt{M^2 - 1} \frac{dV}{V} = v(M)$$

To evaluate the integral and thus find an explicit form of $v_{(M)}$, V must be rewritten in terms of M using the following relationships

$$V = aM$$

$$\frac{a_T^2}{a^2} = \frac{\gamma R T_T}{\gamma R T} = \frac{T_T}{T} = 1 + \frac{\gamma - 1}{2} M^2$$

from which

$$\frac{dV}{V} = \frac{dM}{M} \times \frac{da}{a} = \frac{dM}{M} \left[\frac{1}{1 + \frac{\gamma - 1}{2} M^2} \right]$$

therefore

$$v_{(M)} = \int \frac{\sqrt{M^2 - 1}}{\left(1 + \frac{\gamma - 1}{2} M^2\right) M} dM$$

This integral may be evaluated between two Mach numbers and is called the Prandtl-Meyer function

$$v_{(M)} = \sqrt{\frac{\gamma + 1}{\gamma - 1}} \tan^{-1} \sqrt{\frac{\gamma - 1}{\gamma + 1} (M^2 - 1)} - \tan^{-1} \sqrt{M^2 - 1} \tag{6.57}$$

The constant of integration was chosen such that $v_1 = 0$ when $M_1 = 1$. Thus, for every supersonic Mach there is a corresponding angle v which represents the angle through which a flow that is initially at Mach 1 must turn to achieve that supersonic Mach.

If M_1 , prior to turning is greater than Mach 1, the associated v_1 is greater than zero. To find the Mach following a turn through an angle Δv , it is necessary to add Δv to the v_1 corresponding to M_1 , and find the final Mach, M_2 , corresponding to v_2 .

In equation form, this may be written

$$v_2 = v_1 + |\Delta v| \tag{6.58}$$

where Δv is the turning angle shown in Figure 6.18a. Absolute values of Δv are used to avoid any confusion associated with the sign of the turning angle.

Tables for solving two-dimensional isentropic expansion problems may be found in Reference 6.4 and Figure 6.20 outlines the method to be used. Once the Mach after expansion is known, all of the supersonic flow properties may be calculated from isentropic relations.

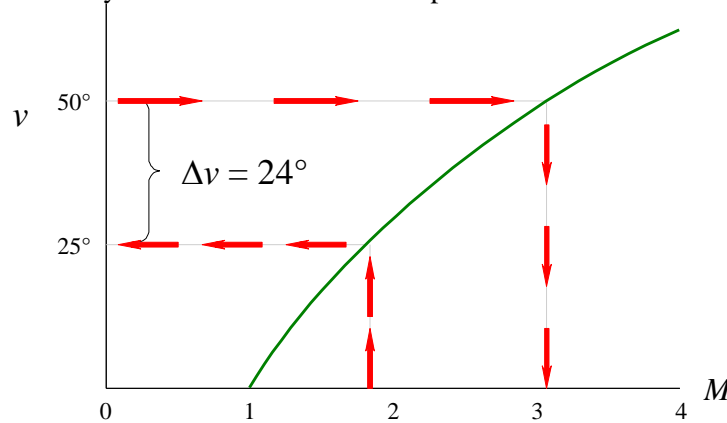


Figure 6.20 Turning Angle as a Function of Mach for Prandtl-Meyer Flow

Consider the problem of $M_1 = 2$ flow expanding through an angle of 24° . What is the Mach after the turn? Enter Figure 6.20 with $M_1 = 2$ and find $v_1 = 26^\circ$. This is the angle $M_1 = 1$ flow must turn through to reach a value of Mach two. Adding $v_1 = \Delta v$ and reentering the figure at this value of 50° , M_2 can be found to have a value of Mach three.

If the Mach in Equation 6.57 goes to infinity, which corresponds to expanding supersonic flow to zero pressure, the maximum turning angle is obtained

$$\Delta v_{\max} = \frac{\pi}{2} \left[\sqrt{\frac{\gamma + 1}{\gamma - 1}} - 1 \right] \tag{6.59}$$

Thus a flow that is initially at Mach 1 can turn 130.5° . But a stream that is initially at 2.5 Mach can turn only 90° . The higher the initial Mach, the lower the turning capability. Using Equations 6.58 and 6.59, an expression for the turning capability, v_{tc} of the flow can be obtained.

$$v_{tc} = \Delta v_{\max} - v_1 \tag{6.60}$$

Attention is called to the fact that these are the theoretical angles at which the flow will leave the surface for any initial Mach and that very high deflection angles are indicated at all Mach. In practice, real fluid effects such as boundary layer and viscosity will greatly reduce the angle at which the flow will leave the surface.

Table 6.1 summarizes the characteristics of the three wave forms encountered in supersonic flow.

Type of wave	Oblique shock wave	Normal shock wave	Expansion wave
--------------	--------------------	-------------------	----------------

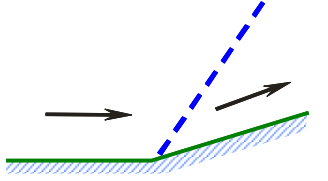
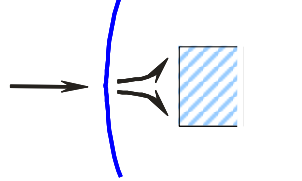
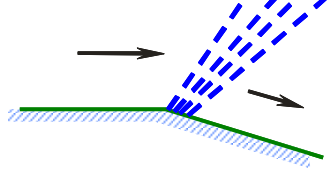
formation			
Flow direction change	“Flow into a corner.” turned into preceding flow.	No change	“Flow around a corner.” turned away from preceding flow.
Effect on velocity and Mach	Decreased but still supersonic	Decreased to subsonic	Increased to higher supersonic
Effect on static pressure and density.	Increase	Great increase	Decrease.
Effect on total pressure	Decrease	Great decrease	No change (no shock).

Table 6.1 Supersonic Wave Characteristics

6.17 Interaction of Wave Forms

Successive oblique wave forms may interfere with one another. Four cases are possible:

1. Expansion followed by expansion
2. Compression followed by compression
3. Compression followed by expansion
4. Expansion followed by compression

This discussion is limited to two-dimensional analysis.

Case one is most easily analyzed because there are no interference effects. This can be seen with reference to Figure 6.21. The final effect is equivalent to flow over a rounded corner with the same total deflection angle.

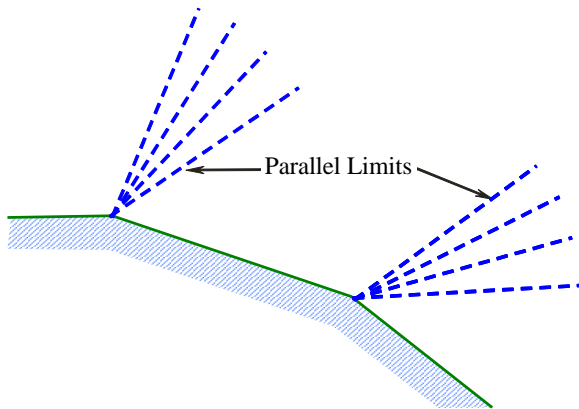


Figure 6.21 Two Expansions

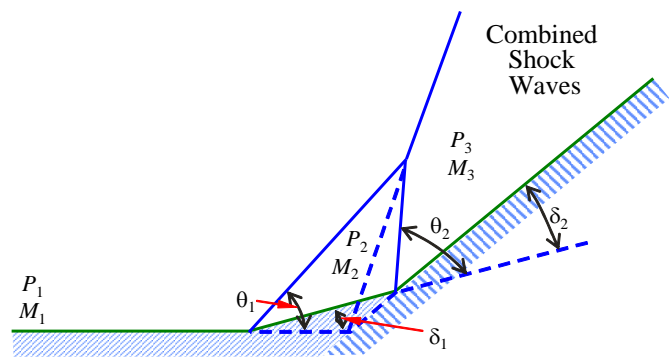


Figure 6.22 Two Compressions

When one oblique shock is followed by another, as in Figure 6.22, interaction must occur and results in a single shock of increased intensity at some distance away from the wall. Recall that the Mach after an oblique shock is always decreased and the flow is bent toward the wave. A second oblique shock generated behind the first with a subsequent second change in flow direction increases the shock wave angle because of the reduction in stream velocity, and the wave will be tilted toward the first oblique

shock due to the initial deflection. Therefore, the two shock lines must intersect. The intersection of the two separate waves must form a wave which has the same angle as that applying to a wave formed by a single intersection of the initial and final surfaces. The wave formed by the combination is therefore stronger than either one alone.

If we have an oblique shock followed by an expansion, we must also have an intersection. Because of the nature of expansion waves, the intersection will be a diffuse effect which tends to weaken the shock at points away from the surface. Because the velocity of the wave is dependent upon its intensity, the weakening effect in the regions away from the surface will reduce the propagation velocity and cause the oblique shock wave front to bend as illustrated in Figure 6.23.

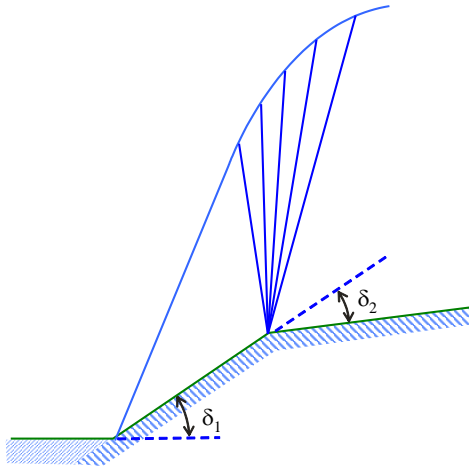


Figure 6.23 Shock Followed by Expansion

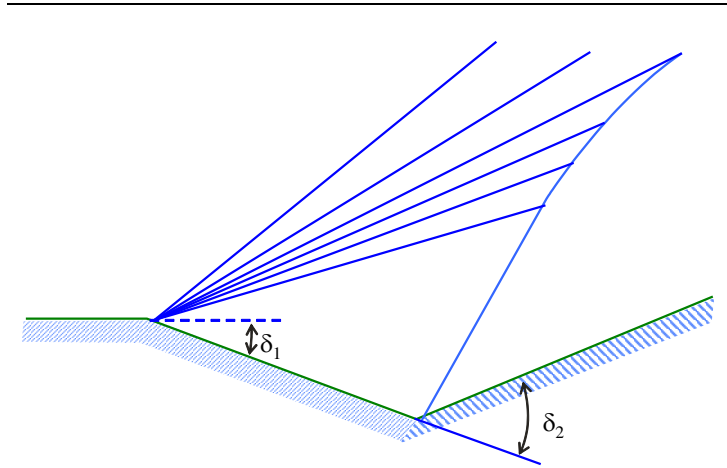


Figure 6.24 Expansion Followed By Shock (6.5:135)

The case of expansion followed by compression is very similar to the case just discussed.

Intersection with a weakening of the shock wave must occur. The details of the intersection are different because the intersection occurs on the free stream side of the shock instead of in the reduced velocity region behind the shock. Intersection cannot be avoided because the shock wave stands at a higher angle with respect to the expanded flow lines than do some or all of the local Mach lines at the expansion corner. This case is illustrated in Figure 6.24 (6.5.132-136).

6.18 Two-Dimensional Supersonic Airfoils

In order to appreciate the effect of these various wave forms upon aerodynamic characteristics in supersonic flow, refer to Figure 6.25. Parts a and b show the wave pattern and resulting pressure distribution for a thin flat plate at a positive angle of attack. The airstream moving over the upper surface passes through an expansion wave at the leading edge and an oblique shock at the trailing edge. Therefore, a uniform suction pressure exists over the upper surface. The airstream moving underneath the flat plate passes through an oblique shock wave at the leading edge and an expansion wave at the trailing edge. Therefore, a uniform positive pressure exists on the underside of the section. This pressure distribution produces a net lift and also a drag due to lift. The drag is analogous to induced drag in subsonic flow but is not a function of downwash as is the case in subsonic flow. Remember that pressure disturbances cannot be transmitted ahead of an object in supersonic flow, so the fluid is not aware of the approaching object.

The flat plate, although aerodynamically quite efficient at supersonic speeds, is not structurally satisfactory. It is difficult to give it enough strength to withstand the loads imposed on the airfoil during high speed flight.

Parts c and d of Figure 6.25 show the wave pattern and pressure distribution for a double wedge airfoil at zero lift. The resulting pressure distribution on the surfaces of the double wedge produces no net lift, but the increased pressure on the forward half along with the decreased pressure on the rear half of the section

produces wave drag. This wave drag is a result of the components of the pressure forces which are parallel to the free stream direction, and can be a large portion of the total drag at high supersonic speeds.

Parts e and f of Figure 6.25 illustrate the wave pattern and resulting pressure distribution for the double wedge airfoil at a small positive angle of attack. The net pressure distribution produces drag due to lift in addition to the wave drag at zero lift. Similarly, parts g and h show the wave pattern and pressure distribution for a circular arc airfoil (also called a bi-convex airfoil) at a small angle of attack.

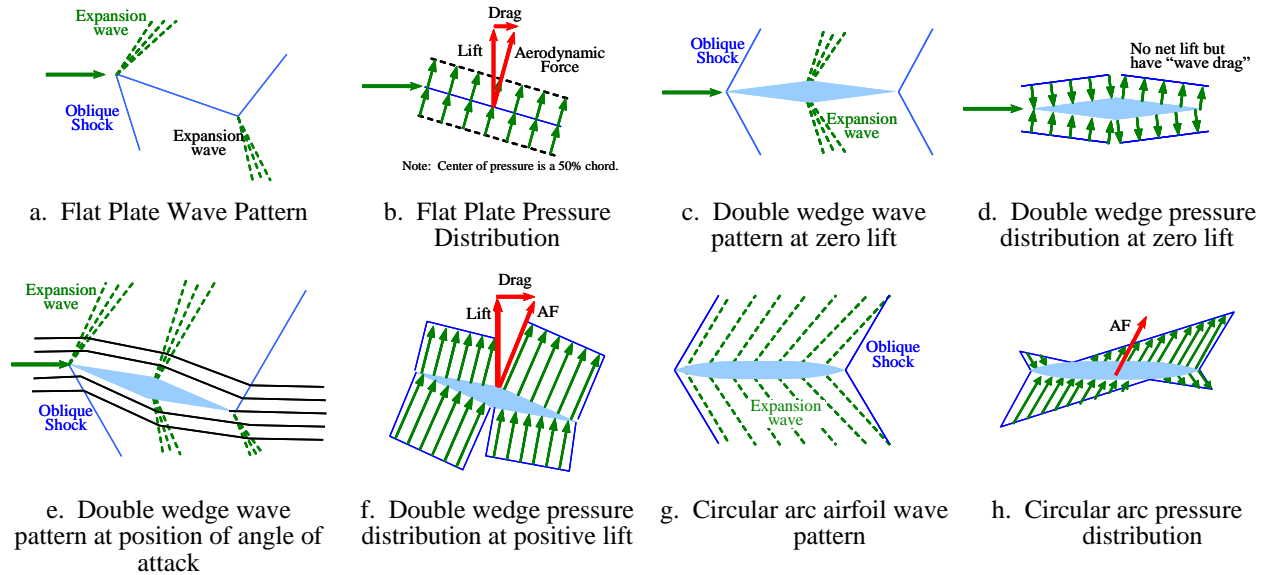


Figure 6.25 Supersonic Flow Pattern and Distribution of Pressure

6.19 Pressure Coefficient for Two-Dimensional Supersonic Airfoils and Infinite Wings

The preceding paragraph on the different supersonic waveforms have developed all of the mathematical tools required to compute the lift and drag on a simple two-dimensional supersonic airfoil. Consider the double wedge or diamond airfoil shown in Figure 6.26.

If the flight Mach, M_∞ , remote ambient pressure, P_∞ , angle of attack, α , and the geometry of the wing are known, pressures in areas 2, 3, 5, and 6 can be computed. Oblique shock relationships can be used to determine P_2 and P_5 from P_∞ , and Prandtl-Meyer relations can be used to determine P_3 and P_6 . from P_2 and P_5 . Once these pressures are known, lift and drag can be readily determined from geometric relationships.

This problem can be attacked in a more systematic manner by recalling the definition of pressure coefficient

$$C_p \equiv \frac{P - P_\infty}{q_\infty}$$

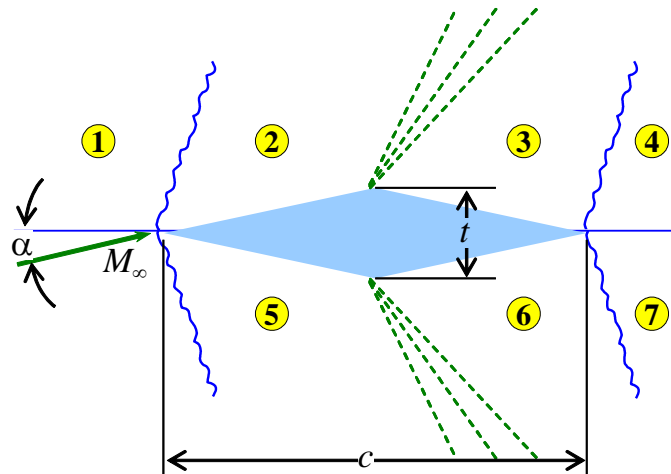


Figure 6.26 Double Wedge Airfoil in Supersonic Flow

For an example of the diamond airfoil, the local pressure coefficient can be expressed as

$$[C_p]_x \equiv \frac{P_x - P_\infty}{q_\infty} \quad (6.61)$$

when $x = 2, 3, 5,$ or $6,$ depending on the area of the airfoil under consideration.

In terms of remote Mach, $M_\infty,$ Equation 6.61 can be rewritten as

$$[C_p]_x \equiv \frac{2}{M_\infty^2 \gamma} \left[\frac{P_x}{P_\infty} - 1 \right] \quad (6.62)$$

Given $\alpha,$ the geometry of the airfoil, $M_\infty,$ and $\gamma = 1.4,$ C_{p_2} and C_{p_5} can be determined directly from Reference 6.4 and use of Equation 6.61.

The evaluation of Equation 6.62 for C_{p_3} and C_{p_6} can also be easily made. In determining C_{p_3} for example,

$$P_3 / P_\infty = [P_2 / P_\infty] [P_{T_2} / P_2] [P_3 / P_{T_3}] \quad (6.63)$$

All of the ratios on the right side of Equation 6.63 are found in Reference 6.4 tables after M_2 and M_3 are determined. After $C_{p_2}, C_{p_3}, C_{p_5},$ and C_{p_6} are determined, the forces normal to each surface can be calculated, since

$$F_x = [C_p]_x q_\infty S$$

when F_x is the force normal to the surface, and again $x = 2, 3, 5,$ or $6,$ depending upon the area of the airfoil under consideration. Once all the F_x 's are known, they can be resolved into components perpendicular to and parallel with the relative wind to determine lift and drag.

6.20 Thin Wing Theory

Although an exact analytic determination of lift and drag forces acting on even a simple two-dimensional supersonic airfoil is a somewhat lengthy problem (as shown in the paragraph on two-dimensional wings), an approximate determination is readily accomplished.

Probably the most widely accepted of the approximate (or thin wing) supersonic theories is the one due to Ackeret which is either called the linear theory or simply the Ackeret theory. For thin airfoils set at relatively small angles of attack, the Ackeret theory agrees well with experimental data from Mach of about 1.2 to 5.0, and therefore the assumptions made in its development are empirically justified.

A pressure coefficient is developed (Derivation F.8 Appendix F) such that

$$C_p = \frac{\Delta P}{q} = \pm \frac{2\delta}{\sqrt{M^2 - 1}}$$

where the minus sign holds for an expansion and the plus sign holds for a compression. For the double wedge, Ackeret Theory predicts that

$$C_L = \frac{4\alpha}{\sqrt{M^2 - 1}} \quad (6.64)$$

$$C_D = \frac{4\alpha^2}{\sqrt{M^2 - 1}} + \frac{4}{\sqrt{M^2 - 1}} \left(\frac{t}{c}\right)^2 \quad (6.65)$$

We can write the drag coefficient of the double wedge in the same form we had for subsonic flow,

$$C_{D_{tot}} = C_{D_i} + C_{D_p} \quad (6.66)$$

Comparing the terms in Equation 6.66 with Ackeret theory gives

$$C_{D_p} = \frac{4(t/c)^2}{\sqrt{M^2 - 1}} \quad (6.67)$$

$$C_{D_i} = \frac{4\alpha^2}{\sqrt{M^2 - 1}} \quad (6.68)$$

As in subsonic flow, C_{D_p} is not a function of α . It is often defined as the wave drag coefficient when $\alpha = 0$. This term is due to the profile shape and is similar to the profile (parasite) drag term of a subsonic wing section, although it does not depend on viscosity. C_{D_p} is a function of Mach and the thickness ratio (t/c) defined in Figure 6.26.

The second term, C_{D_i} , can be defined as drag coefficient due to lift and is a direct function of α^2

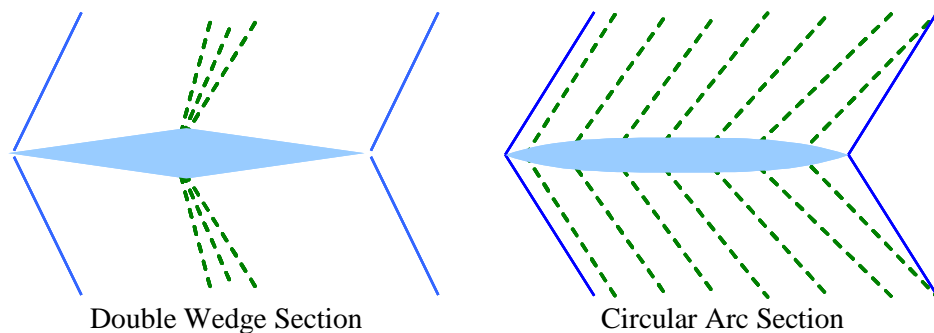
By allowing t to equal zero, Equation 6.65 immediately simplifies to the coefficient of drag equation for a flat plate, Equation 6.69.

$$C_{D_{tot}} = \frac{4\alpha^2}{\sqrt{M^2 - 1}} \quad (6.69)$$

From Ackeret theory the equation for lift coefficient for both the flat plate and for the double wedge turns out to be

$$C_L = \frac{4\alpha}{\sqrt{M^2 - 1}} \quad (6.70)$$

The Ackeret theory presented here may be extended to other airfoil shapes, and in all cases, the form of the equations is similar. Figure 6.27 summarizes the lift and drag coefficient relationships for the double wedge and circular arc airfoils, the two types most commonly used for supersonic flight vehicles.



Wave Drag Coefficient:	$C_{D_p} = \frac{4(t/c)^2}{\sqrt{M^2 - 1}}$	$C_{D_p} = \frac{5.33(t/c)^2}{\sqrt{M^2 - 1}}$
Lift Coefficient:	$C_L = \frac{4\alpha}{\sqrt{M^2 - 1}}$	$C_L = \frac{4\alpha}{\sqrt{M^2 - 1}}$
Drag Due to Lift:	$C_{D_i} = \frac{4\alpha^2}{\sqrt{M^2 - 1}}$	$C_{D_i} = \frac{4\alpha^2}{\sqrt{M^2 - 1}}$
Lift Curve Slope:	$C_{L_\alpha} = \frac{4}{\sqrt{M^2 - 1}}$	$C_{L_\alpha} = \frac{4}{\sqrt{M^2 - 1}}$

where

- (t/c) = Airfoil Thickness Ratio
- α = Angle of Attack (In Radians)
- M = Mach

Figure 6.27 Approximate Equations For Supersonic Section Characteristics

6.21 Supersonic Flow In Three Dimensions

In supersonic three-dimensional flow we must consider the fact that the stream lines do not turn immediately as they do in the two-dimensional case. Therefore, the shock wave for a typical three-dimensional shape, i.e., a cone, will be weaker for a given velocity. The stream lines approach the object's surface in a rather asymptotic fashion. This is seen from the fact that at all points off the apex of the cone, the section presented to the flow is a hyperbolic section rather than a sharp point. Because of this fact, we have the gradual transition shown in Figure 6.28.

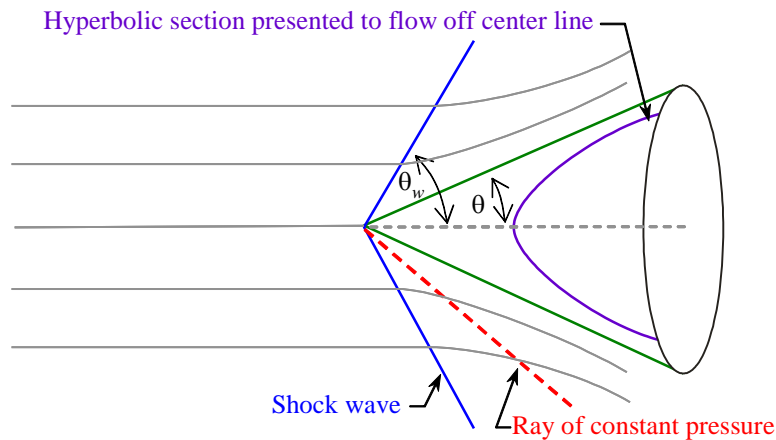


Figure 6.28 Stream Lines about a Cone

As would be expected, the pressure, density, temperature, velocity, and Mach all vary between the shock wave and the surface. After increasing through the shock wave, the static pressure and density would continue to increase along a stream line, and the velocity and Mach would therefore continue to decrease. However, the pressure along any ray from the apex of the cone is constant. Since the surface of the cone is essentially the limiting ray from the apex, the surface pressure is constant. Because of the nature of the flow, this pressure is considerably lower than that found at the surface of an infinite wedge of the same apex angle. For a given vertex angle and free stream flow, the pressure change for a cone is about one-third that for a wedge.

If the cone we have been discussing is suddenly flared out at a new angle, we will have a condition in which the surface is formed by the intersection of two coaxial cones. This situation is illustrated in Figure 6.29.

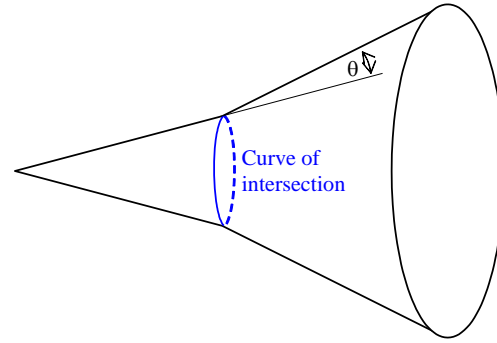


Figure 6.29 The Flared Cone

The curve of intersection of the two surfaces is a circle as shown. If this circle is of large radius, we shall have the approximation of two-dimensional flow at the corner as the air is forced to turn through the angle θ . The effect of the rounded shape, however, acts to relieve the severity of the shock and modify the details of the flow. Because of this action, the line of the shock wave will be a curve rather than a straight line. This is illustrated in Figure 6.30.

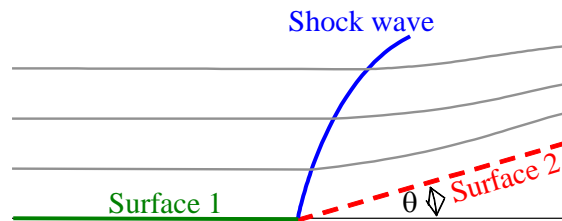


Figure 6.30 Flow in a Round Corner

As shown, the stream lines change direction at the shock wave. However, they continue to change gradually to approach the condition of parallel flow as we expect on the surface of a cone. The bending of the shock line is related to the surface curvature.

Practical application of the three-dimensional effects discussed above could be applied to the juncture of canopy and nose on an aircraft or to conical plugs found in engine inlets such as those on the SR-71.

6.22 Three-Dimensional Supersonic Wings

To this point we have considered only the infinite wing in two-dimensional flow. If we have a finite planform such as that given in Figure 6.31, we can expect the apex to generate a Mach cone as indicated. This will be true in any practical case of an aircraft in flight because of the nose section ahead of the wing. The nose will generate a cone of disturbance in which at least a portion of the wing will fly. As the velocity of flight, V_∞ , increases, the cone narrows as indicated in Figure 6.31b.

When the leading edge of the wing is behind the Mach cone angle as shown in Figure 6.31a, the normal Mach is subsonic, and no shock wave is created at the leading edge. The pressure distribution and the forces resulting will be equivalent to those found in an airfoil normal to the stream at the corresponding subsonic Mach. In this case, it is advantageous to use a subsonic airfoil section rather than a supersonic section if the wing will always be below the effective Mach of unity.

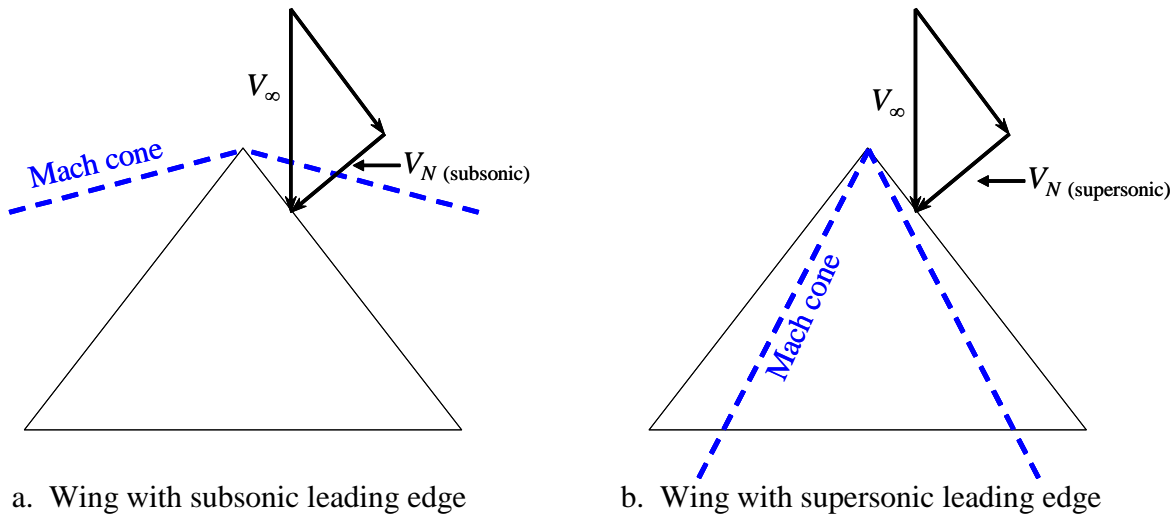


Figure 6.31 Mach Cone Limits

If the Mach cone falls behind the leading edge as shown in Figure 6.31b, the effective flow on the wing is supersonic at the leading edge. However, it is quite possible that the effective flow may be supersonic at the leading edge but subsonic at the trailing edge. This would certainly happen behind a shock cone. The pressure distribution is modified by the transition from supersonic to subsonic flow.

These effects are also involved in the analysis of tip losses. Let us consider a flat plate wing of finite aspect ratio as shown in Figure 6.32.

Since the tip losses are confined to the region within the tip cones, the tips could be cut off at an angle slightly greater than the Mach angle so that none of the wing is contained within the Mach cone. Then there are no induced effects, and the wing acts as in two-dimensional flow, and Equations 6.65 and 6.70 apply.

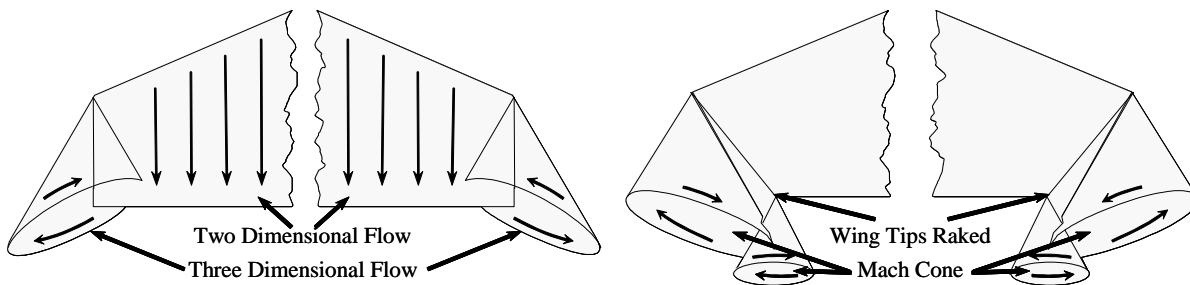


Figure 6.32 Supersonic Tip Effects

6.23 Transonic Flow Regime

In the previous paragraphs, the subject of transonic aerodynamics has been judiciously avoided. It can be seen from Ackeret thin wing theory (Equations 6.67 - 6.70) that lift and drag tend to become infinite in the vicinity of Mach 1. A similar result is also found from subsonic theory proposed by Prandtl and Glauert, shown in Figure 6.33.

From this figure comes the concept of the mythical sonic barrier. In the actual case, the lift coefficient follows a trend more like that indicated by the dotted line.

Transonic flow over a body is complicated by the fact that both subsonic and supersonic flows exist simultaneously on the surface of the aircraft. The interaction between these two types of flow plus the viscous effects in the boundary layer create a condition that defies direct mathematical analysis.

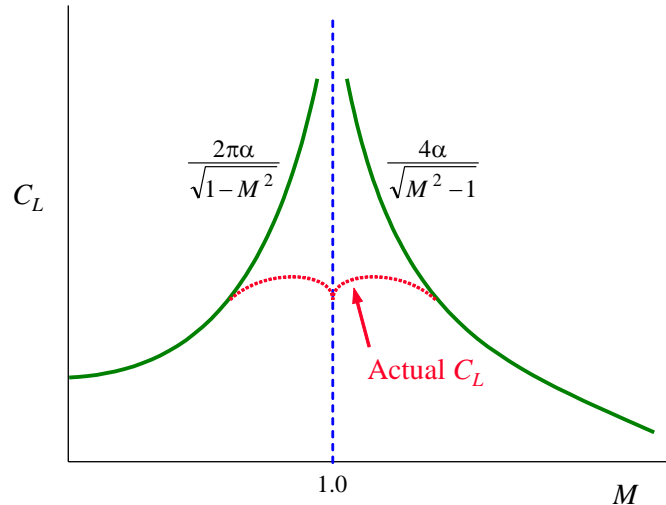


Figure 6.33 Transonic Lift Coefficient Characteristics

Even experimental results in the wind tunnel are difficult to obtain because of the tunnel choking effects caused when a model is placed in the nearly sonic throat of the tunnel. The approach in this chapter will be to extrapolate the concepts of viscous, subsonic flow and nonviscous supersonic flow into this region of mixed flow conditions resulting in a qualitative look at the transonic speed range.

The transonic speed range begins when sonic flow first occurs over the surface of the vehicle and ends when the flow is supersonic over the entire surface (with the possible exception of a small insignificant subsonic region at the leading edge).

From Bernoulli's theorem, it has been shown that the velocity increases and the pressure decreases as air flows subsonically over the surface of an airfoil. As the Mach of the vehicle is increased, the flow near the thickest portion of the airfoil approaches Mach 1 as in Figure 6.34a.

This is the critical Mach of the airfoil and is always less than 1. When the vehicle velocity exceeds the critical Mach, regions of subsonic and supersonic flow are created on the airfoil as shown in Figure 6.34, parts b and c.

A shock always exists at the trailing edge of the supersonic region, and as the vehicle velocity is increased above the critical Mach, the supersonic region grows fore and aft of the point of maximum thickness until it reaches the trailing edge and is very nearly attached to the leading edge as in Figure 6.34e.

When the bow shock attaches to the leading edge, the airfoil has left the transonic speed regime and has entered the supersonic regime.

6.23.1 Thickness

As speed increases from subsonic to transonic, thick, unswept, straight tapered wings show increases in lift-curve slope up to Mach slightly beyond the critical. The slope then drops to a lower value followed by a rise starting near Mach 1 to a value almost as high as the value at the critical Mach. This type of behavior is illustrated in Figure 6.33.

Reducing either the aspect ratio, the wing thickness ratio, or both reduces the magnitude of these effects. For very thin wings and for wings of very low aspect ratio, these transonic nonlinearities do not exist, and the $C_L - M$ curve resembles Figure 6.35.

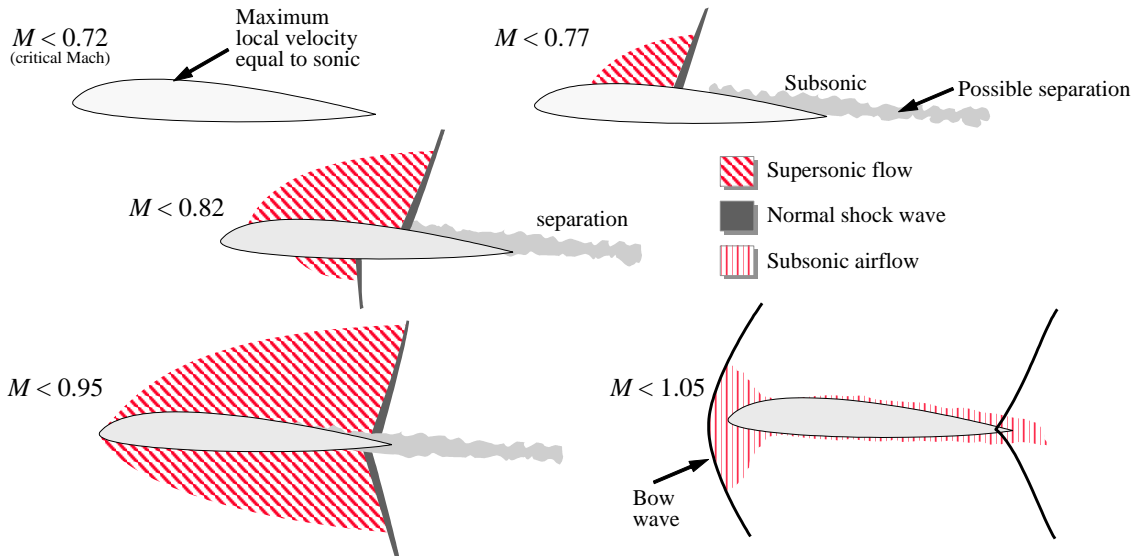


Figure 6.34 Transonic Flow Patterns

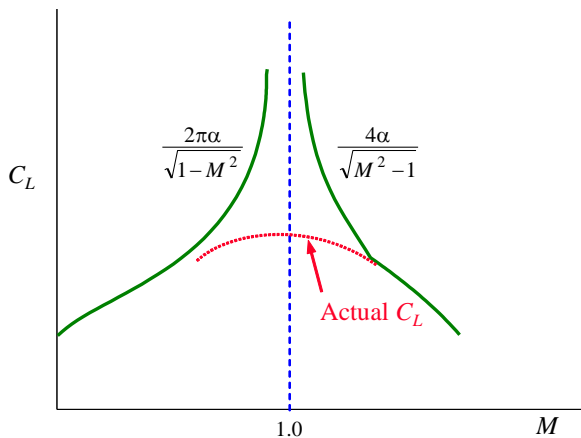


Figure 6.35 Thin Wing Transonic Lift Coefficient

Further evidence of the benefits of reducing airfoil thickness for the transonic flight regime is shown in Figure 6.36, where pressure coefficient as a function of critical Mach is shown for various thicknesses of airfoils.

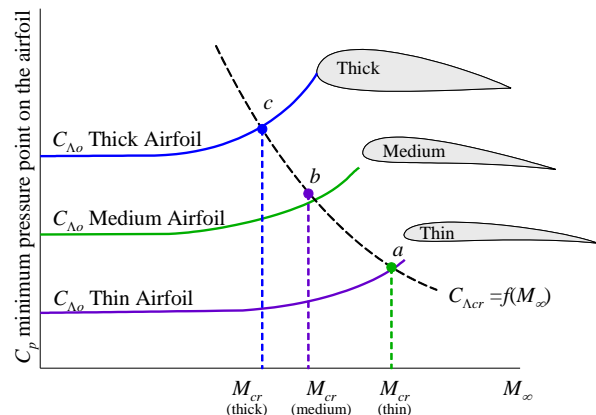


Figure 6.36 Critical Pressure Coefficient and Critical Mach for Airfoils of Different Thicknesses

6.23.2 Supercritical Airfoils

Another method which can be utilized to increase critical Mach and delay the transonic drag rise is to use a supercritical airfoil. Such an airfoil is depicted in Figure 6.37. The supercritical airfoil is thicker than the conventional airfoil; this results in greater rigidity and internal volume. At the same time, the recovery shock wave on top of the wing is weaker and is moved much further aft than on conventional airfoils. The supercritical airfoil causes less boundary layer separation, resulting in a delay in the drag rise which occurs on a conventional airfoil section at the critical Mach. The result is that the drag rise associated with passage through critical Mach is delayed.

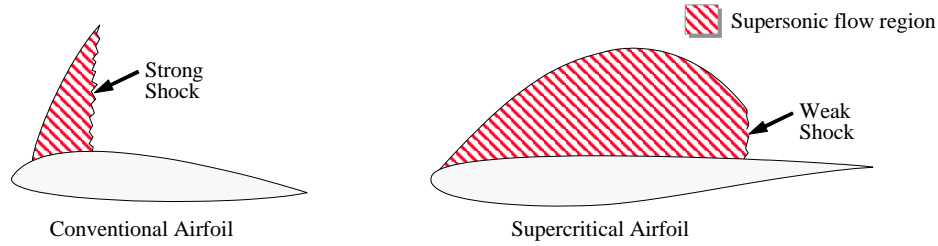


Figure 6.37 Comparison of Drag Rise Phenomena, at Critical Mach

6.23.3 Wing Sweep

The final method to be discussed for delaying critical Mach to higher values is wing sweep. To the airstream, the velocity (or Mach) that is important is the component that is perpendicular to the leading edge of the wing. By referring to Figure 6.38a, it is seen that the component of velocity perpendicular to the leading edge of the wing is less than the free stream value by the cosine of the sweep angle Λ . Therefore, the critical Mach is increased, and the transonic drag rise is delayed. Reduction in drag coefficient as a function of Mach for several values of wing sweep is illustrated in Figure 6.38b.

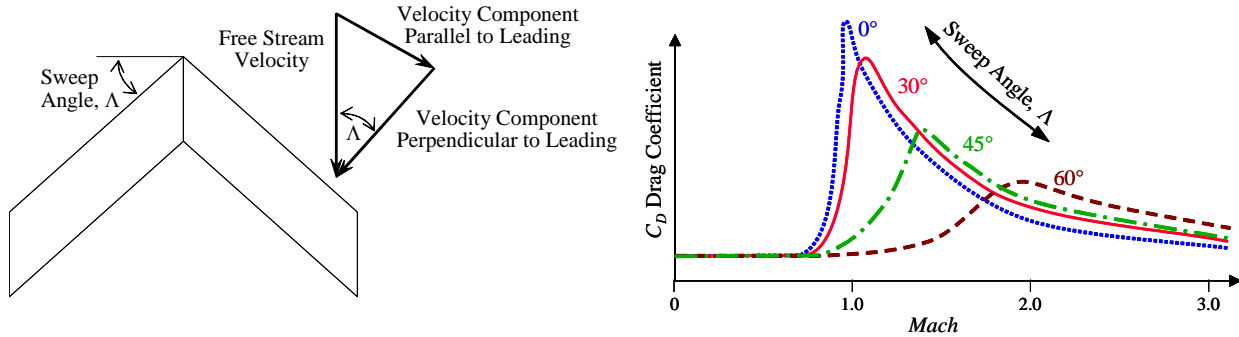


Figure 6.38 General Effects of Sweepback

Spanwise flow in the boundary layer tends to develop from the root toward the tip as depicted in Figure 6.39. This spanwise flow contributes to the strength of wing tip vortices, thereby increasing induced drag at high angles of attack. The swept back wing also tends to separate and stall first at the wing tip. This is, of course, undesirable from a control point of view as ailerons are normally located toward the wing tip. These stall characteristics are also depicted in Figure 6.39. The tendency can be decreased by twisting and/or tapering the wing, but again a penalty arises due to the structural complications caused by bending toward the wing tips; this twists the wing and imposes torsional loading. A further disadvantage of wing sweep is illustrated in Figure 6.40. Note that for the same angle of attack, a straight wing is capable of producing a much higher lift coefficient than a swept wing.

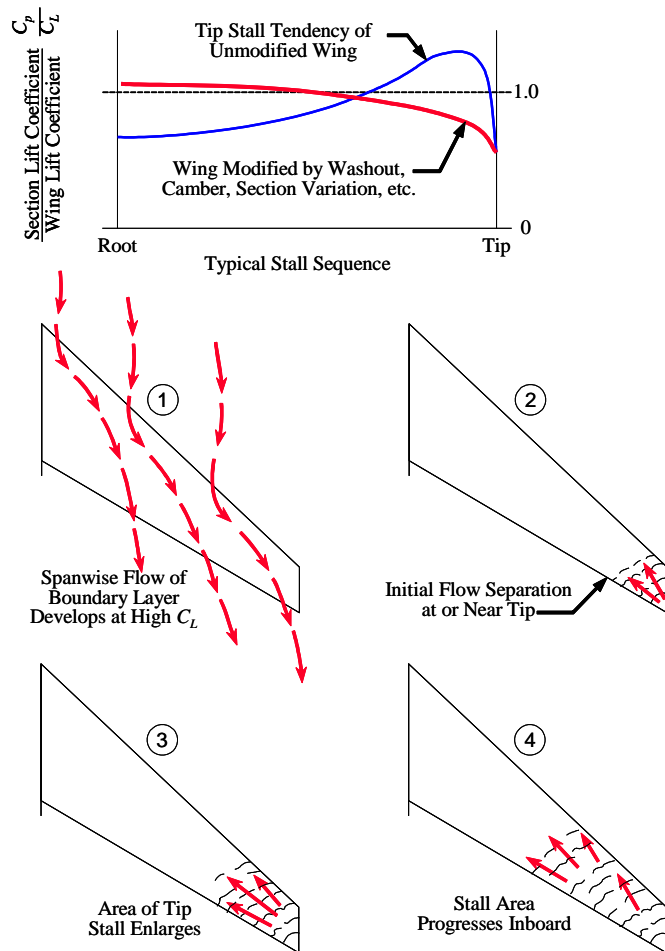


Figure 6.39 Stall Characteristics of Tapered Swept Wing

Aerodynamically, the effect of wing sweep with regard to delaying critical Mach applies to forward sweep as well as sweep back. The spanwise flow on a forward swept wing, however, is from the tip toward the root and tends to be beneficial. The major reason forward swept wings have not been widely used in the past is because of aeroelastic divergence problems. The present day improvement in composite materials has provided us with a material that has the stiffness needed to combat such problems.

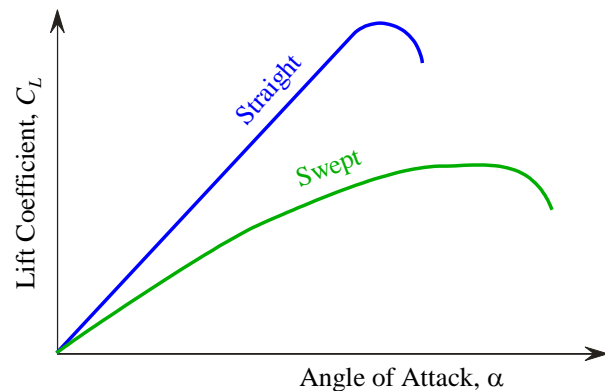


Figure 6.40 Effect of Sweepback on Low Speed Lift Curve

Despite many disadvantages, rearward wing sweep has been for many years the primary method used to delay transonic drag rise. Reference to Figure 6.38b, however, shows that at higher supersonic Mach, a straight wing becomes superior from a drag standpoint.

6.23.4 Fuselage Shape and Area Rule

The onset of shock formation is also accompanied by a very severe drag rise. For an aircraft the best fuselage shape and the best wing fuselage combination that will delay the drag rise and/or tend to limit the severity of its effect is of major interest.

As a matter of both calculation and testing, it is found that a body of revolution with high fineness ratio (ratio of length to diameter) gives the least drag. The nose section should not be a cone. The best shape for the nose resembles that shown in Figure 6.41.

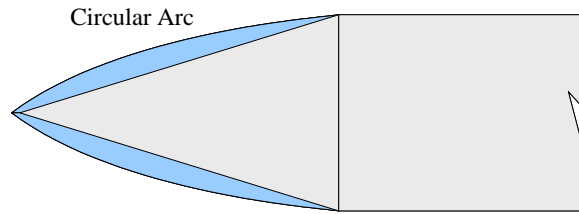


Figure 6.41 Optimum Nose Shape

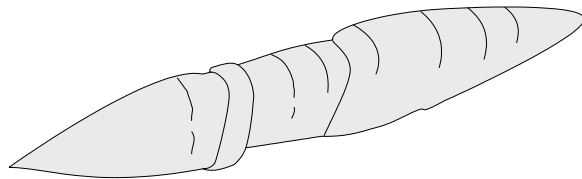


Figure 6.42 Equivalent Body of Revolution

Unfortunately, a true body of revolution is not found in actual vehicles. As an example, the canopy will form a bulge in the fuselage. The wings, when attached, will further modify the shape. However, without the necessity of preserving the exact form of the aircraft, the equivalent effect of wings and canopy can be preserved by making an equivalent body of revolution with the proper bulges located in the appropriate regions. This is shown in Figure 6.42.

The abrupt offsets in the surface will cause an increase in drag above that for the ideal body of revolution. To minimize drag it will be necessary to remove material from the region of the bulges. Because the wings must be present, the contour of the fuselage is changed in this region to compensate for them. The same thing can be done in the region of the canopy. In some instances, it may be necessary to introduce bulges in the fuselage behind or ahead of the wing to introduce the equivalent effect of the smooth aerodynamic contour.

A striking example of this effect is the extending of the "cab" of the Boeing 747. Wind tunnel data show that the Mach at which drag rise shows a significant increase is delayed by smoothing the area distribution by fairing the fuselage-cab juncture. The drag effect of the fairing is insignificant until M_{cr} is reached for the unfaired juncture; then the fairing delays the Mach at which waves are generated. As shown in Figure 6.43, the fairing causes an increase in M_{cr} for $0.3 < C_L < 0.5$.

The application of the transonic area rule will delay the drag rise, but in any event shock formation cannot be avoided if the flight Mach is sufficiently increased. The contour of the fuselage that will be effective at Mach 1 is not as effective at Mach 1.2. In fact, the conditions which provided an advantage in the transonic region may become a disadvantage at higher Mach. It is generally considered that area rule application is pointless above Mach 1.5. Further illustrations of the effects of area ruling are shown in Figure 6.44.

Transonic flow also produces important changes in the aerodynamic pitching moment characteristics of wing sections. The aerodynamic center of airfoils in subsonic flow is located at about the 25% chord point. As the airfoil is subjected to supersonic flow, the aerodynamic center changes to about the 50% chord point. Thus, the aircraft in transonic flight can experience large changes in longitudinal stability because of the large changes in the position of the aerodynamic center. If an aircraft stabilizes in the transonic region, the aerodynamic center may oscillate between the 25% chord point and the 50% chord point, often at very high frequency; this further aggravates longitudinal stability problems.

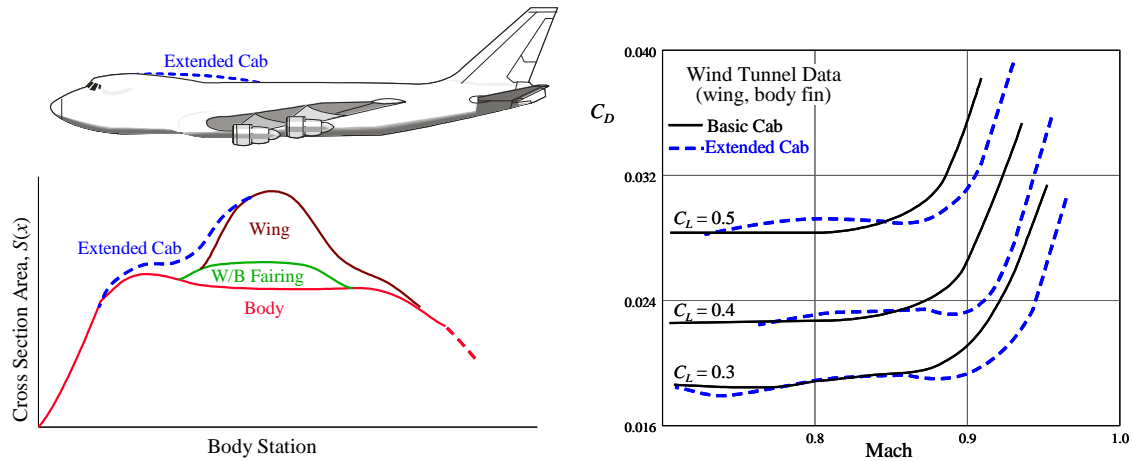


Figure 6.43 Benefits of Area Rule Application



Figure 6.44. "Coke Bottle" Fuselage

6.23.5 Transonic and Supersonic Control Surfaces

The design of control surfaces for transonic and supersonic flight involves many important considerations. This fact is illustrated by the typical transonic and supersonic flow patterns of Figure 6.45. Trailing edge control surfaces can be affected adversely by the shock waves formed in flight above the critical Mach. If the airflow is separated by the shock wave, the resulting buffet of the control surface can be very objectionable. In addition to the buffet of the surface, the change in the pressure distribution due to separation and the shock wave location can create very large changes in control surface hinge moments. Such large changes in hinge moments create very undesirable control forces and present the need for an "irreversible" control system. An irreversible control system would employ powerful hydraulic or electric actuators to move the surfaces upon control by the pilot, and the airloads developed on the surface could not feed back to the pilot. Of course, suitable control forces would be synthesized by bungees, "q" springs, bobweights, etc.

Transonic and supersonic flight can cause a noticeable reduction in the effectiveness of trailing edge control surfaces. The deflection of a trailing edge control surface at low subsonic speeds alters the pressure distribution on the fixed portion as well as the movable portion of the surface. This is true to the extent that a 1° deflection of a 40% chord elevator produces a lift change very nearly the equivalent of a 1-degree change in stabilizer setting. However, if supersonic flow exists on the surface, a deflection of the trailing edge control surface cannot influence the pressure distribution in the supersonic area ahead of the movable control surface. This is especially true in high supersonic flight where supersonic flow exists over the entire chord and the change in pressure distribution is limited to the area of the control surface.

The reduction in effectiveness of the trailing edge control surface at transonic and supersonic speeds necessitates the use of an all movable surface. Application of the all movable control surface to the horizontal tail is most usual since the increase in longitudinal stability in supersonic flight requires a high degree of control effectiveness to achieve required controllability for supersonic maneuvering.

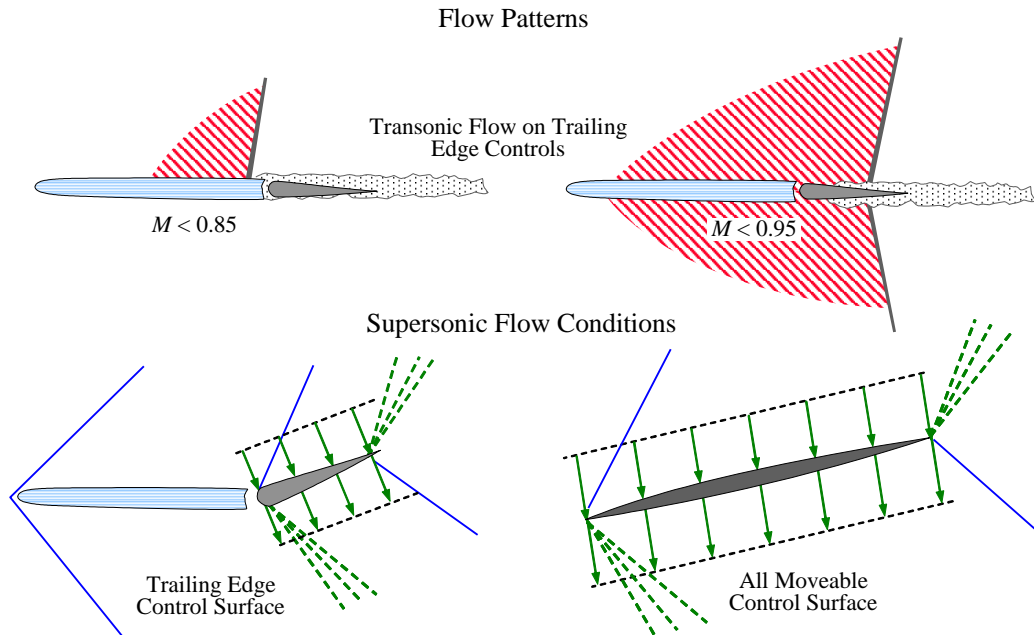


Figure 6.45. Planform Effects and Control Surfaces

6.24 Summary

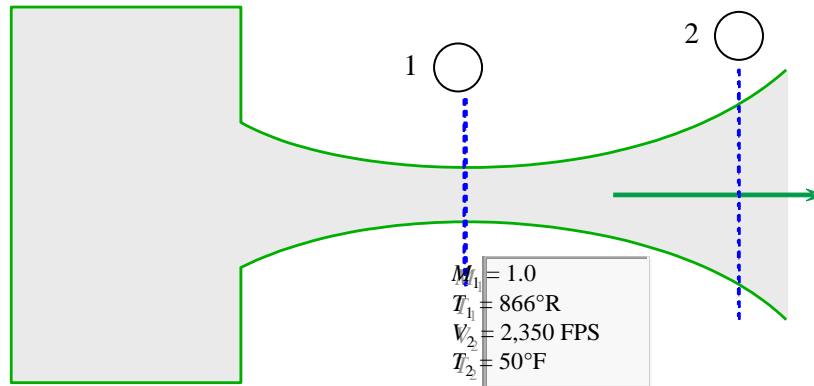
In this chapter we have studied the theory of supersonic and transonic flow. Emphasis was placed on the practical application of the theory to realistic two and three dimensional flow problems about aerodynamic shapes. Understanding and application of supersonic theory will be necessary in Chapter 7 on Propulsion.

Present day supersonic aircraft and space shuttle operations necessitate a thorough understanding of this material by the flight test pilot and flight test engineer.

6.25 Problems

6.1 Calculate the velocity of sound in air at a temperature of 70°F. Express it in (a) knots, and (b) ft/sec.

- Find: (c) At station 1 below, V , in ft/sec.
 (d) At station 2 below, M_2 .

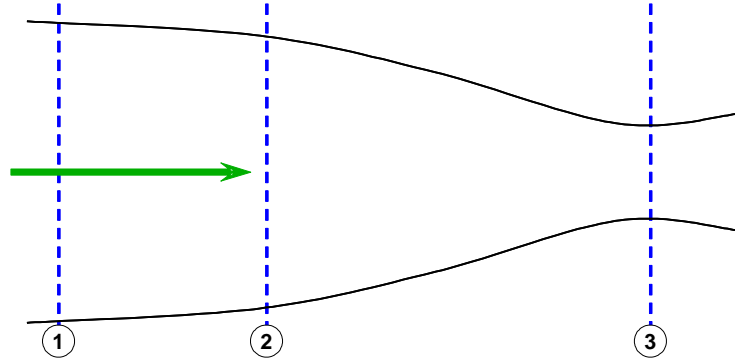


6.2 Sketch the Mach cone for $M = 2$. Show that

$$\mu = \sin^{-1} \frac{1}{M}$$

- 6.3 $P_\infty = 2116 \text{ lb/ft}^2$
 $M_\infty = 4$
 $T_\infty = 165^\circ\text{R}$
 $P_T = ?$
 $T_T = ?$

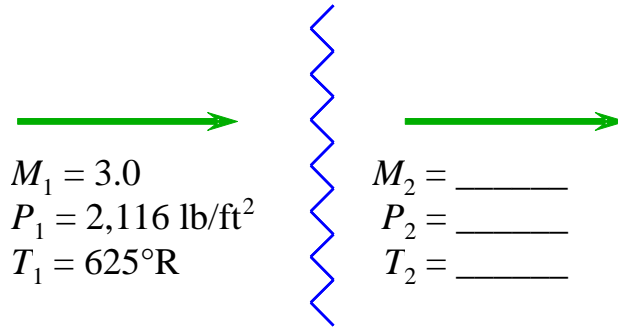
- 6.4 At point 1 in a nozzle, air flows with a velocity of 500 ft/sec, pressure of 2116 lb/ft², temperature of 40°F, and density of 0.0024 slugs/ft³. Assuming isentropic flow,
- Calculate the quantities listed at point 2 where the area is reduced by 15%.
 - Calculate the quantities listed at point 3 where $M = 1$.



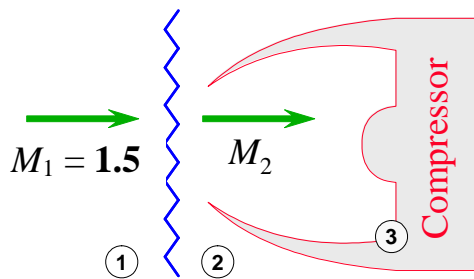
$V_1 = 500$ ft/sec	$V_2 =$	$V_3 =$
$P_1 = 2116$ lb/ft ²	$P_2 =$	$P_3 =$
$\rho_1 = .0024$ slugs/ft ³	$\rho_2 =$	$\rho_3 =$
$T_1 = 40^\circ$ F	$T_2 =$	$T_3 =$
$A_1 = A_1$	$A_2 = 0.85A_1$	$A_3 =$
$M_1 =$	$M_2 =$	$M_3 = 1$
$P_{T_1} =$	$P_{T_2} =$	$P_{T_3} =$
$T_{T_1} =$	$T_{T_2} =$	$T_{T_3} =$
$\rho_{T_1} =$	$\rho_{T_2} =$	$\rho_{T_3} =$

- 6.5 A surface temperature of 1000°R is recorded for a missile that is flying at an altitude of 50,000 ft in a standard atmosphere. Assume that the conditions on the surface are the same as those at a stagnation point after an isentropic compression. What is the velocity of the missile? What is the pressure at the stagnation point on the missile?
- 6.6 An intermittent wind tunnel is designed for mach 4 in the test section. The tunnel operates by sucking air from the atmosphere through a duct and into a vacuum tank. The tunnel is at an elevation of 5,000 ft (standard atmosphere). What will be the static temperature, static density, and velocity in the test section assuming an isentropic process?
- 6.7 Find M_2, P_2, T_2

Normal Shock Wave



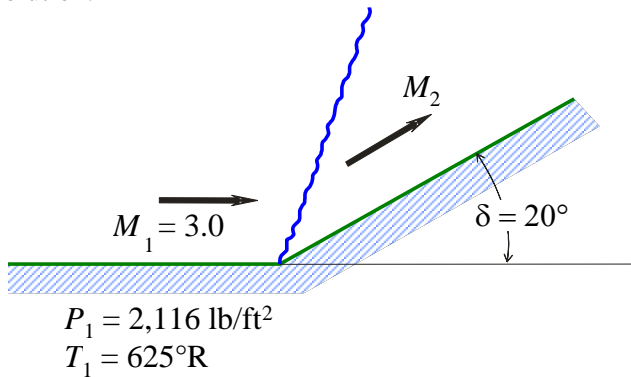
6.8 An intake is a diffuser to slow the flow and recover as much free stream pressure as possible, i.e., to recover all of the total pressure possible while slowing the flow to $M = 0$. The sketch below shows a typical low supersonic inlet (F=100 type).



Find: P_{T_3} / P_{T_1} assuming an isentropic process behind shock from 2 to 3.

$$\frac{P_{T_3}}{P_{T_1}} = \underline{\hspace{2cm}}$$

6.9 Find M_2 , P_2 , T_2 , and maximum δ possible without detaching shock. Assume a weak shock solution.

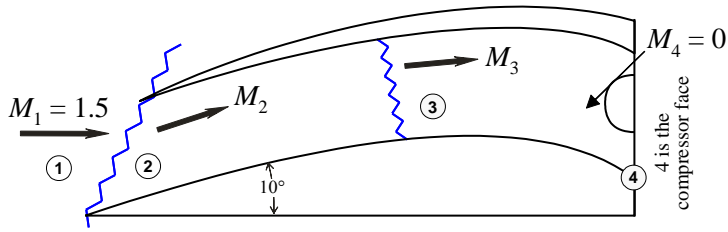


$$M_2 = \underline{\hspace{2cm}}$$

$$P_2 = \underline{\hspace{2cm}}$$

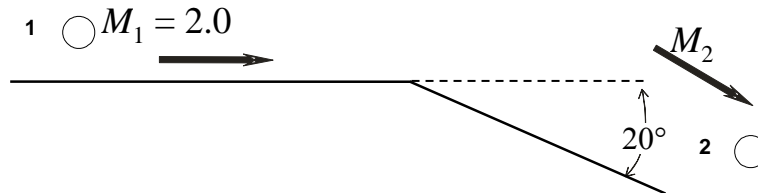
$$T_2 = \underline{\hspace{2cm}}$$

- 6.10 Inlets designed to operate in the high supersonic flight regime (F-104 type inlet) usually utilize multiple shock waves, unlike the F-100 type inlet. Using the tabular information in NACA 1135, you can estimate the improvement in pressure recovery to be expected.



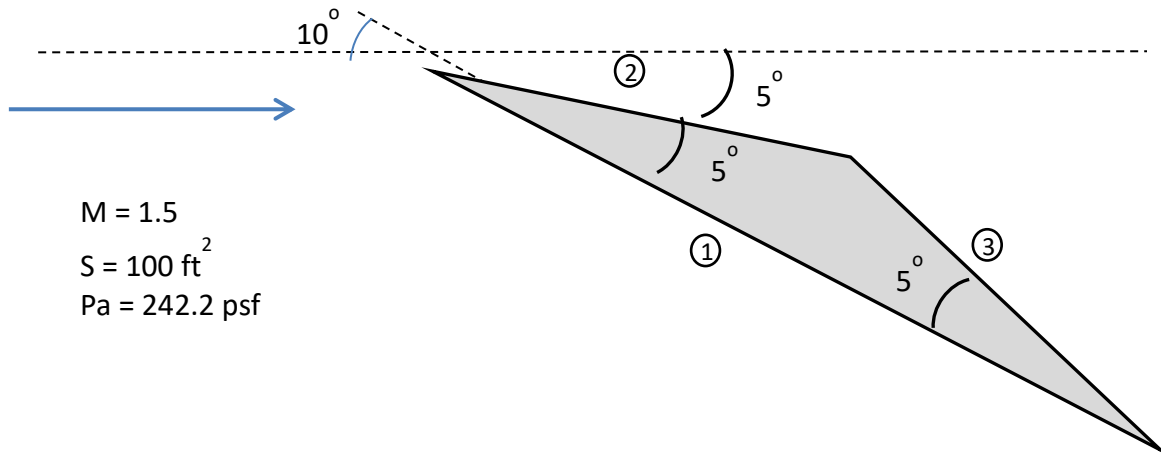
For a weak shock solution from 1 to 2 find P_{T_4} / P_{T_1} assuming and the second shock is a normal shock. Compare this pressure recovery to that of the F-100 type inlet in Problem 6.8.

- 6.11



- Assuming a flow Mach of 2, what will the Mach be after an expansive deflection of 20° as shown above?
- Find T_2/T_1 and P_2/P_1
- What is the entropy change?
- Draw μ_1 and μ_2 and find angle of the expansion fan.

6.12 6.12 Given the following:



- Find the Mach number in each region: 1, 2 and 3
- Find the static pressure on each of the three surfaces: 1, 2 and 3
- Calculate the force on each surface (approximate areas 2 and 3 as simply 50 ft^2)
- Resolve the forces into lift and drag
- Use Ackeret's approximation for a double wedge airfoil using a t/c of 0.044 to calculate lift and drag (hint $q = 1481 \delta M^2 \text{ lb/ft}^2$).

6.26 Answers

- 6.1 (a) 668 kts
(b) 1128 ft/sec
(c) 1442 ft/sec
(d) 2.12
- 6.3 321,283 lb/ft² 693°R
- 6.4 628 ft/sec 1021 ft/sec
 1948 lb/ft² 1291 lb/ft²
 0.00226 slug/ft³ 0.00169 slug/ft³
 488°R 434°R
 0.70A₁
 0.46 0.58
 2446 lb/ft² 2446 lb/ft²
 521°R 521°R
 0.00266 slug/ft³ 0.00266 slug/ft³
- 6.5 2709 ft/sec 6582 lb/ft²
- 6.6 119°R 5.68 x 10⁻⁵ slug/ft³ 2141 ft/sec
- 6.7 0.4752 21858 lb/ft² 1675°R
- 6.8 0.9298
- 6.9 2 8104 lb/ft² 981°R; 34°
- 6.10 98.6% recovery (93% Problem 6.8)
- 6.11 (a) 2.83
(b) 0.692, 0.275
(c) no change in entropy
(d) 29.31°
- 6.12 (a) M₁ = 1.11, P₁ = 403.5 psf
 M₂ = 1.67, P₂ = 188.7 psf
 M₃ = 2.02, P₃ = 110.3 psf
(b) lift: 25,019 lb, drag: 4,758 lb
(c) lift: 23,812 lb, drag: 4,417 lb

6.27 Bibliography

- 6.1 Aerodynamic for Pilots, ATC Pamphlet 51-3, July 1979.
- 6.2 Hurt, H.H., Jr., Aerodynamics for Naval Aviators, NAVWEPS 00-80T-80, Office of the Chief of Naval Operations Aviation Training Division, U.S. Navy, 1960.
- 6.3 Zucker, R.D., Fundamentals of Gas Dynamics. Champaign, IL: Matrix Publishers, Inc., 1977.
- 6.4 NACA Report 1135, Equations, Tables, and Charts for Compressible Flow, Ames Research Staff, Ames Aeronautical Laboratory, Moffett Field, CA.
- 6.5 Carroll, R.L., The Aerodynamics of Powered Flight. New York: John Wiley & Sons, 1960.
- 6.6 Anderson, J.D., Jr., Introduction to Flight. New York: McGraw-Hill Inc., 1978
- 6.7 John, J.E.A., Gas Dynamics. Boston, Mass: Allyn and Bacon, 1969.

Volume 2 – Aerodynamics for Flight Testers

Chapter 7

Pitot-Statics

Table of Contents

- 7.1.1 Introduction 3
 - 7.1.1.1 Impact of Hydrostatic Equilibrium..... 3
- 7.1.2 Incompressible Airspeed Theory 4
 - 7.1.2.1 Dynamic Pressure..... 5
- 7.1.3 Compressible Airspeed Theory 6
 - 7.1.3.1 Equivalent Airspeed 7
 - 7.1.3.2 Calibrated Airspeed..... 7
 - 7.1.3.3 Instrument Error Correction 7
 - 7.1.3.4 Scale Altitude Correction 8
 - 7.1.3.5 Correction Summary 9
 - 7.1.3.6 Compressible Dynamic Pressure..... 10
- 7.1.4 Supersonic Flow 10
- 7.1.5 Measurement of Altitude 11
- 7.1.6 Temperature Measurement 13
- 7.1.7 Mach Number Measurement 15
- 7.1.8 Pitot Static Position Errors 16
 - 7.1.8.1 Total Head Error..... 16
 - 7.1.8.2 Static Source Error 17
- 7.1.9 Test Methods 18
 - 7.1.9.1 Tower Fly-by..... 18
 - 7.1.9.2 Calibrated Aircraft..... 20
 - 7.1.9.3 Ground Course 21
 - 7.1.9.4 Static Bomb 22
 - 7.1.9.5 Trailing Static Cone 23
 - 7.1.9.6 GPS Method 23
 - 7.1.9.7 Summary of Methods 26
- 7.1.10 Position Error Correction Data Analysis 26
 - 7.1.10.1 Effect of Altitude and Weight on Position Errors 26
 - 7.1.10.2 Mach Number Effects on Airspeed Calibration 27
 - 7.1.10.3 Humidity Corrections 28
- 7.1.11 System Lag Errors 28
 - 7.1.11.1 Dynamic Balance 28
 - 7.1.11.2 Sideslip Effects..... 29
- 7.1.12 Rotary-wing Aircraft 29
 - 7.1.12.1 Ground Effect on Static Sources 29
 - 7.1.12.2 Low Airspeed Measurement Systems 29
 - 7.1.12.3 Types of Low Airspeed Measurement Systems 29
- 7.1.13 Pitot Static Requirements 30
 - 7.1.13.1 14 CFR Part 23 Aircraft (Normal Category)..... 30
 - 7.1.13.2 14 CFR Part 25 Aircraft (Transport Category) 30
 - 7.1.13.3 14 CFR Part 27 Rotorcraft (Normal Category) 31

7.1.13.4 14 CFR Part 29 Rotorcraft (Transport Category).....	31
7.1.13.5 Military Requirements.....	31
7.1.14 Summary.....	32
7.1.14.1 References	33

7.1.1 Introduction

Airspeed and altitude are determined in an aircraft by measuring total pressure (pitot) and static pressure. But the airflow around the structure of the aircraft causes changes in pressures and thus can create errors in sensed pressures, resulting in errors in speed and altitude. The most common error source is the static port. Finding a good location for the static port is important to minimizing the errors. Thus the errors are commonly called *position* error corrections (PEC) because of a non-ideal position of the static port.

An accurate knowledge of the aircraft's airspeed and altitude is important for many reasons. Operational safety could be affected. Both civil certification and military specifications put requirements by setting upper limits on the magnitude of the airspeed and altitude errors within the range of speeds used for normal operations. The basic requirements are for speeds to be within $\pm 3\%$ or 5 kts of the real value and for altitude to be within ± 30 ft of the actual pressure altitude per 100 kts. Specific details of various requirements are shown towards the end of this chapter.

7.1.1.1 Impact of Hydrostatic Equilibrium

Civil and military requirements are all stated in terms of values at sea level. Both the airspeed and altimeter are connected to the same static source on the aircraft. This static source does not sense true ambient static pressure because it is influenced by the pressure field surrounding the aircraft. Therefore, the pressure differential between the true ambient static pressure and the static pressure source on the aircraft will cause errors in both the airspeed and the altimeter indications.

Since the design and especially the calibration of both the airspeed and altimeter instruments are based on the "Standard Atmosphere," one more factor needs to be considered. One of the four assumptions on which the Standard Atmosphere is based will have a major impact on the altimeter, i.e. that hydrostatic equilibrium exists. Consider the forces acting on a stagnant element of air. Figure **Error! No text of specified style in document.-1** shows an element in equilibrium with the vertical direction given as H .

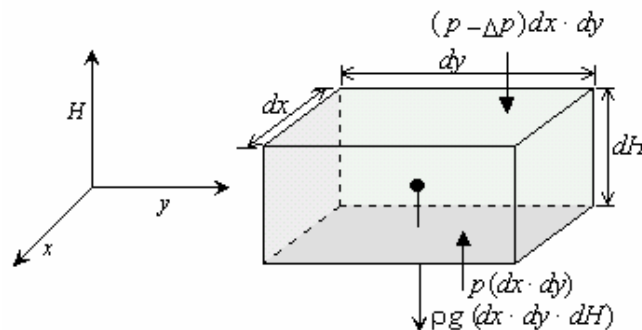


Figure **Error! No text of specified style in document.-1**Hydrostatic Equilibrium

The two types of forces acting on an element of air are the pressure forces from the surrounding air exerted on the surface of the element, and the gravity force due to the weight of the air inside the element. Consider the force in the H direction. The pressure on the bottom surface of the element is p , and therefore the force on the bottom face is $p(dx \cdot dy)$ in the upward direction as shown in Figure **Error! No text of specified style in document.-1**. The pressure on the top face of the element will be less by an increment Δp since the pressure in the atmosphere decreases with altitude. Therefore the pressure force on the top face of the element is in the downward direction. The net pressure force $p(dx \cdot dy) - (p - \Delta p)dx \cdot dy$ in the upward direction is $= \Delta p(dx \cdot dy)$

The gravitational force on the mass of air in the element is the volume of air times the density of the air times the acceleration due to gravity (g) i.e. the force in the downward direction $= \rho g(dx \cdot dy \cdot dH)$. Since equilibrium exists then the forces must be equal and opposite, therefore

$$\Delta p(dx \cdot dy) = -\rho g(dx \cdot dy \cdot dH)$$

$$\Delta p = -\rho g \cdot \Delta H \tag{7.1}$$

Equation 7.1 is called the hydrostatic equation which relates the change in pressure, dp , in air with a change in vertical height, dH . Equation 7.1 governs the variation of atmosphere properties as a function of altitude in the air above us. This same equation will relate altimeter errors (ΔH) to pressure errors (Δp) given an ambient density, ρ . Compared to sea level values, a given pressure error, ΔP , will produce a larger ΔH at higher altitudes (lower density ρ). Thus altimeter position error corrections are calculated for comparison to certification limits *at sea level conditions* (ρ_0).

7.1.2 Incompressible Airspeed Theory

Many methods have been used to determine airspeed. They range from listening to the sound of the wind through the flying wires to pitot-static systems to exotic radar doppler systems. The pitot-static system has proven to be reliable, simple and accurate for the measurement of airspeed, altitude, vertical velocity and Mach number. Pitot-static systems have changed very little throughout the years except that current high performance aircraft tend to use pressure transducers at the probe. These have electrical signaling to cockpit instruments rather than long pneumatic tubing. This eliminates lag in the systems.

Airspeed system theory was first developed with the assumption of *incompressible* flow. This assumption is only useful for speed of 250 kts or less at relatively low altitudes. However, since various concepts and nomenclature of incompressible flow are still in use, it is examined here as a step toward the understanding of compressible flow relations.

Airspeed system theory for all types of flow stems from Euler's equation. It essentially says that, along a streamline, the total energy of the flow is constant. This is reasonable since matter is neither created nor destroyed, and we are assuming frictionless flow. The energy of air is comprised of pressure energy and momentum. Potential energy is not a factor because it is insignificant for air moving along a streamline. The mathematical interpretation of Euler's thinking is that the total energy change is zero:

$$dP + \rho V dV = 0 \tag{7.2}$$

For the incompressible case considered now, density remains constant. Integrating yields:

$$P + \frac{\rho V^2}{2} = Const. \tag{7.3}$$

This equation is called Bernoulli's equation, although it was first presented in this form by Euler. This relation is valid all along the streamline as long as energy is not added to or subtracted from the system. Airspeed indicators are built around this principle that the total energy is constant. Consider a schematic drawing of an airspeed indicator, Figure **Error! No text of specified style in document.-2**.

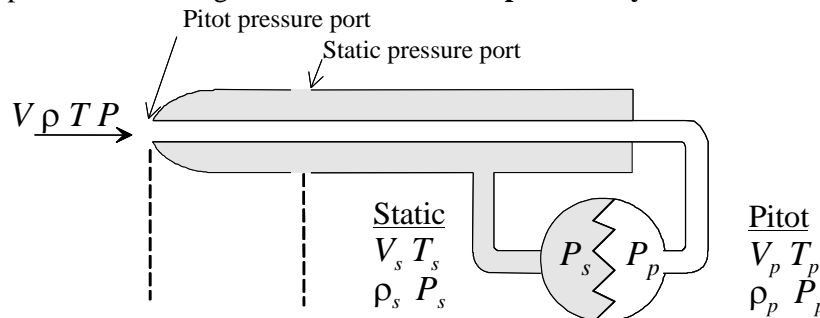


Figure **Error! No text of specified style in document.-2** Pitot-Static Airspeed System

Applying the Bernoulli equation to both the pitot and the static gives

$$P_p + \frac{\rho_p V_p^2}{2} = P_s + \frac{\rho_s V_s^2}{2}$$

But $V_p = 0$ because the airflow stagnates in the pitot tube

$$\text{Therefore } P_p = P_s + \rho_s \frac{V_s^2}{2}$$

Solving for the airspeed, which is a true airspeed (V_T),

$$V_T = \sqrt{\frac{2}{\rho_s}(P_p - P_s)} \quad (7.4)$$

It is possible to use a pitot-static system and build a true airspeed indicator that conforms to this equation. However, there are disadvantages in doing so.

Equation 7.4 shows that differential pressure ($P_p - P_s$) and density are required to determine the true velocity. Differential pressure is easily determined using the bellows in Figure **Error! No text of specified style in document.-2**. Determination of local ambient density (ρ) is very difficult and therefore standard sea level density (ρ_o) is substituted in Equation 7.4. The substitution of sea level density changes the velocity from a true velocity to an equivalent velocity (V_e) i.e.

$$V_e = \sqrt{\frac{2}{\rho_o}(P_p - P_s)} \quad (7.5)$$

A true airspeed indicator on an aircraft is useful for navigational purposes but is hazardous for safety of flight reasons. For example, if a true airspeed indicator is used in an aircraft then the stall speed, structural limitation speeds etc. would be a function of altitude. Pilots prefer, and certification and acceptance standards insist that the pilot have a calibrated airspeed (V_c) system which corresponds to an equivalent airspeed (V_e) at low subsonic speeds. The stall speeds and structural limitation speeds would then be constant for all altitudes and can be marked on an airspeed indicator which improves flight safety.

7.1.2.1 Dynamic Pressure

The differential pressure term in Equation 7.4 and 7.5 ($P_p - P_s$) can be rewritten as

$$(P_p - P_s) = \frac{1}{2} \rho_s V_T^2 = \frac{1}{2} \rho_o V_e^2 \quad (7.6)$$

Note that the differential pressure of $\frac{1}{2} \rho_o V_e^2$ is similar to the equation for kinetic energy $\frac{1}{2} mV^2$ and is essentially a measure of the directed energy of the airflow. This differential pressure for the subsonic case is called dynamic pressure (q) such that

$$q = \frac{1}{2} \rho_s V_T^2 = \frac{1}{2} \rho_o V_e^2 \quad (7.6.1)$$

The above equation can therefore be used to determine the true airspeed if the equivalent airspeed V_e is known.

$$\text{i.e. } V_T = \left(\frac{\rho_o}{\rho_s} \right)^{\frac{1}{2}} V_e \text{ or } V_T = \frac{V_e}{\sqrt{\sigma}} \quad (7.6.2)$$

where σ is the density ratio $\left(\frac{\rho_s}{\rho_o} \right)$ i.e. the ratio of the local ambient static density to the standard atmosphere density at sea level ρ_o .

The dynamic pressure is used extensively in dimensional analysis and aerodynamics to define non-dimensional lift and drag coefficients and stability and control derivatives, e.g.

$$C_L = \frac{L}{qS}, \quad C_D = \frac{D}{qS}, \quad C_M = \frac{M}{qS\bar{c}}$$

Where C_M is the pitching moment coefficient, S is the wing area and \bar{c} is the mean aerodynamic chord.

The concept of using incompressible flow theory to determine V_T and V_e was primarily used before World War II. However, as aircraft speed and altitude capabilities increased, pilots found themselves constantly flying into a headwind. This "headwind" appeared to occur regardless of the direction of flight. It turns out that the theory was too simplified. The error resulted from the assumption that density remains

constant along a streamline. Airspeed indicators for today's aircraft are built to compensate for the air's compressibility.

7.1.3 Compressible Airspeed Theory

Euler's Equation (7.2) is used again to develop the equations for *compressible* flow. Before integrating, several thermodynamic relationships are used to replace the density term:

Poisson's Equation: $Pv^\gamma = \text{Const}$

where $v = \text{specific mass} \frac{1}{\rho g}$ and $\gamma = \text{the ratio of specific heats} (C_p / C_v) = 1.4$ for air.

Rearrange Poisson's equation to get: $P \left(\frac{1}{\rho g} \right)^\gamma = \frac{P}{(\rho g)^\gamma} = C$

$$\text{Or } \frac{P}{\rho^\gamma} = C_1$$

$$\rho = \left(\frac{P}{C_1} \right)^{\frac{1}{\gamma}} = \left(\frac{P}{C_2} \right)^{\frac{1}{\gamma}}$$

Substituting this term into Equation (7.2) and integrating gives Bernoulli's equation for compressible flow:

$$\frac{V^2}{2} + \frac{\gamma}{\gamma-1} \frac{P}{\rho} = \text{Constant} \quad (7.7)$$

Applying this to the pitot-static system in Figure **Error! No text of specified style in document.-2** (where stagnation velocity = 0) gives:

$$\frac{\gamma}{\gamma-1} \frac{P_p}{\rho_p} = \frac{V_s^2}{2} + \frac{\gamma}{\gamma-1} \frac{P_s}{\rho_s} \quad (7.8)$$

$$\text{Since } \frac{P}{\rho^\gamma} \text{ is a constant, then } \frac{P_p}{\rho_p^\gamma} = \frac{P_s}{\rho_s^\gamma} \text{ or } \rho_p = \rho_s \left(\frac{P_p}{P_s} \right)^{\frac{1}{\gamma}}$$

Substituting this into Equation 7.8 yields:

$$\frac{V_s^2}{2} + \frac{\gamma}{\gamma-1} \frac{P_s}{\rho_s} = \left(\frac{\gamma}{\gamma-1} \right) \frac{P_p}{\rho_s \left[\frac{P_p}{P_s} \right]^{\frac{1}{\gamma}}}$$

Solving for V_s , which is a true velocity (the subscript "s" refers to *static* port and the subscript "p" refers to the *pitot* tube port):

$$V_s = \left[2 \left(\frac{\gamma}{\gamma-1} \frac{P_p}{\rho_s \left(\frac{P_p}{P_s} \right)^{\frac{1}{\gamma}}} - \frac{\gamma}{\gamma-1} \frac{P_s}{\rho_s} \right) \right]^{\frac{1}{2}} = \left[\frac{2\gamma}{\gamma-1} \frac{P_s}{\rho_s} \left(\frac{P_p}{P_s \left(\frac{P_p}{P_s} \right)^{\frac{1}{\gamma}}} - 1 \right) \right]^{\frac{1}{2}} = \left[\frac{2\gamma}{\gamma-1} \frac{P_s}{\rho_s} \left(\left[\frac{P_p}{P_s} \right]^{\frac{\gamma-1}{\gamma}} - 1 \right) \right]^{\frac{1}{2}}$$

To put this equation into a form that can be mechanized through simple bellows, add and subtract P_s to the innermost term.

$$V = \left[\frac{2\gamma}{\gamma-1} \frac{P_s}{\rho_s} \left(\left[\frac{P_p - P_s}{P_s} + \frac{P_s}{P_s} \right]^{\frac{\gamma-1}{\gamma}} - 1 \right) \right]^{\frac{1}{2}} = \left[\frac{2\gamma}{\gamma-1} \frac{P_s}{\rho_s} \left(\left[\frac{P_p - P_s}{P_s} + 1 \right]^{\frac{\gamma-1}{\gamma}} - 1 \right) \right]^{\frac{1}{2}} \quad (7.9)$$

This relation for true airspeed can be simplified by substituting 1.4 for γ

$$V_T = \sqrt{7 \frac{P_s}{\rho_s} \left(\left[\frac{P_T - P_s}{P_s} + 1 \right]^{\frac{2}{7}} - 1 \right)} \quad (7.10)$$

Equation 7.9 (or 7.10) is the compressible true airspeed equation and applies at all subsonic airspeeds.

7.1.3.1 Equivalent Airspeed

Just as ρ_o was substituted for ρ_s for the incompressible analysis, it can be done with Equation (7.10). By convention, in the standard atmosphere, the subscript "a" is used instead of the subscript "s". The "a" refers to any *altitude* value of density (ρ) other than the constant sea level density (ρ_o).

$$V_e = \sqrt{7 \frac{P_s}{\rho_o} \left(\left[\frac{P_T - P_s}{P_s} + 1 \right]^{\frac{2}{7}} - 1 \right)} = V_T \sqrt{\frac{\rho_a}{\rho_o}} = V_T \sqrt{\sigma} \quad (7.11)$$

7.1.3.2 Calibrated Airspeed

Equation (7.11) is not practical for mechanization as it contains additional ambient pressure terms. By substituting sea level pressure (P_o) for these terms, the resulting velocity is a function of the differential pressure only. This velocity is known as "calibrated" airspeed since it is calibrated to indicate equivalent velocity at sea level pressure (P_o).

$$V_c = \left[\frac{2\gamma}{\gamma - 1} \frac{P_o}{\rho_o} \left(\left[\frac{P_p - P_s}{P_o} + 1 \right]^{\frac{\gamma - 1}{\gamma}} \right) \right]^{\frac{1}{2}} = \sqrt{7 \frac{P_o}{\rho_o} \left(\left[\frac{P_p - P_s}{P_o} + 1 \right]^{\frac{2}{7}} - 1 \right)} \quad (7.12)$$

The only unknown in equation (7.12) is differential pressure ($P_p - P_s$), therefore, a known pressure differential corresponds to a unique value of calibrated velocity. In practice, all other velocities must be calculated using V_c . Two corrections must be made, however, to determine V_c .

7.1.3.3 Instrument Error Correction

The values for the constants in Equation 7.12 can be inserted to arrive at an equation used in the laboratory to calibrate airspeed indicators at subsonic speeds.

$$V_c = 1478 \sqrt{\left[\frac{P_p - P_s}{2116} + 1 \right]^{\frac{2}{7}} - 1} \quad (7.13)$$

where pressures are in units of lb/ft² and V_c is in terms of knots.

One of the differences between the airspeed seen on the indicator (V_i) and the V_c given by Equation (7.13) is termed the "instrument error" or "instrument error correction". This is a function of the wear of the mechanical linkages in the instrument. To determine this error, the instrument is checked in a laboratory. A known pressure differential is applied to the airspeed indicator. This corresponds to a unique value of velocity (V_c). The difference between what the instrument indicates and what it should be reading is the instrument error correction, ΔV_{ic} . The actual "instrument error correction" (ΔV_{ic}) is the opposite sign of the error. Figure **Error! No text of specified style in document.-3** shows an example of such a curve. Note that the instrument error correction is added to the indicated airspeed i.e.

$$V_{ic} = V_i + \Delta V_{ic} \quad (7.13.1)$$

where V_{ic} is called the instrument-corrected airspeed.

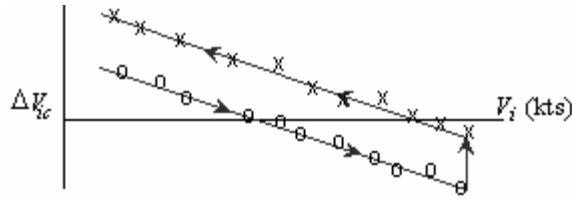


Figure Error! No text of specified style in document.-3 Airspeed Instrument Correction Curve

The difference in ΔV_{ic} at the same V_i with the airspeed increasing and decreasing is due to friction in the mechanical linkages and is called hysteresis. Hysteresis is unacceptable for flight test work. Airspeed indicators which have been stored or not used regularly should be exercised prior to calibration. Exercising means moving the airspeed indicator bellows a number of times within the intended calibration range.

7.1.3.4 Scale Altitude Correction

If V_e is desired, the *scale altitude correction* is applied. This correction gets its name because it reverses the P_o substitution made between Equations (7.11) and 7.12). Figure Error! No text of specified style in document.-4 graphically depicts this correction.

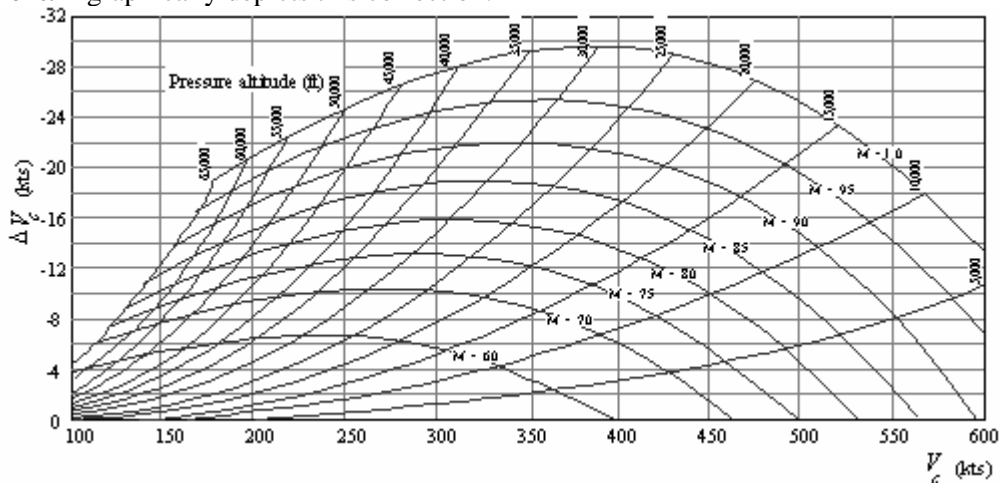


Figure Error! No text of specified style in document.-4 Scale Altitude Correction

This "scale altitude correction" is often incorrectly referred to as the "compressibility correction" and is therefore a continuing source of confusion. In fact, Equations 7.9 through 7.11 already address compressibility effects. When sea level altitude is substituted to obtain an expression for V_c (Equations 7.12, 7.13) the inherent compressibility correction only applies at sea level. If the aircraft is above sea level, then the scale altitude correction will modify the compressibility correction for that altitude.

Rather than determining ΔV_c graphically to calculate V_e , it can be solved for directly using Equation 7.11 where

$$P_T - P_s = P_o \left[\left(\frac{P_o}{P_o} \frac{V_c^2}{7} + 1 \right)^{3.5} - 1 \right]$$

Static ambient pressure, P_s , can be calculated as shown in Equations (7.16) or (7.17).

If the airspeed remains low, i.e. less than 200 kts, and the altitude less than 10,000 feet, then the correction is insignificant and the calibrated airspeed and the equivalent airspeed can be considered the same. The scale altitude correction is always negative. This figure graphically depicts the mysterious "headwinds" encountered by pilots as they began to fly higher and faster. Rotary wing aircraft seldom exceed 200 kts, however, with tilt wing rotorcraft this could change.

7.1.3.5 Correction Summary

True airspeed is primarily a navigation parameter; however, it is also required for Mach meter calibration since Mach number equals aircraft V_T divided by the ambient speed of sound. True airspeed is also required in the flight testing of aircraft flutter modes and in jet engine inlet testing where fuel control systems can be a function of V_T . To calculate true airspeed, we require the equivalent airspeed, and knowledge of ambient pressure and temperature to obtain the ambient atmospheric density ratio. The step-by-step computation of true airspeed follows:

V	Indicated airspeed	as read from the instrument on the aircraft
$+ \Delta V_{ic}$	Instrument error correction	obtained from laboratory tests, Figure Error! No text of specified style in document.-3
$= V_{ic}$	Instrument-corrected airspeed	indicated airspeed corrected for instrument error
$+ \Delta V_{pc}$	Position error correction	compensates for effects of the aircraft pressure field on the static and pitot ports (addressed later)
$= V_c$	Calibrated airspeed	indicated airspeed corrected for instrument and position errors
$+ \Delta V_c$	Scale altitude correction	required to reverse P_o substitutions made in V_e equation
$= V_e$	Equivalent airspeed	calibrated airspeed corrected for compressibility
$\div \sqrt{\sigma}$	Square root of the density ratio	
$= V_T$	True airspeed	actual inertial velocity of the aircraft through the air mass

Table 7.1 Airspeed Correction Summary

7.1.3.6 Compressible Dynamic Pressure

A new term is now defined: *compressible dynamic pressure*, q_c

$$q_c = P_T - P_A \quad (7.14)$$

q_c is generally *not* equal to dynamic pressure ($\frac{1}{2} \rho_s V_T^2 \sim$ derived from incompressible theory). The relation between q_c and q is affected by the amount of compression the air goes through. Rearranging Equation 7.12 and combining it with (7.14) and the relation [$a_o^2 = \gamma P_o / \rho_o$] gives:

$$P_p - P_s = q_c = P_o \left(\left[\left(\frac{V_c}{a_o} \right)^2 \frac{\gamma - 1}{2} + 1 \right]^{\frac{\gamma}{\gamma - 1}} - 1 \right)$$

After a binomial expansion, q_c can be expressed as a function of incompressible dynamic pressure and Mach number. The following subsonic relation is presented without proof.

$$q_c = q \left(1 + \frac{M^2}{4} + \frac{M^4}{40} + \frac{M^6}{1600} + \dots \right) \quad (7.15)$$

Note that below 0.2 Mach number, q_c is less than 1% higher than q . The difference is about 6% at 0.5 Mach. During high speed flight at 0.95 M , q_c is about 25% higher than q . Although q_c is measured by the airspeed indicator, engineers generally require a knowledge of q when working with non-dimensional values. If the Mach number effects cannot be ignored, then the above correction to q_c must be made to obtain q . Alternatively, q can be found by calculating V_e as shown and applying Equation 7.6. Equation 7.15 is also useful for finding q_c if knowing only V_c and Mach number. In this case, $q = \frac{1}{2} \rho_o V_c^2$.

7.1.4 Supersonic Flow

The above theory is limited to subsonic flow. If the flow is supersonic, it must pass through a shock wave in order to slow to stagnation conditions. There is a loss of total pressure when the flow passes through the shock wave. Thus, the indicator does not measure the total pressure of the supersonic flow. The solution for supersonic flight is derived by considering a normal shock compression in front of the total pressure tube and an isentropic compression in the subsonic region aft of the shock. The normal shock assumption is valid, since the pitot tube has a small frontal area. Consequently, the radius of the shock in front of the hole may be considered infinite. The resulting equation is known as the Rayleigh Supersonic Pitot

Equation. It relates the total pressure *behind the shock* (P_T') to the free stream ambient pressure P_a and free stream Mach (V/a).

$$\frac{P_T'}{P_a} = \left[\frac{\gamma + 1}{2} \left(\frac{V}{a} \right)^2 \right]^{\frac{\gamma}{\gamma-1}} \left[\frac{1}{\frac{2\gamma}{\gamma+1} \left(\frac{V}{a} \right)^2 - \frac{\gamma-1}{\gamma+1}} \right]^{\frac{1}{\gamma-1}}$$

This equation is used to calculate the ratio of dynamic pressure to ambient pressure.

$$\frac{P_T' - P_a}{P_a} = \frac{q_c}{P_a} \left[\frac{\gamma + 1}{2} \left(\frac{V}{a} \right)^2 \right]^{\frac{\gamma}{\gamma-1}} \left[\frac{1}{\frac{2\gamma}{\gamma+1} \left(\frac{V}{a} \right)^2 - \frac{\gamma-1}{\gamma+1}} \right]^{\frac{1}{\gamma-1}} - 1 \quad \text{or} \quad \frac{q_c}{P_a} = \frac{166.921 \left[\frac{V_e}{a_o \sqrt{\delta}} \right]^7}{\left(7 \left[\frac{V_e}{a_o \sqrt{\delta}} \right]^2 - 1 \right)^{2.5}} - 1$$

If sea level standard day values are inserted for P_a and the speed of sound, a , and 1.4 is substituted for γ , then the supersonic calibrated airspeed equation results:

$$\frac{q_c}{P_a} = \left[\frac{166.921 \left(\frac{V_e}{a_o \sqrt{\delta}} \right)^7}{\left[7 \left(\frac{V_e}{a_o \sqrt{\delta}} \right)^2 - 1 \right]^{2.5}} \right] - 1 \quad \text{or} \quad \frac{q_c}{P_o} = \left[\frac{166.921 \left(\frac{V_e}{a_o} \right)^7}{\left[7 \left(\frac{V_c}{a_o} \right)^2 - 1 \right]^{2.5}} \right] - 1 \quad M > 1$$

Supersonic V_c cannot be calculated explicitly, but can be determined through iteration or mechanically through an airspeed indicator calibrated according to this equation. Dynamic pressure for a supersonic aircraft can be calculated as $q = \frac{1}{2} \rho_a V_T^2$

7.1.5 Measurement of Altitude

Establishment of a standard atmosphere in which standard values of pressure, density and temperature are assigned for each altitude allows various methods of measuring altitude. The use of the temperature or density variation with altitude to measure altitude presents accuracy problems due to large temperature variations between day and night, close to the ground, temperature inversions and thermal activity in the summer. An absolute pressure instrument calibrated according to the pressure variation with altitude of standard atmosphere is the usual and the most practical method of measuring altitude or height above a reference level, which is normally taken as sea level.

Present day altimeters are designed to follow the hydrostatic equilibrium relation as illustrated in (Equation 7.1). This relation is used to determine standard variation of pressure with altitude within the troposphere (Equation 7.16) and in the stratosphere (Equation 7.17). These equations are combined in Figure **Error! No text of specified style in document.-5**.

$$P_a = P_o (1 - 6.87559 \times 10^{-6} H_c) \quad \text{for } H_c < 36,089 \text{ ft} \quad (7.16)$$

$$P_a = P_o \left[0.223358 e^{-4.80614 \times 10^{-5} (H_c - 36,089)} \right] \quad \text{for } 36,089 \text{ ft} < H_c < 82,021 \text{ ft} \quad (7.17)$$

where P_a = altimeter pressure, inches Hg
 H_c = pressure altitude, feet
 P_o = 29.92126 in Hg = 2116 lb/ft²

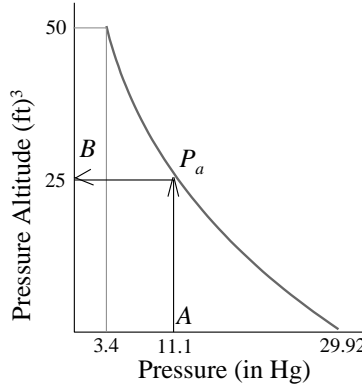


Figure Error! No text of specified style in document.-5 Pressure Variation with Altitude on a Standard Day

Altimeters are calibrated according to the equation in Figure Error! No text of specified style in document.-5. The standard atmosphere sea level pressure (P_0) is 29.92 inches 1013.2 millibars of mercury (Hg). Therefore, on a non-standard sea level pressure day, the altitude reading will be in error. To allow for local pressure changes in the atmosphere, a provision is made in the construction of the altimeter to adjust the barometric setting to the (current) sea level pressure for any given condition, such that the altimeter, when adjusted, will indicate the altitude of the airport. This is known as the local altimeter setting and is given by the tower. This adjustment is important for instrument flying to ensure terrain clearance but is not used in flight testing.

Aerodynamic forces are a function of the local ambient density which can be obtained from knowledge of the local ambient pressure and static temperature. Pressure altitude is defined as the altitude with the altimeter set at 29.92 inches 1013.2 millibars of Hg and is used as the independent variable to measure atmospheric pressure. Pressure altitude is not related to height above the ground except on a standard atmospheric day. Pressure altitude is only a measure of the pressure of the atmosphere in which the test aircraft is flying. Flight testing requires that the local ambient pressure and the temperature of the air be known, from which the actual air density is calculated. Therefore, the altimeter is set at 29.92 inches 1013.2 millibars of Hg for all flight tests.

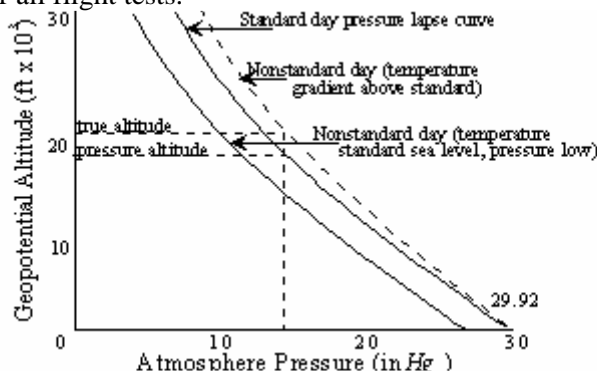


Figure Error! No text of specified style in document.-6 Standard Day and Test Day Pressure Variation with Altitude

The heart of the altimeter is an evacuated bellows which expands or contracts with changes in outside pressure. The bellows is connected to a series of gears and levers which cause a pointer to move. It is through this network that Equations (7.16) and (7.17) are mechanized. The mechanism is placed in an airtight case and is vented to the static source. Altimeter construction is shown in Figure Error! No text of specified style in document.-7. Such an instrument is subject to wear and tear, calibration errors, friction, and hysteresis problems. As with airspeed indicators, the altimeter instrument error must be determined in a laboratory.

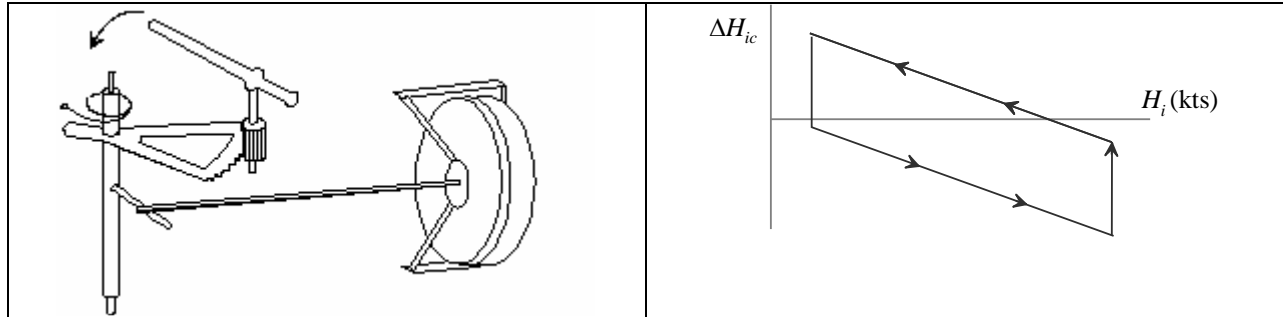


Figure Error! No text of specified style in document.-7 Altimeter Schematic Figure Error! No text of specified style in document.-8 Altimeter Instrument Correction

A step-by-step process to obtain a calibrated pressure altitude from an indicated altitude (with the altimeter set at 29.92) is given below.

H_i	Indicated pressure altitude	as read from the instrument on the aircraft
$+\Delta H_c$	Instrument error correction	obtained from laboratory
$= H_{ic}$	Instrument-corrected altitude	indicated altitude corrected for instrument error
$+\Delta H_{pc}$	Position error correction	compensates for effects of the aircraft pressure field on the static and pitot ports (addressed later)
$= H_c$	Calibrated altitude	equals calibrated <i>pressure altitude</i> if 29.92 is set

Table 7.2 Altitude Correction Summary

7.1.6 Temperature Measurement

Knowledge of the air temperature outside the aircraft is essential to measuring true airspeed and density. The temperature indicated on the gauge must be corrected for Mach effects, recovery factor and instrument errors.

When a probe is inserted into the freestream, it does not see a uniform temperature on its surface. The leading edge suffers from the problem that the energy of the airflow at the stagnation point is included. This increases the probe temperature above the static ambient temperature. Applying Bernoulli's theorem to the freestream and the probe's stagnation point:

$$\frac{\gamma}{\gamma - 1} \frac{P_T}{\rho_T} = \frac{V^2}{2} + \frac{\gamma}{\gamma - 1} \frac{P_s}{\rho_s} \tag{7.8}$$

where the total indicated test (stagnation) condition is denoted by the subscript "T". We can substitute $[P = \rho gRT]$ and $[a^2 = \gamma gRT]$ into the above equation and rearrange it to see the effect of Mach number on stagnation temperature:

$$T_T = T_a \left[1 + \frac{\gamma - 1}{2} M^2 \right]$$

where T_a is the ambient static temperature. This relation was derived assuming adiabatic flow (no addition or loss of heat while bringing the flow to stagnation). In reality, however, the temperature probe is hotter than the surrounding air and will, in fact, radiate some of its energy. This heat loss is expressed mathematically by putting a recovery factor (K) into the above equation

$$T_T = T_a \left[1 + \frac{K(\gamma - 1)}{2} M^2 \right] = T_a + \frac{\gamma - 1}{2} T_a K M^2 \tag{7.18}$$

The recovery factor, K , indicates how closely the temperature sensor actually observes the total temperature. Its value generally varies from 0.7 to 1.0. For flight test systems, a range of 0.95 to 1.0 is more common. A value of 1.0 for K is ideal, but greater values may be observed when heat is added to the sensors by conduction (hot material around the sensor) or radiation (exposure to direct sunlight). In any

case, K must be determined through flight test. Indicated velocity, altitude and temperature are recorded and corrected to calibrated airspeed, calibrated altitude, and instrument-corrected temperature, respectively. Mach number can be computed directly from V_c and altitude (Equations 7.19 and 7.20). By applying Equation (7.18) and plotting T_{ic} vs M^2 as shown in Figure **Error! No text of specified style in document.-9**, the recovery factor is determined from the slope of the line.

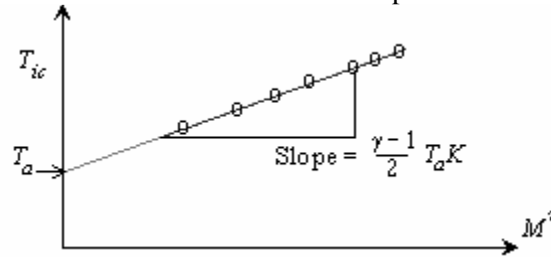


Figure **Error! No text of specified style in document.-9** Corrected Indicated Temperature vs Mach Number Squared

where T_{ic} is the sensed test temperature corrected for instrument error.

$$T_{ic} = T_i + \Delta T_{ic}$$

As with airspeed indicators and altimeters, ΔT_{ic} is determined in a laboratory. Although ΔT_{ic} is called instrument correction, it is more than that. It accounts for many system errors collectively from the indicator to the temperature probe.

Finally, substituting values for T_i , ΔT_{ic} , γ , and M into Equation (7.18) to obtain an equation for ambient temperature:

$$T_a = \frac{T_i + \Delta T_{ic}}{1 + .2KM^2}$$

Because K is affected by solar radiation, the temperature probe should be shielded from direct sunlight.

7.1.7 Mach Number Measurement

The Mach number is defined as the ratio of the true airspeed to the ambient speed of sound.

$$M = \frac{V_T}{a} = \frac{V_T}{\sqrt{\gamma gRT}} \text{ where } \frac{P}{\rho} = gRT \text{ therefore } M = \frac{V_T}{\sqrt{\gamma \frac{P}{\rho}}}$$

Substituting this into the true velocity Equation given in (7.9) and rearranging gives:

$$M = \sqrt{\frac{2}{\gamma - 1} \left[\left(\frac{P_p - P_s}{P_s} + 1 \right)^{\frac{\gamma - 1}{\gamma}} - 1 \right]}$$

$$\text{or } \frac{P_p}{P_s} = \left(1 + \frac{\gamma - 1}{2} M^2 \right)^{\frac{\gamma}{\gamma - 1}}$$

This equation, which relates Mach to the freestream total and ambient pressures, is valid for supersonic as well as subsonic flight. Remember, however, that P_T rather than P_p is measured in supersonic flight. By using the Raleigh pitot equation and substituting for the constants, the supersonic equation for Mach number is also derived.

$$\frac{q_c}{P_s} = (1 + 0.2M^2)^{3.5} - 1 \text{ or } M = \sqrt{5 \left[\left(\frac{q_c}{P_s} + 1 \right)^{2/7} - 1 \right]} \text{ for } M < 1 \tag{7.19}$$

$$\frac{q_c}{P_s} = \frac{166.92M^7}{(7M^2 - 1)^{2.5}} - 1 \text{ for } M > 1 \tag{7.20}$$

The Mach meter is essentially a combination altimeter and airspeed indicator designed to solve these equations. An altimeter capsule and an airspeed capsule simultaneously supply signals to a series of gears and levers to produce the Mach indication, Figure Error! No text of specified style in document.-10. Since the construction of the Mach meter requires two bellows, one for q_c and another for P_s , it is complex, difficult to calibrate, and inaccurate. As a result, the Mach meter is not used in flight test work except as a reference instrument.

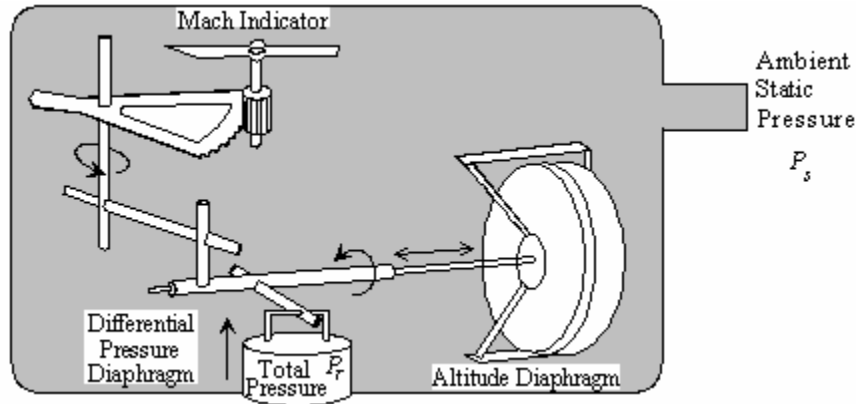


Figure Error! No text of specified style in document.-10 Mach Meter Schematic

Equations (7.19) and (7.20) show that Mach number is a function of total pressure and ambient pressure only. Mach is independent of temperature, and when flying at a given H_c and V_c ,

$$M_{\text{test}} = M_{\text{std}}$$

7.1.8 Pitot Static Position Errors

The airspeed system depends upon accurate measurements of ambient static pressure and total pressure. Static and pitot pressure are sensed by the pitot-static tube which gives true readings in an undisturbed freestream; however, when attached to an aircraft which has its own pressure field, the pitot-static tube will be affected by the pressure field and flow angularity.

The calibration equation for the airspeed and altimeter systems assumes that the static pressure sensed (P_s) is the true ambient reference pressure (P_{ref}) at the altitude of the aircraft. Unfortunately, the pressure field of the aircraft itself will affect the static pressure readings and cause errors. These errors are a function of the position of the static pressure source (sensor) on the aircraft and the aircraft angle of attack.

7.1.8.1 Total Head Error

The capability of a total head tube to sense true total pressure (P_T) is a function of the flow angularity and the geometry of the nose of the total head tube. Wind tunnel tests on pitot tubes at various angles of attack have been performed and typical results are shown below:

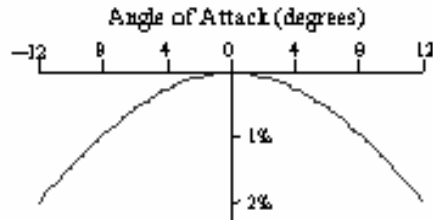


Figure Error! No text of specified style in document.-11 Percent Error in Total Pressure

As can be seen from Figure Error! No text of specified style in document.-11, if a rounded or sharp-nosed pitot tube is chosen, the resulting error in total head pressure should be less than 1% for the angle of attack range of most conventional fixed-wing aircraft. However, for high lift STOL or V/STOL applications where angle of attack changes of greater than 20 degrees could be expected, then a Kiel tube total head or a swiveling total head should be considered. If large changes in angle of attack or sideslip angle are to be expected, then the total head error must be determined by comparing the aircraft total head ($P_{PA/C}$) to a reference total head ($P_{P_{ref}}$) that is known to have zero error. Two reference total heads are: (a) the swiveling type, which is free to rotate into the local freestream and (b) the Kiel tube which is a shrouded total head, Figure Error! No text of specified style in document.-12.

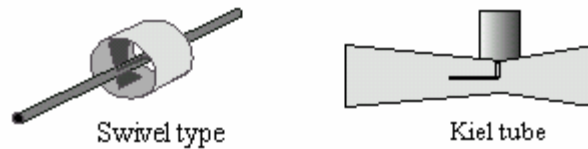


Figure Error! No text of specified style in document.-12 Reference Pitot-Tubes

The Kiel tube is simple to make and is often used as a reference. However, with the swiveling total head, the inclusion of potentiometers in the swivel can give readouts of the local angle of attack and the sideslip angle. If a reference total head is used in the calibration flight tests, then the pitot position error corrections can be determined by connecting a calibrated pressure differential gauge between the reference total head and the aircraft total head. Figure Error! No text of specified style in document.-13 shows other simple pitot inlets and the angle of attack range where each retains less than 1% error. In general, it is accurate to say that as long as the total pressure sensor is not located behind a propeller, in the wing wake, boundary layer, or region of localized supersonic low, then the total pressure error (ΔP_p) is negligible.

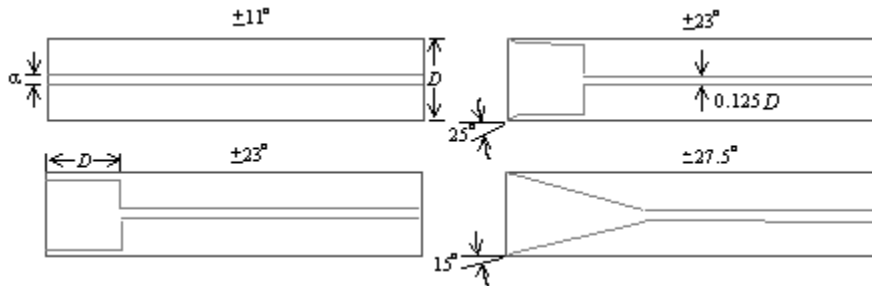


Figure Error! No text of specified style in document.-13 Accuracy of Various Pitot Tube Configurations

7.1.8.2 Static Source Error

A typical subsonic pressure distribution about an aircraft is shown below and it can be seen that the best place for the static source on these types of aircraft is in the rear fuselage, approximately halfway between the trailing edge of the wing and the leading edge of the horizontal tail. Static pressure sensors are generally on both sides of the fuselage and connected to reduce errors due to sideslip.

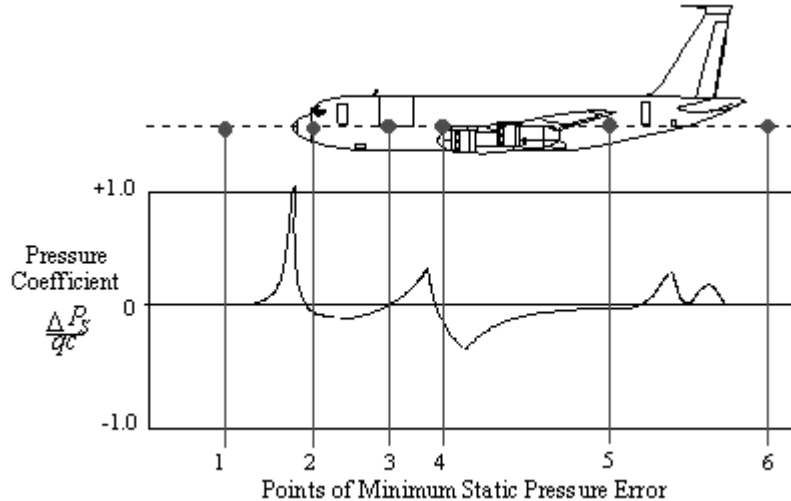


Figure Error! No text of specified style in document.-14 Pressure Distribution About a Subsonic Aircraft

Figure Error! No text of specified style in document.-14 shows that the error is greatly affected by the location of the sensor - yielding the name "position error". Aircraft engaged in flight testing generally have a pitot-static probe mounted on a long boom attached to the aircraft nose section or the wingtip (Figure Error! No text of specified style in document.-15). This removes the static source from the influence of the aircraft's pressure field, thereby reducing position error corrections. Wingtip booms give reasonable results at low values of C_L if the boom is $\frac{1}{2}$ chord length ahead of the leading edge. Results are good at most moderate values of C_L if the boom is two chords ahead of the wing. Nose boom installations are adequate if the boom length is greater than $\frac{1}{2}$ fuselage diameter ahead of the fuselage.

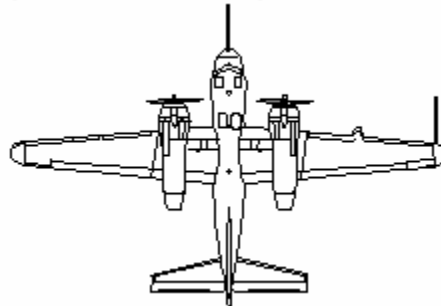


Figure Error! No text of specified style in document.-15 Typical Location of Pitot Tubes for Flight Testing

7.1.9 Test Methods

There are many methods of determining position error corrections. The principle behind each technique is the same; compare a known true value (airspeed or altitude) to the corrected indicated value and use the theory to correlate this error to pressure error.

7.1.9.1 Tower Fly-by

Since the altimeter and airspeed system use the same static source, it is possible to correlate the altimeter position error directly to the airspeed error. This method assumes that there is no error in the total head system.

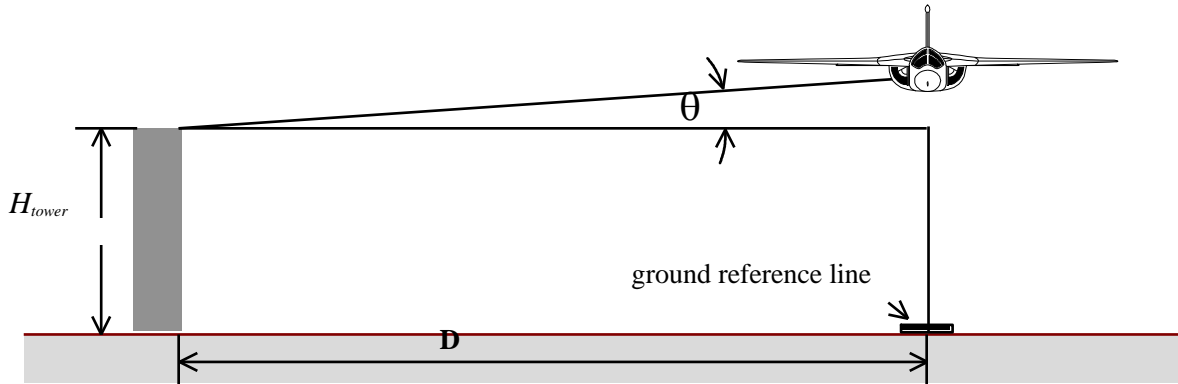


Figure **Error! No text of specified style in document.**-16 Tower Fly-By Method

The test technique is to fly the aircraft along a ground reference line, past the tower, in stabilized flight at a constant airspeed and at the approximate height of the tower. The primary piloting task is to maintain a constant indicated altitude during the run. The tower is equipped with a sensitive altimeter and a means of determining the relative angle (θ) of the aircraft. The data recorded during each run are the calibrated pressure altitude of the tower, ($H_{c_{tower}}$), the angle θ , and the aircraft's indicated pressure altitude, airspeed and temperature (H_i , V_i and T_i), as it passes the tower. The actual pressure altitude of the aircraft is:

$$H_{c_{a/c}} = (H_{c_{tower}} + \Delta H_{i_{c_{tower}}}) + D \tan \theta \frac{T_s}{T_{test}}$$

Where T_s is the standard day absolute temperature at the test altitude and T_{test} is the test day temperature in absolute units. The difference between the actual pressure altitude and the aircraft's instrument-corrected pressure altitude is the position error *correction*. The T_s / T_{test} temperature correction is to convert the geometric height to the aircraft above the reference grid line in the tower ($D \tan \theta$) to a pressure height that can be added to the pressure altitude of the tower $H_{c_{tower}}$.

$$\Delta H_{pc} = H_{c_{a/c}} - H_{ic} = H_{c_{a/c}} - (H_i + \Delta H_{ic})$$

where H_i is the indicated pressure altitude in the aircraft as it passes the tower and ΔH_{ic} is the aircraft altimeter instrument correction. The hydrostatic equilibrium equation states that the pressure *error* at the static source is

$$\Delta P_s = \rho g \Delta H_{pc} \quad (7.21)$$

This equation yields the pressure *error correction* from an altitude correction. Knowing the static pressure error is useful as it allows calculation of the calibrated airspeed and airspeed correction.

To compute the position error correction for the airspeed system knowing ΔP_s and V_{ic} , the following equation is needed:

$$\Delta P_D = \Delta P_s - \Delta P_T = \frac{1}{2} \rho_o V_c^2 \left(1 + \frac{M_c^2}{4} \right) - \frac{1}{2} \rho_o V_{ic}^2 \left(1 + \frac{M_{ic}^2}{4} \right) \quad (7.22)$$

The tower fly-by method assumes no errors in the total head, therefore ΔP_T in the above equation would be zero, and $\Delta P_D = \Delta P_s$. Only the first two terms of the binomial expansion on the Mach number are used. Equation 7.22 is solved for V_c and the position error correction for the airspeed is:

$$\Delta V_{pc} = V_c - V_{ic} \quad (7.23)$$

The above calculations are repeated for each airspeed tested and plots of ΔV_{pc} and ΔH_{pc} versus V_{ic} are generated. For FAA/JAA certification ΔH_{pc} at sea level is required i.e. $\Delta P_s = \rho_o g \Delta H_{pc}$.

The tower fly-by method is relatively simple and provides a reasonable calibration technique for the altimeter system. Accurate position error corrections for the airspeed systems using this method depend upon the magnitude of V_{ic} in Equation (7.22) and on the accuracy in reading the altimeter as well as in using the grid. The results of an error analysis on the use of the tower fly-by method to determine airspeed position errors are plotted in Figure **Error! No text of specified style in document.-17**. If the cumulative error of tower and aircraft pressure altitude readings is 25 feet, then to measure ΔV_{pc} to within one knot, the aircraft airspeeds must be greater than 250 knots.

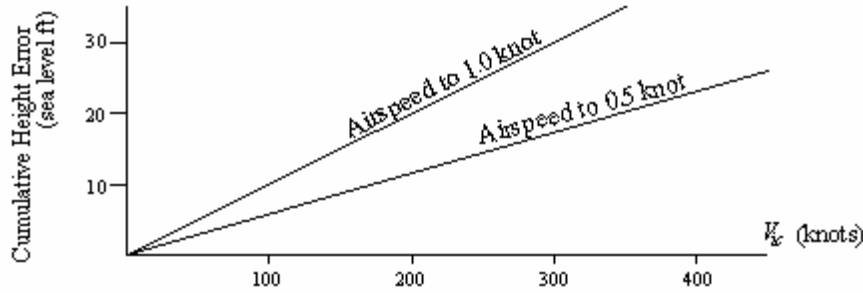


Figure **Error! No text of specified style in document.-17** Error Analysis of Tower Fly-By Method for Airspeed Calibration

The major problems with this method are the requirements of a tower, an unobstructed flight path near the ground, a line marked on the ground a known distance from the tower and the inability to test at airspeeds near stall or in the transonic region. While conducting a tower fly-by, the test pilot's first priority is maintaining a constant altitude. Maintaining proper distance is second priority, while maintaining airspeed is 3rd.

7.1.9.2 Calibrated Aircraft

This method is similar to the tower fly-by method except that a calibrated aircraft is used as the aerial tower. The pace method is not formation flying. Although both aircraft are at the same altitude, if they are too close to each other the pressure field of one will affect the other and vice versa. However the pace aircraft must be close enough to ensure no relative movement exists between the two aircraft.

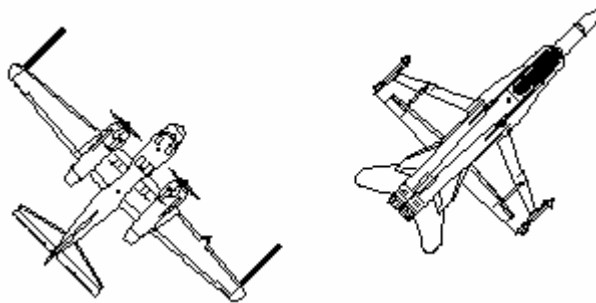


Figure **Error! No text of specified style in document.-18** Calibrated Pace Aircraft

The two aircraft stabilize at a constant altitude and various airspeeds, both aircraft record V_i , H_i , T_i , M and fuel weight. Equations (7.21) through (7.23) are applied as before to obtain the position error corrections. Another method is for the calibrated aircraft to lay down a smoke trail at a known altitude and the test aircraft to fly along the smoke trail in a manner similar to the tower fly-by technique. The smoke trail

technique from a calibrated aircraft is very useful for conducting airspeed calibrations in the transonic speed region.

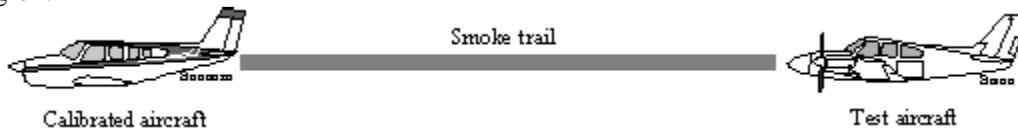


Figure Error! No text of specified style in document.-19 Smoke Trail Method

The disadvantages of these techniques are that smooth air is required as well as an expensive calibrated aircraft which must be recalibrated regularly using one of the other techniques. Formation flying is required, and any unknown errors of the calibrated aircraft are passed on to the test aircraft.

Since many test flights require a safety chase aircraft, a first hack at airspeed and altimeter position error corrections can be obtained very early in the flight test program, prior to dedicated pitot-static calibration flights, if the safety chase is a calibrated aircraft.

A final option is to have a calibrated aircraft fly within range of a precision tracking radar. The radar will measure geometric altitude and true ground velocity. When the test aircraft flies at some indicated altitude, this value can be compared to the height determined by the radar, Figure Error! No text of specified style in document.-20. This method is the easiest of all operationally if both a calibrated aircraft and precision radar are available.



Figure Error! No text of specified style in document.-20 Calibrated Radar Method

7.1.9.3 Ground Course

The true speed of an aircraft can be determined by timing the aircraft over a known distance marked on the ground. By comparing the instrument-corrected airspeed, to the actual calibrated airspeed, position error corrections can be computed. The ground speed course should be flat and long enough so that the shortest time of any run will be greater than 45 seconds. The aircraft should be flown at a height above the ground greater than the wing span to ensure no ground proximity effects on the airspeed system. To allow for wind effects, two runs at the same airspeed in opposite directions should be performed on the course. The aircraft should be allowed to drift with the crosswind, i.e. fly the aircraft on the magnetic heading of the ground course. The ground course FTT is often used to calibrate the pitot-static systems on helicopters.

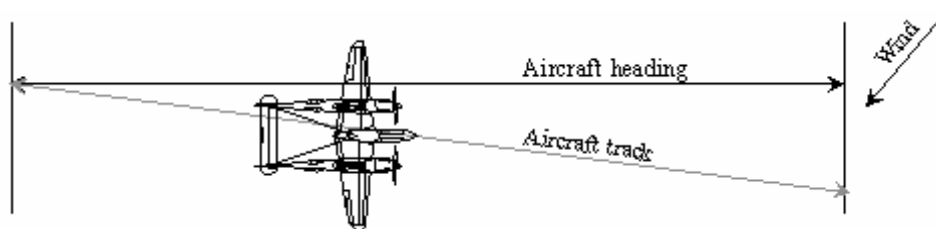


Figure Error! No text of specified style in document.-21 Schematic of Ground Course Technique

The primary piloting task is to hold a constant airspeed at a reasonably constant indicated altitude over the speed course. Data recorded are V_i , H_i , T_i , and elapsed time in each direction. Data reduction proceeds as follows:

1. Calculate ground speed in each direction and average them to get V_T : $V_T = \frac{1}{2} \left[\frac{S}{T_1} + \frac{S}{T_2} \right]$
2. From H_i and T_i of the test aircraft, calculate density ratio and compute equivalent airspeed (V_e) from average V_T in step (a): $V_e = V_T \sqrt{\sigma}$
3. Correct V_i for instrument error correction and obtain V_{ic} : $V_{ic} = V_i + \Delta V_{ic}$
4. $\Delta V_{pc} = V_c - V_{ic}$ where $V_c = V_e$ since the scale altitude correction is negligible near sea level.
5. Knowing V_c , calculate ΔP_D , $\Delta P_D = \frac{1}{2} \rho_o (V_c^2 - V_{ic}^2)$
6. $\Delta P_D = q_c - q_{ic}$
7. $\Delta P_D = \Delta P_S - \Delta P_T$ assuming all the errors are in the static source: $\Delta P_D = \Delta P_S$
8. Calculate altimeter position error $\Delta H_{pc} = \Delta P_S / \rho_o g$
9. Plot ΔV_{pc} and ΔH_{pc} versus V_{ic} . Note that ΔV_{pc} does not assume $\Delta P_T = 0$

The ground course method is generally used for slow, subsonic aircraft including helicopters. The time over a three mile course is reasonably long and small timing errors are not a major factor in the results. Figure Error! No text of specified style in document.-22 shows the inaccuracies in ΔV_{pc} if there is a 0.5 second timing error during the test. Another consideration is winds. If the aircraft is flying into the wind on one pass and with it on the return pass, different times will result. It is important to average the velocities for each pass, not the times. Averaging the times would result in an error because the aircraft is battling the headwind for a longer period of time than it benefits from a tailwind.

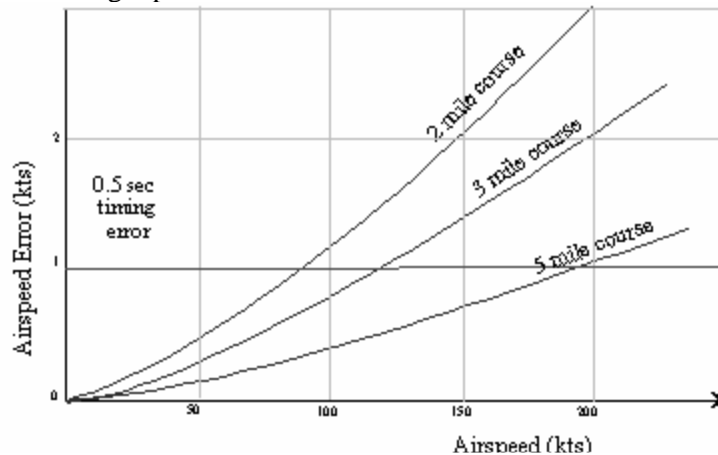


Figure Error! No text of specified style in document.-22 Error Analysis of Ground Course Method

Figure Error! No text of specified style in document.-23 illustrates the effect of changing wind between speed runs.

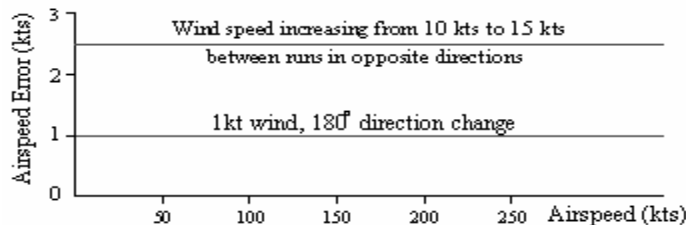


Figure **Error! No text of specified style in document.**-23 Ground Course Error Resulting from Wind Changes

7.1.9.4 Static Bomb

A reference static source (bomb) which has been previously calibrated in a wind tunnel is trailed behind and below the aircraft, out of its pressure field (Figure **Error! No text of specified style in document.**-24). The pressure transmitted up the tube gives the true freestream ambient pressure which is compared directly to the static source being tested. This direct measurement of ΔP_s is performed with a pressure differential gauge, $\left[\Delta P_s = P_{S_{A/C}} - P_{S_{ref}} \right]$. If desired, the same comparison can be done for the pitot source: Use a ΔP_p gauge to measure the difference between the reference pitot pressure and that for the test probe, $\Delta P_T = P_{T_{a/c}} - P_{T_{ref}}$.

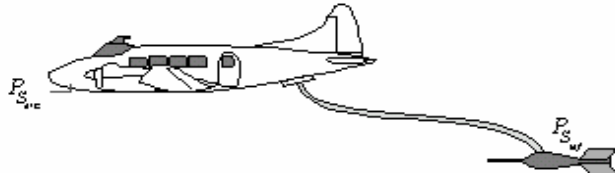


Figure **Error! No text of specified style in document.**-24 Trailing Static Bomb Pilot technique consists of flying at stabilized airspeeds at constant altitude. Data recorded are V_i , H_i , T_i , ΔP_p and ΔP_s at each airspeed. Data reduction is as follows:

1. Apply instrument corrections to all readings to obtain V_{ic} , H_{ic} , T_{ic} .
2. $\Delta P_D = \Delta P_T - \Delta P_S$. ΔP_T may be assumed to be zero if not instrumented.
3. Calculate V_c from ΔP_D and V_{ic} , Equation (7.22)
4. $\Delta V_{pc} = V_c - V_{ic}$.
5. Compute the altimeter position error correction: $\Delta H_{pc} = \Delta P_s / \rho_0 g$

The trailing static bomb method has disadvantages in that a stable static source is required, a deployment and recovery system is required and there are upper speed limitations due to the bomb's rising into the aircraft wake. Trailing bombs are generally used at speeds of 150 knots or less and are often used in the pitot static calibration of helicopters.

7.1.9.5 Trailing Static Cone

An alternative to the trailing bomb is the trailing cone. In this case, the reference static pressure port is trailed behind the aircraft and the tubing is kept taut by means of a stabilizing drag device. This device is normally a simple 35° cone with stabilizing holes as shown in Figure **Error! No text of specified style in document.**-25. A mechanical swivel between the cone and the tube will prevent twisting of the tube.



Figure **Error! No text of specified style in document.**-25 Trailing Static Cone

The test technique is similar to the trailing static bomb method and the data analysis is exactly the same. The trailing cone technique has no speed limitations and often the aircraft can take-off and land with the cone trailed. The disadvantages are that the trailing tubing may be at an angle to the local freestream in the slow flight regime thereby causing local pressure effects on the trailing static source. The trailing cone method is not used on helicopters due to possible entanglement in the tail and main rotors.

7.1.9.6 GPS Method

This method is essentially another way to do the traditional ground method. The procedures detailed below are a variation of methods previously documented (ref. 7.10 and 7.11) in 1995 and 1997. This particular variation was laid out in an unpublished paper by Doug Gray (ref. 7.12) in 1998. As an historical note, the same concept (obviously without GPS and computer spreadsheets) was used by NACA in 1927 to measure the true airspeed of a dirigible airship, the U.S.S. Los Angeles (ref. 7.13).

The advantage of this method over the traditional ground course method is that it doesn't have to be flown near the ground, thus it can be done at very slow speeds as long as the aircraft can be held stable at constant speed, altitude and heading.

The basic procedure is to fly at least three legs at the same airspeed and altitude. Using a handheld GPS, note ground speed and ground track on each leg. Assuming the aircraft's true airspeed and the wind speed and direction are constant on each of the three legs, then three equations in three unknowns can be solved giving wind speed, wind direction, and true airspeed. The solution can be understood by realizing that the ground speed vector (magnitude and direction) is the vector sum of the wind and the true airspeed. This is graphically shown in Figure **Error! No text of specified style in document.**-26. If three ground track vectors are placed with the heads at the same point, then a circle drawn through the tails of the three vectors will have a radius equal to the true airspeed and the difference between the center of the circle and the three heads will be the wind speed and direction.

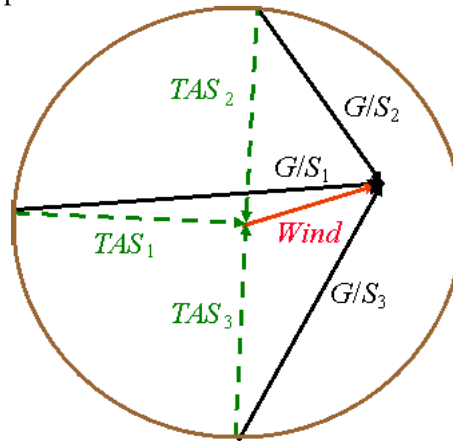


Figure **Error! No text of specified style in document.**-26 GPS Method Vectors

The solution of the data is best accomplished using a spreadsheet. The solution shown in Table 7.3 is from reference 7.11

	A	B	Result
1	Ground Speed 1	184	184
2	Track 1	265	265
3	Ground Speed 2	178	178
4	Track 2	178	178
5	Ground Speed 3	185	185
6	Track 3	82	82
7	X1	=B1*SIN(PI()*(360-B2)/180)	183.3
8	Y1	=B1*COS(PI()*(360-B2)/180)	-16.0
9	X2	=B3*SIN(PI()*(360-B4)/180)	-6.2
10	Y2	=B3*COS(PI()*(360-B4)/180)	-177.9
11	X3	=B5*SIN(PI()*(360-B6)/180)	-183.2
12	Y3	=B5*COS(PI()*(360-B6)/180)	25.7
13	M1	=-1*(B9-B7)/(B10-B8)	-1.17
14	B1	=(B8+B10)/2-B13*(B7+B9)/2	6.71
15	M2	=-1*(B11-B7)/(B12-B8)	8.77
16	B2	=(B8+B12)/2-B15*(B7+B11)/2	4.42
17	Wx	=(B14-B16)/(B15-B13)	0.2
18	Wy	=B13*B17+B14	6.4
19	Wind Speed	SQRT(B17^2+B18^2)	6.4
20	Wind Direction	MOD(540-(180/PI()*ATAN2(B18,B17)),360)	177.9
21	True Airspeed	=SQRT((B7-B17)^2+(B8-B18)^2)	184.4

Table 7.3 GPS Method Spreadsheet Solution with Example Data

The inflight procedures to apply the GPS method should be as follows:

1. Perform a stable trim shot at the desired airspeed and configuration. Pick an altitude and geographic location where you would expect steady wind.
2. Once stable, note everything that would affect true airspeed (indicated airspeed, pressure altitude, and outside air temperature).
3. After allowing sufficient settling time (perhaps 10 seconds after the aircraft is stable, no change in ground speed or track), record the GPS ground speed and track.
4. Turn 60° to 120° and repeat step 3 at the same airspeed and altitude. Small changes in altitude are much preferred over any change in airspeed. A one knot speed error will produce one knot or more error in true airspeed, but a 100 ft error in altitude will have a relatively insignificant error on true airspeed. A constant ground track is important.
5. Turn again and repeat at the same airspeed and altitude. Three legs are required to complete one data point (one speed/configuration). If four legs are done at the same conditions then the data can be averaged taking four legs, three at a time, four different ways.

There is no technical requirement to use a specially certified or differential GPS. The indication of accuracy of the derived true airspeed can come from the repeatability of the derived wind vector. If several points are flown at different speeds (each “point” being at least three legs at the same speed) and give the same derived wind speed and direction, then a high degree of confidence can be placed in the results. If on the other hand, regardless of how sophisticated the GPS equipment is, if the derived wind vector is not consistent, then the data can not be relied upon. If the wind is inconsistent the reason could be one of several things – a variable wind or temperature, failure to hold airspeed and/or heading constant during the data gathering process, changing airspeed between legs of a point, or even poor GPS satellite coverage.

7.1.9.7 Summary of Methods

A summary of test methods and applicable airspeeds is shown in Figure Error! No text of specified style in document.-27.

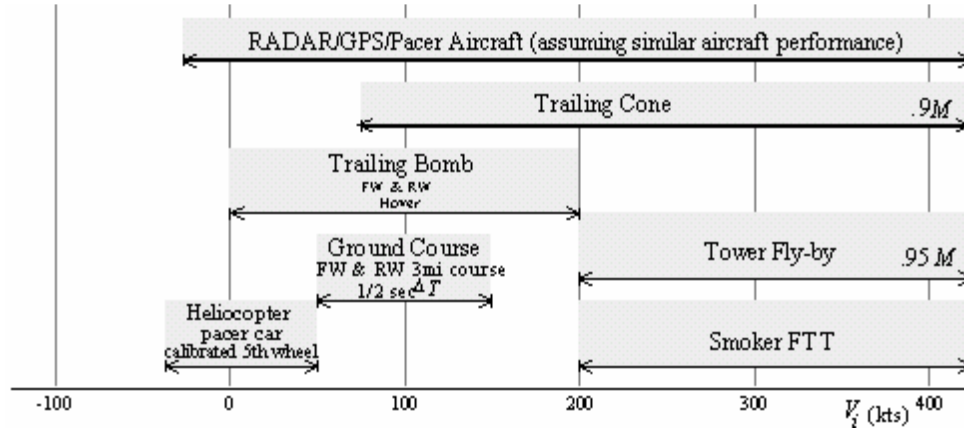


Figure Error! No text of specified style in document.-27 Summary of PEC Test Methods

With most of the above methods it is assumed that the total head position error correction is zero; however, if a reference total head is used in the airspeed calibration tests and a pressure differential gauge is used to measure the difference between the reference total head and the aircraft total head, then the pressure differential is designated ΔP_p . Also if ΔP_s is the difference between the reference and the aircraft static sources, then the complete airspeed position error is $\Delta P_D = \Delta P_p - \Delta P_s$.

7.1.10 Position Error Correction Data Analysis

7.1.10.1 Effect of Altitude and Weight on Position Errors

The pressure field around an aircraft is a function of angle of attack, and therefore C_L , as well as flap configuration. There are obviously many combinations of weight and speed that will give the same C_L . Therefore, position error corrections for both airspeed and altimeter are functions of aircraft weight if plotted versus V_{ic} as shown in Figure Error! No text of specified style in document.-28.

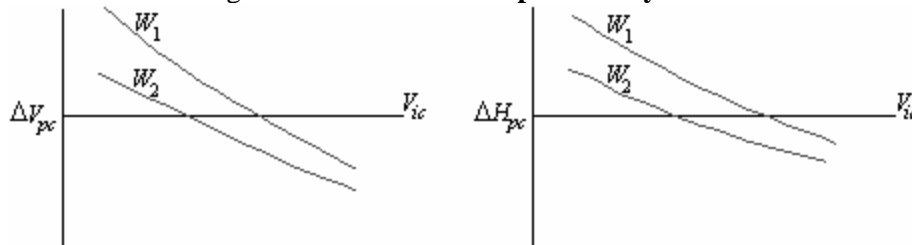


Figure Error! No text of specified style in document.-28 Effect of Weight on Position Errors

Note that since equivalent airspeeds are used, altitude has no effect on airspeed position error correction. This is not true, however, for the altimeter position error corrections since the ambient density term (ρ_a) is in the equation:

$$\Delta H_{pc} = \frac{\Delta P_s}{\rho_a g} \tag{7.24}$$

Therefore altimeter correction curves are a function of *both weight and altitude*, Figure **Error! No text of specified style in document.-29**. Many position error correction curves are required if plotted as a function of airspeed, weight and altitude.

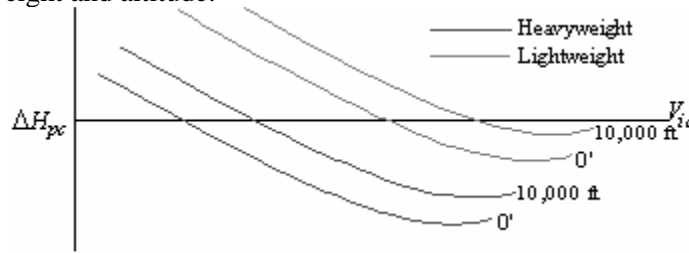


Figure **Error! No text of specified style in document.-29** Altimeter Position Error Curves

Plotting a pressure coefficient versus lift coefficient reduces the number of curves to one curve, Figure **Error! No text of specified style in document.-30**. This curve is valid for all aircraft weights. C_L is easy to calculate and thus a direct relation to α and is used instead of α . Regardless of the plots used, a differently configured aircraft will have a different pressure field which may affect the static source. If this is the case, a separate calibration curve is required.

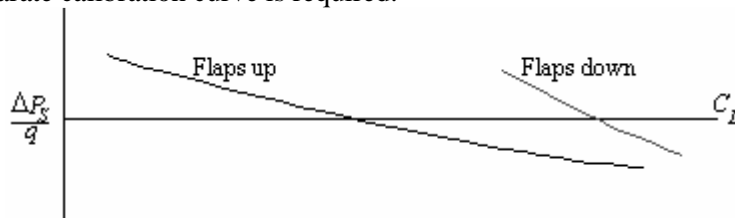


Figure **Error! No text of specified style in document.-30** $\frac{\Delta P_s}{q_c}$ vs C_L Curve

From the $\frac{\Delta P_s}{q} \sim C_L$ data plotted in Figure **Error! No text of specified style in document.-30**, the data for the curves in 7.29 and 7.30 can be calculated using assumed value of weight and altitude.

7.1.10.2 Mach Number Effects on Airspeed Calibration

Because it neglects Mach effects, the above technique for consolidating all data into a single plot works well for slow flying aircraft only. Generally

$$C_p = \Delta P_s / q = f(C_L, M) \tag{7.25}$$

At Mach numbers above 0.3, compressibility effects must be considered.

$$C_L = \frac{nW}{\frac{1}{2} \rho_a V_T^2 S} \text{ where } V_T^2 = (Ma)^2 = (Ma_o \sqrt{\theta})^2 = M^2 a_o^2 \theta; \text{ also } \sigma = \frac{\delta}{\theta} \text{ or } \rho_a \theta = \delta \rho_o$$

Combining and substituting values for constants yields:
$$C_L = \frac{\frac{nW}{\delta}}{1481M^2 S}$$

or $C_L = f\left(\frac{nW}{\delta}, M\right)$ for any given aircraft.

Combining this with Equation (7.24) shows that

$$\frac{\Delta P_s}{q} = f\left(\frac{nW}{\delta}, M\right)$$

where $\frac{nW}{\delta}$ is proportional to α for any given Mach number. For low Mach numbers, the compressibility effect is negligible and the relation simplifies to that in Figure **Error! No text of specified style in document.-30**.

document.-29. As the Mach number increases, both $\frac{nW}{\delta}$ and M affect $\frac{\Delta P_s}{q}$. Note that the position error correction is a function of load factor, weight or altitude. At high subsonic speeds the α changes very little and the position error correction is due to Mach number only. Figure **Error! No text of specified style in document.**-31 illustrates the most common method of presenting this data.

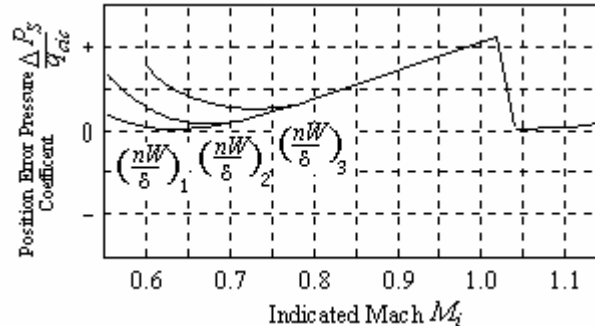


Figure **Error! No text of specified style in document.**-31 Indicated Mach Corrected for Instrument Error, Mic

At supersonic speeds, the situation is similar. Provided the static source is ahead of the fuselage bow wave, as with a nose boom installation, the static pressure will not be affected by the pressure field of the aircraft. Any static pressure error will be due to the design of the pitot-static head only. Generally the P-S head is calibrated in a wind tunnel prior to installation on the aircraft.

Since the pitot head will have a local shock wave, the total pressure registered will be less than predicted by Bernoulli's equation and the Raleigh Equation (7.20) must be used. The Raleigh equation assumes a normal shock at the entry of the pitot tube.

7.1.10.3 Humidity Corrections

If the relative humidity is high and the temperature is above 0°C, the errors introduced by neglecting humidity in the computations of relative density may become appreciable for high speed aircraft. Moist air will have less mass density than dry air for the same pressure and temperature conditions. Airspeed and density altitudes will be affected by this lower density. Whenever the humidity factor becomes appreciable, humidity must be measured at the time of test. Note that the FAA does not require humidity corrections to pitot-static calibrations.

7.1.11 System Lag Errors

The presence of a time lag error in pressure measurements is generally associated with climbing/descending or accelerating/decelerating flight. This pressure lag error is a result of the following:

1. Pressure drop in tubing caused by viscous friction.
2. Inertia of the air mass in the tubing.
3. Instrument inertia and viscous and kinetic friction.
4. The finite speed of pressure propagations, i.e. acoustic lag.

System lag errors show up as errors in the airspeed when the ambient static pressure is changing, such as when the aircraft is climbing or descending. The primary reason for this is the difference in volume between the pitot side of the system and the static side of the system. The volume differences can be due to excessively long static lines in large aircraft and also due to the static source's being connected to the altimeter and vertical velocity indicator as well as to the airspeed systems. Although a lag time constant ground test can be performed on the pressure systems and corrections made to the data, it is better if lag errors are eliminated by dynamic balancing.

7.1.11.1 Dynamic Balance

If it is necessary to calibrate the airspeed system while the aircraft is either descending or climbing, such as in glider flights, it is necessary to make sure that the total pressure and static lines are dynamically balanced. Generally this means that the volume of the static and the total sides of the airspeed system must be equal. Dynamic testing can also determine the maximum allowable climb/sink rate for a given pitot-static system. Install the complete airspeed system in a pressure chamber with the variable bleed rate corresponding to a maximum rate of climb or rate of sink expected. If the system fails, vary the volume of either the static or total side until the airspeed indicator no longer responds to the rate of change of altitude in the chamber.

7.1.11.2 Sideslip Effects

To minimize the effect of sideslip on the pitot-static system, static ports are often arranged on both sides of the aircraft and connected together prior to routing to the airspeed, altimeter, Mach and vertical speed system. On some aircraft only a single static source is used which can result in huge airspeed errors when constant heading sideslips are performed.

Inadvertent stalls have been performed in flight test when doing constant heading sideslips at low speed in the take-off and landing configurations when the pilot is using the aircraft's pitot-static system. To prevent such incidences a swivelling pitot-static system should be used for the instrumentation system with an airspeed and altimeter readout for the pilot.

7.1.12 Rotary-wing Aircraft

7.1.12.1 Ground Effect on Static Sources

The helicopter spends a great deal of its useful time in ground effect. The rotor downwash will have an effect on the pressure field around the helicopter, and the effect will diminish as the helicopter climbs to out of ground effect, where the effect will be minimal. The effect will be seen as a decrease in pressure altitude as power is applied, reaching a maximum deviation from the rotor stopped value as the helicopter just lifts off. The effect will depend on the weight of the helicopter and the wind, with the worst effect being on a calm day at very heavy weights. There is no point correcting for this as the helicopter should not be operating with respect to pressure altitude in this regime. Set the altimeter with the rotor at flat pitch, or stopped for greatest accuracy.

7.1.12.2 Low Airspeed Measurement Systems

For a long time helicopters and VSTOL aircraft have had to operate in the low airspeed environment (below 40 kts) with little or no airspeed information. When helicopters operated VFR only, this was not a problem. Low airspeed data was not seen as essential, but rather as desirable. However, as airspeed data is now often fed into many mission-critical systems, such as navigation, fire control systems, etc., this problem is receiving considerable attention.

Although conventional pitot-static systems work well for aircraft traveling forward at speeds greater than 30 to 40 kts, the problems associated with the accurate measurement of very low airspeeds (down to zero and beyond, i.e. rearwards flight) are currently the subject of many research projects. As well as all the problems already discussed for conventional systems, low airspeed measurement systems have two further major problems: the accurate transformation of very low dynamic pressures into airspeed signals, and the very complex airflows in which these systems have to operate, e.g., the recirculation effects from helicopter rotors.

7.1.12.3 Types of Low Airspeed Measurement Systems

LASSIE. The Low Airspeed Sensing System and Indicating Equipment developed by GEC-Marconi, is basically a swiveling pitot-static probe which works by aligning itself to the local airstream. At speed this system behaves very much like a conventional pitot-static sensor aligned with the aircraft longitudinal

axis. At low speed, however, where it would be in the influence of the rotor downwash, it uses the airflow velocity (probe angle and airspeed) to resolve the airspeed. In this way the problem of measuring very low pressures is eliminated, as in the hover (zero forward airspeed) the probe will be aligned to, and measuring the rotor downwash, which will be in the order of 40 kts. Once installed, such a system requires a series of characterization flights, usually against a pace vehicle, to obtain the calibration for the aircraft. This data is then loaded into the air data computer and will be valid as long as no changes are made to the airframe. Currently, this system is fitted to the AH-1S where it provides information to the fire control system for increased rocket and cannon accuracy, and to the EH-101 where it is being evaluated as a complete air data system.

LORAS. This system, produced by Pacer Systems Inc, works by rotating a pair of pitot heads, which point in opposite directions. The difference between the pressures indicated by the pitot heads is measured and combined with the aircraft's normal static source in an air data computer. In the hover the system will still detect airspeed (or wind) due to the rotation of the pitot heads. The rotation of the pitot heads allows both x- and y-components of the speed to be computed and, hence, sideslip or relative wind angle can be derived. As the pitot heads are "fixed" in the horizontal plane of the longitudinal axis the system will be subject to errors caused by changes in aircraft attitude and angle of attack.

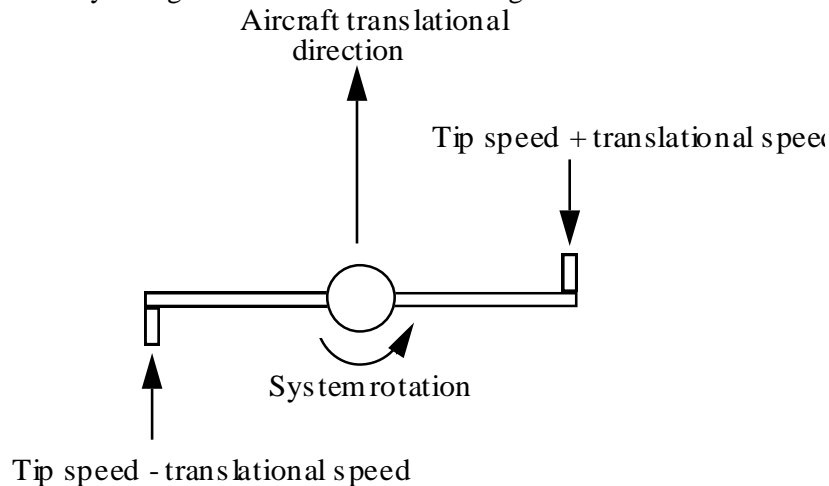


Figure **Error! No text of specified style in document.**-32 Schematic of LORAS

Ultrasonic methods, pitot tubes in rotor blade tips, and flush-mounted pressure sensors in rotor blades have all been attempted as means to obtain the low airspeed signals necessary. One additional method uses the control positions compared to a known position in the hover to generate airspeed information.

7.1.13 Pitot Static Requirements

7.1.13.1 14 CFR Part 23 Aircraft (Normal Category)

The FAA requires that an airspeed system indicate true airspeed (at sea level on a standard day) with minimum practical calibration error. The airspeed position error correction, may not exceed ± 3 percent or ± 5 knots, whichever is greater, throughout the following speed ranges: {CFR 23.1323(a)(b)}

(a) $1.3 V_{S1}$ to V_{MO}/M_{MO} or V_{NE} with flaps retracted.

(b) $1.3 V_{S1}$ to V_{FE} with flaps extended.

CFR 23.1325 addresses the static pressure systems. Essentially the static pressure system must be isolated from the cabin interior and leak checked. The maximum altimeter position error correction allowable at sea level is ± 30 feet per 100 knots speed between $1.3 V_{S0}$ with flaps extended and $1.8 V_{S1}$ with flaps retracted. However, the error need not be less than ± 30 feet.

7.1.13.2 14 CFR Part 25 Aircraft (Transport Category)

CFR Part 25 requirements for airspeed and altitude calibrations are very similar to Part 23 except for minor details on the inflight speed ranges required plus a requirement for calibration during the take-off ground roll. CFR 25.1323(b) states that the airspeed systems must be calibrated in during the acceleration take-off ground run from 0.8 of the minimum value of V_1 to the maximum value of V_2 with the flaps and power settings corresponding to the values determined in the establishment of the take-off path.

7.1.13.3 14 CFR Part 27 Rotorcraft (Normal Category)

CFR 27.1323 states that the maximum airspeed errors at sea level must not be more than ± 3 percent or ± 5 knots at forward speeds above 80% of the climb out speed. The airspeed system must also be calibrated at all speeds down to 20 kts. CFR 27.1325 does not specify a maximum error on altitude but does require that the difference between primary and or alternate static sources must not exceed 50 feet.

7.1.13.4 14 CFR Part 29 Rotorcraft (Transport Category)

CFR 29.1323(b) states that the airspeed system must be calibrated to determine system errors excluding instrument errors at speeds above 20 kts and over an appropriate range of speeds for flight conditions of climb and autorotation.

CFR 29.1323(c)(2) for Category A Rotorcraft states that the airspeed system errors, excluding instrument errors may not exceed three percent or five knots whichever is greater at speeds above 80 percent of take-off safety speed (V_{TOSS}) and at speeds within the range of ± 10 kts of V_{TOSS} the system errors may not exceed 10 kts. For Category B rotorcraft the maximum allowable system errors are ± 3 percent or ± 5 kts whichever is greater in level flight at speeds above 80 percent of the climb out speed attained at 50 feet when complying with CFR 29.63 Category B take-off requirements.

CFR 29.1325(b) states that the maximum allowable error between the primary and the alternate static sources is 50 feet. CFR 29.1325 (f) states that the altimeter system error may not exceed ± 30 feet per 100 kts speed. As in Parts 23 and 25, the error need not be less than ± 30 feet.

7.1.13.5 Military Requirements

MIL-SPEC-P-26292C requires that the non-dimensional static source error must be within curve A of Figure Error! No text of specified style in document.-33 for all conditions. Furthermore, an air data computer is required if the error is not less than curve B.

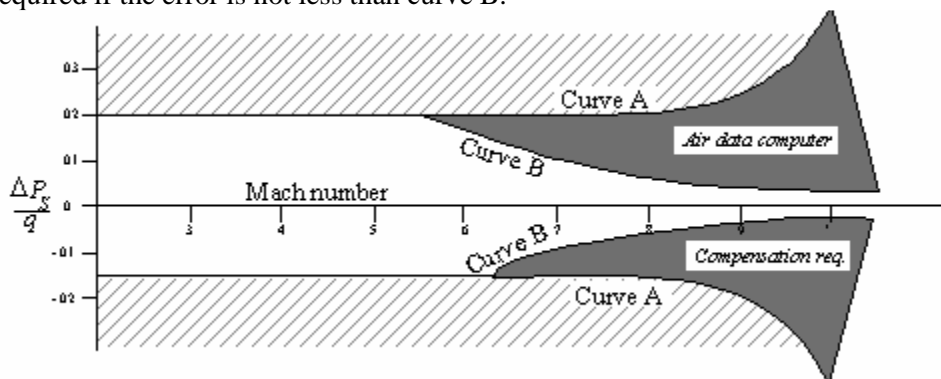


Figure Error! No text of specified style in document.-33 MIL-SPEC-P-26292 C Position Error Tolerance

A completely different military document, MIL-I-6115A, requires airspeed and altimeter errors to be less than those shown in Table 7.4. In addition, the instruction specifies limits on errors with sideslips and use of alternate controls such as speed brakes. Interestingly, the FAA puts no limits on errors in sideslips or during the use of alternate controls.

Configuration	Speed Range	Airspeed	Altimeter
Approach	$V_S \rightarrow V_S + 50$	± 4.0 kts	25ft per 100 kts,
Clean/Cruise Power	Speed for best range	$\pm 1/2\%$ V_i	25ft per 100 kts,
Clean	Stall to V_N	± 4.0 kts	25ft per 100 kts,
Dive	Max speed w/dive brakes	± 6.0 kts	50ft per 100 kts,

Table 7.4 MIL-I-6115A Tolerances on Airspeed and Altimeter Readings

7.1.14 Summary

Different kinds of airspeed information are required for different applications. *True* airspeed is useful for navigation and during flight testing of certain flutter modes, and engine controls. Dimensional analysis shows that incompressible dynamic pressure is the key parameter for evaluating aerodynamic forces. This parameter is directly proportional to *equivalent* airspeed squared. Aircraft structural loads and the hinge moments on the controls (which in a reversible control system directly affect the pilot's ability to maneuver the aircraft) are also a direct function of V_e^2 .

The *calibrated* airspeed given in Equation (7.12) is a more practical speed for a pilot. Since it is not a function of temperature, V_C test day is the same as V_C standard day. Since compressibility effects are negligible near stall, the aircraft stall speed is defined by V_c . It is not a significant function of altitude unless changes in Reynolds number change the maximum lift coefficient of the wing.

Dimensional analysis shows that *Mach* number is also an important parameter to know precisely. Although defined as the ratio between true velocity and the speed of sound, it is not affected by temperature. Test day Mach number is the same as standard day Mach number. Finally, the reader should note this text defines ΔV_{pc} and ΔH_{pc} as corrections but some other documents define them as errors (such as some MILSPEC's).

7.1.14.1 References

1. USAF Test Pilot School, *Flight Test Handbook*, Edwards AFB, August, 1979.
2. US Navy Test Pilot School, *Fixed Wing Performance Theory and Flight Test Technique*, USNTPS -FTM- No. 103 Patuxant River, MD, 1975.
3. Owen E. and Pankhurst R.C., *The Measurement of Air Flow*, Pergamon Press, 1966.
4. Army Air Forces Technical Report No. 5069, "Performance Flight Testing Methods in Use by the Flight Section", January 15, 1944.
5. CFR, Part 23, "Airworthiness Standards; Normal, Utility and Acrobatic Category Airplanes".
6. FAA Advisory Circular 23-8B, Flight Test Guide for Certification of Part 23 Airplanes, Appendix 9, March 14, 2003.
7. FAA Advisory Circular 25-7A, Flight Test Guide for Certification of Transport Category Airplanes, August 31, 1998.
8. "Pitot and Static Pressure Systems, Installation and Inspection of", MIL-P-26292C (U.S.A.F.), December 3, 1969.
9. U.S.A.F. Flight Test Center, *Flight Test Engineering Handbook*, FTC-TR-6273, Edwards AFB, January, 1966.
10. "Is Your Speed True?" David Fox, *KITPLANES*, February, 1995.
11. "A Flight Test Technique Using GPS for Position Error Correction Testing", Gregory Lewis, *COCKPIT*, Society of Experimental Test Pilots Quarterly Publication, Jan-Feb-Mar, 1997.
12. "Using GPS to Accurately Establish True Airspeed", David Gray, unpublished paper available at www.ntps.edu/downloads.htm, June 1998.
13. NACA Report 318, 1927. Speed and Deceleration Trails of the U.S.S. Los Angeles.
14. Army Report AMCP 701-204 Performance Flight Test Methods.

Volume 2 – Aerodynamics for Flight Testers

Appendix A

Glossary

Table of Contents

A.1 Abbreviations.....	2
A.2 Greek Symbols.....	4
A.3 Subscripts.....	4
A.4 Greek Alphabet.....	4
A.5 Prefix Multiples / Prefix Symbol	4
A.6 Constants.....	6
A.7 Useful Relations.....	6
A.8 Conversions.....	7

A.1 Abbreviations

a	speed of sound	C_Y	side force coefficient
a	linear acceleration (ft/sec ² or m/sec ²)	$C_{y\beta}$	side force due to sideslip coefficient
a	lift curve slope	$C_{y\delta_r}$	side force due to rudder coefficient
AC	aerodynamic center	D	drag (lbs)
AGL	above ground level	D	diameter
AOA	angle of attack	ΔD	drag increment
ATC	air traffic control	E	energy
AR	aspect ratio = b^2 / S	E	lift-to-drag ratio (C_L/C_D)
a_x	longitudinal acceleration	e	Oswald efficiency factor
a_y	lateral acceleration	EGT	exhaust gas temperature
b	span of wing (feet)	E_{max}	maximum lift-to-drag ratio
BHS	brake horse power	EPR	engine pressure ration
BSFC	brake specific fuel consumption	E_s	specific energy
c	brake specific fuel consumption (BSFC)	ESHP	equivalent shaft horsepower
c	aerodynamic chord of a wing	deg	degrees
\bar{c}	mean aerodynamic chord (MAC) of a wing	db	decibels
$^{\circ}C$	degrees centigrade... see T	f	frequency hertz (originally cycles per seconds)
C_D	coefficient of drag	$^{\circ}F$	degrees Fahrenheit
C_{D_i}	induced drag coefficient	FAA	Federal Aviation Administration
C_{D_o}	zero lift drag coefficient (also parasitic drag coefficient for symmetric wing)	F_a	aileron force
C_f	coefficient of friction	F_e	elevator force
cg	center of gravity (normally in % MAC)	F_{ex}	excess thrust
CH	hinge moment coefficient	F_r	rudder force
C_M	moment coefficient	F_g	gross thrust
C_m	pitching moment coefficient	F_n	net thrust, force pounds = $(550 \eta_p \text{ SHP})/V_T$
C_L	dimensionless coefficient	F_n	net thrust
C_l	rolling moment coefficient	F_n/δ	corrected thrust parameter
CLHQ	closed loop handling qualities	F_g	gross thrust
C_{l_p}	roll damping coefficient	F.S.	fuselage station
C_{l_r}	roll moment due to yaw rate coefficient	ft	feet
$C_{l_{\beta}}$	(dihedral) rolling moment due to sideslip	ft-lb	English unit of work foot-pound..
$C_{l_{\delta}}$	aileron power coefficient	fwd	forward
C_m	pitching moment coefficient	G	gravitational constant (also g_o 32.174 ft/sec ²)
C_{m_a}	longitudinal static stability coefficient	g_o	acceleration due to gravity at sea level
C_{m_q}	pitch damping coefficient	g	acceleration due to gravity at altitude
$C_{m_{\delta_e}}$	elevator power coefficient	H	altitude
C_n	yawing moment coefficient	h	% MAC
$C_{n\beta}$	directional stability coefficient	H_c	calibrated altitude (assumed to be pressure altitude in flight test)
$C_{n_{\delta_a}}$	adverse yaw coefficient	$h\bar{c}$	mean aerodynamic cord moment arm (ft or in)
$C_{n_{\delta_r}}$	rudder power coefficient	H_D	density altitude
C_{n_r}	yaw damping coefficient	Hg	mercury
cnst	constant	H_i	indicated altitude
CP	center of pressure	h_m	stick-fixed maneuver point (%MAC)
C_p	propeller power coefficient	h'_m	stick-fixed maneuver point (%MAC)
		h_n	stick-fixed neutral point (%MAC)
		h'_n	stick-free neutral point (%MAC)
		hr	hour
		H_z	hertz
		ΔH_{ic}	altimeter instrument correction
		ΔH_{pc}	altimeter position error correction

IAS	indicated airspeed	N_g	lateral load factor (g's)
IFR	instrument flight rules	NM,nm	nautical mile (6080 feet)
ILS	instrument landing system	N_x	longitudinal load factor (g's)
in	inch	N_y	normal load factor (g's)
INS	inertial navigation system	N_1	low pressure compressor speed
I_x, I_y, I_z	moments of inertia	N_2	high pressure compressor speed
I_{xy}, I_{xz}, I_{yz}	products of inertia	OAT	outside air temperature
J	propeller advance ratio	OEI	one engine inoperative
J	joules energy, (Newton-Meter)	p	aircraft roll rate (degrees/sec)
$^{\circ}K$	degrees Kelvin	P	pressure (N/m ² pounds per square inch)
K	temperature probe recovery factor	P_a	ambient pressure
k	constant	PIO	pilot induced oscillations
KCAS	knots calibrated airspeed	P_{iw}	total thrust horsepower required at sea level standard day and standard weight
KEAS	knots equivalent airspeed	PLF	power for level flight
kg	kilogram, metric unit of mass	P_o	standard atmospheric pressure (2116.22 lb/ft ²)
KIAS	knots indicated airspeed	P_p	pitot pressure
Kt	knots	P_s	static pressure
KTAS	knots true airspeed	Prop	propeller
k_1, k_2, k_3	constants	PSI	pounds per square inch
L	rolling moment	P_T	total pressure
L	Lift (lbs)	ΔP_P	pitot pressure error
l	length	ΔP_s	static pressure error
lat	lateral	Q	engine torque
lb	pound	q	dynamic pressure = $0.5\rho V^2$
lb _f	english unit of force, often just lb (pound)	q	aircraft pitch rate
lb _m	english unit of mass, often just lb (slug)	q_c	impact pressure ($P_t - P_a$)
\ln	natural logarithm	R	perfect gas constant
l_t	distance from cg to tail's aerodynamic center	R	range
L_{δ_a}	rolling moment due to aileron deflection	r	aircraft yaw rate (degrees/sec)
L/D	lift-to-drag ration	r	earth radius
M	Mach number	$^{\circ}R$	degrees Rankin = $^{\circ}F + 459.67$
M	moment (ft-lbs)	rad	radians
M	pitching moment	RAF	resultant aerodynamic force
m	meter (length)	RAT	ram air turbine
m	mass	Re	Reynolds number (dimensionless)
M_{cr}	critical Mach number	RF	range factor
M_d	drag divergence Mach number	RPM	revolution per minute (a.k.a N)
MGC	mean geometric chord	RTO	refused takeoff
M_{ic}	instrument-corrected Mach number (not corrected for position error)	R/C	rate of climb
Mil Spec	military specification	S	wing area (ft ² or m ²)
min	minute (time)	S_a	horizontal distance between liftoff and specified height or between specified height and touchdown.
MP	manifold pressure	SE	specific endurance
N	Newton force	sec	seconds (time)
N	rotational speed (RPM)	SFC	specific fuel consumption
N	yawing moment	S_g	ground roll distance
n	load factor (g's)	SHP	shaft horsepower
NACA	National Advisory Committee for Aeronautics		

SL	sea level	V_{LO}	max speed while operating landing gear
SR	specific range	V_{LOF}	lift off speed
S_T	total takeoff or landing distance ($S_a + S_g$)	V_{mc}	minimum directional control speed
S_t	tail area	V_{mca}	minimum directional control speed in the air
STOL	short takeoff and landing	V_{mcg}	minimum directional control speed on the ground
S/N	serial number	V_{mu}	minimum unstuck speed
T, t	time (sec)	V_W	wind velocity
T	period of oscillation	V_{NE}	never exceed
T	temperature	V_{no}	max structural cruising speed
t	thickness	V_{opt}	optimum velocity for endurance flight
T_a	ambient temperature	VOR	omnidirectional range
TAS	true airspeed	V_{Pmin}	velocity for minimum power
T_{as}	standard temperature at altitude	$V_{Pmin,SL}$	velocity for minimum power at sea level
TED	trailing edge down	V_R	rotation speed
TEU	trailing edge up	V_S	stall speed
TER	trailing edge right	V_{S0}	stall speed in landing configuration
TEL	trailing edge left	V_{S1}	stall speed in some defined configuration
TD	touchdown	VSTOL	vertical/short takeoff and landing
THP	Thrust Horsepower	V_T	True airspeed
THP_{alt}	horsepower required at altitude	VTOL	vertical takeoff & landing
THP_{max}	maximum horsepower available	V_x	speed for best angle of climb
THP_{min}	minimum horsepower required	V_y	speed for best rate of climb
THP_{SL}	horsepower required at sea level	V_2	takeoff safety speed
TIT	turbine inlet temperature	V_1	takeoff decision speed
T/O	takeoff	ΔV_c	scale altitude correction to airspeed
T_o	standard sea level temperature (59.0° F, 15°C)	ΔV_{ic}	instrument correction to airspeed indicator
TSFC	thrust specific fuel consumption	ΔV_{pc}	correction for airspeed position error
T_t	total temperature	V_{mo}/M_{mo}	maximum operating limit speed
T/W	thrust to weight ratio	W	weight
u	velocity along aircraft's x-axis	w	component of velocity along aircraft's Z-axis
UHF	ultra high frequency	\dot{W}_f	fuel weight
v	velocity along aircraft's lateral axis	\dot{W}_f	fuel flow (lb/sec) also $\dot{\omega}_f$
V_A	design maneuvering speed	$\frac{\dot{W}_f}{\delta\sqrt{\theta}}$	corrected fuel flow parameter
V_B	design speed for max gust intensity	W/δ	weight-to-pressure ratio
V_b	buffet airspeed	X	aircraft longitudinal axis, a line running through the nose & tail
V_{br}	velocity for best range	X_{ac}	distance from leading edge to aerodynamic force along y-axis
V_T	true airspeed	Y	aircraft lateral axis, a line running the wingtip
V_c	calibrated airspeed	y	aircraft vertical or yaw axis, a line perpendicular to the longitudinal and lateral axes
V_D	design diving speed	z	when positioned over variable means a time derivative, single = velocity, double = acceleration
V_e	equivalent velocity	•	infinity, or freestream condition
V_{FE}	maximum flap extended speed	∞	
VFR	visual flight rules		
V_g	ground speed		
VHF	very high frequency		
V_i	indicated airspeed		
V_{ic}	indicated airspeed corrected for instrument error		
V_{iw}	velocity at sea level std day and std weight		
V_{LE}	max speed with landing gear extended		

A.2 Greek Symbols

α	angle of attack (degrees or radians)
α_τ	tail angle of attack
β	angle of sideslip (degrees)
γ	flight path angle relative to horizontal
γ	specific heat ratio (1.4 for air)
δ	relative pressure ratio (P_a/P_o)
δ_α	aileron deflection angle
δ_r	rudder deflection angle
δ_e	elevator deflection angle
ε	downwash angle at tail (degrees)
ζ	damping ratio
η	propeller efficiency
θ	body axis/pitch angle (degree)
θ	relative temperature ratio, T_a/T_o
ι	angle of incidence
ι_F	thrust angle of incidence
ι_T	horizontal tail angle of incidence
λ	pressure lag constant
Λ	wing sweep angle
μ	coefficient of absolute viscosity = $\rho\nu$
μ	Mach cone angle
ν	kinematic viscosity = μ/g
π	nondimensional parameter
ρ	air density
ρ_a	ambient air density
ρ_o	standard atmospheric density (slugs/ft ³)
σ	air density ratio (ρ_a/ρ_o)
σ_c	ceiling density ratio
σ_{cr}	critical density
τ	shear stress (pounds per square inch) psi
τ_R	Roll Mode Time Constant (sec)
ϕ	bank angle (degrees)
ψ	aircraft heading (degrees)
ω	frequency
ω_d	damped natural frequency
ω_n	natural undamped frequency

A.3 Subscripts

a	aileron
a	ambient
alt	at test altitude
avg	average
c	calibrated
e	elevator
e	equivalent

E	endurance leg of mission
F	final
I	initial
i	inbound leg of mission
i	indicated
ic	instrument corrected
l	subscript for coefficient of rolling moment
m	mission conditions
m	subscript for coefficient of pitching moment
n	subscript for coefficient of yawing moment
O	outbound leg of mission
o	sea-level standard day
o	sea-level
r	reserve leg of mission
r	rudder
S	standard day
s	standard day at altitude
SL	sea level
T	True
t	test day

A.4 Greek Alphabet

A	α	Alpha	N	ν	Nu
B	β	Beta	Ξ	ξ	Xi
Γ	γ	Gamma	O	o	Omicron
Δ	δ	Delta	Π	π	Pi
E	ε	Epsilon	P	ρ	Rho
Z	ζ	Zeta	Σ	σ	Sigma
H	η	Eta	T	τ	Tau
Θ	θ	Theta	Y	υ	Upsilon
I	ι	Iota	Φ	ϕ	Phi
K	κ	Kappa	X	χ	Chi
Λ	λ	Lambda	Ψ	ψ	Psi
M	μ	Mu	Ω	ω	Omega

A.5 Prefix Multiples / Prefix Symbol

10^{18}	exa	E
10^{15}	peta	P
10^{12}	tera	T
10^9	giga	G
10^6	mega	M
10^3	kilo	K
10^{-2}	deci	d
10^{-3}	milli	m
10^{-6}	micro	μ
10^{-9}	nano	n
10^{-12}	pico	p

10^{-15} femto f
 10^{-18} atto a

A.6 Constants

$$P_o = 2116.22 \text{ lb/ft}^2 = 14.696 \text{ lb/in}^2 = 29.921 \text{ in Hg} = 1013 \text{ mb} = 760 \text{ mm Hg}$$

$$T_o = 288.15 \text{ }^\circ\text{K} = 518.67 \text{ }^\circ\text{R} = 58.67 \text{ }^\circ\text{F} = 15 \text{ }^\circ\text{C}$$

$$\rho_o = .002377 \text{ slugs/ft}^3 = .00004426 \text{ lbm/in}^3 = 1,225 \text{ kg/m}^3$$

$$a_o = 1116.45 \text{ ft/sec} = 661 \text{ KTAS} = 761.14 \text{ mph}$$

$$R = 1716 \text{ lb(ft)/slugs(}^\circ\text{R)} = 3089.7 \text{ lb(ft)/slugs(}^\circ\text{K)}$$

$$g = 32.174 \text{ ft/sec}^2$$

$$\gamma = 1.4 \text{ for air}$$

A.7 Useful Relations

$$C_L = L/qS \quad Re = \rho_a V_T l/\mu \quad m = 1/\pi A P \epsilon \quad C_F = f(M, Re, \alpha) \quad \text{Perfect gas law: } P = \rho RT$$

$$M = \frac{V_T}{a} = \left(\left[\left[\frac{P_t - P_a}{P_a} + 1 \right]^{2/7} - 1 \right] 5 \right)^{1/2} \quad \mu = [338.5 + .575(^{\circ}\text{F})] \times 10^{-9}$$

$$a = a_o \sqrt{\theta} = \sqrt{\gamma RT} = 49.1 \sqrt{^{\circ}\text{R}} (\text{ft/sec}) = 38.967 \sqrt{^{\circ}\text{K}} (\text{kts})$$

$$C_D = \frac{D}{qs} = C_{D_o} + C_{D_i} \quad q = 1/2 \rho_o V_e^2 = 1/2 \rho_a V_T^2 \quad Cp = \frac{\Delta P}{q} = \frac{P - P_\infty}{\frac{1}{2} \rho_\infty V_\infty^2}$$

$$\delta = \sigma \theta \quad \text{where } \delta = P_a/P_o, \quad \sigma = \rho_a/\rho_o, \quad \theta = T_a/T_o$$

Power = Force x Velocity or Torque x Angular Velocity

$$C_D = C_{D_o} \div \sqrt{1 - M^2} \quad (\text{below } \sim 7M) \quad V_T = [V_i + \Delta V_{ic} + \Delta V_c + \Delta V_{pc}] \div \sqrt{\sigma}$$

A.8 Conversions

	From	To	Multiply by
Length	meter	ft	3.28084
	centimeter	inch	0.3937
	feet	in	12
	kilometer	ft	3280.84
	kilometer	mile	0.621371
	kilometer	m	10 ³
	mile	km	1.60934
	mile (statute)	ft	5280
	Mile (Nautical)	ft	6076
	yard	in	36
yard	m	0.9144	
Velocity	ft/sec	knots	1.689
	ft/sec	mph	1.467
	m/sec	ft/sec	3.2808
	m/sec	knots	1.943
	m/sec	mph	2.23
	mph	km/hr	0.9113
	mph	knots	1.151
Mass	gram	pound	0.0022046
	kilogram	pound	2.20462
	pound	ounce	16
	pound	kilogram	0.453
Density	kg/m ³	slug/ft ³	0.001935
Pressure	atm	inHg	29.92
	atm	psi	14.96
	atm	pa (n/m ²)	101330
	bar	inHg	29.53
	pa	atm	9.8692E-06
	pa	inHg	0.0002953
	pa	psi	14.504
Angular Velocity	deg/sec	rpm	0.166
	rad/sec	deg/sec	57.29
Angular Accel.	deg/sec ²	rpm ²	10
	rad/sec ²	deg/sec ²	57.29
Power	Horse Power (HP)	foot-lbs/(sec)	550
	Horse Power (HP)	watts	745.7
Area	square foot	square meter	0.092
	square inch	square centimeter	6.45
	square mile	square kilometer	2.589
Volume	cubic foot	cubic meter	0.0283

	cubic inch	cubic centimeter	16.4
	quarts	pints	2
	From	To	Multiply by
Volume	US Gallon	cubic feet	0.134
	US Gallon	liters	3.785
	US Gallon	quarts	4
Force	kilogram	Newton	9.8
	Newton	pounds	0.224
	Newton	poundals	7.233
	Newton	kilogram	0.101
	pound	poundals	32.174
	pound	slugs	0.03108
	pound	Newton	4.44
Energy	B.T.U	joules	1050
	B.T.U	kilowatt hours	0.000293
	B.T.U	foot-lbs	778
	B.T.U	calories	251.8
	foot-lbs	B.T.U	0.001285
	foot-lbs	kilowatt hours	0.00000376
	joules	B.T.U	0.000947
	joules	kilowatt hours	0.0000027
	joules	foot-lbs	0.737

Volume 2 – Aerodynamics for Flight Testers

Appendix B

Standard Atmosphere Table

Table of Contents

B.1 Troposphere - below 36,089 ft	1
B.2 Stratosphere	1
B.3 Table B – 1 Standard Atmosphere	1

B.1 Troposphere - below 36,089 ft

$$\theta = 1 - (L/T_o)h \quad \sigma = \theta^{n-1} \quad \delta = \theta^n$$

where $L = 0.0019812 \text{ K /ft}$ $T_o = 288.15 \text{ K}$ $n = 5.25585$ $h = \text{altitude}$

B.2 Stratosphere

Between 36,089 ft and 65,616 ft the standard day temperature is a constant 216.66°K, therefore:

$$\theta = 0.7519 \quad \sigma = 0.29707e^{-0.00004806(h - 36,089)} \quad \delta = 0.223358e^{-0.00004806(h - 36,089)}$$

$P_o = 2116.22 \text{ lb/ft}^2 = 14.696 \text{ lb/in}^2 = 29.921 \text{ in Hg} = 1013.25 \text{ mb} = 760 \text{ mm Hg}$
 $T_o = 288.15 \text{ K} = 518.67 \text{ }^\circ\text{R} = 58.67 \text{ }^\circ\text{F} = 15.15 \text{ }^\circ\text{C}$
 $\rho_o = 0.002377 \text{ slugs/ft}^3 = 0.07647 \text{ lbm/in}^3 = 1.225 \text{ kg/m}^3$
 $a_o = 1116.45 \text{ ft/s} = 340.29 \text{ m/s} = 661 \text{ KTAS} = 761.2 \text{ mph}$
 $a = a_o \sqrt{\theta}$

B.3 Table B – 1 Standard Atmosphere

Altitude (ft)	$\delta = P_o/P_o$	$\theta = T_o/T_o$	$\sigma = \rho_o/\rho_o$	$\sqrt{\sigma}$	T (K)	a (kts)
-500	1.0182	1.0034	1.0147	1.0073	289.2	662.6
-400	1.0145	1.0028	1.0118	1.0059	289	662.4
-300	1.0109	1.0021	1.0088	1.0044	288.8	662.2
-200	1.0072	1.0014	1.0059	1.0029	288.6	661.9
-100	1.0036	1.0007	1.0029	1.0015	288.4	661.7
0	1	1	1	1	288.2	661.5
100	0.9964	0.9993	0.9971	0.9985	288	661.2
200	0.9928	0.9986	0.9942	0.9971	287.8	661
300	0.9892	0.9979	0.9913	0.9956	287.6	660.8
400	0.9856	0.9972	0.9883	0.9942	287.4	660.8
500	0.9821	0.9966	0.9855	0.9927	287.2	660.3
600	0.9785	0.9959	0.9826	0.9912	287	660.1
700	0.975	0.9952	0.9797	0.9898	286.8	659.9
800	0.9714	0.9945	0.9768	0.9883	286.6	659.7
900	0.9679	0.9938	0.9739	0.9869	286.4	659.4
1,000	0.9644	0.9931	0.9711	0.9854	286.2	659.2
1,100	0.9609	0.9924	0.9682	0.984	286	659
1,200	0.9574	0.9917	0.9654	0.9825	285.8	658.7
1,300	0.9539	0.9911	0.9625	0.9811	285.6	658.5
1,400	0.9504	0.9904	0.9597	0.9796	285.4	658.3

Altitude (ft)	$\delta = P_a/P_o$	$\theta = T_a/T_o$	$\sigma = \rho_a/\rho_o$	$\sqrt{\sigma}$	T (K)	a (kts)
1,500	0.947	0.9897	0.9568	0.9782	285.2	658.1
1,600	0.9435	0.989	0.954	0.9767	285	657.8
1,700	0.9401	0.9883	0.9512	0.9753	284.8	657.6
1,800	0.9366	0.9876	0.9484	0.9738	284.6	657.4
1,900	0.9332	0.9869	0.9456	0.9724	284.4	657.1
2,000	0.9298	0.9862	0.9428	0.971	284.2	656.9
2,100	0.9264	0.9856	0.94	0.9695	284	656.7
2,200	0.923	0.9849	0.9372	0.9681	283.8	656.5
2,300	0.9196	0.9842	0.9344	0.9667	283.6	656.2
2,400	0.9163	0.9835	0.9316	0.9652	283.4	656
2,500	0.9129	0.9828	0.9289	0.9638	283.2	655.8
2,600	0.9096	0.9821	0.9261	0.9623	283	655.5
2,700	0.9062	0.9814	0.9234	0.9609	282.8	655.3
2,800	0.9029	0.9807	0.9206	0.9595	282.6	655.1
2,900	0.8996	0.9801	0.9179	0.958	282.4	654.8
3,000	0.8962	0.9794	0.9151	0.9566	282.2	654.6
3,100	0.8929	0.9787	0.9124	0.9552	282	654.4
3,200	0.8897	0.978	0.9097	0.9538	281.8	654.2
3,300	0.8864	0.9773	0.9069	0.9523	281.8	653.9
3,400	0.8831	0.9766	0.9042	0.9509	281.4	653.7
3,500	0.8798	0.9759	0.9015	0.9495	281.2	653.5
3,600	0.8766	0.9752	0.8988	0.9481	281	653.2
3,700	0.8733	0.9746	0.8961	0.9466	280.8	653
3,800	0.8071	0.9739	0.8934	0.9452	280.6	652.8
3,900	0.8669	0.9732	0.8908	0.9438	280.4	652.5
4,000	0.8637	0.9725	0.8881	0.9424	280.2	652.3
4,100	0.8605	0.9718	0.8854	0.941	280	652.1
4,200	0.8573	0.9711	0.8828	0.9396	279.8	651.9
4,300	0.8541	0.9704	0.8801	0.9381	279.6	651.6
4,400	0.8509	0.9697	0.8775	0.9367	279.4	651.4
4,500	0.8477	0.9691	0.8748	0.9353	279.2	651.2
4,600	0.8446	0.9684	0.8722	0.9339	279	650.9
4,700	0.8414	0.9677	0.8695	0.9325	278.8	650.7
4,800	0.8383	0.967	0.8669	0.9311	278.7	650.5
4,900	0.8352	0.9663	0.8643	0.9297	278.5	650.2
5,000	0.8321	0.9656	0.8617	0.9283	278.3	650
5,100	0.8289	0.9649	0.8591	0.9269	278.1	649.8
5,200	0.8258	0.9642	0.8565	0.9255	277.9	649.5
5,300	0.8228	0.9636	0.8539	0.9241	277.7	649.3
5,400	0.8197	0.9629	0.8513	0.9226	277.5	649.1

Altitude (ft)	$\delta = P_a/P_o$	$\theta = T_a/T_o$	$\sigma = \rho_a/\rho_o$	$\sqrt{\sigma}$	T (K)	a (kts)
5,500	0.8166	0.9622	0.8487	0.9212	277.3	648.8
5,600	0.8135	0.9615	0.8461	0.9198	277.1	648.6
5,700	0.8105	0.9608	0.8435	0.9184	276.9	648.4
5,800	0.8074	0.9601	0.841	0.917	276.7	648.2
5,900	0.8044	0.9594	0.8384	0.9157	276.5	647.9
6,000	0.8014	0.9587	0.8359	0.9143	276.3	647.7
6,100	0.7984	0.9581	0.8333	0.9129	276.1	647.5
6,200	0.7954	0.9574	0.8308	0.9115	275.9	647.2
6,300	0.7924	0.9567	0.8282	0.9101	275.7	647
6,400	0.7894	0.956	0.8257	0.9087	275.5	646.8
6,500	0.7864	0.9553	0.8232	0.9073	275.3	646.5
6,600	0.7834	0.9546	0.8207	0.9059	275.1	646.3
6,700	0.7805	0.9539	0.8182	0.9045	274.9	646.1
6,800	0.7775	0.9532	0.8156	0.9031	274.7	645.8
6,900	0.7746	0.9526	0.8131	0.9017	274.5	645.6
7,000	0.7716	0.9519	0.8107	0.9004	274.3	645.4
7,100	0.7687	0.9512	0.8082	0.899	274.1	645.1
7,200	0.7658	0.9505	0.8057	0.8976	273.9	644.9
7,300	0.7629	0.9498	0.8032	0.8962	273.7	644.7
7,400	0.76	0.9491	0.8007	0.8948	273.5	644.4
7,500	0.7571	0.9484	0.7983	0.8935	273.3	644.2
7,600	0.7542	0.9477	0.7958	0.8921	273.1	644
7,700	0.7514	0.9471	0.7934	0.8907	272.9	643.7
7,800	0.7485	0.9464	0.7909	0.8893	272.7	643.5
7,900	0.7456	0.9457	0.7885	0.888	272.5	643.3
8,000	0.7428	0.945	0.786	0.8866	272.3	643
8,100	0.74	0.9443	0.7836	0.8852	272.1	642.8
8,200	0.7371	0.9436	0.7812	0.8838	271.9	642.6
8,300	0.7343	0.9429	0.7787	0.8825	271.7	642.3
8,400	0.7315	0.9422	0.7763	0.8811	271.5	642.1
8,500	0.7287	0.9416	0.7739	0.8797	271.3	641.9
8,600	0.7259	0.9409	0.7715	0.8784	271.1	641.6
8,700	0.7231	0.9402	0.7691	0.877	270.9	641.4
8,800	0.7203	0.9395	0.7667	0.8756	270.7	641.2
8,900	0.7176	0.9388	0.7644	0.8743	270.5	640.9
9,000	0.7148	0.9381	0.762	0.8729	270.3	640.7
9,100	0.7121	0.9374	0.7596	0.8715	270.1	640.4
9,200	0.7093	0.9367	0.7572	0.8702	269.9	640.2
9,300	0.7066	0.9361	0.7549	0.8688	269.7	640
9,400	0.7039	0.9354	0.7525	0.8675	269.5	639.7

Altitude (ft)	$\delta = P_a/P_o$	$\theta = T_a/T_o$	$\sigma = \rho_a/\rho_o$	$\sqrt{\sigma}$	T (K)	a (kts)
9,500	0.7012	0.9347	0.7502	0.8661	269.3	639.5
9,600	0.6985	0.934	0.7478	0.8648	269.1	639.3
9,700	0.6958	0.9333	0.7455	0.8634	268.9	639
9,800	0.6931	0.9326	0.7431	0.8621	268.7	638.8
9,900	0.6904	0.9319	0.7408	0.8607	268.5	638.6
10,000	0.6877	0.9312	0.7385	0.8594	268.3	638.3
11,000	0.6614	0.9244	0.7156	0.8459	266.4	636
12,000	0.636	0.9175	0.6932	0.8326	264.4	633.6
13,000	0.6113	0.9106	0.6713	0.8194	262.4	631.2
14,000	0.5875	0.9037	0.65	0.8062	260.4	628.8
15,000	0.5644	0.8969	0.6293	0.7933	258.4	626.4
16,000	0.542	0.89	0.609	0.7804	256.5	624
17,000	0.5203	0.8831	0.5892	0.7676	254.5	621.6
18,000	0.4994	0.8762	0.5699	0.7549	252.5	619.2
19,000	0.4791	0.8694	0.5511	0.7424	250.5	616.8
20,000	0.4596	0.8625	0.5328	0.7299	248.5	614.3
21,000	0.4406	0.8556	0.515	0.7176	246.6	611.9
22,000	0.4223	0.8487	0.4976	0.7054	244.6	609.4
23,000	0.4047	0.8419	0.4807	0.6933	242.6	606.9
24,000	0.3876	0.835	0.4642	0.6813	240.6	604.4
25,000	0.3711	0.8281	0.4481	0.6694	238.6	601.9
26,000	0.3552	0.8212	0.4325	0.6577	236.6	599.4
27,000	0.3398	0.8144	0.4173	0.646	234.7	596.9
28,000	0.325	0.8075	0.4025	0.6344	232.7	594.4
29,000	0.3107	0.8006	0.3881	0.623	230.7	591.9
30,000	0.297	0.7937	0.3741	0.6117	228.7	589.3
31,000	0.2837	0.7869	0.3605	0.6005	226.7	586.7
32,000	0.2709	0.78	0.3473	0.5893	224.8	584.2
33,000	0.2586	0.7731	0.3345	0.5783	222.8	581.6
34,000	0.2467	0.7662	0.322	0.5675	220.8	579
35,000	0.2353	0.7594	0.3099	0.5567	218.8	576.4
36,000	0.2243	0.7525	0.2981	0.546	216.8	573.8
37,000	0.2138	0.7518	0.2843	0.5332	216.7	573.6
38,000	0.2037	0.7519	0.271	0.5205	216.7	573.6
39,000	0.1942	0.7519	0.2582	0.5082	216.7	573.6
40,000	0.1851	0.7519	0.2461	0.4961	216.7	573.6
41,000	0.1764	0.7519	0.2346	0.4843	216.7	573.6
42,000	0.1681	0.7519	0.2236	0.4728	216.7	573.6
43,000	0.1602	0.7519	0.2131	0.4616	216.7	573.6

Altitude (ft)	$\delta = P_a/P_o$	$\theta = T_a/T_o$	$\sigma = \rho_a/\rho_o$	$\sqrt{\sigma}$	T (K)	a (kts)
44,000	0.1527	0.7519	0.2031	0.4506	216.7	573.6
45,000	0.1455	0.7519	0.1935	0.4399	216.7	573.6
46,000	0.1387	0.7519	0.1844	0.4295	216.7	573.6
47,000	0.1322	0.7519	0.1758	0.4193	216.7	573.6
48,000	0.126	0.7519	0.1675	0.4093	216.7	573.6
49,000	0.1201	0.7519	0.1597	0.3996	216.7	573.6
50,000	0.1144	0.7519	0.1522	0.3901	216.7	573.6
51,000	0.1091	0.7519	0.145	0.3808	216.7	573.6
52,000	0.1039	0.7519	0.14	0.3718	216.7	573.6
53,000	0.0991	0.7519	0.1317	0.363	216.7	573.6
54,000	0.0944	0.7519	0.1256	0.3543	216.7	573.6
55,000	0.09	0.7519	0.1197	0.3459	216.7	573.6
56,000	0.0857	0.7519	0.114	0.3377	216.7	573.6
57,000	0.0817	0.7519	0.1087	0.3297	216.7	573.6
58,000	0.0779	0.7519	0.1036	0.3218	216.7	573.6
59,000	0.0742	0.7519	0.0987	0.3142	216.7	573.6
60,000	0.0707	0.7519	0.0941	0.3067	216.7	573.6
61,000	0.0674	0.7519	0.0897	0.2995	216.7	573.6
62,000	0.0643	0.7519	0.0855	0.2923	216.7	573.6
63,000	0.0612	0.7519	0.0815	0.2854	216.7	573.6
64,000	0.0584	0.7519	0.0776	0.2786	216.7	573.6
65,000	0.0556	0.7519	0.074	0.272	216.7	573.6

Table B – 1 Standard Atmosphere